Cranfield UNIVERSITY

Enhanced pyroelectric effect through product property and its applications

Harrison Hoon Seok Chang

Supervised by **Dr. Zhaorong Huang**

Microsystems and Nanotechnology Centre, Department of Materials,
School of Applied Sciences, Cranfield University,
MK43 0AL, UK

October 2009

This dissertation is submitted in partial fulfillment of the requirements for the degree of Doctor of Philosophy.

To my family, Prof. Choo-Hwan Chang,
Mrs. Myung-Hee Rim, and Miss Seon-Hee Chang

In loving memory of my grandparents…

My deepest gratitude is reserved for my supervisor, Dr. Zhaorong Huang, whose support, guidance, and contributions have made this dissertation possible. Meanwhile, my sincerest gratitude also goes to Prof. Roger W. Whatmore of Tyndall National Institute, Ireland, with whom invaluable discussions regarding this work took place.

Dr. Chris Shaw, Mr. Andrew Stallard, and Dr. Hsien-Chun Chung are owed my warmest gratitude for their contributions during the experimental phase of this research, while I am also very grateful to Dr. Rob Dorey, Dr. Steve Dunn, Dr Glenn Leighton, and many other colleagues at Microsystems and Nanotechnology centre for their support during the course of this research.

The moral support I received from my family, Dr. Kyung-Sub Sung, Dr. Chang-Sub Park, Miss Borame Dickens, Mr. Josu Lopez de Aretxaga grijalba, Dr. Katja Jantos, Dr. Katherine Rickus, Miss Kyung-Ah Kwon, Mr. Jin-Hyun Yu, and Mr. Jung-Soo Chung are all greatly appreciated of and thankful for.

Financial support from EPSRC and Cranfield University are also acknowledged.

"The Road goes ever on and on
Down from the door where it began.
Now far ahead the Road has gone,
And I must follow, if I can,
Pursuing it with eager feet,
Until it joins some larger way
Where many paths and errands meet.
And whither then? I cannot say."
- J. R. R. Tolkien

Abstract

Pyroelectric materials have the ability to generate electrical response when they experience a thermal stimulus. This has lead to their deployment in applications such as Infra-Red detectors/sensors, energy harvesting, and ferroelectric electron emission cathodes, among others. All the "Figures of merit" presented in the literature for assessing pyroelectric materials are proportional to the pyroelectric coefficient. Hence, enhancing this coefficient should improve the performance of the pyroelectric element in any application. This research has been conducted to find ways of enhancing the pyroelectric coefficient of a given material through product property in the secondary pyroelectric effect arising from thermal expansion coefficient mismatch.

Analytical model for describing such enhancement in 2-2 connectivity laminate composites has been developed and simulated on Mathematics package Maple, while Finite Element Analysis package ANSYS® was used to perform thermo-structural analysis investigating the effect of bonding/interfacial layer on the strain transfer between the laminate layers. Indicators for judging the credentials of various pyroelectric materials in pyroelectric coefficient enhancement have been identified and evaluated for six different pyroelectric materials. These six pyroelectric materials were paired with six different non-pyroelectric materials to form thirty-six 2-2 connectivity laminate composites for the purpose of comparing pyroelectric coefficient enhancements, whereby various factors affecting the enhancement have been determined. Potential applications of this enhancement and what it may mean in terms of improvement in the outputs of these applications has been reviewed. In particular, two electrical boundary conditions, namely short and open circuit conditions, have been explored while the effects of thermal mass variation due to the introduction of non-pyroelectric layer have also been inspected.

Experimental verification of pyroelectric coefficient enhancement under short circuit condition in Lead zirconate titanate/Stainless steel 2-2 connectivity laminate composites has been conducted with observed pyroelectric coefficient enhancements of more

than 100 % while theoretical enhancements of up to 800 % is predicted in certain laminate composites of Lead zirconate titanate/Chlorinated polyvinyl chloride thermoplastic. Consideration of the open circuit condition pyroelectric coefficients and their enhancements revealed significant dissimilarities from their short circuit condition counterparts, prompting the need for more distinction to be made between the two than it has previously been thought. For instance, appraising employment credentials of pyroelectric elements in applications such as pyroelectric X-ray generation, electron accelerator, and nuclear fusion should involve the use of open circuit pyroelectric coefficient rather than the short circuit one.

The effects of thermal mass has also been considered using quantities termed "Figures of merit for efficiency", comparing the laminate composite's thermal-to-electrical conversion efficiency to that of stand alone pyroelectric material. Up to twenty fold increase in thermal-to-electrical conversion efficiency under short circuit condition has been predicted in laminate composites of Lead zirconate titanate/Chlorinated polyvinyl chloride thermoplastic, insinuating a potential for increased employment of Lead zirconate titanate in areas such as pyroelectric sensors and pyroelectric energy harvesting.

Pyroelectric energy harvesting application has been examined in detail as a potential beneficiary of this enhancement, with various analysis tools for assessing pyroelectric energy harvesting performance of a given pyroelectric element presented and evaluated. A pyroelectric energy harvesting system was designed as a hypothetical application of pyroelectricity and pyroelectric coefficient enhanced 2-2 connectivity laminate composites. Theoretical analysis confirms that large improvement in pyroelectric energy harvesting performance can be expected in Lead zirconate titanate materials by converting them into 2-2 connectivity laminate composites. The use of newly defined "New electrothermal coupling factor for composites" (k^2_{New}) for assessing credentials of particular pyroelectric element in pyroelectric energy harvesting application has been proposed and vindicated while the experimental samples from the pyroelectric coefficient enhancement study were demonstrated to show significant improvement in their pyroelectric energy harvesting performance via pyroelectric coefficient enhancement.

The analysis techniques used in this dissertation provide a methodology for assessing the potentials of particular pyroelectric material and its 2-2 connectivity laminate composites for applications under both short and open circuit conditions.

Nomenclature

η_{Carnot}	Carnot cycle efficiency
η_{Res}	Efficiency for resistive load PY energy harvesting
Θ_H	High temperature, hot reservoir temperature or temperature at which SMA is in austenite phase
Θ_L	Low temperature, cold reservoir temperature or temperature at which SMA is in martensite phase
Θ_{PY}	Temperature of PY element
Θ_{SMA}	Temperature of SMA springs
f	Thermal (heating/cooling) cycle frequency
F_{eff}^{a}	Figure of merit for efficiency type a, the ratio between the same total volume of pyroelectric material and 2-2 connectivity composite
F_{eff}^{b}	Figure of merit for efficiency type b, the ratio between a pyroelectric material and a composite with the pyroelectric material of the same thickness
k^2	Electrothermal coupling factor from literature
k_{New}^2	New electrothermal coupling factor for laminate composites
P_{denMax}	Maximum power density
R	Thickness ratio between thicknesses of PY and NP materials ($\frac{^{PY}t}{^{NP}t}$)
R_{min}	Minimum R value of 0.005

Al	Aluminium
BTO	Barium titanate
cf.	confer(Please refer to)
coef	coefficient
CPVC	Chlorinated polyvinyl chloride thermoplastic
Cu	Copper
Cur temp	Epoxy/adhesive curing temperature
dc1/dc2/dc3	Indicators for pyroelectric coefficient enhancement potentials (Eq 4.1)
Eff	Efficiency / Thermal-to-electrical conversion efficiency
FE	Ferroelectric
Invar36	Invar 36
IPA	Isopropyl alcohol
KOH	Potassium hydroxide
LNO	Lithium niobate
LTO	Lithium tantalate
Normal pre-stress	pre-stress parallel to 3 axis
NP	Non-pyroelectric
OC	Open circuit condition
Op. temp	Operating temperature, temperature at which the measurement takes place
P_S	Spontaneous polarisation
PA	Paraelectric

Planar pre-stress	pre-stress parallel to 1 and 2 axes
PLZT	Lead-lanthanum-zirconate-titanate
PMN-PT	Lead magnesium niobate-Lead titanate single crystal
PTFE	Poly-tetrafluoroethylene or Teflon
PVDF	Poly-vinylidene fluoride
PVDF-HFP	Poly(vinylidene fluoride-hexafluoropropylene)
PY	Pyroelectric
pyro-rig	Pyroelectric coefficient measurement rig
PZST	Lead zirconate stannate titanate
PZT	Lead zirconate titanate
RTD	Resistive temperature detector
SC	Short circuit condition
SECE	Synchronised electric charge extraction
SMA	Shape Memory Alloys
SSDI	Synchronised switch damping on inductor
SSHI	Synchronised switch harvesting on inductor
St	Stainless steel
Zn	Zinc

Table of Contents

List of Figures

List of Tables

List of Equations

Chapter 1

Introduction

1.1 Research rationale

Pyroelectric materials have the ability to generate electrical response when they experience a thermal stimulus. This has lead to their deployment in applications such as Infra-Red detectors/sensors[110,123,188,189], energy harvesting[138], and ferroelectric electron emission cathodes[166], among others. Depending on the application of these materials, it is convenient to define appropriate "Figures of merit" for the comparison purposes, three of which are[110,187,188]: $F_i = \frac{p}{c}$, $F_v = \frac{p}{c\varepsilon}$, and $F_D = \frac{p}{c(\varepsilon tan\delta)^{1/2}}$, where p is the pyroelectric coefficient, c the volume specific heat, ε the relative permittivity, and $tan\delta$ the dielectric loss of the material. F_i applies to a thin pyroelectric disc feeding current into a low impedance amplifier, F_v to such a disc supplying a voltage to a high impedance amplifier whose inherent noise of which limits the sensitivity of detection, while F_D also applies to a voltage mode, but under the assumption of the dominant source of noise being the pyroelectric element[188]. It is evident that all these "figures of merit" are proportional to the pyroelectric coefficient. By improving this coefficient, one should be able to improve the performance of the pyroelectric element in any such application.

The main aim of this research is to improve the pyroelectric effect of a given material through product property in the secondary pyroelectric effect. The pyroelectric coefficient can be divided into various parts, each a contribution from different phenomena transpiring inside the material stemming from the thermal stimuli. The secondary pyroelectric effect is a contribution from piezoelectricity. It will become apparent from the following chapters that this physical property is also a product property in composites[181], and hence it can be greatly increased with relatively small magnitude of change in one or

more of its constituents. It is hoped that by achieving this goal, the areas of employment of pyroelectric effect will be enlarged due to the enhancement of pyroelectric coefficient, leading to superior thermal sensitivity and greater charge response from the material, for example. At the outset of this research, pyroelectricity application of interest was pyroelectric X-ray generation. However, due to single crystal pyroelectric materials (pyroelectric materials mainly used in X-ray application) displaying limited enhancement, pyroelectric energy harvesting application (where various pyroelectric materials including Lead zirconate titanate are used) became the focus of this research.

1.2 Research objectives

1. Demonstration of the enhancement through product property potentials:
   (a) Development of a mathematical model for describing the potential enhancement in pyroelectric effect.
   (b) Investigation into the possible configurations of composites and materials to achieve this enhancement using the model developed in 1a.
   (c) Experimental verification of the predicted enhancement.
2. Investigation into potential applications of this enhancement.

1.3 Research methodology

In order to achieve the stated objectives in Section 1.2 following tasks will be undertaken.

1. Develop a mathematical model so that the composite's thermal-electrical performance can be conjectured and accounted for. (Objective 1a : Chapters 3 and 8)
2. Search for the best suited pyroelectric and thermally active material, as this will lead to greater improvement. (Objective 1b : Chapter 4)
3. Find the best possible configuration, be it laminar or matrix composite, for the chosen set of materials. (Objective 1b : Chapter 3 and 4)

4. Fabricate the composite and examine its performance, ensuring its behaviours are fully justified and compatible with the developed model. (Objective 1c : Chapters 5-7)

5. Theoretically consider the conditions under which the applications of these composites may operate. (Objective 2 : Chapters 8-10)

6. Consider various potential applications of these enhanced composites, evaluating their performance for a chosen application, namely pyroelectric energy harvesting. (Objective 2 : Chapters 12-14)

Among the tasks stated above, undertaking tasks 1-4 resulted in journal articles accepted by Journal of Applied Physics for publication[45] and published in Applied Physics Letters[43]. In these two articles, we compared thirty-six different pyroelectric and non-pyroelectric pairs for their enhancement and application potentials under short circuit electrical boundary condition through detailed analysis of their pyroelectric coefficient and thermal-to-electrical energy conversion efficiency, while presenting the results from our experimentation on Lead zirconate titanate and Stainless steel composites (cf. Appendices C.1 and C.3). Task 5 resulted in the published paper on Journal of Applied Physics[44], where similar considerations were given, but under open circuit electrical boundary condition (cf. Appendix C.2).

1.4 Contents of this dissertation

1.4.1 Part I

In this part of the dissertation, the possibility of pyroelectric coefficient enhancement will be considered. Mathematical modelling of the enhancement under short and open circuit electrical boundary conditions via thermodynamics and beam theory will be presented, while the findings from experimental verification of this enhancement under short circuit condition in Stainless steel/Lead zirconate titanate 2-2 connectivity laminate composites will also be revealed. Various parameters affecting this enhancement measurement will also be investigated, while their impact on the enhancement will be analysed.

Chapter 2 will consist of two sections. In Section 2.1, the definition of pyroelectricity and piezoelectricity will be presented, followed by the crystal classes that are said to be pyroelectric, finishing with some historical background in the relationship between

pyroelectricity and piezoelectricity. Section 2.2 will deal with what the author means by "enhancement" and introduce the readers to some work conducted by other researchers on the subject of the effect of pre-stress in piezoelectric/pyroelectric materials.

In Chapter 3, the fundamental concepts behind our pyroelectric coefficient enhancement will be presented with some analytical modelling and finite element analysis. At the outset, Section 3.1 will investigate the differences between short and open circuit electrical boundary conditions via boundary condition definitions (cf. Subsection 3.1.1). Section 3.2 will then propose a mathematical description of our enhancement under short circuit condition through consideration of thermodynamics, beam theory, and force balance equations, the consequence of which is the general pyroelectric coefficient expression for the 2-2 connectivity laminate composites of pyroelectric material of any crystal structure. This is followed by Section 3.3 exhibiting our finite element analysis results on the effects of adhesive/bonding/epoxy layer, concluding with Section 3.4, where simplified pyroelectric coefficient expressions for our samples used in the experimentation is derived via symmetry considerations and interface factors, k-factors, are introduced with the view to taking the results of the finite element analysis into account.

Six different pyroelectric materials and non-pyroelectric materials were paired and analysed for their enhancement potentials for this dissertation and Chapter 4 gives a brief introduction to these materials. Section 4.1 will give examples of some of the other materials we have considered for our pairing, but decided against it. Sections 4.2 and 4.3 will list the pyroelectric materials we have investigated, while the latter will also demonstrate the reasons behind the deployment of 2-2 connectivity configuration for our laminate composites and provide the indicators for judging the pyroelectric coefficient enhancement credentials of various pyroelectric materials. This chapter will then finish with the list of non-pyroelectric materials we have reviewed and the reasons behind their selection.

Chapter 5 consists of three sections. In Section 5.1, as well as the fabrication techniques used in creating our samples, some of the parameters that may affect our PY coef enhancement measurement will also be presented. Section 5.2 introduces the readers to our two planned experimental studies, Curing temperature (cf. Subsection 5.2.1) and Enhancement study (cf. Subsection 5.2.2). The aim of the former, which is also one of the main preliminary experimentation the author has conducted, is to investigate some of the potential parameters such as bonding layer thickness, epoxy curing temperature

(Cur temp), PY coef measurement temperature (operating temperature or Op. temp), and others that may affect the latter. The Enhancement study is designed to test the accuracy of our analytical model developed in Chapter 3, and its results form an integral part of this PhD dissertation. The final Section 5.3 illustrates parameters that may arise from the actual experimentation that may also affect the outcome of our investigation. Brief introduction to our experimental kit, pyro-rig, and the experimental procedures are presented, identifying features that may also affect the enhancement measurements. The preliminary experiments and their findings are also presented here. Randomly selected samples of the exactly same fabrication and measurement parameters were additionally created and compared to ensure the reproducibility of, and removal of any anomaly from, these studies.

Two sections make up Chapter 6. Section 6.1 presents the experimental results from the Curing temperature study and the derivation/analysis of the mathematical expression for pre-stresses parallel to all three axes. The outcomes from this section determined Cur and Op. temps to be employed in the Enhancement study, the results of which are presented in Section 6.2, and compared with the theoretical expectations of the analytical model from Chapter 3.4. Pyroelectric coefficient enhancement potentials of various Pyroelectric-Non-pyroelectric pairs will be discussed and analysed as well.

Chapter 7 summarizes the work undertaken in Chapters 2 - 6 and findings from this work, drawing conclusions from them. In essence, this work has successfully modelled the enhancements in pyroelectric coefficients of 2-2 connectivity laminate composites, followed by experimental verification of more than 100% enhancement in Stainless steel/Lead zirconate titanate composites.

Initial consideration of pyroelectric X-ray generation as the potential application for this research meant that pyroelectric effect under open circuit condition had to be considered since the X-ray application utilises pyroelectricity under open circuit condition. Although this dissertation mainly deals with another pyroelectric application, namely pyroelectric energy harvesting, which usually operates under short circuit condition, analyses undertaken for pyroelectricity under open circuit condition have resulted in some very interesting findings and hence these will be presented in Chapters 8 - 10 largely based on the author's journal publications[44,45].

Chapter 8 consists of two sections. It will start with the derivation of pyroelectric coefficient under open circuit condition for 2-2 connectivity laminate composites and

comparison with that under short circuit condition in Section 8.1, followed by Section 8.2 introducing the readers to the concept of the thermal-to-electrical conversion efficiency (Eff), its derivation process and use in Figure of merit for efficiencies.

Chapter 9 will analyse the short and open circuit condition pyroelectric coefficient enhancement and thermal-to-electrical conversion efficiencies of the laminate composites. In Section 9.1, the author will comment on and compare the enhancement potentials of various Pyroelectric-Non-pyroelectric pairs under the two electrical boundary conditions. The differences between pyroelectric coefficients measured under short and open circuit conditions will be highlighted and discussed. Section 9.2, will deal with the thermal-to-electrical conversion efficiencies of Pyroelectric-Non-pyroelectric pairs under both electrical boundary conditions, namely short and open circuit conditions. Evaluation procedures introduced in 8.2.3 and 8.2.3 will be followed to calculate the Figures of merit for efficiency for the pairs under short and open circuit conditions, respectively.

Chapter 10 summarizes the work undertaken in Chapters 8 - 9 and findings from this work, drawing conclusions from them. In essence, the secondary pyroelectric coefficient under open circuit condition has been described and compared to that under short circuit condition analytically. The differences between various materials and their 2-2 connectivity laminate composites have been presented. With other potential applications of these laminate composites in mind, the issue of thermal mass change by the introduction of non-pyroelectric layer to the pyroelectric material has been investigated using a quantity termed "efficiency", a measure for the laminate composites' thermal-to-electrical conversion efficiency, along with Figures of merit for efficiency (F^a_{eff} and F^b_{eff}) derived to be a ratio between the efficiencies of stand alone pyroelectric material and its laminate composite. Using these figures of merit for efficiency, various Pyroelectric-Non-pyroelectric pairs and their potential efficiency improvements under both electrical boundary conditions were analysed.

1.4.2 Part II

In this part of the dissertation, various applications where pyroelectric coefficient enhancement may find use in will be considered. In particular, its applicability in pyroelectric energy harvesting will be analysed via analytical modelling of a hypothetical pyroelectric energy harvesting system. How the enhancement affects the system's performance will be assessed while the parameters that play a significant role in this assessment

will be identified. The energy harvesting potentials of thirty-six 2-2 connectivity laminate composites and the experimental samples of Enhancement study from Part I will also be assessed.

The literature review in Chapter 11 provides an overview of the potential applications of the enhanced pyroelectric effect described in Part I. Although some of the applications listed here are not discussed in great detail, the author believes they are areas where this enhancement could also have an impact. At the outset, the application of most interest for this project was Pyroelectric X-ray generation presented in Section 11.2. However, as the project progressed it became apparent that evaluating the potential impact the enhancement can have on this particular application would be rather difficult. Even the theoretical description behind this particular X-ray generation phenomenon is problematic, making theoretical approximation impossible at this stage. With experimental verification under open circuit condition out of the question due to time and equipment constraints, it was decided that the energy harvesting application (cf. Section 11.1) will be the key area of interest.

In Chapter 12, theoretical analysis and formulation of pyroelectric energy harvesting application using 2-2 connectivity laminate composites will be presented. Section 12.1 will illustrate a simple energy harvesting arrangement which can turn a typical spatial temperature gradient into a temporal one, and hence enabling the use of pyroelectric materials in applications where thermoelectric routes would normally have been taken. For the analysis/formulation in Section 12.2, only the energy harvesting potentials of the 2-2 connectivity laminate composites under short circuit condition will be considered since the experimental measurements taken in Section 6.2 were under this condition. As the author has already demonstrated the differences between the short and open circuit conditions in Chapter 8, it should pose no problem for other researchers to derive the analogous expressions for the open circuit condition by themselves.

Section 13.1 of Chapter 13 will present the findings from the analysis performed on the thirty-six Pyroelectric-Non-pyroelectric 2-2 connectivity laminate composites using techniques from Chapter 12 with regards to pyroelectric energy harvesting application. Various parameters in pyroelectric energy harvesting application will be evaluated and compared for these laminate composites and their pyroelectric material only counterparts, while a new parameter termed "New electrothermal coupling factor (k^2_{New})" will be derived for assessing the pyroelectric energy harvesting potentials of laminate compos-

ites. This will then be followed by Section 13.2, where the author will focus the readers' attention on a particular pair, namely Stainless steel/Lead zirconate titanate composites, exploring the energy harvesting potentials of these experimentally measured samples from Section 6.2. During the analyses of these composites, recommendations will also be made on how to improve PY energy harvesting efficiency and output.

Chapter 14 summarizes the work undertaken in Chapters 11 - 13, drawing conclusions from them. In essence, numerous parameters for assessing a material or laminate composite's pyroelectric energy harvesting credentials have been identified, while a brief comparison with Figures of merit for efficiency (F^a_{eff} and F^b_{eff}) derived in previous part of the dissertation has been made. The use of New electrothermal coupling factor for composites (k^2_{New}) for such assessment has been vindicated while the experimental samples are demonstrated to show significant improvement in their pyroelectric energy harvesting performance via pyroelectric coefficient enhancement. Finally, some recommendations have been made to improve the performance of 2-2 connectivity laminate composites in this application.

1.4.3 Summary

Summarizing the work presented in this dissertation, Chapter 15 will give brief details of findings of this research and outline what this may mean in the applicability of pyroelectric coefficient enhancement.

1.4.4 Future work

Chapter 16 will list a number of potential research the author would like to see conducted. These works vary from those involved in developing better analytical models to pyroelectricity applications.

Part I

Pyroelectric coefficient enhancement through product property

In this part of the dissertation, the possibility of pyroelectric coefficient enhancement will be considered. After mathematically modelling the enhancement under short circuit electrical boundary condition via thermodynamics and beam theory, the findings from experimental verification of this enhancement in Stainless steel/Lead zirconate titanate 2-2 connectivity laminate composites will be presented. Various parameters affecting this enhancement measurement will also be investigated, while their impact on the enhancement will be analysed. The pyroelectric coefficient enhancement under open circuit condition will also be modelled, followed by the consideration of the thermal mass.

Chapter 2

Literature review - Pyroelectricity

This chapter will consist of two sections. In Section 2.1, the definition of pyroelectricity and piezoelectricity will be presented, followed by the classes of materials that are said to be pyroelectric, finishing with some historical background in the relationship between pyroelectricity and piezoelectricity. Section 2.2 will deal with what the author means by "enhancement" and introduce the readers to work conducted by other researchers on the subject of the effect of pre-stress in piezoelectric/pyroelectric materials.

2.1 Pyroelectric effect

2.1.1 Definition of pyroelectricity[40,82,99,133,190]

Oxford dictionary defines the prefix "pyro-" as a word originating from the Greek phrase "pyr", meaning "fire", that implies a relation to fire or heat. Therefore, it would be logical to deduce that pyroelectricity, or pyroelectric (PY) effect, must describe a relation between thermal and electrical entity. It is a phenomenon where there is a temperature dependence of the spontaneous polarisation in certain anisotropic solids, where spontaneous polarisation is an instantaneous charge quantity associated with the dipolar or free charge in a dielectric. To be more precise, pyroelectricity is the ability of certain crystals, which lack a centre of symmetry and also have polar directions, to generate an electrical potential when they are either heated or cooled. Therefore, for obvious reasons pyroelectricity can only be exhibited in crystallised non-conducting substances having at least one axis of symmetry that is polar, i.e. that has no centre of symmetry. Such conditions are fulfilled by only ten of the thirty-two crystal classes, which will be identified

later in 2.1.3.

Pyroelectricity can also be visualised as one side of a triangle, where each corner represents energy states in the crystal as illustrated by Figure 2.1:

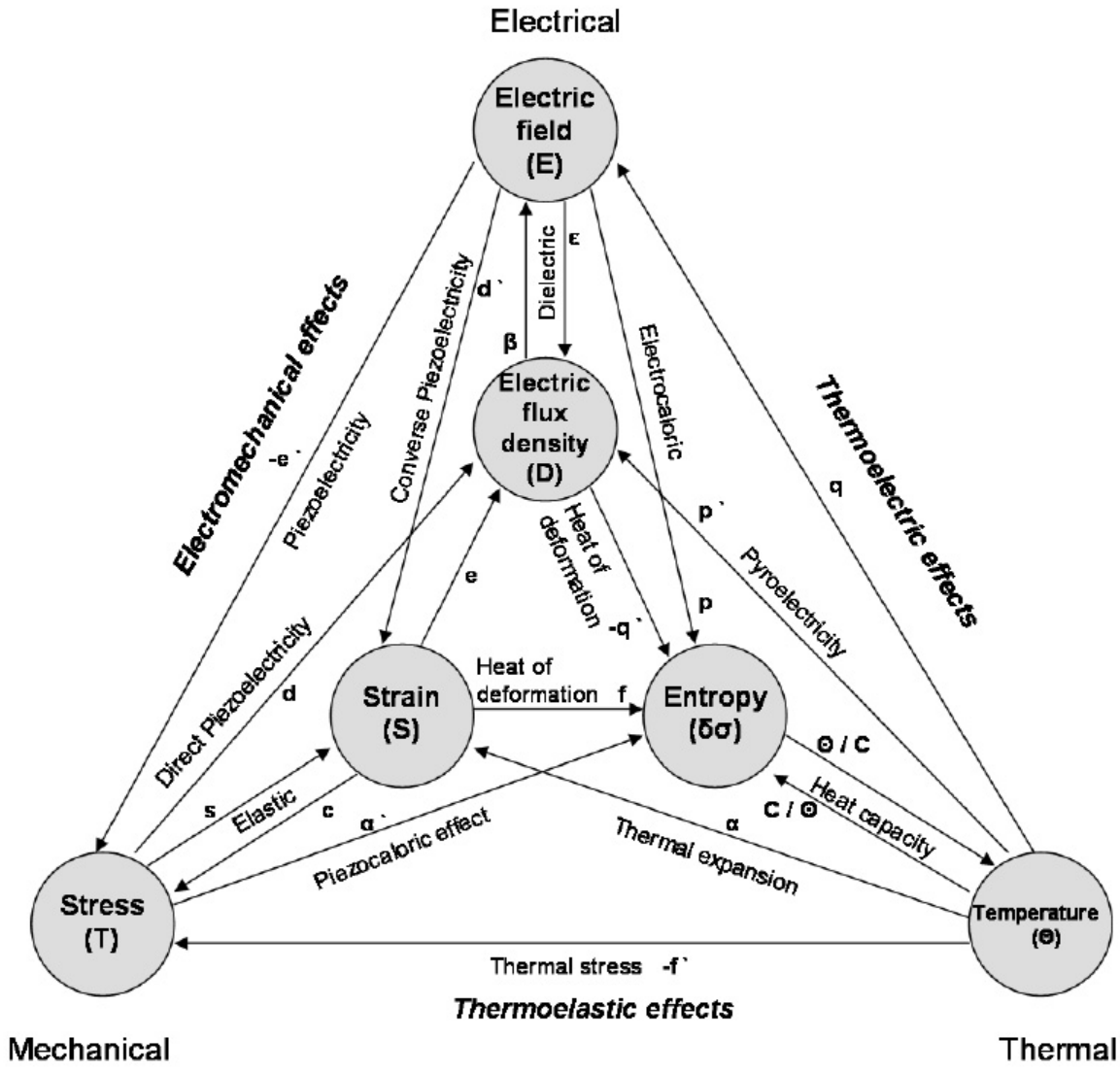

Figure 2.1: Interaction processes between the electrical, mechanical, and thermal systems[133].

The mechanism behind pyroelectricity can be described as follows: The unit cells of pyroelectric materials have a dipole moment. The dipoles are packed so that the components of the dipole moment in each unit cell add up in the direction normal to the flat surface. The dipole moment per unit volume of the material is called the spontaneous polarisation, P_S. Always a non-zero quantity in a pyroelectric material, P_S exists in the absence of an applied electric field and is equivalent to a layer of bound charge on each

flat surface of the sample. This is obvious since the electrical potential, i.e. the bound charge on the surface, is established by the polarisation of the material, to put in other terms migration of positive and negative charges moving in opposite directions. This potential on the surface is, in general, compensated by the nearby free charges such as electrons or ions.

If the temperature of the sample is kept constant, then P_S also remains constant. However, if an increase in temperature is experienced the net dipole moment and, consequently, the spontaneous polarisation will decrease in most single crystals and ceramics. Then the potential on the surface also decreases, and the redistribution of free charges to compensate for the change in potential occurs. Had the sample been cooled, instead of heated, the signs of the charges on opposite surfaces would have been reversed. It should also be noted at this point that the pyroelectric effect is only observable during the period in which the temperature changes occur;

$$\Delta P_{Si} = p_i \Delta\Theta, \qquad i = 1, 2, 3 \tag{2.1}$$

where ΔP_{Si} = Dipole moment per unit volume, i.e. Spontaneous polarisation, in i-direction

$\Delta\Theta$ = Uniform temperature change

p_i = Pyroelectric coefficient (PY coef) in i-direction

Under normal circumstances, even polar materials do not display a net dipole moment. As a consequence, there are no electric dipole equivalents of bar magnets because the intrinsic dipole moment is neutralized by "free" electric charge that builds up on the surface by internal conduction or from the ambient atmosphere. Polar crystals only reveal their nature when perturbed in some fashion that momentarily upsets the balance with the compensating surface charge, an example of this would be a sudden temperature change in pyroelectric crystals leading to pyroelectric effect.

2.1.2 Definition of piezoelectricity [82,133]

Discovered by the Curie brothers in 1880 and termed by Hankel's proposal as "piezoelectricity", derived from Greek word for "press", piezoelectricity is an interaction between electrical and mechanical systems (cf. Figure 2.1 for further details). The direct piezoelectric effect is when the electric polarisation is produced by mechanical stress.

Closely related to it is the converse effect, whereby a crystal becomes strained when an electric field is applied. Both effects are manifestations of the same fundamental property of the crystal.

The linear relation between the stress, T_{kl}, applied to a piezoelectric material, and the resulting charge density, D_m is called the direct piezoelectric effect and may be written as; $D_m = d_{mkl}T_{kl}$, where d_{mkl} is the piezoelectric coefficient. The converse piezoelectric effect describes the strain, S_{ij}, that is developed in a piezoelectric material when the electric field, E_n, is applied; $S_{ij} = d_{nij}E_n = d^t_{ijn}E_n$ where ^{t} denotes the transposed matrix.

The well-established piezoelectric constitutive equations are:

$$\begin{aligned} dS_{ij} &= s^{E,\Theta}_{ijkl}dT_{kl} + d_{ijn}dE_n \\ dD_m &= d_{mkl}dT_{kl} + \varepsilon^T_{mn}dE_n \end{aligned} \tag{2.2}$$

where $s^{E,\Theta}_{ijkl}$ = Elastic compliance at constant temperature and electric field
ε^T_{mn} = Dielectric constant at constant stress

2.1.3 Classes of pyroelectric materials[133]

The fundamental postulate of crystal physics, known as "Neumann's Principle", displays how the symmetry of a crystal is related to the symmetry of its physical properties:

> "The symmetry elements of any physical property of a crystal must include the symmetry elements of the point group of the crystal"

The point group of a crystal is the group of macroscopic symmetry elements that its structure possesses. On this basis the crystal structures can be divided into thirty-two classes, or point groups, according to the number of rotational axes and reflection planes, which ensures that the crystal structure does not get altered when an operation has been applied[22]. Of the thirty-two crystal classes, twenty-one are non-centro-symmetric (i.e. lack a centre of symmetry), and of these, twenty exhibit direct piezoelectricity (i.e. they are piezoelectric), the remaining one being the cubic class 432.

Any material which develops a dielectric polarisation when an electric field is applied, but also possesses such natural charge separation even in the absence of a field, is called

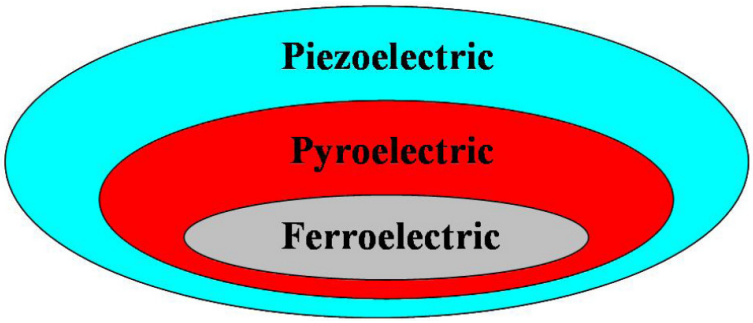

Figure 2.2: All ferroelectric materials are pyroelectric and all pyroelectric materials are piezoelectric.

a polar material. Whether a material is polar or not is determined solely by its crystal structure. Only ten of these twenty piezoelectric point groups are polar and these constitute the pyroelectric materials. They spontaneously polarise and possess a dipole in their unit cell, which leads to the phenomenon of pyroelectricity. If this dipole can be reversed by the application of an electric field, then the materials are also said to be ferroelectric.

- Piezoelectric crystal classes: 1, 2, m, 222, 2mm, 4, $\bar{4}$, 422, 4mm, $\bar{4}$2m, 3, 32, 3m, 6, $\bar{6}$, 622, 6mm, $\bar{6}$m2, 23, $\bar{4}$3m
- Pyroelectric crystal classes: 1, 2, m, 2mm, 4, 4mm, 3, 3m, 6, 6mm

There are a few crystal structures, notably the perovskite structure, which exhibit ferroelectric behaviour. This is analogous to ferromagnetism, in that, in the absence of an electric field during production, the ferroelectric crystal does not exhibit a polarisation. Upon the application of an electric field of sufficient magnitude, the crystal becomes permanently polarised. This polarisation can be reversed by a sufficiently large counter-charge, in the same way that a ferromagnet can be reversed. However, it is important to note that, although they are called ferroelectrics, the effect is due to the crystal structure, not the presence of a ferrous metal.

2.1.4 History behind the close association between pyroelectricity and piezoelectricity[40,82,99,133]

The definition of pyroelectricity as a phenomenon due to a change in net dipole moment is a rather modern concept. In fact, the first account of pyroelectric phenomenon is believed to have been recorded by a Greek philosopher, Theophrastus, who in 314 BC noted that tourmaline becomes charged when heated. He described a stone, called lyngourion in Greek, or lyncurium in Latin, that had the property of attracting straws and

bits of wood. Those attractions were no doubt the effects of electrostatic charges produced by temperature changes in the mineral, namely tourmaline. However, as Theophrastus and other writers of that period were far more interested in the origin of the stone and its possible therapeutic properties, scientific explanations for the reasons behind this phenomenon were never properly explored at that time.

Two millennia after Theophrastus, accounts of tourmalines unusual physical properties resurfaced in Europe in the form of a published book in 1707. Titled "Curiose Speculationes bey Schlaflosen Nachten (Curious speculations during sleepless nights)" and written by Johann Georg Schmidt, also known as "Immer Gern Speculirt (Always gladly speculating)", the book contained a section describing the experiences of Dutch gem cutters when they tested the durability of tourmaline in a fire. A passage from this book reads:

> "The ingenious Dr. Daumius, chief physician to the Polish and Saxon troops on the Rhine, told me that, in the year 1703, the Dutch first brought from Ceylon in the East Indies a precious stone called tourmaline, turmale, or trip, which had the property of not only attracting the ashes of the warm or burning coals, as the magnet does iron, but also repelling them again."

The first scientific description of pyroelectricity was reported in a journal by a physician and chemist Louis Lemery in 1717. Pyroelectric property of tourmaline was first related to electricity by a naturalist Carl von Linne (Linnaeus), who used the term "mineral lapis electricus", i.e. electric stone. With the development of more sophisticated research techniques, progressively quantitative understanding of pyroelectricity emerged during the 19th century. In 1824, Sir David Brewster, well known for his work in optics, observed the pyroelectric effect with various kinds of crystals and coined the term "pyroelectricity" for the first time. One of the materials he studied was a "tartrate of soda and potash", i.e. Rochelle salt, the same material in which Joseph Valasek discovered ferroelectricity almost exactly a century later. The first precise measurements of pyroelectric charges were made in 1859 by John Mothee Gaugain, made possible by the development of electrometer by Antoine Becquerel and others. From these measurements Gaugain deduced some important conclusions. He derived that the total quantity of electricity produced by a crystal of tourmaline depends uniquely on the limits within which its temperature is varied. Within those limits, the amount of electricity produced during heating is the same as that of cooling, but with the signs of the charges reversed.

In addition, the amount of charge produced is proportional to the cross-sectional area of the crystal, and independent of its length.

William Thomson, also known as Lord Kelvin, widely known for his work on the Kelvin scale for absolute temperature measurements, published the first major theoretical treatment of pyroelectricity in 1878, in which he also predicted the electrocaloric effect (cf. Figure 2.1 for further details on this effect). Lord Kelvin noted that pyroelectricity was due to permanent polarisation. According to his theory, the pyroelectric effect is simply a manifestation of the temperature coefficient of this polarisation. Hence, this effect was known to be an interaction between electrical and thermal systems (Figure 2.1).

Meanwhile, Pierre Curie and his brother, Jacques Curie, studied pyroelectricity around 1880s and proposed that the electrical effects due to non-uniform heating of quartz crystals might have been caused by pressure, a speculation that led to their discovery of some of the mechanisms behind piezoelectricity in 1880. Pierre Curie had previously studied the relation between pyroelectricity and crystal symmetry. This study led the brothers to foresee in what direction pressure should be applied and in which crystal classes the effect was to be expected. The same phenomena known as piezoelectricity have also been observed in many other crystals, such as those of tourmaline and Rochelle salt. In the year following this discovery of the direct piezoelectric effect, Lippmann predicted the existence of the converse effect from thermodynamic considerations. His prediction was verified by the Curies before the end of 1881. They showed in a later paper that the piezoelectric coefficient of quartz had the same value for the converse as for the direct effect.

Ever since the discovery of piezoelectricity, however, the relationship between pyro- and piezo-electricity generated much discussion, and Woldemar Voigt pointed out that a distinction must be made between the true (as defined by Lord Kelvin) and false (piezoelectric component due to thermal expansion) pyroelectricity. Please refer to Figure 2.3 for further details:

Both Lord Kelvin in 1878 and Voight in 1897 laid foundation to the development of a theory describing the processes behind pyroelectricity today. The phenomenological theory of piezoelectricity is also based on the thermodynamic principles enunciated by Lord Kelvin. The piezoelectric formulation was carried out in more detail by Pierre Duhem and F. Pockets, but Voigt proved to be the most active person in this field.

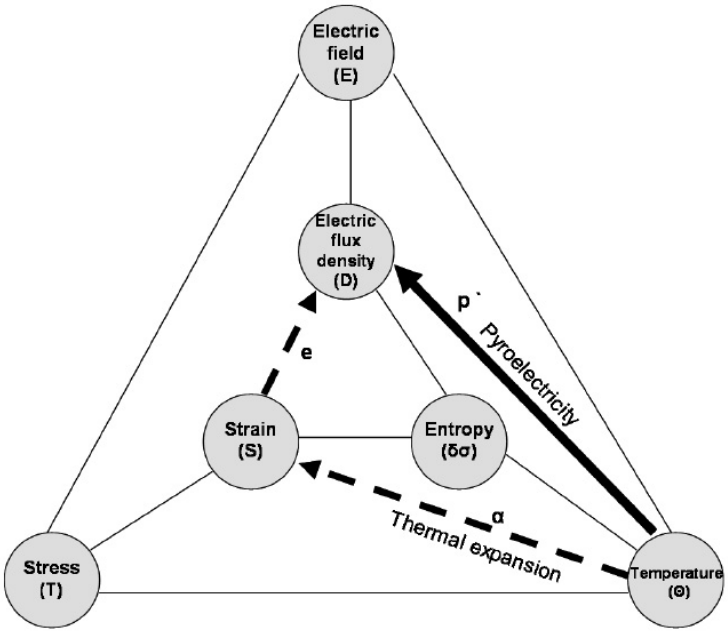

Figure 2.3: Primary and secondary pyroelectricity. The full line illustrates the primary effect (with strain constant) and the broken line illustrates the secondary effect which can occur when the crystal is free to deform [41,133].

The formulation we use today in crystal physics owes much to Voigts monumental work, "Lehrbuch der Kristallphysik", which appeared in 1910. Since then, Max Born published a lattice-dynamical theory in 1920, and Bragg and Gibbs demonstrated an atomic model for the qualitative explanation of piezoelectric polarisation in quartz by X-ray analysis in 1925.

In 1920, Joseph Valasek studied the properties of Rochelle salt and discovered ferroelectricity. Then the interest in pyroelectricity virtually vanished until 1938, when Yeou Ta, a chemist at the Sorbonne in Paris, published a paper that initiated the great growth in research activities that continues in the field till today. The paper contained a proposal for the tourmaline crystals as Infra-Red (IR) sensors in spectroscopy. This, with its obvious military application, led to some research being conducted on pyroelectric IR detectors during, and immediately after, World War II in the UK, US and Germany. Subsequently, the first detailed analysis of the behaviour of fast IR detectors was published by J. Cooper, following his experiments with barium titanate ($BaTiO_3$) in 1962.

Pyroelectricity is definitely not a new concept, but research and application of this useful property continues to this day.

2.2 Pyroelectric coefficient enhancement

2.2.1 The concept of enhancement

Over the years, there have been a large number of research being conducted on the secondary pyroelectric coefficient[21,186]. In particular, the effect of a substrate on pyroelectric thin films, owing to the thermal expansion mismatch, has been a topic of interest to many researchers[21,123,162,163,202]. In general the consensus was that for perovskite-based ferroelectric materials the product term $d_{mkl}^{E,\Theta} c_{ijkl}^{E,\Theta} \alpha_{ij}^{T,E}$ is much smaller than the primary term $p^{S,E}$ and hence the effect of this mismatch would be rather limited[123,202] (cf. subsection 3.2.1 for further details on what these symbols stand for and what these terms mean).

However, the possibility of utilising this secondary pyroelectric effect and thermal expansion mismatch to enhance the total pyroelectric coefficient has been suggested by Newnham et al.[129] and Nan[125,126] despite such limitation. Prior to their research Suchtelen's report[181] on product properties in phenomena such as magnetoelectric effect in composites of magnetostrictive and piezoelectric materials[146,147] also insinuated the secondary pyroelectric effect as a product property between piezoelectricity and thermal expansion, hinting a potentially high impact from this property in turn. Then, the work by Newnham et al. and Nan led to the development of various composites with superior mechanical flexibility accompanied by good pyroelectric characteristics[47,98,177,195,196] including improved pyroelectric figure of merit[28,130], but with only very limited enhancement in pyroelectric coefficient if any. As others did, they also concluded that in most cases due to the small hydrostatic piezoelectric effect, arising from cancellation between coefficients of opposite signs, the enhancement available through the secondary contribution is rather limited.

As it will become evident from the following sections of this dissertation, somewhat ironically it is this dissimilar signs of piezoelectric coefficients that we intend to exploit to achieve our large pyroelectric coefficient enhancement. By considering our pyroelectric materials and its piezoelectric coefficients symmetry and asymmetry respectively (cf. section 3.2), we concluded that a 2-2 connectivity laminate of pyroelectric Lead zirconate titanate (PZT) and non-pyroelectric (NP) Stainless steel (St), with much larger thermal expansion coefficient, should lead to a substantial pyroelectric coefficient enhancement, and verified that theoretically and experimentally[43] (cf. section C.3). Although the

mathematical expression for the pyroelectric coefficients of certain composites have been developed by others[126,129,130] based on volume fractions of each constituent, these expressions are not sufficient in describing our pyroelectric coefficient enhancement, and hence a new expression will be derived in Chapter 3.

2.2.2 Effect of pre-stress

There has been some research into the effect of pre-stress on the piezoelectric and dielectric responses of piezoelectric ceramics such as Lead zirconate titanate[199–201]. As our enhancement is expected to be induced by the stress/strain resulting from thermal expansion mismatch, this will undoubtedly put extra stress on to the pyroelectric material. General consensus seems to be that a significant increase in the dielectric and piezoelectric performances are expected over a small uniaxial compressive pre-stress range up to around 25-30 MPa for soft PZTs, beyond which predominant mechanical depolarisation effect makes the material exhibit hardly any piezoelectric effect. Although the nature of the stresses involved in our enhancement is not uniaxial nor entirely compressive, this may well suggest that under certain conditions we may observe rather limited enhancement when extremely large enhancement is expected due to large thermal expansion coefficient difference leading to large external stress/strain experienced by the pyroelectric material (cf. Eq 3.28).

As our pyroelectric coefficient enhancement is expected to come from the secondary pyroelectric coefficient, which is essentially a coupled physical property between piezoelectricity and thermal expansion, the author conducted some research into this aspect of our potential enhancement, which might be interesting to investigate further. Although this PhD dissertation does not deal with this specifically, it definitely is a subject area where further research could take place (cf. Sections 6.1 and 16.1 for the study undertaken for this project and the author's recommendation for future work directions, respectively).

Chapter 3

Basic Concept - Pyroelectric coefficient enhancement

In Chapter 3, the fundamental concepts behind our pyroelectric coefficient enhancement will be presented with some analytical modelling and finite element analysis. At the outset, Section 3.1 will investigate the differences between short and open circuit electrical boundary conditions via boundary condition definitions in Subsection 3.1.1. Section 3.2 will then propose a mathematical description of our enhancement under short circuit condition through consideration of thermodynamics, beam theory, and force balance equations, the consequence of which is the general pyroelectric coefficient expression for the 2-2 connectivity laminate composites of pyroelectric material of any crystal structure. This is followed by Section 3.3 exhibiting our finite element analysis results on the effects of adhesive/bonding/epoxy layer, concluding with Section 3.4, where simplified pyroelectric coefficient expressions for our samples used in the experimentation is derived via symmetry considerations and interface factors, k-factors, are introduced with the view to taking the results of the finite element analysis into account.

3.1 Two electrical boundary conditions

3.1.1 Definition of the electric boundary conditions

Although both Eq. 3.3 and 8.1 are correct expressions for the same PY coef, distinction between the two is essential to facilitate for the introduction of two alternative boundary conditions that may arise in practice. These two boundary conditions to be considered are short circuit and open circuit conditions. Following comments illustrate some differences between the two conditions[109,133,186]:

- Short circuit condition (abbreviated to SC henceforth)

Under short (closed) circuit condition, the electric potential on the whole of the surface of the crystal is perceived as being the same. This implies $d\boldsymbol{E} = 0$, i.e. electric field ($\boldsymbol{E}$) is assumed to be constant and $d\boldsymbol{E}$ to be zero. Sometimes also termed as electrically free, this is the condition under which most measurements of PY coef are taken and therefore Eq 3.9 is the expression conventionally used for the derivation of PY coef.

- Open circuit condition (abbreviated to OC henceforth)

Under open circuit condition, electric displacement ($\boldsymbol{D}$) is assumed to be constant in a crystal. This implies $d\boldsymbol{D} = \varepsilon_0 d\boldsymbol{E} + d\boldsymbol{P} = 0$ where ε_0 is the permittivity of free space and $\boldsymbol{P}$ is the total polarisation, and hence the need for Eq 8.1 as a prerequisite for the PY coef expression under OC. In general, when $d\boldsymbol{D} = 0$, the crystal is said to be electrically clamped.

3.2 Mathematical treatment

3.2.1 Short circuit pyroelectric coefficient

In this subsection, we shall derive the pyroelectric coefficient (PY coef) from Gibbs free energy of piezoelectric crystals[109,133]. Although we shall only derive the expression for PY coef under short circuit condition (SC) for the moment, that under open circuit condition (OC) will also be presented in Section 8.1.

Definition of pyroelectric coefficient under SC

The PY coef is a measure of pyroelectricity. However, since all pyroelectric materials are also piezoelectric, the pyroelectric coefficient, which is usually measured at constant stress $p^{T,E}$, consists of the primary pyroelectric coefficient measured at the constant strain $p^{S,E}$ and the secondary pyroelectric coefficient arising from strain[133];

$$p_m^{T,E} = p_m^{S,E} + d_{mkl}^{E,\Theta} c_{ijkl}^{E,\Theta} \alpha_{ij}^{T,E} \tag{3.1}$$

where $d_{mkl}^{E,\Theta}$ = Piezoelectric constant at constant temperature and electric field
$c_{ijkl}^{E,\Theta}$ = Elastic stiffness at constant temperature and electric field
$\alpha_{ij}^{T,E}$ = Thermal expansion coefficient at constant stress and electric field
E = Electric field
Θ = Temperature
i,j,k,l,m = 1..3

Please notice the use of Einstein summation convention which will be used throughout this report along with Voigt notation.

Also, it should be noted that there is a third contribution to the pyroelectricity termed tertiary pyroelectric effect which arises from either inhomogeneous temperature distributions within the crystal[27] or a temperature gradient through the specimen thickness[158]. As our intended samples have dimensions that should minimise this effect and our preliminary tests demonstrated negligible contribution from this effect in our measurements (cf. Subsection 5.3.3), its contribution will be ignored in our theory. However should the preliminary testing depicted a contribution, the techniques used by Newsome and Andrei[84] could be employed to determine the magnitude of this contribution.

As we intend to use our PY coef expression to derive that of a laminate composite (cf. section 5.1), it is necessary to generalise the mathematical model of the PY coef as much as possible since the final configuration will consist of a PY material attached to a thermally active material (NP material such as Stainless steel or Shape Memory Alloys), which will then exert 'thermally motivated external' stress onto the PY material. This implies previous models for PY coef given by others[73,99,109,129,130,133,186,194], Eq 3.1 for instance, do not supply sufficient enough description of the mechanisms behind our desired effect. So, let us derive the expression for the pyroelectric coefficient (p_i) again from its fundamental definition[133,186]:

$$p_i = \frac{\Delta P_{Si}}{\Delta\Theta} = \frac{dP_{Si}}{d\Theta}, i = 1..3 \tag{3.2}$$

where ΔP_{Si} = Dipole moment per unit volume, i.e. Spontaneous polarisation, in i-direction

$\Delta\Theta$ = Uniform temperature change

dP_{Si} = Change in spontaneous polarisation vector's component in i-direction

$d\Theta$ = Change in temperature

p_i = Pyroelectric coefficient in i-direction

Also, $\boldsymbol{D} = \varepsilon_0\boldsymbol{E} + \boldsymbol{P}$ in any dielectric material and $\boldsymbol{P} = \boldsymbol{P}_S + \boldsymbol{P}_{Ind}$ in piezo- or pyroelectric materials with $\boldsymbol{P}_{Ind} = \varepsilon_0\boldsymbol{\chi}_e\boldsymbol{E}$[45,183].

$\Rightarrow \boldsymbol{D} = \varepsilon_0\boldsymbol{\varepsilon_r}\boldsymbol{E} + \boldsymbol{P}_S \qquad \therefore P_{Si} = D_i - \varepsilon_0(\varepsilon_r)_i E_i$

Therefore for short circuit condition, $dE_i = 0$ (cf. subsection 3.1.1);

$$p_i = \frac{dP_{Si}}{d\Theta} = \frac{dD_i}{d\Theta} \tag{3.3}$$

where $\boldsymbol{P}$ = Total polarisation

$\boldsymbol{P}_S$ = Spontaneous polarisation

$\boldsymbol{D}$ = Electric displacement (Electric flux density)

$\boldsymbol{E}$ = Electric field (intensity)

$\boldsymbol{P}_{Ind}$ = Induced polarisation owing to $\boldsymbol{E}$

$\boldsymbol{\chi}_e = \boldsymbol{\varepsilon}_r - \boldsymbol{I}$ = Dielectric susceptibility

$\boldsymbol{I}$ = Identity matrix/vector

ε_0 = Permittivity of free space

$\boldsymbol{\varepsilon_r}$ = Relative dielectric constant (Relative permittivity)

(Note that for the purpose of our studies, as in practice most measurements are taken under constant stress condition, where they are not mechanically clamped and free to deform, we can safely assume that $((\varepsilon_r)_i = (\varepsilon_r^T)_i$, i.e. relative dielectric constants are evaluated under constant stress.)

Pyroelectric coefficient under SC

According to the first and second law of thermodynamics, the reversible change dU in the internal energy U of an elastic dielectric subjected to a small change of the strain dS, electric displacement dD, and entropy $d\sigma$ is given by;

$$dU = \Theta d\sigma + T_{kl} dS_{ij} + E_n dD_m \tag{3.4}$$

where Θ is the temperature of the material.

If one wishes to investigate systems under isothermal conditions, and use electric field, E, and stress, T, as the independent variables, a Legendre transformation of U has to be performed by adding the expression $-S_{ij}T_{kl} - D_m E_n - \sigma\Theta$ to U. This results in the following free energy function, which is also know as the Gibbs free energy, G, of a piezoelectric crystal[109,133];

$$G = U - S_{ij}T_{kl} - D_m E_n - \sigma\Theta \tag{3.5}$$

where i, j, k, l, m, n = 1..3

Any natural process occurs if and only if the associated change in G of the process is negative. Likewise, a system reaches an equilibrium when the associated change in G is zero.

In order to derive the pyroelectric coefficient expression under short circuit condition, we commence with the assumption of constant external electric field, i.e. $dE_n = 0\ \forall n$, from the definition of short circuit condition (cf. subsection 3.1.1). To make the resulting constitutive equations from Eq 3.5 solvable, we must choose the independent variables accordingly. So, for SC we define the temperature (Θ), stress (T_{ij}) and electric field (E_m) as the independent variables.

By considering the conventional nine components of the second order strain and stress tensors, while the magnetic effect is ignored as usual, we have:

$$
\begin{aligned}
&G = G(T_{ij}, E_m, \Theta) \\
&\Rightarrow \quad dS_{ij} \quad = \sum_k \sum_l \left(\frac{\partial S_{ij}}{\partial T_{kl}}\right)_{E,\Theta} dT_{kl} + \sum_n \left(\frac{\partial S_{ij}}{\partial E_n}\right)_{T,\Theta} dE_n + \left(\frac{\partial S_{ij}}{\partial \Theta}\right)_{T,E} d\Theta \\
&\text{and} \\
&\qquad dD_m \quad = \sum_k \sum_l \left(\frac{\partial D_m}{\partial T_{kl}}\right)_{E,\Theta} dT_{kl} + \sum_n \left(\frac{\partial D_m}{\partial E_n}\right)_{T,\Theta} dE_n + \left(\frac{\partial D_m}{\partial \Theta}\right)_{T,E} d\Theta
\end{aligned}
\tag{3.6}
$$

Assuming constant external electric field (i.e. $dE_n = 0 \; \forall n$ for SC) and using Einstein's summation indexing method: Eq 3.6

$$
\begin{aligned}
&\Rightarrow \quad dS_{ij} \quad = \left(\frac{\partial S_{ij}}{\partial T_{kl}}\right)_{E,\Theta} dT_{kl} + \left(\frac{\partial S_{ij}}{\partial \Theta}\right)_{T,E} d\Theta \\
&\text{and} \\
&\qquad dD_m \quad = \left(\frac{\partial D_m}{\partial T_{kl}}\right)_{E,\Theta} dT_{kl} + \left(\frac{\partial D_m}{\partial \Theta}\right)_{T,E} d\Theta
\end{aligned}
\tag{3.7}
$$

From Eq 3.7 with $(\partial S_{ij}/\partial T_{kl})^{-1}_{E,\Theta}$ denoting the inverse tensor of $(\partial S_{ij}/\partial T_{kl})_{E,\Theta}$, which is assumed to exist as $(\partial S_{ij}/\partial T_{kl})_{E,\Theta} = s^{E,\Theta}_{ijkl}$:

$$
\begin{aligned}
&\Rightarrow \quad dT_{kl} \quad = \left(\frac{\partial S_{ij}}{\partial T_{kl}}\right)^{-1}_{E,\Theta} \left[dS_{ij} - \left(\frac{\partial S_{ij}}{\partial \Theta}\right)_{T,E} d\Theta\right] \\
&\Rightarrow \quad dD_m \quad = \left(\frac{\partial D_m}{\partial T_{kl}}\right)_{E,\Theta} \left(\frac{\partial S_{ij}}{\partial T_{kl}}\right)^{-1}_{E,\Theta} \left[dS_{ij} - \left(\frac{\partial S_{ij}}{\partial \Theta}\right)_{T,E} d\Theta\right] + \left(\frac{\partial D_m}{\partial \Theta}\right)_{T,E} d\Theta \\
&\Rightarrow \quad \frac{dD_m}{d\Theta} \quad = \left(\frac{\partial D_m}{\partial \Theta}\right)_{T,E} - \left(\frac{\partial D_m}{\partial T_{kl}}\right)_{E,\Theta} \left(\frac{\partial S_{ij}}{\partial T_{kl}}\right)^{-1}_{E,\Theta} \left[\left(\frac{\partial S_{ij}}{\partial \Theta}\right)_{T,E} - \frac{dS_{ij}}{d\Theta}\right]
\end{aligned}
\tag{3.8}
$$

Substituting Eq 3.8 into Eq 3.3:

$$\begin{aligned}\therefore p_m^{SC} &= \frac{dD_m}{d\Theta} \\ &= \left(\frac{\partial D_m}{\partial \Theta}\right)_{T,E} - \left(\frac{\partial D_m}{\partial T_{kl}}\right)_{E,\Theta} \left(\frac{\partial S_{ij}}{\partial T_{kl}}\right)^{-1}_{E,\Theta} \left[\left(\frac{\partial S_{ij}}{\partial \Theta}\right)_{T,E} - \frac{dS_{ij}}{d\Theta}\right] \\ &= p_m^{T,E} - d_{mkl}^{E,\Theta}(s_{ijkl}^{E,\Theta})^{-1}\left[\alpha_{ij}^{T,E} - \frac{dS_{ij}}{d\Theta}\right] \\ &= p_m^{T,E} - d_{mkl}^{E,\Theta} c_{ijkl}^{E,\Theta}\left[\alpha_{ij}^{T,E} - \frac{dS_{ij}}{d\Theta}\right]\end{aligned} \tag{3.9}$$

where p_m^{SC} = Total pyroelectric coefficient under SC

$\frac{dDm}{d\Theta}$ = Change in electric displacement per temperature change

= Measured/observed value of pyroelectric coefficient from Eq 3.2

$p_m^{T,E}$ = Pyroelectric coefficient at constant stress (free boundary condition) and electric field

$d_{mkl}^{E,\Theta}$ = Piezoelectric constant at constant temperature and electric field

$s_{ijkl}^{E,\Theta}$ = Elastic compliance at constant temperature and electric field

$c_{ijkl}^{E,\Theta} = (s_{ijkl}^{E,\Theta})^{-1}$

= Elastic stiffness at constant temperature and electric field

$\alpha_{ij}^{T,E}$ = Thermal expansion coefficient at constant stress and electric field

dS_{ij} = Total strain experienced by the pyroelectric material

i,j,k,l,m = 1..3

(Please compare this expression with the expression from the literature, Eq 3.1, for better understanding of the difference.)

In addition, since the primary pyroelectric coefficient $p^{S,E}$ is measured when $dS_{ij} = 0$;

$$p_m^{S,E} = p_m^{T,E} - d_{mkl}^{E,\Theta} c_{ijkl}^{E,\Theta}(\alpha_{ij}^{T,E}) \tag{3.10}$$

which agrees with the literature[133].

Please note that all these expressions only deal with linear effects. In the case of strong fields or strongly non-linear materials, which is not the case for this project, these expressions must be extended to include higher order terms.

3.2.2 Laminate structures and related strains

We now move on to the derivation of the pyroelectric coefficient for the symmetric laminate structure (2-2 connectivity three layer laminate composite configuration as illustrated in Figure 3.1 (a)) which is the configuration chosen for this project for their theoretical elimination of the bending effect, simplifying the mathematical considerations required for our theories.

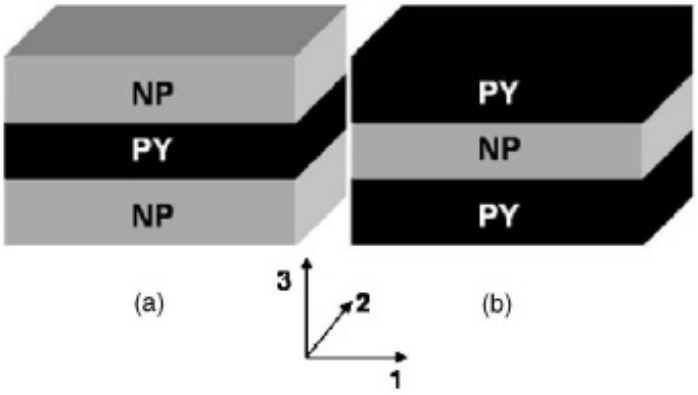

Figure 3.1: 2-2 Connectivity three layer laminate composite configurations [43]

Derivation of the strain expression to be substituted into the pyroelectric coefficients

Since we now have the expression for the pyroelectric coefficient (under SC cf. Eq 3.9 and under OC cf. Eq 8.6 in subsection 8.1.1), we shall proceed to deriving the expressions for the strains the pyroelectric material will experience due to the thermal expansion mismatch between itself and the non-pyroelectric (thermally active) material.

Please note that the pyroelectric material will be termed as 'PY' and non-pyroelectric material as 'NP' henceforth. In addition, for the purpose of deriving the desired strain expressions, various constants will not be distinguished between SC and OC (namely into $s_{ij}^{E,\Theta}$ or $c_{ij}^{E,\Theta}$ or ${}^{PY}\alpha_j^{T,E}$ for SC and $s_{ij}^{D,\Theta}$ or $c_{ij}^{D,\Theta}$ or ${}^{PY}\alpha_j^{T,D}$ for OC), as in both cases the derivation process will be identical.

Force balance equation

In general, any solid material has the following elastic relations between the strain (S_j) and stress (T_k);

$$S_j = \sum_{k=1}^{6} s_{jk} T_k \qquad \& \qquad T_k = \sum_{j=1}^{6} c_{kj} S_j \tag{3.11}$$

By utilising the previously stated relations of PY and NP, and considering their interactions at the interface between the PY and NP layer, we can now construct a mathematical model of the two constituents' mechanical interaction, the solution of which will give us the strain the PY will experience when a temperature change is applied to the symmetric laminate structure consisting of PY and NP. As the system is symmetrical about the 1-2 plane, two layer laminar theory should present a good approximation to our three layer case, while generalised Hooke's law for orthotropic materials[101] and the assumptions of the state of plane stress conditions[111] should make the mathematical model much simpler and hence solvable.

Assume[42,60,151]:

1. State of plane stress, i.e. only S_1, S_2, S_3, and S_6 are non-zero (but $T_3 = T_4 = T_5 = 0$),

2. The shear stress in 1-2 plane, i.e. $T_6 = \tau_{12}$, is negligible (this means S_6 is also negligible since $S_6 = \frac{1}{G_{12}} T_6$).

Hence, we only need to consider S_j for j=1..3 and T_k for k=1..2. So, Eq 3.11 becomes:

$$S_j = \sum_{k=1}^{2} s_{jk} T_k \qquad \& \qquad T_k = \sum_{j=1}^{3} c_{kj} S_j \tag{3.12}$$

Using force balance law at the interface:

$$\begin{aligned} 0 &= {}^{PY}F_1 + {}^{NP}F_1 = {}^{PY}F_2 + {}^{NP}F_2 \\ &= {}^{PY}T_1\,{}^{PY}A_1 + {}^{NP}T_1\,{}^{NP}A_1 = {}^{PY}T_2\,{}^{PY}A_2 + {}^{NP}T_2\,{}^{NP}A_2 \end{aligned}$$

$$\Rightarrow \quad 0 = \left[\sum_{j=1}^{3} {}^{PY}c_{1j}\,{}^{PY}S_j\right] {}^{PY}A_1 + {}^{NP}T_1\,{}^{NP}A_1 \tag{3.13}$$

and

$$0 = \left[\sum_{j=1}^{3} {}^{PY}c_{2j}\,{}^{PY}S_j\right] {}^{PY}A_2 + {}^{NP}T_2\,{}^{NP}A_2 \tag{3.14}$$

where A_i = Surface area perpendicular to i-axis

F_i = Force acting perpendicular to A_i and along the i-axis

Beam model for the non-pyroelectric (NP) material and the force balance equation

Now, for ${}^{NP}T_k$ (k=1..2), in general the stiffness matrix of a NP material is unknown, therefore we use the general stress-strain relationship for the materials with orthotropic symmetry and negligible shear stresses[42,60,151]:

$$\begin{pmatrix} {}^{NP}S_1 \\ {}^{NP}S_2 \\ {}^{NP}S_3 \end{pmatrix} = \begin{pmatrix} \frac{1}{E_1} & \frac{-\nu_{21}}{E_2} & \frac{-\nu_{31}}{E_3} \\ \frac{-\nu_{12}}{E_1} & \frac{1}{E_2} & \frac{-\nu_{32}}{E_3} \\ \frac{-\nu_{13}}{E_1} & \frac{-\nu_{23}}{E_2} & \frac{1}{E_3} \end{pmatrix} \begin{pmatrix} {}^{NP}T_1 \\ {}^{NP}T_2 \\ {}^{NP}T_3 = 0 \end{pmatrix}$$

$$\begin{aligned} \Rightarrow \quad {}^{NP}S_1 &= \left(\frac{1}{E_1}\right) {}^{NP}T_1 + \left(\frac{-\nu_{21}}{E_2}\right) {}^{NP}T_2 \\ {}^{NP}S_2 &= \left(\frac{-\nu_{12}}{E_1}\right) {}^{NP}T_1 + \left(\frac{1}{E_2}\right) {}^{NP}T_2 \\ {}^{NP}S_3 &= \left(\frac{-\nu_{13}}{E_1}\right) {}^{NP}T_1 + \left(\frac{-\nu_{23}}{E_2}\right) {}^{NP}T_2 \\ \Rightarrow \quad {}^{NP}T_1 &= \frac{E_1\left({}^{NP}S_1 + \nu_{21}\,{}^{NP}S_2\right)}{1-\nu_{21}\nu_{12}} = X_1\,{}^{NP}S_1 + X_2\,{}^{NP}S_2 \\ {}^{NP}T_2 &= \frac{E_2\left({}^{NP}S_2 + \nu_{12}\,{}^{NP}S_1\right)}{1-\nu_{21}\nu_{12}} = Y_1\,{}^{NP}S_1 + Y_2\,{}^{NP}S_2 \end{aligned}$$

where $X_1 = \dfrac{E_1}{1-\nu_{21}\nu_{12}}$, $X_2 = \dfrac{E_1\nu_{21}}{1-\nu_{21}\nu_{12}}$, $Y_1 = \dfrac{E_2\nu_{12}}{1-\nu_{21}\nu_{12}}$, $Y_2 = \dfrac{E_2}{1-\nu_{21}\nu_{12}}$,
E = Young's modulus, and ν = Poisson's ratio.

Therefore, Eq 3.13 and 3.14 become:

$$0 = \left[\sum_{j=1}^{3} {}^{PY}c_{1_j}\,{}^{PY}S_j\right] {}^{PY}A_1 + \left[X_1\,{}^{NP}S_1 + X_2\,{}^{NP}S_2\right] {}^{NP}A_1 \tag{3.15}$$

and

$$0 = \left[\sum_{j=1}^{3} {}^{PY}c_{2_j}\,{}^{PY}S_j\right] {}^{PY}A_2 + \left[Y_1\,{}^{NP}S_1 + Y_2\,{}^{NP}S_2\right] {}^{NP}A_2 \tag{3.16}$$

Relationship between the strains along each axis inside the pyroelectric (PY) material

From Eq 3.12;

$$\begin{aligned} {}^{PY}S_3 &= s_{31}T_1 + s_{32}T_2 \\ &= s_{31}\left(c_{11}\,{}^{PY}S_1 + c_{12}\,{}^{PY}S_2 + c_{13}\,{}^{PY}S_3\right) + s_{32}\left(c_{21}\,{}^{PY}S_1 + c_{22}\,{}^{PY}S_2 + c_{23}\,{}^{PY}S_3\right) \end{aligned}$$

Hence,

$$\begin{aligned} {}^{PY}S_3 &= \frac{\left(s_{31}c_{11} + s_{32}c_{21}\right){}^{PY}S_1 + \left(s_{31}c_{12} + s_{32}c_{22}\right){}^{PY}S_2}{\left[1 - \left(s_{31}c_{13} + s_{32}c_{23}\right)\right]} \\ &= {}^{PY}\Lambda_1\,{}^{PY}S_1 + {}^{PY}\Lambda_2\,{}^{PY}S_2 \end{aligned} \tag{3.17}$$

where ${}^{PY}\Lambda_1 = \dfrac{\left(s_{31}c_{11} + s_{32}c_{21}\right)}{\left[1 - \left(s_{31}c_{13} + s_{32}c_{23}\right)\right]}$ and ${}^{PY}\Lambda_2 = \dfrac{\left(s_{31}c_{12} + s_{32}c_{22}\right)}{\left[1 - \left(s_{31}c_{13} + s_{32}c_{23}\right)\right]}$.

Force balance equation and its boundary conditions

Following Figure 3.2 represents the boundary conditions for the force balance equation, which must be solved to derive the expression for our enhancement:

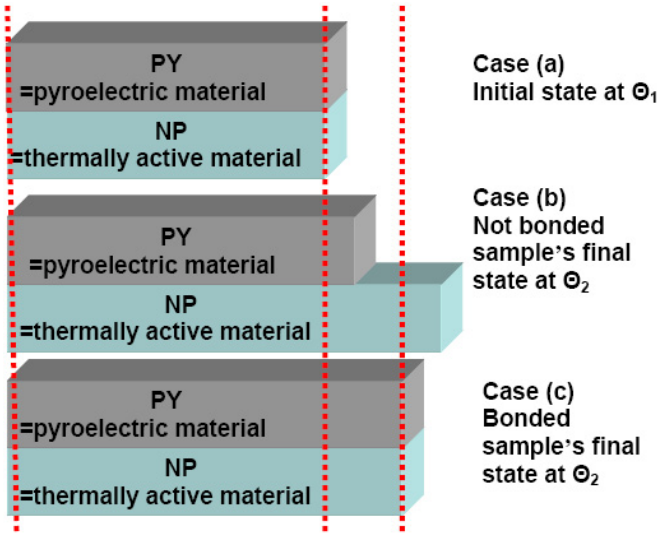

Figure 3.2: Dimensional changes for the force balance equation [42]

The dimensions for each material at each case in Figure 3.2 are (please note that NP = Thermally active material = Non-pyroelectric material):

- Case (a) ← this is the initial state of the samples

$^{PY}l_j^I,\ ^{PY}A_j^I,\ ^{NP}l_j^I,\ ^{NP}A_j^I \quad \forall j = 1..2$

- Case (b)

$^{PY'}l_j^{II},\ ^{PY'}A_j^{II},\ ^{NP'}l_j^{II},\ ^{NP'}A_j^{II} \quad \forall j = 1..2$

$$\Rightarrow {}^{PY'}l_j^{II} = {}^{PY}l_j^I(1 + {}^{PY}\alpha_j d\Theta) \quad \text{and} \quad {}^{NP'}l_j^{II} = {}^{NP}l_j^I(1 + {}^{NP}\alpha_j d\Theta) \qquad \forall j = 1..2 \quad (3.18)$$

where ^{PY} denotes PY material and ^{NP} denotes NP material

l = the length of the materials at that state

A = the cross-sectional area of the material at that state

α = thermal expansion coefficient

$d\Theta$ = change in temperature = $\Theta_2 - \Theta_1$

j denotes which axis this length is parallel to

I denotes the entity at initial temperature (Θ_1)

II denotes the entity at final temperature (Θ_2)

- Case (c) ← this is the actual final state of bonded samples

$${}^{PY}l_j^{II},\ {}^{PY}A_j^{II},\ {}^{NP}l_j^{II},\ {}^{NP}A_j^{II} \quad \forall j = 1..2$$

$$\Rightarrow \text{Min}({}^{PY'}l_j^{II}, {}^{NP'}l_j^{II}) \quad < \quad {}^{PY}l_j^{II} = {}^{NP}l_j^{II} \quad < \quad \text{Max}({}^{PY'}l_j^{II}, {}^{NP'}l_j^{II}) \qquad \forall j = 1..2 \tag{3.19}$$

Therefore, the force balance equation is required to obtain these lengths at equilibrium demonstrated by Case (c) in Figure 3.2 and Eq 3.19 (i.e. final lengths for the bonded samples). Once the force balance equation is solved, the resulting expressions will lead us to the final strain terms arising from the interaction between the two constituents, namely PY and NP. Substituting these strain expressions into Eq 3.9 and 8.6 will then yield in the expressions for the pyroelectric coefficient under SC and OC respectively, for a given symmetric laminate system. It must also be noted that the final strain values for SC and OC will differ as they will be functions of constants evaluated under different conditions, ${}^{PY}\alpha_j^{T,E}$ and ${}^{PY}\alpha_j^{T,D}$ respectively, for example (cf. Chapter 8).
(Please note that from here on, all the expressions are true for $\forall j = 1..2$ unless stated otherwise.)

In order to acquire the strain expressions for the force balance equation: (Note: ${}^{PY}S_j \& {}^{NP}S_j$ in force balance equation are when ${}^{PY}l_j^{II} \& {}^{NP}l_j^{II}$ are achieved)

At Θ_2, force balance must occur:
Initial state for force balance equation $\equiv {}^{PY'}l_j^{II},\ {}^{NP'}l_j^{II}$
← corresponds to Case (b) from Figure 3.2
Final state for force balance equation $\equiv {}^{PY}l_j^{II},\ {}^{NP}l_j^{II} = L_j^{II}$
← corresponds to Case (c) from Figure 3.2
(NB: since bonded, ${}^{PY}l_j^{I} = {}^{NP}l_j^{I} = L_j^{I}$ as well)

$\Rightarrow$ From Eq 3.18: ${}^{PY'}l_j^{II} = L_j^I(1 + {}^{PY}\alpha_j d\Theta)$ and ${}^{NP'}l_j^{II} = L_j^I(1 + {}^{NP}\alpha_j d\Theta)$

$\Rightarrow$ Strains at final state are:

$$\begin{aligned} {}^{PY}S_j &= \frac{L_j^{II} - L_j^I(1 + {}^{PY}\alpha_j d\Theta)}{L_j^I(1 + {}^{PY}\alpha_j d\Theta)} = \frac{L_j^{II}}{L_j^I(1 + {}^{PY}\alpha_j d\Theta)} - 1 \\ {}^{NP}S_j &= \frac{L_j^{II} - L_j^I(1 + {}^{NP}\alpha_j d\Theta)}{L_j^I(1 + {}^{NP}\alpha_j d\Theta)} = \frac{L_j^{II}}{L_j^I(1 + {}^{NP}\alpha_j d\Theta)} - 1 \end{aligned} \tag{3.20}$$

Solution to the force balance equation

Before we can solve this force balance equation, we require another relationship between ${}^{PY}S_j$ and ${}^{NP}S_j$.

Solving Eq 3.20 for L_j^{II} (since L_j^{II} is the only unknown term in the pair of equations, it needs to be eliminated in order to find the relationship):
$L_j^{II} = \left({}^{PY}S_j + 1\right) L_j^I \left(1 + {}^{PY}\alpha_j d\Theta\right) = \left({}^{NP}S_j + 1\right) L_j^I \left(1 + {}^{NP}\alpha_j d\Theta\right)$

$$
\begin{aligned}
{}^{PY}S_j &= \frac{\left({}^{NP}S_j + 1\right)\left(1 + {}^{NP}\alpha_j d\Theta\right)}{1 + {}^{PY}\alpha_j d\Theta} - 1 = \frac{{}^{NP}S_j\left(1 + {}^{NP}\alpha_j d\Theta\right) + \left({}^{NP}\alpha_j - {}^{PY}\alpha_j\right) d\Theta}{1 + {}^{PY}\alpha_j d\Theta} \\
{}^{NP}S_j &= \frac{\left({}^{PY}S_j + 1\right)\left(1 + {}^{PY}\alpha_j d\Theta\right)}{1 + {}^{NP}\alpha_j d\Theta} - 1 = \frac{{}^{PY}S_j\left(1 + {}^{PY}\alpha_j d\Theta\right) + \left({}^{PY}\alpha_j - {}^{NP}\alpha_j\right) d\Theta}{1 + {}^{NP}\alpha_j d\Theta}
\end{aligned}
\tag{3.21}
$$

Now, looking back at the force balance equation (cf. Eq 3.15, 3.16, and 3.17) and substituting Eq 3.21 in:

$\Rightarrow$

$$
\begin{aligned}
0 &= \left[c_{11}{}^{PY}S_1 + c_{12}{}^{PY}S_2 + c_{13}{}^{PY}S_3\right]{}^{PY}A_1 + \left[X_1{}^{NP}S_1 + X_2{}^{NP}S_2\right]{}^{NP}A_1 \\
&= {}^{PY}A_1\left[c_{11}{}^{PY}S_1 + c_{12}{}^{PY}S_2 + c_{13}\left\{{}^{PY}\Lambda_1{}^{PY}S_1 + {}^{PY}\Lambda_2{}^{PY}S_2\right\}\right] \\
&+ {}^{NP}A_1\left[X_1\frac{{}^{PY}S_1\left(1 + {}^{PY}\alpha_1 d\Theta\right) + \left({}^{PY}\alpha_1 - {}^{NP}\alpha_1\right) d\Theta}{1 + {}^{NP}\alpha_1 d\Theta}\right. \\
&\qquad \left. + X_2\frac{{}^{PY}S_2\left(1 + {}^{PY}\alpha_2 d\Theta\right) + \left({}^{PY}\alpha_2 - {}^{NP}\alpha_2\right) d\Theta}{1 + {}^{NP}\alpha_2 d\Theta}\right]
\end{aligned}
$$

and

$$
\begin{aligned}
0 &= \left[c_{21}{}^{PY}S_1 + c_{22}{}^{PY}S_2 + c_{23}{}^{PY}S_3\right]{}^{PY}A_2 + \left[Y_1{}^{NP}S_1 + Y_2{}^{NP}S_2\right]{}^{NP}A_2 \\
&= {}^{PY}A_2\left[c_{21}{}^{PY}S_1 + c_{22}{}^{PY}S_2 + c_{23}\left\{{}^{PY}\Lambda_1{}^{PY}S_1 + {}^{PY}\Lambda_2{}^{PY}S_2\right\}\right] \\
&+ {}^{NP}A_2\left[Y_1\frac{{}^{PY}S_1\left(1 + {}^{PY}\alpha_1 d\Theta\right) + \left({}^{PY}\alpha_1 - {}^{NP}\alpha_1\right) d\Theta}{1 + {}^{NP}\alpha_1 d\Theta}\right. \\
&\qquad \left. + Y_2\frac{{}^{PY}S_2\left(1 + {}^{PY}\alpha_2 d\Theta\right) + \left({}^{PY}\alpha_2 - {}^{NP}\alpha_2\right) d\Theta}{1 + {}^{NP}\alpha_2 d\Theta}\right]
\end{aligned}
$$

Simplifying this simultaneous linear equation:

$$\begin{aligned}
0 &= \left\{ {}^{PY}A_1 \left(c_{11} + c_{13}\, {}^{PY}\Lambda_1 \right) + {}^{NP}A_1 X_1 \Gamma_{11} \right\} {}^{PY}S_1 \\
&\quad + \left\{ {}^{PY}A_1 \left(c_{12} + c_{13}\, {}^{PY}\Lambda_2 \right) + {}^{NP}A_1 X_2 \Gamma_{12} \right\} {}^{PY}S_2 + {}^{NP}A_1 \left\{ X_1\Gamma_{21} + X_2\Gamma_{22} \right\} \\
&= \Omega_{11}\, {}^{PY}S_1 + \Omega_{12}\, {}^{PY}S_2 + {}^{NP}A_1 \left\{ X_1\Gamma_{21} + X_2\Gamma_{22} \right\} \\
&\text{and} \\
0 &= \left\{ {}^{PY}A_2 \left(c_{21} + c_{23}\, {}^{PY}\Lambda_1 \right) + {}^{NP}A_2 Y_1 \Gamma_{11} \right\} {}^{PY}S_1 \\
&\quad + \left\{ {}^{PY}A_2 \left(c_{22} + c_{23}\, {}^{PY}\Lambda_2 \right) + {}^{NP}A_2 Y_2 \Gamma_{12} \right\} {}^{PY}S_2 + {}^{NP}A_2 \left\{ Y_1\Gamma_{21} + Y_2\Gamma_{22} \right\} \\
&= \Omega_{21}\, {}^{PY}S_1 + \Omega_{22}\, {}^{PY}S_2 + {}^{NP}A_2 \left\{ Y_1\Gamma_{21} + Y_2\Gamma_{22} \right\}
\end{aligned} \tag{3.22}$$

where $\Gamma_{11} = \dfrac{1 + {}^{PY}\alpha_1 d\Theta}{1 + {}^{NP}\alpha_1 d\Theta}$, $\Gamma_{12} = \dfrac{1 + {}^{PY}\alpha_2 d\Theta}{1 + {}^{NP}\alpha_2 d\Theta}$, $\Gamma_{21} = \dfrac{\left({}^{PY}\alpha_1 - {}^{NP}\alpha_1 \right) d\Theta}{1 + {}^{NP}\alpha_1 d\Theta}$, and $\Gamma_{22} = \dfrac{\left({}^{PY}\alpha_2 - {}^{NP}\alpha_2 \right) d\Theta}{1 + {}^{NP}\alpha_2 d\Theta}$.

At this stage, it must be noted that ${}^{PY}A_j$ and ${}^{NP}A_j$ ($\forall j = 1..3$) can also be expressed in terms of ${}^{PY}S_j$ ($j = 1..3$). However, this will destroy the linearity of this force balance equation and potentially introduce unnecessary solutions. Being area, the change in ${}^{PY}A_j$ and ${}^{NP}A_j$ with $d\Theta$ is very small since the change in ${}^{PY}l_j$ and ${}^{NP}l_j$ are much less than 1. Therefore, it is sufficient to assume that the areas remain constant even after the linear thermal expansions in all three directions. So, ${}^{PY}A_1 = L_2\, {}^{PY}t$, ${}^{PY}A_2 = L_1\, {}^{PY}t$, ${}^{NP}A_1 = L_2\, {}^{NP}t$ and ${}^{NP}A_2 = L_1\, {}^{NP}t$ when ${}^{PY}l_j^I = {}^{NP}l_j^I = L_j \forall j = 1..2$, ${}^{PY}l_3^I = {}^{PY}t$ and ${}^{NP}l_3^I = {}^{NP}t$.

Solving the force balance equation, i.e. Eq 3.22, in terms of ${}^{PY}S_1$ and ${}^{PY}S_2$, we obtain the following expressions for both strains and ${}^{PY}S_3$ (cf. Eq 3.17):

$$\begin{aligned}
&\therefore \quad \text{The strains are} \\
{}^{PY}S_1 &= \frac{{}^{NP}A_1\Omega_{22}\left\{ X_1\Gamma_{21} + X_2\Gamma_{22} \right\} - {}^{NP}A_2\Omega_{12}\left\{ Y_1\Gamma_{21} + Y_2\Gamma_{22} \right\}}{\Omega_{12}\Omega_{21} - \Omega_{22}\Omega_{11}} \\
{}^{PY}S_2 &= \frac{{}^{NP}A_2\Omega_{11}\left\{ Y_1\Gamma_{21} + Y_2\Gamma_{22} \right\} - {}^{NP}A_1\Omega_{21}\left\{ X_1\Gamma_{21} + X_2\Gamma_{22} \right\}}{\Omega_{12}\Omega_{21} - \Omega_{22}\Omega_{11}} \\
{}^{PY}S_3 &= {}^{PY}\Lambda_1\, {}^{PY}S_1 + {}^{PY}\Lambda_2\, {}^{PY}S_2 \\
&= \frac{{}^{NP}A_1\{X_1\Gamma_{21}+X_2\Gamma_{22}\}\left({}^{PY}\Lambda_1\Omega_{22} - {}^{PY}\Lambda_2\Omega_{21} \right) + {}^{NP}A_2\{Y_1\Gamma_{21}+Y_2\Gamma_{22}\}\left({}^{PY}\Lambda_2\Omega_{11} - {}^{PY}\Lambda_1\Omega_{12} \right)}{\Omega_{12}\Omega_{21} - \Omega_{22}\Omega_{11}}
\end{aligned} \tag{3.23}$$

$$
\begin{aligned}
\text{where } X_1 &= \frac{E_1}{1-\nu_{21}\nu_{12}}, \quad X_2 = \frac{E_1\nu_{21}}{1-\nu_{21}\nu_{12}}, \quad Y_1 = \frac{E_2\nu_{12}}{1-\nu_{21}\nu_{12}}, \quad Y_2 = \frac{E_2}{1-\nu_{21}\nu_{12}}, \\
{}^{PY}\Lambda_1 &= \frac{s_{31}c_{11}+s_{32}c_{21}}{1-(s_{31}c_{13}+s_{32}c_{23})}, \quad {}^{PY}\Lambda_2 = \frac{s_{31}c_{12}+s_{32}c_{22}}{1-(s_{31}c_{13}+s_{32}c_{23})}, \\
\Gamma_{11} &= \frac{1+{}^{PY}\alpha_1 d\Theta}{1+{}^{NP}\alpha_1 d\Theta}, \quad \Gamma_{12} = \frac{1+{}^{PY}\alpha_2 d\Theta}{1+{}^{NP}\alpha_2 d\Theta}, \\
\Gamma_{21} &= \frac{\left({}^{PY}\alpha_1 - {}^{NP}\alpha_1\right) d\Theta}{1+{}^{NP}\alpha_1 d\Theta}, \quad \Gamma_{22} = \frac{\left({}^{PY}\alpha_2 - {}^{NP}\alpha_2\right) d\Theta}{1+{}^{NP}\alpha_2 d\Theta}, \\
\Omega_{11} &= {}^{PY}A_1\left(c_{11}+c_{13}{}^{PY}\Lambda_1\right) + {}^{NP}A_1 X_1 \Gamma_{11}, \\
\Omega_{12} &= {}^{PY}A_1\left(c_{12}+c_{13}{}^{PY}\Lambda_2\right) + {}^{NP}A_1 X_2 \Gamma_{12}, \\
\Omega_{21} &= {}^{PY}A_2\left(c_{21}+c_{23}{}^{PY}\Lambda_1\right) + {}^{NP}A_2 Y_1 \Gamma_{11}, \qquad \text{and} \\
\Omega_{22} &= {}^{PY}A_2\left(c_{22}+c_{23}{}^{PY}\Lambda_2\right) + {}^{NP}A_2 Y_2 \Gamma_{12},
\end{aligned}
$$

Correction for the strain expressions before they can be applied to the pyroelectric coefficients and their final form

Although we now have the solution for the force balance equation (cf. Eq 3.23), we must remember that the strain expressions in the force balance equation have different lengths at their initial state when compare to the strain expression in the pyroelectric coefficient (please compare the initial state in the derivation for Eq 3.20 with that in Figure 3.2). Therefore we must compensate for this by:

dS_j (strain in pyroelectric coefficient) is the strain with the initial state at ${}^{PY}l_j^I = {}^{NP}l_j^I = L_j^I$. However, ${}^{PY}S_j$ in the force balance equation is the strain with the initial state at ${}^{PY'}l_j^{II} = L_j^I\left(1+{}^{PY}\alpha_j d\Theta\right) \neq {}^{NP'}l_j^{II} = L_j^I\left(1+{}^{NP}\alpha_j d\Theta\right)$.

$$
\Rightarrow \qquad dS_j = \frac{L_j^{II}-L_j^I}{L_j^I} \quad \text{and} \quad {}^{PY}S_j = \frac{L_j^{II}-L_j^I\left(1+{}^{PY}\alpha_j d\Theta\right)}{L_j^I\left(1+{}^{PY}\alpha_j d\Theta\right)}
$$

$\Rightarrow$ after equating for L_j^{II} we get:

$$
\begin{aligned}
\therefore \qquad dS_j &= \frac{\left({}^{PY}S_j+1\right)\left\{L_j^I\left(1+{}^{PY}\alpha_j d\Theta\right)\right\} - L_j^I}{L_j^I} \\
&= \left({}^{PY}S_j+1\right)\left(1+{}^{PY}\alpha_j d\Theta\right) - 1 \qquad\qquad \forall j = 1..3
\end{aligned}
\tag{3.24}
$$

This expression along with Eq 3.23 can be used for both SC and OC cases and their pyroelectric coefficients. As stated before, the only difference between the two cases would

be the use of the elastic compliance, elastic stiffness, and thermal expansion coefficients all evaluated under different electric boundary conditions (cf. Subsection 3.2.1 for SC and Section 8.1 for OC). For instance, $s_{ij}^{E,\Theta}$ or $c_{ij}^{E,\Theta}$ or ${}^{PY}\alpha_j^{T,E}$ for SC and $s_{ij}^{D,\Theta}$ or $c_{ij}^{D,\Theta}$ or ${}^{PY}\alpha_j^{T,D}$ for OC.

Universal evaluation procedure for a pyroelectric coefficient

The procedure is as follows:

1. By substituting appropriate material data into Eq 3.23, evaluate the solution to the force balance equation while paying due attention to the conditions the material data has been evaluated under, i.e. making sure that $s_{ij}^{E,\Theta}$ or $c_{ij}^{E,\Theta}$ or ${}^{PY}\alpha_j^{T,E}$ are used for SC and $s_{ij}^{D,\Theta}$ or $c_{ij}^{D,\Theta}$ or ${}^{PY}\alpha_j^{T,D}$ are used for OC.

2. Use Eq 3.24 and the calculated values from Step 1 to evaluate the final strain values, dS_j for j=1..3.

3. Evaluate the pyroelectric coefficient by substituting the final strain values calculated from Step 2 into Eq 3.9 and Eq 8.6 for SC and OC, respectively.

3.3 Finite Element Analysis

3.3.1 FEA analysis of a sandwich structure with thermal expansion mismatch

Prior to giving our due attention to the final theoretical model of the enhancement phenomena (cf. Section 3.4), the author would first like to consider certain behaviours of our 2-2 connectivity laminate composites our analytical model (cf. Eq 3.24 in Section 3.2) can not portray. These include the existence of shear stresses and curvature profile of the sides of the laminate structure arising from these shear stresses and the existence of the bonding/epoxy layer (cf. Figure 3.3). Suggested improvements to address these issues analytically are presented in Subsection 16.1.1. However, for the scope of this PhD, it was deemed that our model was ample enough to describe the enhancement and experimental data, provided a minor addition (cf. k-factors) to the expression of the expected strain in the PY material has been made, which will be dealt with in more detail in Section 3.4.

With above stated issues in mind, subsequent to developing the mathematical model for the phenomena, we have also attempted to model the enhancement using Mathematics package Maple 9.5 (cf. Appendix D.2) and Finite Element Analysis package ANSYS® 11 (cf. Appendix D.1). The results of the modelling with Maple are presented throughout this dissertation. Rather regrettably however, the attempts at modelling the behaviour with ANSYS® has not yielded with a full model. The software just does not seem to provide the facility necessary for modelling the full pyroelectric effect (cf. Subsection 16.1.2). Its capability for modelling thermal, structural, and piezoelectric effects have, however, resulted in the following figure illustrating the curvature profile of the laminate structure in Figure 3.3(a) and the effect of the bonding/epoxy layer in Figure 3.3(b) (for further details on our FEA model, please refer to Appendix D.1):

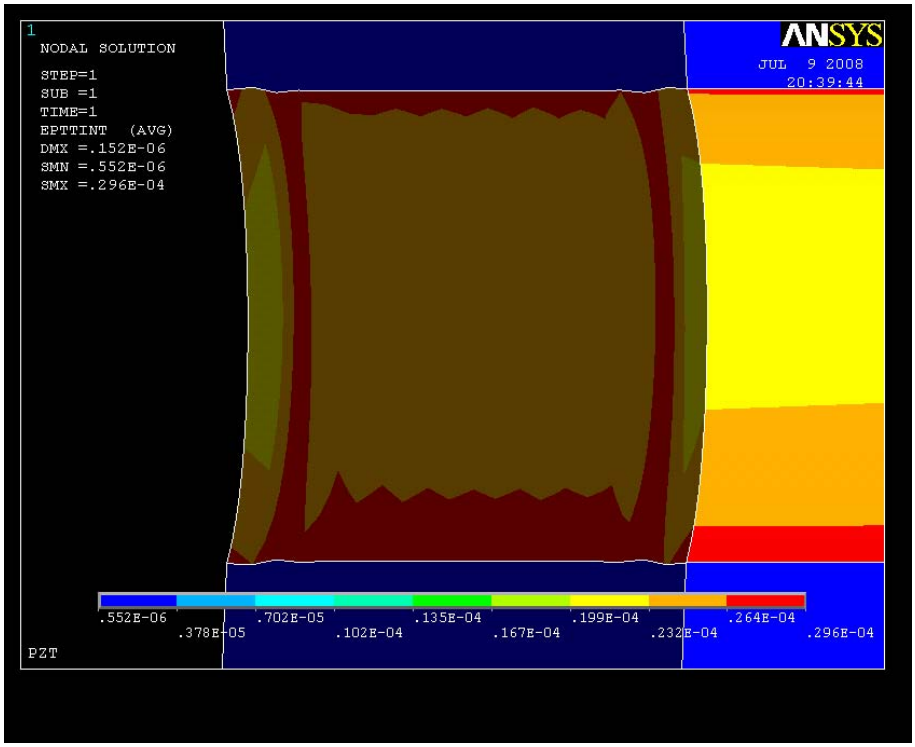

(a) Three layer St/PZT-5H/St structure

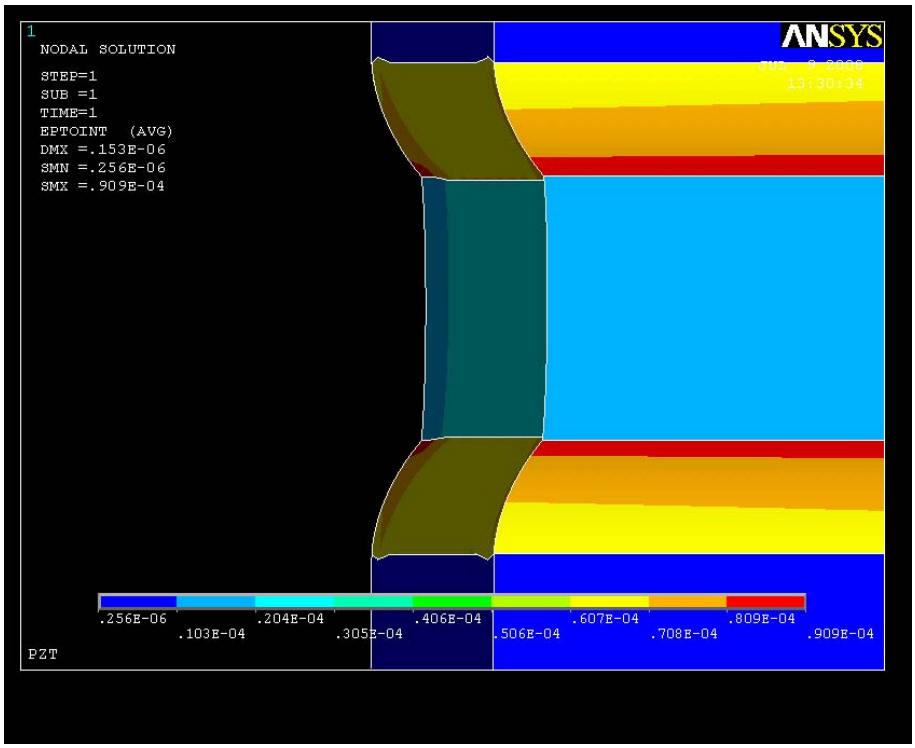

(b) 2-2 connectivity laminate with epoxy layers in between

Figure 3.3: FEA models after temperature variation has been applied

Figure 3.3(a) represents our Stainless steel (St)/PZT/St case (cf. Figure 3.1 (a)), evidently portraying the expected curvature across PY material with the largest of the strains being experienced in the PZT-5H layer, illustrated by its red and yellow colour. Meanwhile, Figure 3.3(b) portrays a more realistic description where the existence of the bonding (epoxy) layer is incorporated into the model with the largest strain being experienced by the softest material, namely epoxy layer.

The epoxy layer, represented in yellow and red due to their large strains, behaves like an elastic layer between PY and NP layers absorbing some of the strain that is being transferred through. This implies that the model proposed in Section 3.2 was not sufficient enough to depict the enhancement phenomenon with ample accuracy. Hence a measure called k-factor was introduced to the theory, consequences of which will be presented in the later sections of this dissertation.

Following Figure 3.4 demonstrates some of the Finite Element Analysis results we get from our FEA model with the configuration of St/Epoxy/PZT/Epoxy/St (same as that displayed in Figure 3.3(b)), with dimensions (length $\times$ width $\times$ thickness) :

- St : $2cm \times 1cm \times 250\mu m$ each
- Epoxy : $2cm \times 1cm \times {}^{EP}t\mu m$ each, where ${}^{EP}t$ is varied to investigate the effect of the epoxy layer thickness on the overall enhancement
- PZT : $2cm \times 1cm \times 127\mu m$
- Hence the thickness ratio ($R = \frac{{}^{PY}t}{{}^{NP}t}$) is $\frac{127}{500} = 0.254$.

(Please note that these dimensions were chosen as they represent the best case scenario of our approximation to our enhancement experimentation samples used in Chapter 5.)

Note that NDiv is the number of divisions for each edge for creating the elements and it is clear from Figure 3.4 that the FEA model converges to a solution when NDiv $\geqslant$ 12. Although higher values of NDiv were used in the preliminary FEA modelling, as the solution seems to converge this dissertation will mainly present the results from NDiv = 20. In addition, the strain and PY coef enhancement values expected from our analytical model, presented as dotted lines, are constant as our analytical model does not take the epoxy layer into account. Despite this short-coming, our analytical model's Total PY coef and PY coef enhancement values were found to be only around 3.1 and 5.3 % different from the FEA model (with ${}^{EP}t = 40\mu m$)'s as illustrated in Table 3.1.

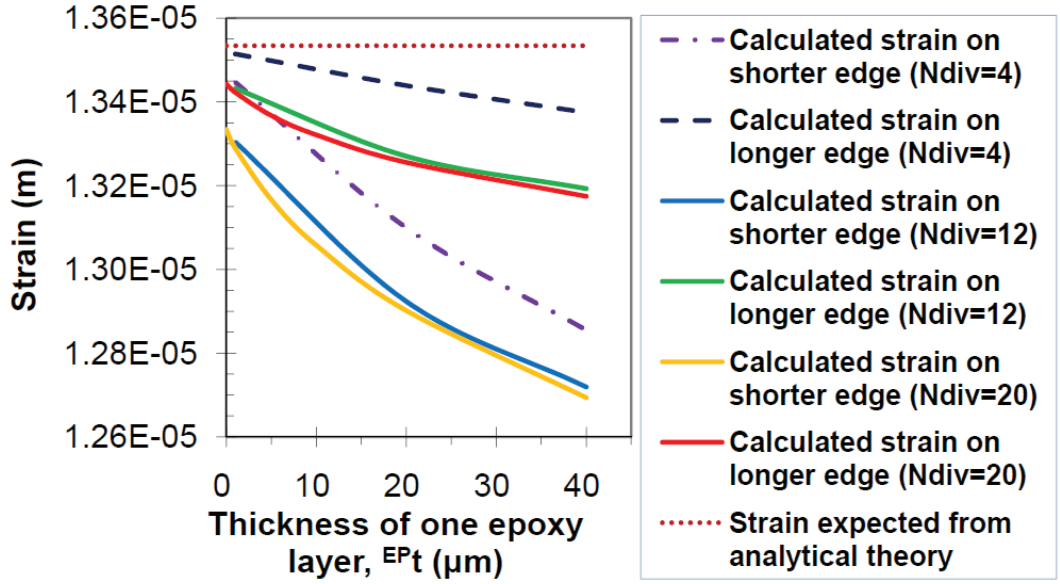

(a) Strain vs thickness of one epoxy layer

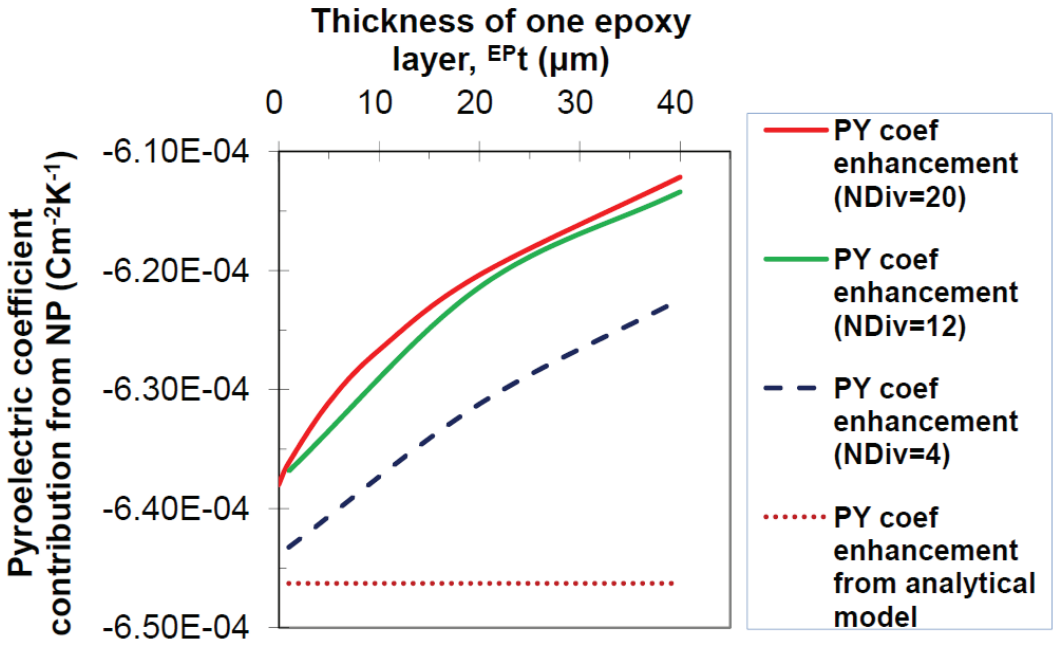

(b) PY coef enhancement vs thickness of one epoxy layer

Figure 3.4: Strain variations with varying epoxy layer thickness

It is evident from Figure 3.4(a) that the amount of strain PY experiences does depend on the thickness of the epoxy layer, as expected. Meanwhile, the strain experienced by the nodes on the longer edge (represented as ${}^{PY}S_1$ in our analytical model) and the shorter edge (represented as ${}^{PY}S_2$ in our analytical model) of the FEA model seem to be influenced by dissimilar amounts. This may well be due to the curvature

Table 3.1: FEA results using 20 divisions vs Analytical model

	FEA (${}^{EP}t = 0$)	FEA (${}^{EP}t = 40$)	Analytical model
${}^{PY}S_1$	13.443	13.174	13.534
${}^{PY}S_2$	13.333	12.694	13.534
${}^{PY}S_3$	-13.299	-12.586	-13.528
PY coef enhancement	-6.380	-6.122	-6.463
Total PY coef	-10.907	-10.649	-10.990

Units: - ${}^{PY}S_i$: $\times 10^{-6}$ - PY coef : $\times 10^{-4}$ $Cm^{-2}K^{-1}$

observed in Figure 3.3, owing to the 'tilting' (cf. work by Tsai[179]), and the interaction between various shear strains. ANSYS® predicts that while the epoxy layer's thickness increases from 0 to 40μm, ${}^{PY}S_1$ decreases from 13.443μm to 13.174μm and ${}^{PY}S_2$ from 13.333μm to 12.694μm, i.e. around 2.0 % and 4.8 % decrease respectively (cf. Table 3.1). Table 3.1 and Figure 3.4(b) also predicts that ${}^{PY}S_3$, PY coef enhancement, and total PY coef drop by 5.4, 4.0, and 2.4 % respectively, ab interim.

3.4 Analytical model

3.4.1 Pyroelectric coefficient for our samples used in the experimentation

As we have appraised certain issues concerning our analytical model through FEA (cf. Section 3.3), we can now move on to evaluating the pyroelectric coefficient under SC so that we can verify the enhancement in PY coef through analytical modelling supported by an experiment. Hence, to exemplify the use of the earlier stated expressions for the PY coef of a 2-2 connectivity laminate configuration (cf. Eq 3.9 and 3.24), we shall calculate the PY coef of our samples to be used in the experiments (cf. Chapter 5), which are laminate structures that consist of a PZT-5H (PY) sandwiched between two stainless steel laminates (NP) of equal thickness. To start with, material data required for the calculations are acquired from the relevant manufacturers[3,4,9]. (Please refer to Appendix A for material properties of PZT-5H and St)

From Appendix A, it is apparent that the possibility exists for further simplification of the PY coef expressions in Eq 3.9 and 3.24 by considering the symmetry of the PY materials. This should make the evaluation process of a PY coef as succinct as possible.

Pyroelectric coefficients under SC for PZT

From Eq 3.9 and with PZT's symmetry (cf. Appendix A.1) in mind[78,103,133,192]:

For PZT under SC, from Eq 3.9:

$$\begin{aligned} p_3^{SC} &= p_3^{T,E} - \sum_{i,j} \left[d_{3i}^{E,\Theta} c_{ij}^{E,\Theta} \left\{ \alpha_j^{T,E} - \frac{dS_j}{d\Theta} \right\} \right] \qquad \text{for } i,j = 1..6 \\ &= p_3^{T,E} - d_{31}^{E,\Theta} \sum_{j=1}^{3} \left[(c_{1j}^{E,\Theta} + c_{2j}^{E,\Theta}) \left\{ \alpha_j^{T,E} - \frac{dS_j}{d\Theta} \right\} \right] - d_{33}^{E,\Theta} \sum_{j=1}^{3} \left[c_{3j}^{E,\Theta} \left\{ \alpha_j^{T,E} - \frac{dS_j}{d\Theta} \right\} \right] \end{aligned} \tag{3.25}$$

Note that this is the same for all PY materials considered except PVDF owing to their symmetries in the elastic constants (cf. Appendix A.1). The effects of the piezoelectric coefficients such as d_{15} disappear, which draws parallel to Bogdanov's work[31] on piezoelectric effect in pyroelectric crystals, where d_{14} and d_{25}'s non-existence were investigated.

The expression for the strains experienced by PZT under both SC and OC

As we have applied the symmetry of our PY material to simplify the PY coef expression, we can also carry out the same procedure on the force balance equation solution, Eq 3.23, which will eventually give us the strain experienced by PY material. This will make the strain expression in Eq 3.23 more intelligible through the consideration of the symmetry of PZT, leading to a more comprehensible PY coef expression for our 2-2 connectivity laminate composites[78,103,133,192].

From PZT's symmetry (cf. Appendix A.1) we know that all non-zero elastic constants of a PZT are:

$c_{11} = c_{22}$	$s_{11} = s_{22}$
$c_{12} = c_{21}$	$s_{12} = s_{21}$
$c_{13} = c_{23} = c_{31} = c_{32}$	$s_{13} = s_{23} = s_{31} = s_{32}$
c_{33}	s_{33}
$c_{44} = c_{55}$	$s_{44} = s_{55}$
c_{66}	s_{66}

In addition, partially due to the limited availability of the material data information and with the aim of simplifying our mathematical model, following reasonable assumptions can also be made (only PVDF among 6 PY materials considered does not satisfy these assumptions, for whom the full solution to the force balance equation was used):

For both PY and NP material: ${}^{PY}\alpha = {}^{PY}\alpha_j \quad \forall j = 1..2 \quad \& \quad {}^{NP}\alpha = {}^{NP}\alpha_j \quad \forall j = 1..3 \quad \text{and} \quad Y = E_1 = E_2 \quad \& \quad \nu = \nu_{12} = \nu_{21}$

Substituting earlier stated relations into the expressions in Eq 3.23:

$$
\begin{aligned}
&\Rightarrow X_1 = Y_2 = \frac{Y}{1-\nu^2}, \quad X_2 = Y_1 = \frac{Y\nu}{1-\nu^2}, \quad {}^{PY}\Lambda_1 = {}^{PY}\Lambda_2 = \frac{s_{13}\left(c_{11}+c_{12}\right)}{1-2s_{13}c_{13}} = \Lambda, \\
&\Gamma_{11} = \Gamma_{12} = \frac{1+{}^{PY}\alpha d\Theta}{1+{}^{NP}\alpha d\Theta}, \quad \Gamma_{21} = \Gamma_{22} = \frac{\left({}^{PY}\alpha - {}^{NP}\alpha\right) d\Theta}{1+{}^{NP}\alpha d\Theta}, \\
&\Omega_{11} = {}^{PY}A_1\left(c_{11}+c_{13}\Lambda\right) + {}^{NP}A_1 X_1 \Gamma_{11}, \quad \Omega_{12} = {}^{PY}A_1\left(c_{12}+c_{13}\Lambda\right) + {}^{NP}A_1 X_2 \Gamma_{11}, \\
&\Omega_{21} = {}^{PY}A_2\left(c_{12}+c_{13}\Lambda\right) + {}^{NP}A_2 X_2 \Gamma_{11}, \quad \text{and} \quad \Omega_{22} = {}^{PY}A_2\left(c_{11}+c_{13}\Lambda\right) + {}^{NP}A_2 X_1 \Gamma_{11}
\end{aligned}
\tag{3.26}
$$

Now, substituting these relations, namely Eq 3.26, into Eq 3.23 along with ${}^{PY}A_1 = L_2{}^{PY}t$, ${}^{PY}A_2 = L_1{}^{PY}t$, ${}^{NP}A_1 = L_2{}^{NP}t$ and ${}^{NP}A_2 = L_1{}^{NP}t$, and simplifying the whole expression we attain the following:

$$
\begin{aligned}
{}^{PY}S_1 = {}^{PY}S_2 &= \frac{\left({}^{NP}\alpha - {}^{PY}\alpha\right) d\Theta}{\frac{(1-\nu)}{Y}\left(\frac{c_{11}+c_{12}}{1-2s_{13}c_{13}}\right)\left(1+{}^{NP}\alpha d\Theta\right) R + \left(1+{}^{PY}\alpha d\Theta\right)} \\
\text{and} \quad {}^{PY}S_3 &= {}^{PY}\Lambda_1{}^{PY}S_1 + {}^{PY}\Lambda_2{}^{PY}S_2 = 2\Lambda{}^{PY}S_1 \\
&= \left(\frac{2s_{13}\left(c_{11}+c_{12}\right)}{1-2s_{13}c_{13}}\right)\frac{\left({}^{NP}\alpha - {}^{PY}\alpha\right) d\Theta}{\frac{(1-\nu)}{Y}\left(\frac{c_{11}+c_{12}}{1-2s_{13}c_{13}}\right)\left(1+{}^{NP}\alpha d\Theta\right) R + \left(1+{}^{PY}\alpha d\Theta\right)} \\
&= \frac{2s_{13}\left({}^{NP}\alpha - {}^{PY}\alpha\right) d\Theta}{\frac{(1-\nu)}{Y}\left(1+{}^{NP}\alpha d\Theta\right) R + \left(\frac{1-2s_{13}c_{13}}{c_{11}+c_{12}}\right)\left(1+{}^{PY}\alpha d\Theta\right)} \\
\text{where } R = \frac{{}^{PY}t}{{}^{NP}t} &\qquad \text{(Note the solution fails at } R = 0 \text{ and hence minimum } R \\
\text{considered in this dissertation is } R_{min} &= 0.005)
\end{aligned}
\tag{3.27}
$$

In order to obtain the strain expression to be substituted into the pyroelectric coefficient expression in Eq 3.25 and 8.12, substitute Eq 3.27 into Eq 3.24:

$$
\begin{aligned}
d\left({}^{PY}S_1\right) &= d\left({}^{PY}S_2\right) \\
&= \left({}^{PY}S_1 + 1\right)\left(1+{}^{PY}\alpha d\Theta\right) - 1 = {}^{PY}S_1\left(1+{}^{PY}\alpha d\Theta\right) + {}^{PY}\alpha d\Theta \\
&= \frac{\left({}^{NP}\alpha - {}^{PY}\alpha\right) d\Theta\left(1+{}^{PY}\alpha d\Theta\right)}{\frac{(1-\nu)}{Y}\left(\frac{c_{11}+c_{12}}{1-2s_{13}c_{13}}\right)\left(1+{}^{NP}\alpha d\Theta\right) R + \left(1+{}^{PY}\alpha d\Theta\right)} + {}^{PY}\alpha d\Theta \\
&= \frac{Y\left(1-2s_{13}c_{13}\right)\left(1+{}^{PY}\alpha d\Theta\right)\left({}^{NP}\alpha - {}^{PY}\alpha\right) d\Theta}{(1-\nu)\left(c_{11}+c_{12}\right)\left(1+{}^{NP}\alpha d\Theta\right) R + Y\left(1-2s_{13}c_{13}\right)\left(1+{}^{PY}\alpha d\Theta\right)} + {}^{PY}\alpha d\Theta
\end{aligned}
$$

and

$$
\begin{aligned}
d\left({}^{PY}S_3\right) &= {}^{PY}S_3\left(1+{}^{PY}\alpha_3 d\Theta\right) + {}^{PY}\alpha_3 d\Theta \\
&= \frac{2s_{13}\left({}^{NP}\alpha - {}^{PY}\alpha\right) d\Theta\left(1+{}^{PY}\alpha_3 d\Theta\right)}{\frac{(1-\nu)}{Y}\left(1+{}^{NP}\alpha d\Theta\right) R + \left(\frac{1-2s_{13}c_{13}}{c_{11}+c_{12}}\right)\left(1+{}^{PY}\alpha d\Theta\right)} + {}^{PY}\alpha_3 d\Theta \\
&= \frac{2Ys_{13}\left(c_{11}+c_{12}\right)\left(1+{}^{PY}\alpha_3 d\Theta\right)\left({}^{NP}\alpha - {}^{PY}\alpha\right) d\Theta}{(1-\nu)\left(c_{11}+c_{12}\right)\left(1+{}^{NP}\alpha d\Theta\right) R + Y\left(1-2s_{13}c_{13}\right)\left(1+{}^{PY}\alpha d\Theta\right)} + {}^{PY}\alpha_3 d\Theta
\end{aligned}
\tag{3.28}
$$

Evaluation procedure for a pyroelectric coefficient of our samples, where materials such as PZT is used as PY material

The procedure is as follows:

1. By substituting appropriate material data into Eq 3.28, evaluate the final strain values, dS_j for j=1..3, while paying attention to the conditions the material data has been evaluated under, i.e. making sure that $s_{ij}^{E,\Theta}$ or $c_{ij}^{E,\Theta}$ or ${}^{PY}\alpha_j^{T,E}$ are used for SC and $s_{ij}^{D,\Theta}$ or $c_{ij}^{D,\Theta}$ or ${}^{PY}\alpha_j^{T,D}$ are used for OC.

2. Evaluate the pyroelectric coefficient by substituting the final strain value calculated from Step 1 into Eq 3.25 and 8.12 for SC and OC, respectively.

Pyroelectric coefficient under SC for our samples (St/PZT-5H/St)

By employing the mathematics package Maple 9.5 (cf. Appendix D.2), the author was able to estimate the value of the pyroelectric coefficient for our samples and analyse what our theory tells us in terms of the relationship between the pyroelectric coefficient enhancement and the sample dimensions, namely the thicknesses of PZT and stainless steel (St) in particular.

Evaluating PY coef using the earlier quoted procedure (cf. Subsubsection 3.4.1) leads to the PY coef of[43];

$$p_3^{SC} = -5.0 \times 10^{-4} - \frac{6.5 \times 10^{-4}}{0.32 \times R + 1.0} \qquad Cm^{-2}K^{-1}$$
$$\text{where} \quad \text{R = thickness of PZT / thickness of stainless steel} \tag{3.29}$$

3.4.2 k-factors

Introduction of k-factor as an interface factor

The solution obtained in the previous section (cf. Eq 3.29) describes the PY coef of a 2-2 connectivity laminate composite of a pyroelectric PZT and elastic laminae configuration when the bonding between the PZT and the elastic layer (NP or St layer) is ideal. However, in practice this is never the case due to finite thickness of the bonding layer

(otherwise called epoxy layer) and other possible bonding defects (cf. Section 3.3). Hence, in order to depict the real measurements of pyroelectric coefficients more accurately, an interface factor termed 'k-factor' can be introduced. A similar idea to the k interface coupling factor utilised by Bichurin et al.[29], this should help us to portray the actual boundary conditions under which our experiments will take place (cf. Chapter 5).

We have tried employing two different kinds of k-factors, termed in the maple codes (please refer to the Maple code in Appendix D.2) as 'k_1' and 'k_2'. What each of these two k-factors stands for is illustrated in the following:

- k_1

k_1 is applied after solving the force balance equation. This means when the strain expression with k_1 is fed back into the original force balance equation the equality no longer holds, implying that the actual force exerted by the NP layer, namely stainless steel, is lost while being transmitted through the epoxy layer, i.e. ${}^{PY}F_i \neq -{}^{NP}F_i$ for i=1..2, as ${}^{Epoxy}F$ is also present and the values of ${}^{Epoxy}F_i$ (for i=1..2) at the opposite faces of the epoxy layer are no longer the same, owing to the work done by the forces to deform the epoxy layer.

- k_2

k_2 is applied before solving the force balance equation using Maple. This implies that when the strain expression with k_2 is fed back into the original force balance equation, it still holds true, entailing that no force is lost during the transmission through the epoxy layer. This means that the values of ${}^{Epoxy}F_i$ (for i=1..2) at the opposite faces of the epoxy layer are still the same, and the only loss in the strain experienced by PY layer is due to the elastic deformation of the epoxy layer only. As the stiffness of the epoxy layer is very small when compared to the other two layers (PZT-5H and stainless steel), the work done involved to achieve this deformation may be negligible, which could make this k-factor a better approximation than k_1.

The PY coef of PZT-5H with stainless steel evaluated with these two k-factors are:

$$p_3^{SC}(k\_1) = -5.0 \times 10^{-4} - \frac{6.5 \times 10^{-4}(k\_1)}{0.32 \times R + 1.0} \qquad Cm^{-2}K^{-1}$$

$$p_3^{SC}(k\_2) = -5.0 \times 10^{-4} - \frac{5.0 \times 10^{5}(k\_2)}{2.5 \times 10^{8} \times R(k\_2) + 7.7 \times 10^{8}} \qquad Cm^{-2}K^{-1}$$

where R = thickness of PZT / thickness of stainless steel

(3.30)

The suitability of which of these two k-factors needs to be employed depends largely on the stiffness of PY, NP, and epoxy layers (as an indicator for the degree of importance the epoxy layer's elastic deformation play in the overall strain loss) and whether there exists other means of strain loss due to thermal expansion coefficient mismatch. If the stiffness of epoxy layer is much smaller than that of PY and NP layers and only negligible quantity of strain is lost to other means (deformation of PY layer itself, for instance) then k_2 would make a better approximation (cf. Figure 3.5), and vice-versa for k_1.

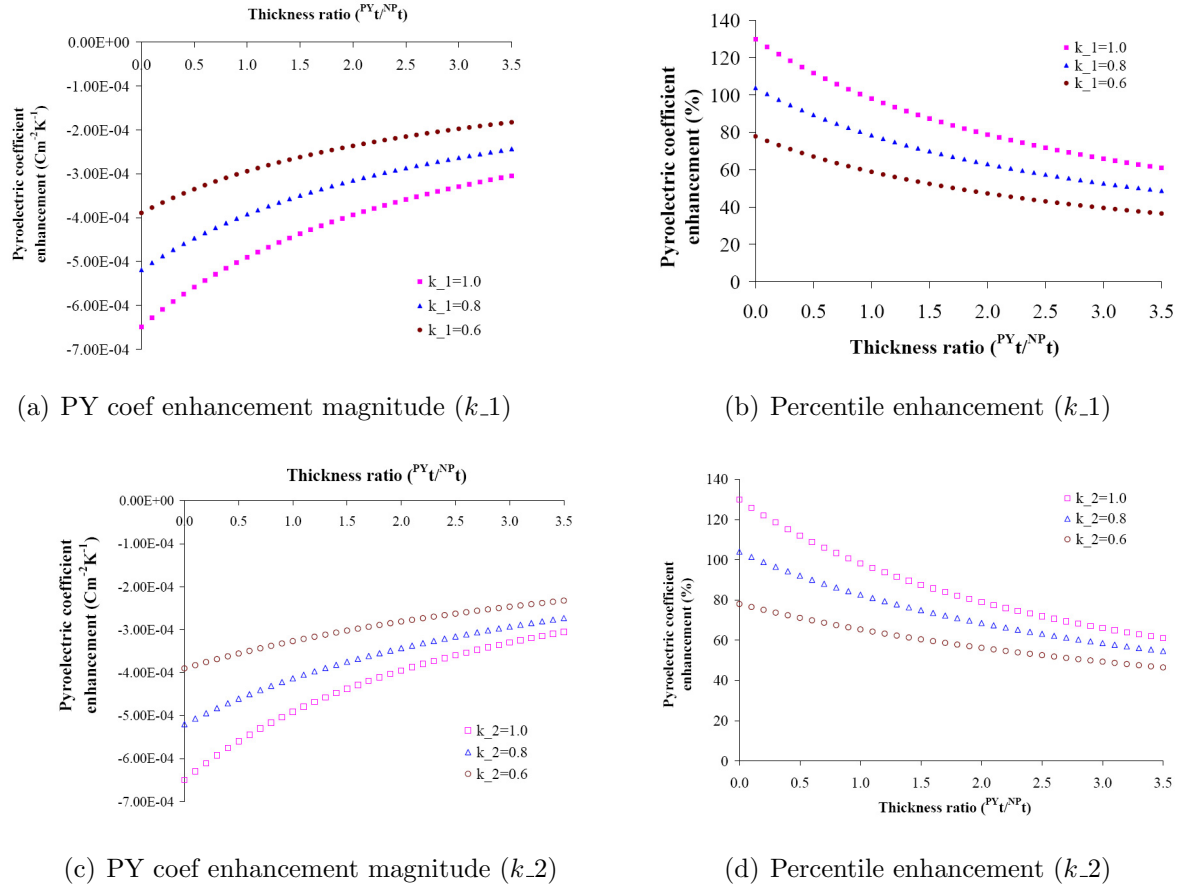

(a) PY coef enhancement magnitude (k_1)

(b) Percentile enhancement (k_1)

(c) PY coef enhancement magnitude (k_2)

(d) Percentile enhancement (k_2)

Figure 3.5: Pyroelectric coefficient enhancement in St/PZT/St laminates predicted by the k-factors

It is evident from Figure 3.6 that k_1 and k_2 depict very similar trends in the PY coef enhancement for small values of thickness ratio (R = $\frac{^{PY}t}{^{NP}t}$). However, as R increases the differences between them become exaggerated, with k_2 maintaining high levels of enhancement over larger R values. This supports the idea that k_2 factor will only describe the strain loss owing to the elastic deformation of the epoxy layer. As Figure 3.6 and our FEA results demonstrate, which is backed up by other researchers (cf. Section 3.3 and Subsection 16.1.1), the stresses involved in our samples are big enough to introduce other means of strain-loss ('tilting' and possibly large pre-stresses at high R values for

example), and that is the reason why the author has made the decision to work mainly with k_1, a simpler, more straightforward k-factor that can be employed as a more general loss factor.

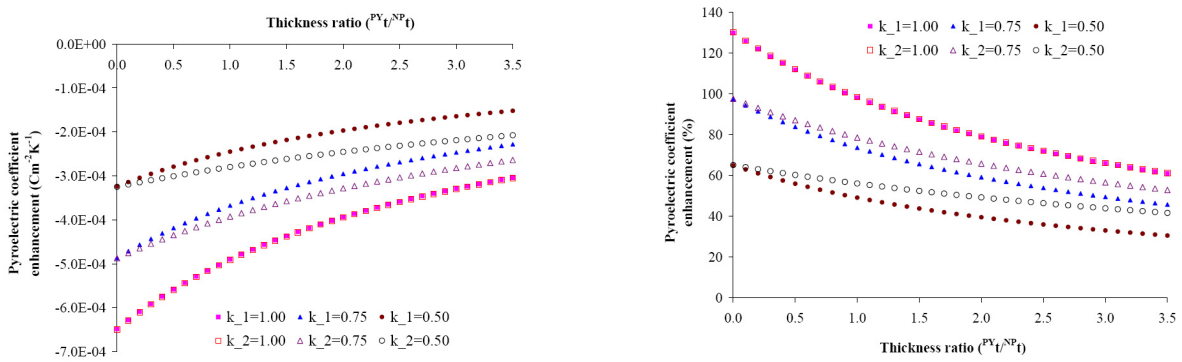

(a) PY coef enhancement magnitude

(b) Percentile enhancement

Figure 3.6: Comparison between the enhancement predictions from the two k-factors

To aid with further comprehension on what these k-factors represent analytically, following derivation processes are presented for both k-factors (please also refer to Appendix D.2 for Maple codes to this effect):

Derivation of pyroelectric coefficient with k_1

This factor, 'k_1', represents the overall loss in the strain the PY material experiences. Its range is between zero and one with former depicting no bonding between the NP and PY layers at all and the latter describing the case of perfect bonding between them. It is applied after the force balance equation has been solved. This means considering this factor as a physical measure of mechanical loss between the two layers due to the existence of bonding layer might not be entirely correct as such loss would also affect the solution to the whole force balance equation, hence leading to the need for an investigation into another factor, namely 'k_2'. However, it also implies that 'k_1' could be better suited as a measure of overall loss regardless of its cause, be it mechanical or otherwise.

To evaluate PY coef, 'k_1', is applied to Eq 3.24. This results in;

$$\begin{aligned} dS_j &= \frac{\left\{\left(k\_1 \times {}^{PY}S_j\right)+1\right\} L_j^I \left(1+{}^{PY}\alpha_j d\Theta\right) - L_j^I}{L_j^I} \\ &= \left\{\left(k\_1 \times {}^{PY}S_j\right)+1\right\}\left(1+{}^{PY}\alpha_j d\Theta\right) - 1 \qquad \forall j = 1..3 \end{aligned} \tag{3.31}$$

Following the subsequent steps after Eq 3.24 presented in the earlier part of this dissertation exactly the same after this application of 'k_1' leads to the first PY coef expression in Eq 3.30.

Derivation of pyroelectric coefficient with k_2

This factor, 'k_2', is introduced before solving the force balance equation which ensures that this factor describes the loss due to the mechanical bonding between the two layers, namely PY and NP, more accurately. Likewise to 'k_1', this factor also varies between zero and one with former describing the no bonding case and the latter the perfect bonding.

In this case, 'k_2' is applied to Eq 3.21. Basically, we introduce a new strain expression ($New\_^{PY}S_j$) such that $New\_^{PY}S_j = (\mathrm{k\_2})^{PY}S_j$, and solve the force balance equation for $New\_^{PY}S_j$ instead of ${}^{PY}S_j$. The consequences of which are;

$$
\begin{aligned}
New\_^{PY}S_j = (k\_2) \times {}^{PY}S_j \qquad &= (k\_2) \times \left[\frac{\left({}^{NP}S_j + 1\right)\left(1 + {}^{NP}\alpha_j d\Theta\right)}{1 + {}^{PY}\alpha_j d\Theta} - 1 \right] \\
&= (k\_2) \times \left[\frac{{}^{NP}S_j \left(1 + {}^{NP}\alpha_j d\Theta\right) + \left({}^{NP}\alpha_j - {}^{PY}\alpha_j\right) d\Theta}{1 + {}^{PY}\alpha_j d\Theta} \right] \\
\text{and } {}^{NP}S_j = \frac{\left({}^{PY}S_j + 1\right)\left(1 + {}^{PY}\alpha_j d\Theta\right)}{1 + {}^{NP}\alpha_j d\Theta} - 1 &= \frac{\left[\dfrac{New\_^{PY}S_j}{k\_2} + 1 \right]\left(1 + {}^{PY}\alpha_j d\Theta\right)}{1 + {}^{NP}\alpha_j d\Theta} - 1 \\
&= \frac{\left(\dfrac{New\_^{PY}S_j}{k\_2} \right)\left(1 + {}^{PY}\alpha_j d\Theta\right) + \left({}^{PY}\alpha_j - {}^{NP}\alpha_j\right) d\Theta}{1 + {}^{NP}\alpha_j d\Theta} \quad \forall j = 1..2
\end{aligned}
$$

Note $New\_^{PY}S_3 = (k\_2) \times {}^{PY}S_3$ also holds since at this stage of the derivation ${}^{PY}S_3$ is a linear function of ${}^{PY}S_1$ and ${}^{PY}S_2$.

(3.32)

Following the subsequent steps after Eq 3.21 presented in the earlier parts of this dissertation exactly the same after this application of 'k_2' while replacing all '${}^{PY}S_j$' with '$New\_^{PY}S_j$', leads to the second PY coef expression in Eq 3.30.

With these analytical models in our arsenal, we can now move on to the actual experimentation to verify our enhancement predictions from this model.

Chapter 4

Materials considered for 2-2 connectivity pairing

Six different pyroelectric materials and non-pyroelectric materials were paired and analyzed for their enhancement potentials for this dissertation and Chapter 4 gives a brief introduction to these materials. Section 4.1 will give examples of some of the other materials we have considered for our pairing, but decided against it. Sections 4.2 and 4.3 will list the pyroelectric materials we have investigated, while the latter will also demonstrate the reasons behind the deployment of 2-2 connectivity configuration for our laminate composites and provide the indicators for judging the pyroelectric coefficient enhancement credentials of various pyroelectric materials. This chapter will then finish with the list of non-pyroelectric materials we have reviewed and the reasons behind their selection.

4.1 Initial choices

In this section, the author would first like to discuss a few materials we have considered that did not make it into our final thirty-six pairs.

4.1.1 Shape Memory Alloys

In Chapter 3, we developed a mathematical model for our 2-2 connectivity laminate composites. In particular, Eq 3.9 suggests that larger the strain NP material can exert on PY (dS_{ij} or dS_j), higher the enhancement/reduction of PY coef. Hence we first searched

for a NP material that can produce large strains given a finite amount of thermal stimulus, i.e. temperature variation.

Initially, it seemed Shape Memory Alloys (SMA) fitted the bill perfectly. The phenomenal thermo-mechanical behaviour of SMA made it look like the perfect accompaniment to any PY material. However, difficulty in modelling their behaviours accurately, issues with fatigue/re-training/fabrication techniques meant that we decided to stick to a more conventional NP materials that did not require such elaborate modelling and preparation techniques. Although it may well be the case that SMA might provide us with the largest enhancement/reduction in PY coef, the uncertainty it brings in describing our enhancement phenomena was judged to be far too much of a risk. The caution urged by Hodgson[79] summarizes this difficulty the best:

> "More than any other engineering material this author has encountered, the shape memory metal's properties are so interrelated with slight compositional variations, fabrication and processing history, training history... one must take each case on its own."

SMA are metallic alloys that are able to recover their original shape (or develop large reaction forces when they have their recovery restricted) through the imposition of a temperature and/or a stress field, due to phase transformations the material undergoes. Although SMA present several thermo-mechanical behaviours, their main, and probably most useful, phenomena are pseudo-elasticity, shape memory effect, which can be one-way or two-way, and phase transformation due to the temperature variation.

Due to the large potential SMA possess, there has been numerous research being carried out to develop a suitable mathematical model for describing its thermo-mechanical behaviours. They can be modelled either from microscopic or from macroscopic points of view.

The first approach, in fact, considers either microscopic or mesoscopic phenomena. The microscopic approach treats phenomena in molecular level while mesoscopic approach is related to the level of lattice particles, and its modelling assumes negligible fluctuations of the molecular particles. These approaches have been studied by several researchers including Warlimont et al.[184], Perkins[143], Nishiyama[131], Achenbach and Mueller[16], Sun and Hwang[175], Fischer and Tanaka[56], Lu and Weng[112], Gall et al.[58], Sittner and Novˊk[167], Kloucek et al.[93], Muller and Seelecke[121], among others.

On the other hand, the macroscopic approach is much more focused on Shape Mem-

ory Alloys phenomenological features. Examples of such models are:

- Falk and Konopkas one-dimensional model based on Devonshires theory[55]

This model assumes a polynomial-free energy potential, which allows for pseudo-elasticity and one-way shape memory effect description. The great advantage of Falks model is its simplicity.

- Assumed phase transformation kinetics models

These consider pre-established simple mathematical functions to describe the phase transformation kinetics. This kind of formulation was first proposed by Tanaka and Nagaki[176], which motivated other researchers who presented modified transformation kinetics laws. Such researches include; Liang and Rogers[107], Brinson[34], Ivshin and Pence[83], Boyd and Lagoudas[33], among others. These models probably are the most popular ones in the literature.

Although the author has made an attempt at using these assumed phase transformation kinetics models to describe a laminate composite structure consisting of a PY and a SMA layer, a comprehensive model remains to be developed. Once such a model is acquired in the future, it should be possible to estimate $\frac{dS_{ij}}{d\Theta}$ by incorporating this with present model of PY coef.

4.1.2 Thunder™

There are a number of multilayered piezoelectric actuators currently under research with some already commercially available. These include Lightweight Piezoceramic Composite Actuators (LIPCA)[72], THin layer UNimorph ferroelectric Driver and sEnoR (Thunder™)[119], and Reduced And INternally Biased Oxide Wafer (RAINBOW)[193] among others. They achieve high displacement using a pre-stressed PY material, which has been bent to a dome shape and put under stress by the substrate which has a different thermal expansion coefficient to the PY layer. As our 2-2 connectivity configuration is nearly identical to this, except ours having the symmetry about the 1-2 plane being a tri-layer, it would be a good idea to investigate these further. Purely due to ease of availability reasons, we chose Thunder™.

Originally developed by the National Aeronautics and Space Administration (NASA), Face(R) International Corporation's Thunder^{TM} actuators produce comparatively higher force together with larger displacement compared to traditional piezoelectric actuators. They are manufactured by binding a thin sheet of piezoelectric ceramic (PZT-5A) under hydrostatic pressure between a metal substrate (stainless steel-304) and an aluminium electrode at 320 °C. During the cooling process the difference in the thermal expansion coefficients between various layers cause the actuator to deform to a shallow dome shape. Then the ceramic is poled in the perpendicular direction to the metal interface, which completes its manufacturing process. This particular manufacturing process introduces

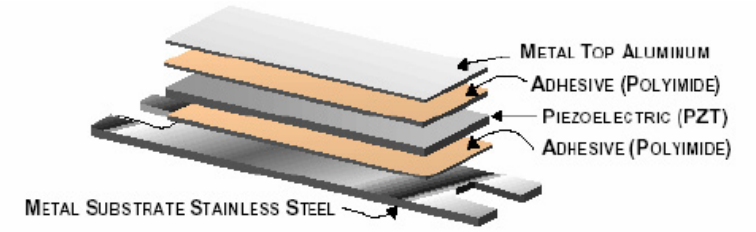

Figure 4.1: Thunder^{TM} actuator

internal stresses inside the actuator, which in turn improves its piezoelectric performance owing to a variety of mechanisms including stress-induced domain alignment[120,140] and ferroelastic switching at high stresses[140]. Even though this actuator is not specifically designed for thermal actuation like SMA, as this particular product was designed with variances in thermal expansion coefficients in mind, it seemed logical to conduct initial test experiments with this actuator to see if there indeed is any kind of contribution to the PY coef from their thermal expansion coefficient differences and internal stress. These experiments were performed by cutting a Thunder^{TM} actuator sheet (TH-6R[119]) into smaller samples and by comparing their PY coefs with other samples of the same Thunder^{TM} actuator, which have been de-laminated from their stainless steel substrate.

Unfortunately, our initial tests did not show any enhancement in the PY coef of the whole sample when compared to that of the de-laminated PZT-5A from the same Thunder^{TM} sample. In fact, it actually showed slight reduction. The reason behind this reduction was attributed to the shallow dome shape of the actuator. As our PY coef measurement rig (pyro-rig)'s surface was flat, Thunder^{TM}'s shape meant that we were unable to vary the temperature of the whole Thunder^{TM} sample as quickly and easily as

the de-laminated PZT-5A, which were flat. Although we attempted to address this issue using thermally conductive paste and aluminium substrate, which filled the gap between the pyro-rig's sample stand and Thunder^{TM}, this then introduced rather large quantity of additional thermal mass (since more material needs to be heated up to reach the same temperature variation), again leading to the same observations. Hence it was decided that in order for us to confirm our theoretical findings of potential PY coef enhancement in 2-2 connectivity laminate composites, we will have to fabricate our own samples, which will be discussed further in Section 5.1.

4.2 Pyroelectric materials

Now we move on to the six pyroelectric materials we did perform our analysis on. The pyroelectric materials investigated are:

- Lead zirconate titanate (PZT); PZT-5H and PZT-5A

Crystal symmetry at room temperature: Tetragonal (4mm)
PZTs are piezoelectric ceramics specifically designed and manufactured for piezoelectric applications. As secondary PY coef is essentially a piezoelectric effect, these demonstrate high enhancement given the right conditions. One hindrance is their high dielectric constants (cf. Appendix A.1), which somewhat limits their application potential under OC. The choice of PZT-5H and PZT-5A were made since they are widely available.

- Barium titanate (BTO)

Crystal symmetry at room temperature: Tetragonal (4mm)
A single crystal perovskite ferroelectric material with the same crystal symmetry as PZT. The same dissimilarity in signs of its piezoelectric coefs and a very large proportion (nearly 45 %, which is 4 times larger than PZT-5Hs) of the total PY coef being attributed to secondary effect indicates potential for high enhancement. However, as exhibited in Table B.3 very large Youngs modulus, largest of all the materials, and comparatively large thermal expansion coef points to lower enhancement than otherwise would have been expected.

- Lithium tantalate (LTO) and Lithium niobate (LNO)

Crystal symmetry at room temperature: Trigonal (3m)
Single crystal perovskite ferroelectric materials with similar applications as that of BTO. However, LTO and LNO possess much lower dielectric constants (cf. Appendix A.1), enabling their deployment in many applications where BTO may not be suited. As exhibited in Table B.3, LTO and LNO both have dc1, dc2, and dc3 (definitions of which will be presented in Section 4.3) of the same sign, implying that the enhancement/reduction in PY coef available in these materials is rather limited due to the cancellation owing to conflicting alteration in the strains corresponding to 1- and 2-axes, and 3-axis from Poisson effect.

- Poly-vinylidene fluoride (PVDF)

⇐ Only uni-axially oriented poled PVDF was investigated in our case
Crystal symmetry at room temperature: Orthorhombic (2mm)
PVDF is an organic ferroelectric polymer that exhibits a variety of characteristic mechanical and electric properties, such as piezoelectricity, the largest among the synthetic polymers, pyroelectricity and many others. As depicted in Table B.3, it has rather anisotropic thermal expansion behavior due to uni-axial orientation with very large thermal expansion coefficients and very small Youngs modulus. Although minute size of Youngs modulus suggests potential for high enhancement, it in fact also leads to extremely small dc1, dc2, and dc3 values which results in diminutive secondary contribution. The sum terms dc1, dc2, and dc3 also have opposite signs to that of PZTs insinuating that for PVDF, NP materials of smaller thermal expansion coefficients should introduce enhancement.

It must also be noted that the material properties of PVDF can vary greatly among different PVDF samples[50,53] fabricated using dissimilar preparation techniques. Due to dispersion of information available on this particular material, the material parameters quoted in Appendix A.2, and hence used for the analysis, have rather diverse sources. As different sources attribute different proportions of the total PY coef to the secondary effect, Kepler and Anderson[90] approximately half and Nix et al.[132] at only 10-60 %, the absolute magnitude of our secondary contribution must be considered with these conflicting views in mind. This is the reason why the comparison of the enhancement in PVDF is made in terms of percentile enhancement of the secondary contribution alone rather than the absolute magnitude, the conclusions of which are presented in later sections of this dissertation.

4.3 Pyroelectric materials assessment

Although previously stated six PY materials present the choice of materials we decided to work with, the author feels it is also equally important to introduce the readers to a method he has found to be most useful for assessing PY materials in their potential for PY coef enhancement.

$$\begin{aligned} dc1 &= d_{31}^{E,\Theta}\left(c_{11}^{E,\Theta}+c_{21}^{E,\Theta}\right)+d_{33}^{E,\Theta}c_{31}^{E,\Theta} \\ dc2 &= d_{31}^{E,\Theta}\left(c_{12}^{E,\Theta}+c_{22}^{E,\Theta}\right)+d_{33}^{E,\Theta}c_{32}^{E,\Theta} \\ dc3 &= d_{31}^{E,\Theta}\left(c_{13}^{E,\Theta}+c_{23}^{E,\Theta}\right)+d_{33}^{E,\Theta}c_{33}^{E,\Theta} \end{aligned} \tag{4.1}$$

When Eq 3.25 is evaluated for a typical PZT, e.g. PZT-5H, the sums of $d_{mkl}^{E,\Theta}c_{ijkl}^{E,\Theta}$ terms for each direction, i.e. corresponding to dS_1 or dS_2 and dS_3, termed "dc1" or "dc2" and "dc3" henceforth, are dc1 = dc2 = -15.9 and dc3 = 16.0 Cm^{-2} as evident from Eq 4.1 and displayed in Table B.3. This implies that positive strains in 1 and 2 directions accompanied by a negative strain in 3 direction would lead to a larger negative secondary contribution, resulting in the greatest PY coef enhancement for PZT-5H. The best configuration for this requirement is a 2-2 connectivity laminate since, with increasing temperature, it can lead to PY material's strains in 1 and 2-axes being positive whilst strain in 3-axis becomes negative as a consequence of Poisson effect. This is the reason why we observe such high enhancements in PZTs as illustrated in Chapter 6.

These dc1, dc2, and dc3 values are the main indicators of the potential for PY coef enhancement. The results from similar analysis on all six PY materials considered are presented in Table B.3 from Appendix B.2 (cf. Appendix A.1 for detailed material parameters used for creating this table).

4.4 Non-pyroelectric materials

The list of the six non-pyroelectric materials used as thermally-active component will be presented with their main properties. In addition, the reasons for their selection will

also be provided here.

Non-pyroelectric materials investigated and their material properties are (cf. Appendix A.2 for the actual numerical value of the properties) :

- Stainless steel (St); Goodfellow stainless steel 15-7PH[9]

This is a standard stainless steel, which was used in our previous publication[43] with experimentation confirming our theoretical predictions on St/PZT/St structures. Although its high Youngs modulus promises large enhancement, its low thermal expansion coefficient implies otherwise.

- Poly-tetrafluoroethylene (PTFE or Teflon)

PTFE, also known as Teflon, is a synthetic fluoro-polymer with inhibited water adhesion on its surface. Hence its applications as a non-stick coating for pans and various other cookware. As evident in Table A.4, its high thermal expansion coef, second highest of the analyzed NP materials, and low volumetric heat capacity, lowest among all materials, indicates to high enhancement and high Efficiency (definition of which will be presented in Section 8.2). However, its very low Youngs modulus, lowest of all materials, hinders its enhancement potential somewhat at high thickness ratios.

- Chlorinated polyvinyl chloride thermoplastic (CPVC)

Chlorinated polyvinyl chloride thermoplastic (CPVC) is a thermoplastic produced by chlorination of polyvinyl chloride (PVC) resin. Its applications include hot/water pipes and industrial liquid handling. It has the highest thermal expansion coef among all the materials examined, but has second lowest Youngs modulus, again entailing potential for higher enhancements at low thickness ratios. It also has second lowest volumetric heat capacity, indicating to a relatively high Efficiency.

- Aluminium (Al)

Widely available metal with lowest Youngs modulus among all metals considered, but with thermal expansion coef that lies between that of St and Zinc (Zn).

- Zinc (Zn)

Zinc is a moderately reactive bluish grey metal that finds application in galvanization of

steel, manufacture of brass and many others. Its comparable Youngs modulus along with highest thermal expansion coef among all the metals, means it promises large adjustment in the PY coef.

- Invar 36 (Invar36)

Invar is a metal used in applications in which a high degree of dimensional stability under changing temperatures is desired. It is used in precision mechanical systems in many different industries including opto-mechanical engineering applications. Invar is a low expansion Iron-Nickel alloy with Invar36 being one of the best known varieties. Invar36 is composed of 64 % Fe (Iron) and 36 % Ni (Nickel) and is the most common Iron-Nickel alloy used in opto-mechanical engineering. The most important property of Invar is its low thermal expansion coef, which makes it the perfect NP material for introducing opposite sign strains in 1- and 2- axes when compared to that of other NP materials, which should make it the ideal companion for PVDF.

Chapter 5

Experimental procedure - Pyroelectric coefficient enhancement

This chapter consists of three sections. In Section 5.1, as well as the fabrication techniques used in creating our samples, some of the parameters that may affect our PY coef enhancement measurement will also be presented. Section 5.2 introduces the readers to our two planned experimental studies, Curing temperature (cf. Subsection 5.2.1) and Enhancement study (cf. Subsection 5.2.2). The aim of the former, which is also one of the main preliminary experimentation the author has conducted, is to investigate some of the potential parameters such as bonding layer thickness, epoxy curing temperature (henceforth referred to as Cure temp), PY coef measurement taking temperature (henceforth referred to as operating temperature or Op. temp), and others that may affect the latter. The Enhancement study is designed to test the accuracy of our analytical model developed in Chapter 3, and its results form an integral part of this PhD dissertation. The final Section 5.3 illustrates parameters that may arise from the actual experimentation that may also affect the outcome of our investigation. Brief introduction to our experimental kit, pyro-rig, and the experimental procedures are presented, identifying features that may also affect the enhancement measurements. The preliminary experiments and their findings are also presented here.

Please note that randomly selected samples of the exactly same fabrication and measurement parameters were additionally created and compared to ensure the reproducibility of, and removal of any anomaly from, these studies.

5.1 Fabrication of laminar sandwich samples

After theoretically considering various materials, as illustrated in Chapter 4, it was decided that we will use Stainless steel (St) as NP material and PZT-5H as PY for our experiments in verifying the expected PY coef enhancement, owing to their wide availability and ample potential for the enhancement. Although we also conducted some experiments with PZT-5A, the experimental data with PZT-5A is not as complete as PZT-5H's whilst demonstrating similar results, and hence those results are not presented in this dissertation.

5.1.1 Fabrication technique

Although revised to our own requisites, this fabrication technique is largely based on those used in Chung's work[48], who designed and fabricated a PZT unimorph actuators by bonding PZT-5H to a Molybdenum or Stainless steel substrates. His extensive research into various adhesive selection and bonding conditions have concluded optimal bonding methods for PZT-5H and Stainless steel adhesion, which we have exploited in our own fabrication technique.

Adhesive choice

One of the main differences between Chung's work and ours is the use of thermal stimuli in the latter. As ours utilises PY effect, it is essential that our adhesive layer does not become a dominant influence on the thermal capacity or conductivity of our whole sample. Piezoelectricity at its heart, Chung's work did not require for this potential hinderance to be explored. Hence, the choice of Epotek 301-2 in Chung's work may not necessarily mean ours would also be the same. Unfortunately however, Epotek 301-2's manufacturer Epotek Technology, Inc.[7] were unable to provided us with any information on its thermal conductivity, making the assessment of this epoxy in our particular application rather difficult. In order to address this issue, we decided to look at other thermally conductive epoxies and compare their thermal performance with Epotek 301-2 experimentally, hence ensuring it is the right choice for our application as well. Some of the thermally conductive epoxies considered are illustrated in Table 5.1.

The best thermal conductivity was found on Epotek H70S. With its good shear strength and decent cure temperature range, it looked very promising. However, as

Table 5.1: Thermally conductive epoxies considered

Manufacturer	Product ID	Maximum lap shear strength	Curing temperature	Thermal conductivity	Weight ratio (A:B)
Timtronics	TIM-815	2400	70	1.53	100:35
Timtronics	TIM-811	1400	25	1.50	1:1
Epotek	301-2	> 2000	80	Unknown	3:1
Epotek	930	658	80	4.57	100:3
Epotek	930-1	1636	80	1.07	100:4
Epotek	930-4	1927	80	1.67	100:3
Epotek	TZ101	1726	150	0.93	N/A
Epotek	H31	1700	150	1.10	N/A
Epotek	H70S	> 2000	80-175	0.44	1:1
Eastern	ERA-182	2300	25-90	1.25	4:1
3M	3M-TC2810	3000	23-50	0.80-1.40	1:2
Fischer	WLK30	$\approx$ 1400-2900	40-190	0.82	10:1

Units: - Max. lap shear strength : PSi - Curing temp. : °C - Therm. cond. : $Wm^{-1}K^{-1}$
Manufacturers: - Timtronics[10] - Epotek : Epotek Tech. Inc.[7] - Eastern : Eastern resins corp.[8] - 3M[6] - Fischer : Fischer Elektronik GmbH[11]

the optimal bonding condition has already been worked out for Epotek 301-2 and it was readily available, it was decided that should Epotek 301-2 fare well in our preliminary testing phase, it will be used in our samples. As WLK30 epoxy also has quite good thermal conductivity and it was easily attainable, it was put against Epotek 301-2. It turns out that at the very least for the heat rate we intended on using, the effect of Epotek 301-2 bonding layer was negligible where the thermal conductivity was concerned, and hence this epoxy was used for all our samples then on.

Adhesive bonding conditions

Once the decision was made on which epoxy to use as an adhesive, the author set out to determine the optimal conditions for the adhesive bonding with this epoxy. Chung's

optimised conditions for adhesive bonding with Epotek 301-2[48] were:

- Spreading method : spinner
- Spin rate : 3,500 rpm
- Spin time : 20 s
- Dead weight : 2 kg
- Curing temperature : 100 °C
- Curing time : 5 hours

After consultation with Dr. Chung and our own preliminary testing we have concluded on the following optimal Epotek 301-2 bonding conditions for our own samples:

- Spreading method : brush/knife edge
- Dead weight : 4-5 kg

(Please note that spin coating was not deemed necessary for our application as we were able to achieve sufficiently thin bonding layer through direct application of the epoxy with brush/knife. Increased Dead weight ensures high likelihood of such thin layers.)

Table 5.2: Curing conditions for the adhesive bonding process

Curing temperature (°C)	Curing time (hours)
80 - 90	≥ 4
40 - 50	≥ 12
30 - 40	≥ 24

Fabrication procedure

Now that the selection of the adhesive to be deployed has been made and optimal conditions for the bonding to take place has been identified, we now move on to the actual fabrication procedure of our samples. Following are the procedures used for the fabrication of our samples displayed in Figure 5.1:

1. PY and NP material preparation

   Using diamond saw, cut PY and NP materials to the dimensions we require. As thicknesses are already set by the manufacturer, we only had to cut them to required surface area. In general, the samples were fabricated to have the surface area of around $1cm \times 2cm$ although during PY coef measurement, the actual areas were measured and taken into consideration in the calculation for the PY coef (cf. Eq 5.1[190]). This dimension was chosen as it was not too small to cause difficulties in handling/bonding the sample while being not overly large to cause any thermal

mass issues. It also ensures our samples have dimensions suitable for plates or beams, enabling us to use already established mechanics regarding these structures (cf. Subsection 3.2.2). Please note that in order to make sure the whole surface of PY material (PZT-5H) was bonded on to NP material (St), the surface area of St was cut so that it was slightly bigger than that of PZT-5H's, leaving some room of error during the bonding procedure.

2. Prepare PY and NP materials surfaces for bonding

   (a) Synthesize 10 % Potassium hydroxide (KOH)
   Weigh KOH flakes and mix it with pure water at H_2O:KOH = 10:1 ratio

   (b) NP material surface

      i. Place the NP substrate into KOH solution for about 15 minutes to remove any impurity from its surface

      ii. Clean the surface with Isopropyl alcohol (IPA) and Acetone, then rinse with de-ionised water

      iii. Carry out the water dispersion test by washing the NP substrate with de-ionised water, ensuring that no water droplet is formed, indicating clean surface

      iv. Dry off inside a drying chamber set at 35-45 °C

   (c) PY material surface

      i. Clean the PY material's surface with IPA and Acetone, then rinse with de-ionised water

      ii. Dry off inside a drying chamber set at 35-45 °C

3. Turn the oven on to the required temperature for bonding
   To avoid depolarisation of the PY material whilst achieving fastest epoxy curing time possible, around 4-5 hours at 80-90 °C of curing conditions were used where appropriate[48]

4. Prepare the epoxy (Epotek 301-2) to be used for the bonding
   (Please note that although Epotek 301-2 (by Epotek technology, Inc.[7]) epoxy was used for the most of the experiments, during the preliminary experiment stage thermally conductive adhesive called WLK30 (by Fischer Elektronik GmbH[11]) was

also used as illustrated in Figure 5.1(c). As the main experiment was conducted with the former only, only the procedure for the former epoxy will be provided.)

(a) Take the Part A out from the fridge (In general, A is stored in the crystallised state)

(b) Place Part A in the drying chamber at around 30 °C for 20 minutes to de-crystallise it

(c) Using pipettes and a scale, mix Parts A and B in ratio A:B = 3:1 and stir the mixture to form the adhesive epoxy

(d) Let the epoxy settle for about 30 minutes so that all the bubbles disappear

(e) Store Part A in the fridge and Part B in Chemicals cupboard

5. PY and NP materials for bonding

(a) Place an aluminium foil on the baking tray or the weight on top of which the sample will be left to bond. Place the cellotape on the very end edges of St, hence fixing the bottom St layer, while making sure as little surface area as possible is covered by the tape

(b) Apply the epoxy mixture on to the St's surface, ensuring the whole surface is covered while the minimum thickness of the epoxy layer possible is pursued

(c) Place PZT-5H on St's surface that has just been applied with epoxy, while making sure the cellotape is visible from the top and hence ensuring that PZT-5H is not sitting on top of the tape, but just St

(d) Apply another layer of epoxy on the top surface of PZT-5H, again ensuring the whole surface is covered with minimum thickness of the epoxy possible

(e) Place the other St on top of PZT-5H's epoxy applied surface, making sure the whole surface of PZT-5H is in contact with St

(f) Cover a weight amounting to about 4-5 kg with an Al foil and place it on top of the whole sandwich structure (cf. Figure 5.1(a))

6. Place the whole contraption into the pre-heated oven and wait for the curing to complete (for the amount of time required cf. Table 5.2)

7. Take the sample out from the oven and remove the top weight and the baking tray/bottom weight

8. While taking care not to apply too much stress or pressure on to the sample, remove the excess epoxy and the whole Al foil using a sharp knife

9. Let the sample cool down to room temperature

(a) Typical dead weight used

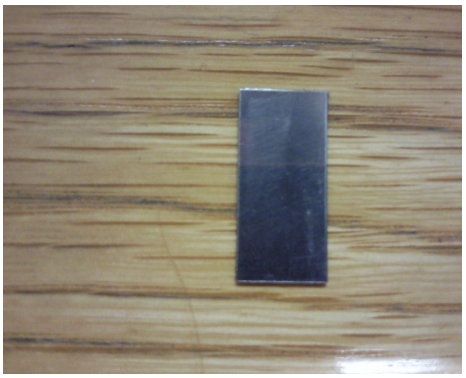

(b) Typical laminate composite sample

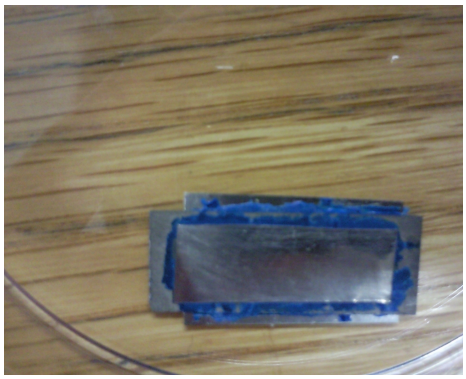

(c) Sample fabricated using WLK30 adhesive

(d) Typical laminate composite sample with an electrical wire attached

Figure 5.1: Sample fabrication

5.1.2 Possible parameters that may affect the experimental data

Now that we can fabricate our samples, this subsection will detail any potential parameters that may root from this fabrication procedure which could affect the PY coef measurement.

Electrical isolation between top and bottom surfaces of the sample

Should the top and bottom St layers make contact, the electrical isolation between these two surfaces will disappear as St is conductive. This means the potential between the top and bottom St layers will be the same and hence no pyroelectric current will be observed. Therefore, a careful consideration must be given to this issue during the bonding process (Step 5) to maintain this electrical isolation.

Bonding quality

As we investigated in Section 3.3, even a perfect bonding between the layers will still lead to some loss in the strain transfer between NP and PY layers. Should the quality of this bonding be anything but perfect, then even further loss will occur in the strain transfer, resulting in the observation of reduced PY coef enhancement. Good surface preparation, namely Step 2, is essential in achieving this, as otherwise rather large loss will have to be described by the k-factors (cf. Subsubsection 3.4.2). Following few paragraphs describe the factors that may also affect the bonding quality.

Type of epoxy used Depending on the adhesive used and its characteristics, lap shear strength for instance, the quality of the bonding can be affected greatly. All three, thermal, mechanical, and electrical properties of our samples can be affected by the choice of the type of the epoxy deployed in the sample.

The general criteria for the best choice would be epoxies with higher thermal conductivity, thermal expansion coefficients, and Young's modulus, accompanied by lower thermal capacity and viscosity. Epotek 301-2's thermal expansion coefficient of 37×10^{-6} $mm^{-1}K^{-1}$ [7] is even higher than that of St (cf. Table A.4), and hence possibly reducing any strain loss that the epoxy layer may introduce. In addition, epoxy capable of forming amply thin adhesive layer (lower viscosity in general leads to thin adhesive layer) must be employed as this will ensure that there is an electrical contact between the surfaces of porous dielectric PY layer and the conductive NP layer, which also acts as the electrodes

in St/PZT-5H/St's case[48], whilst also reducing the loss in strain from the mechanical deformation of the adhesive layer.

Notice that the electrical conductivity of epoxy itself is not as important since it is not a necessity that NP layers must act electrodes as well. Very thin layer of conductor can always be deposited onto PY material as electrodes when required.

It is the author's firm belief that given the circumstances Epotek 301-2 was the right choice for this particular PhD project. However, it may well be the case that other epoxy might be able to achieve even higher enhancement and in some cases, just the application of the epoxy layer itself without NP could lead to some enhancement. Epotek H70S from Table 5.1 seems very promising in this aspect.

Bonding thickness As illustrated in Section 3.3, the thickness of the epoxy layer plays a crucial role on the amount of the strain that can be transferred between PY and NP layers. Thinner the adhesive layer the better as long as it covers the whole surface of PY and NP materials that are in contact. Measurements with a micrometer have revealed that on average we were able to achieve bonding layer thickness of 20-25 μm each utilising the optimised dead weight during the bonding process.

Epoxy curing time The bonding strength and quality depends heavily on the curing conditions. Depending on the curing temperature used (cf. Table 5.2 for Epotek 301-2), the samples must remain in the heated oven for sufficient enough time for the adhesion layer to harden. However, prolonged exposure to heat could de-polarise PY material, so optimising the amount of time the sample must remain in the curing temperature is essential for achieving good bond quality and subsequent high enhancement.

Curing temperature As with curing time, each epoxy must be cured above certain curing temperature for good mechanical bonding. Too low temperature will lead to weak bonding between PY and NP layers, while excessively high temperatures can cause the bonding to fail altogether through the degradation of the epoxy layer or cause the depolarisation of the PY layer.

Since epoxy curing temperatures and PY coef measuring temperature (or operating temperature) are not always identical, there is bound to be some pre-stress/residual stress present in the sample. This also means its effect on piezoelectric and dielectric properties of our sample[199–201] (cf. Subsections 2.2.2 and 16.1.3) could also influence

our measurement. In must be stated here that during the preliminary testing phase (cf. Section 6.1), the author has conducted a series of experiments to quantify how much of an impact this can potentially have on the overall PY coef enhancement measurement. Unfortunately, the results were inconclusive although it was apparent that where the overall magnitude of the PY coef is concerned the impact can be minimised by the use of 80-100 °C curing temperature and PY coef measuring temperature around the room temperature, i.e. 25-35 °C.

5.2 Methodology

5.2.1 Curing and operating temperature variation and the effect of pre-stress

To investigate some of the potential parameters such as bonding layer thickness, epoxy curing temperature (Cur temp), PY coef measurement taking temperature (operating temperature or Op. temp), and others that may affect the Enhancement study planned in Subsection 5.2.2, results of which are presented in Section 6.2, this Curing temperature study was planned as one of the main preliminary experimentation. It will consist of two phases, Samples fabrication and PY coef measurement phase.

Samples fabrication phase

In order to fabricate samples cured at various curing temperatures for comparison purposes, following common parameters were used for all the samples listed in Table 5.3 (based on the optimal epoxy curing conditions in Subsubsection 5.1.1):

- PY material thickness: 127 μm PZT-5H
- NP material thickness: 250 μm Stainless steel
- Epoxy used : Epotek 301-2
- Spreading method : brush/knife edge
- Dead weight : 4-5 kg
- Op. temp for PY coef measurement before bonding the sample : 25-35 °C

Table 5.3: Samples fabricated for Curing temperature study

Name	Aimed Cur temp (°C)	Actual Cur temp	Curing time (time in the oven)
XII1	≈ 40	≈ 48-50	≈ 2 days
XII2	≈ 60	≈ 60	≈ 1 day
XII3	≈ 80	≈ 82-84	≈ 3-4 hrs
XII4	≈ 100	≈ 100	≈ 2-3 hrs
XII5	≈ 120	≈ 115-120	≈ 2-3 hrs

All the samples had their piezoelectric coefficient measured before bonding to confirm their poled state and their thicknesses were also measured after the bonding to record

the bonding layer thickness. The samples created are listed in Table 5.3.

Although the curing times are decided upon previous research results and the manufacturer's recommendation, it must be noted that the time used for XII5 sample was more that was quoted as necessary since this sample showed some dissimilarity from others in its behaviour as illustrated in Section 6.1. To ensure this was not due to bonding failure owing to short curing time, more than one sample were created with this prolonged curing time.

PY coef measurement phase

Following Op. temps were employed for measuring PY coef enhancement in all the samples displayed in Table 5.3 to investigate the effect of Cur temp and Op. temp difference:

- 25-35 °C
- 35-45 °C
- 55-65 °C
- 75-85 °C

Heating rate of 2 °C per minute was used (this was the optimum value decided after our preliminary experiments in Subsubsection 5.3.3) with each measurement being carried out over at least 3 cycles of heating-cooling-heating to identify any potential anomaly. It must be pointed out that the time the samples were exposed to pre-stress due to the temperature difference between Cur temp and room temperature (around 25-35 °C) is varied despite the author's efforts to carry out all the measurements within 1-3 hours from taking the samples out from the oven. The effect of this is unknown at present, but it should not be too influential as the stresses involved are not huge when compared to those values quoted by Zhou et al.[201], where they observed large decrease in piezoelectric activity in soft PZTs above compressive uniaxial stress of around 25-30 MPa. The results of this Curing temperature study are presented in Section 6.1.

5.2.2 Pyroelectric coefficient enhancement study

Once the preliminary experiments and Curing temperature study have been conducted, we should be able to conduct a controlled PY coef measurement where we only allow one parameter to affect the outcome. As our analytical model developed in Section 3.4 predicts the dependence of PY coef enhancement on the thickness ratio between the thicknesses of PY and NP materials, this Enhancement study will create samples of various thickness ratios ($R = \frac{PY_t}{NP_t}$) and compare their PY coef enhancement with that

predicted by the model with the hope of validating our analytical model, the results of which are presented in Section 6.2.

The samples manufactured for this study are displayed in Table 5.4.

Table 5.4: Samples fabricated for Enhancement study

Name	PZT thickness (μm)	Each St thickness (μm)	Thickness ratio (R)
XI1	127	50	1.270
XI2	127	125	0.508
XI3	127	250	0.254
XI4	191	50	1.910
XI5	191	250	0.382
XI6	267	50	2.670
XI7	267	125	1.068
XI8	267	250	0.534

A typical PY coef enhancement measurement procedure is:

1. Measure the pyroelectric coefficient of a bare PZT-5H and yet-to-be-bonded stainless steel (St) laminates in the stack configuration of St/PZT/St.
2. Bond the exact same St/PZT/St stack with epoxy (EPOTEK301-2)
3. Measure the pyroelectric coefficient of the bonded stack and compare with that of Step 1 to calculate the enhancement.

Please note that Op. temp used for all the measurement in this study is room temperature, i.e. 25-35 °C range, while all the samples fabricated for this study were cured at approximately 100 °C with the following epoxy bonding parameters (cf. the optimal bonding condition shown in Subsubsection 5.1.1):

- PY material : PZT-5H (PZT)
- NP material : Stainless steel (St)
- Epoxy spreading method : brush/knife edge
- Epoxy used : Epotek 301-2
- Dead weight : 4-5 kg
- Cur temp : 100 °C
- Curing time : 2-3 hours
- Op. temp for PY coef measurements : 25-35 °C

The results of this Enhancement study are presented in Section 6.2.

5.3 Pyroelectric coefficient measurement

In Section 5.1, as well as the fabrication techniques used in creating our samples, some of the parameters that may affect our PY coef enhancement measurement were also presented in Subsection 5.1.2. The author would now like to introduce the readers to parameters that may arise from the actual experimentation itself which could also affect the outcome of our investigation. Brief introduction to our experimental kit, pyro-rig, and the procedures for our experiments are presented first in Subsection 5.3.1, followed by Subsection 5.3.2 identifying the experimental features that may also affect the enhancement measurements. Then Subsection 5.3.3 will draw this section to a close with our preliminary experiments and their findings.

5.3.1 Experimental kit and procedures

In general, pyroelectric coefficients are measured by applying a thermal variation to the PY material and then measuring the charge released at the surface of the PY material, which can be detected as a pyroelectric current, i. Once i is measured one can deduce the material PY coef using the following expression[186]:

$$i = Ap_m \frac{d\Theta}{dt} \tag{5.1}$$

where i = Pyroelectric current generated by potential difference across m-axis of the pyroelectric material
A = Surface area perpendicular to m-axis
p_m = Pyroelectric coefficient in m-direction
$\frac{d\Theta}{dt}$ = Rate of temperature variation

As the surface area, A, is assumed to be constant, in most cases as long as the rate of thermal change is known calculating p_m is very easy once i is measured. Our experimental kit, pyro-rig, whose details will follow shortly, enables us to do exactly this as illustrated by Figure 5.2.

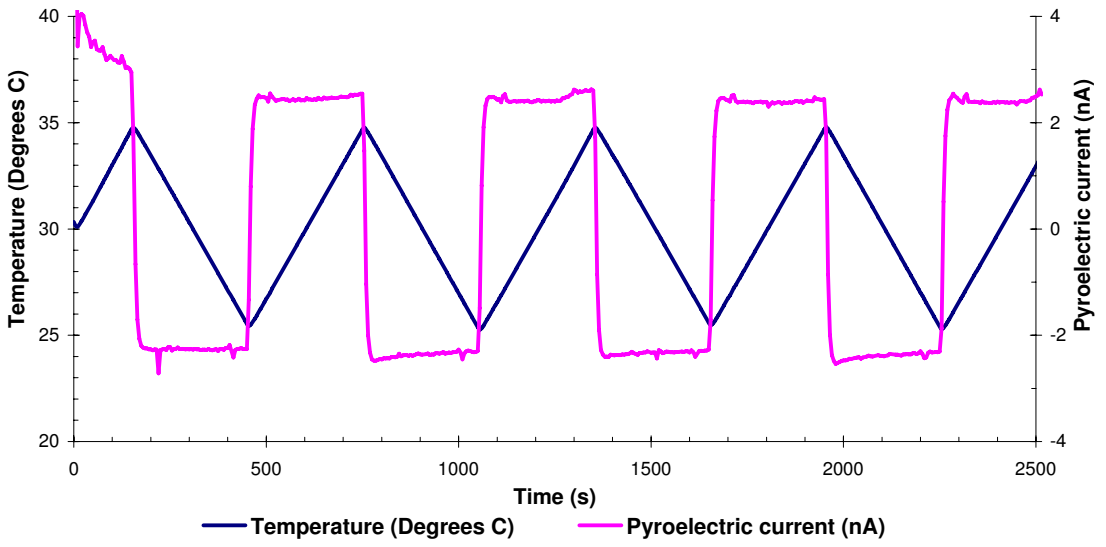

(a) Typical pyroelectric current output and temperature profile from pyro-rig

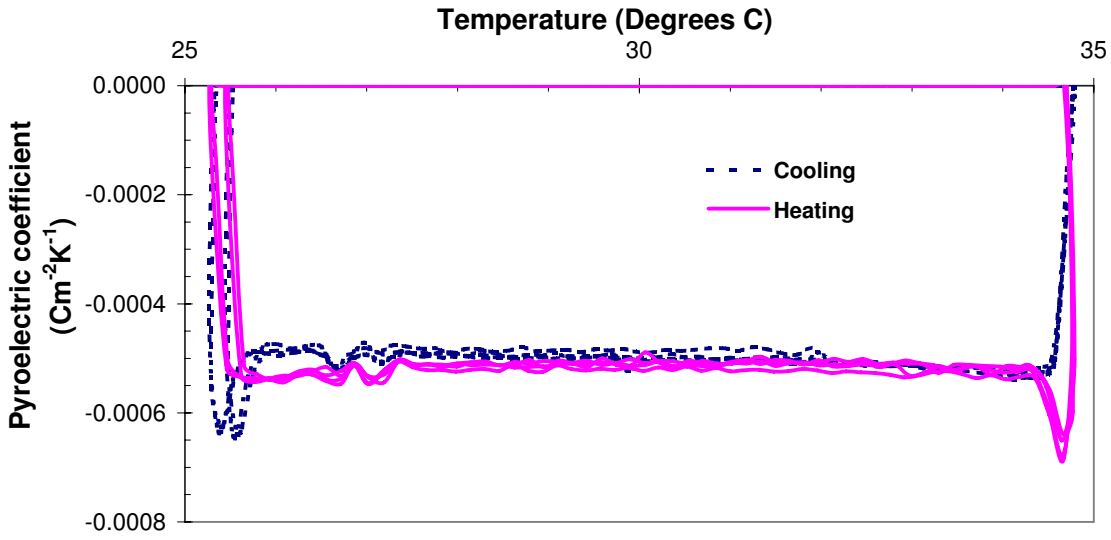

(b) Evaluated pyroelectric coefficient from pyroelectric current using Eq 5.1

Figure 5.2: Pyroelectric current and coefficient from pyro-rig

Pyro-rig

The schematics of the pyro-rig is displayed in Figure 5.3, while its components are described in the following paragraphs. Figure 5.4(a) is an actual view of the pyro-rig and Figure 5.4(b) depicts the vacuum chamber with a sample placed on top Cu substrate in preparation for measurement.

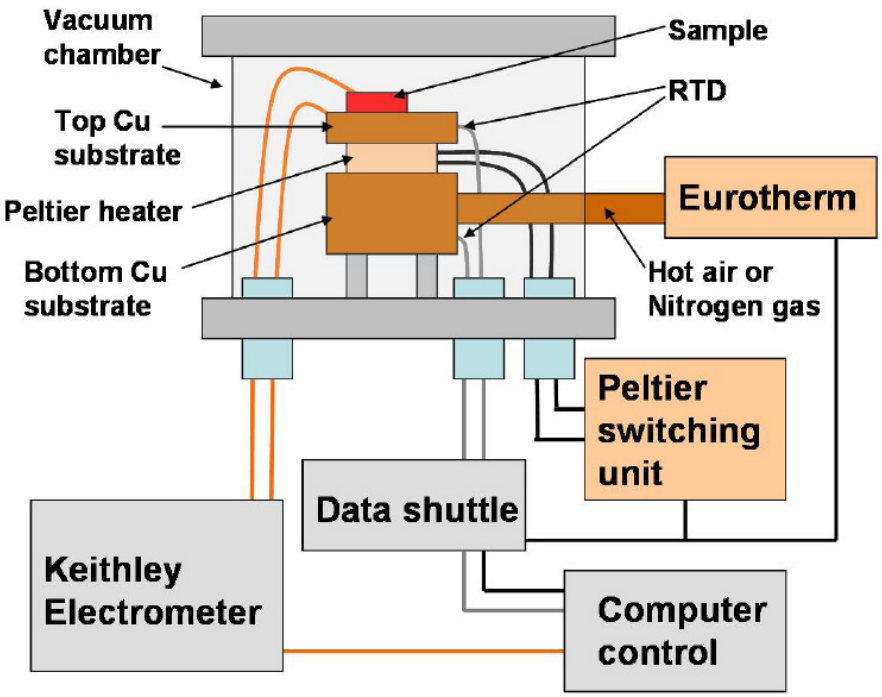

Figure 5.3: Schematics of the pyro-rig

Vacuum chamber A sealable chamber where our sample will be placed. It also houses the Peltier heater and top and bottom copper (Cu) substrates. The quality of vacuum achievable in this chamber was reasonable enough for our PY coef measurements under short circuit condition although it is anticipated that better quality may be required for open circuit condition measurements.

Keithley 6517 Electrometer Capable of measuring small currents down to pA, it is connected to an IBM PC to which it sends the PY current data. It measures the real time PY current (i) from the surfaces of the PY sample housed inside the vacuum chamber and feeds it to the PC so that it can log it against the time of the observation.

Data shuttle This processes the top plate and copper substrate temperature data and sends it to the Peltier switching unit and Eurotherm so that desired temperature requested from the PC can be achieved.

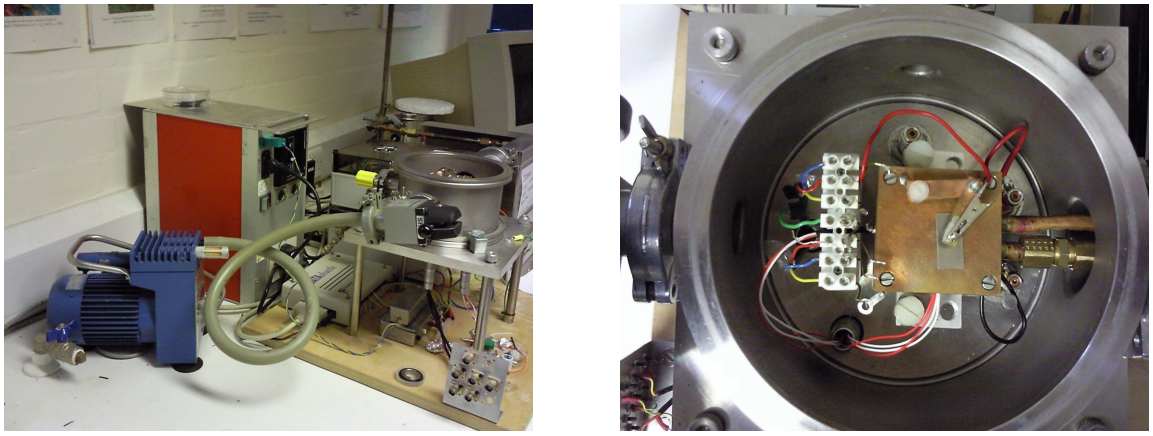

(a) The actual pyro-rig (b) Vacuum chamber with sample in place

Figure 5.4: Pictures of the pyro-rig

Peltier switching unit Connected to the Data shuttle via two BNC cables, Peltier switching unit controls the Peltier heater with the data from Data shuttle as feedback. The Peltier heater is in contact with two Cu substrates and transfers the heat from one to the other, hence attaining the required temperature. The top Cu substrate is where the subject to be measured is placed, and its temperature is monitored by the Resistive temperature detectors (RTD) that feed this temperature information back to Data shuttle (which is relayed on to the PC as well so that the rate of temperature variation can be evaluated). Peltier heater is capable of achieving temperature variation of up to around 30 °C.

Eurotherm This heats the hot air that is blown into the chamber via Cu pipes that provide heat to the bottom Cu substrate should higher temperatures than what Peltier heater can provide is desired. Although it is capable of much higher temperatures, the fragility of the Peltier heater means only temperatures up to 90-100 °C is allowed on pyro-rig.

Air pump Pumps air out from the vacuum chamber, creating a reasonable vacuum condition after around 2 minutes of pumping.

Pyroelectric coefficient measurement procedure

1. Turn on the "Vacuum" tube (grey knob)
2. Check cable connections
   (a) Sample chamber to Keithley (BNC cable)
   (b) Keithley to PC (IEEE cable)
   (c) Data shuttle to Peltier switching unit (BNC cable)
   (d) Data shuttle to PC (DDC cable)
   (e) If high temperatures are required
      i. Data shuttle to Eurotherm (Cable with green plug)
      ii. Power supply from Eurotherm to Cu pipe heater (To be connected only after the run has started)
      iii. Place the stand to support the heating Cu pipes
3. If vacuum is required
   (a) Turn the inlet valve on the Vacuum chamber to "Open"
   (b) Pump air out
   (c) Turn the inlet valve to "Shut"
   (d) Turn the Air pump off
4. Turn the power to Data shuttle, PC, and Keithley on
5. Set "Work Bench Base" with right parameters
   (a) Work Bench mode must be set to "Standard"
   (b) Set "Slider00" module, which is the wave frequency generator, to the value of $\frac{1}{f}$ where f is the frequency of the temperature variation
   (c) Set "Generator00" module, which is the wave magnitude setter, to the value of the amplitude of the temperature variation ($\pm\alpha$ for example)
   (d) Set "Formula00" module, which is the experiment condition setter, to the base temperature ($IN(0) + \beta$ for example)
   Note that this means our temperature variation range is $\beta \pm \alpha$°C

(e) Check the input/output of the "Board1:A1" module which deals with the temperature readings from RTDs from the top Cu substrate

(f) Check the input/output of the "GPIB2" module which deals with the PY current data from Keithley

(g) Configure "Formula03" module, which sets the units, to $\times 10^{-9}$ so that the reading is recognised as being measured in nA

6. Run the experiment on Work Bench Base

7. Turn the power to Peltier switching unit and Eurotherm (its connection to the Cu pipe as well), if high temperatures are required, on

8. Observe the screen logging the data

9. When all the data has been collected, unplug Peltier switching unit and Eurotherm, including its connection to the Cu pipe

10. Save the collected data as an ASCI file

11. If another run is required, follow steps 6 - 10 again. Otherwise, turn off and unplug Data shuttle, PC, and Keithley.

12. De-pressurise the vacuum chamber by opening the outlet valve

5.3.2 Possible parameters from pyro-rig's operation that may affect the experimental data

Some examples of the possible parameters that can potentially influence the experimental data are identified here. In depth assessment on these, and those presented in Subsection 5.1.2's, potential effect on our experimental results will be carried out in Subsection 5.3.3.

Vacuum quality

Electrical isolation across the thickness of the sample can be influenced by the quality of vacuum inside the chamber. Although the requirement of the vacuum for SC measurements is not as strict as that of OC, it is still desirable. Under OC, if poor vacuum is used the charge released on the surface of the PY material can be instantaneously

compensated by the atmosphere, resulting in wrong readings. As the lack of background noise in the readings from the preliminary testing (cf. Subsection 5.3.3) suggests, under SC the vacuum quality achievable with our pyro-rig is sufficient enough for PY coef measurements.

Uniform thermal stimulation

Although our samples' large aspect ratio, the pyro-rig's surface to surface contact with the sample, and relatively big top Cu substrate means the contribution to the PY coef measurement from the tertiary pyroelectric effect[57] would be rather limited, its effect must be checked. Non-uniform thermal stimulation to the sample could increase the tertiary contribution, and hence in the preliminary testing thermally conductive (but electrically insulating) pastes were used to surround the sample surfaces. This influences the thermal distributions within the sample and any temperature gradient that might be present across the sample thickness, i.e. the causes of tertiary pyroelectric effect, so that any changes in the measurements would be an indication of the presence of the tertiary PY effect in the overall measurement.

Thermal mass issue

If our samples have large thermal mass and high rate or frequency of temperature variation (termed heating rate henceforth) is used, the samples may not achieve the necessary temperature variations intended, leading to reduced perceived PY coef. In order to assess this issue, various heating rates will be tested on various sizes of samples with some theoretical work in Subsection 5.3.3.

Electrical condition

There are two electric conditions a measurement can take place (cf. Section 3.1). Although the author has attempted to carry out the measurement under both conditions, it was concluded that our pyro-rig can only carry out the measurements under SC. Therefore all our experimental data will be under SC.

5.3.3 Preliminary experimentation

Preliminary experiments were conducted to determine the extent to which previously stated parameters may affect our PY coef measurements.

Samples used in the preliminary experiments

Although many more were created, these are the main samples whose experimental data are presented in this section of the treatise:

Table 5.5: Samples created for the preliminary experiments

Name	PZT thickness	Each St thickness	Structure	Epoxy used	Cur temp
VI_3	127	50	3-layer	Not bonded	N/A
VI_4	127	50	3-layer	Epotek 301-2	50
VII_3	127	50	3-layer	Epotek 301-2	50
VII_6	127	50	3-layer	Epotek 301-2	80-90
IX_5	267	50	3-layer	Epotek 301-2	80-90
IX_6	267	50	3-layer	WLK30	80-90
IX11	267	N/A	N/A	PZT only	N/A

Units: - thickness : μm - temperature : °C

Please note that only IX_5 and IX_6 were actually bonded for the measurements carried out during the preliminary phase. Most of the samples were bonded later on in the main experiments stage.

Time constant calculation

The aim of this part of the dissertation is to confirm that the heating rate employed in the experiments, namely maximum 2 degrees per minute, was a justifiable limit with thermal conductivity of the samples in consideration. This should give us some theoretical insight when dealing with thermal mass issue stated in Subsubsection 5.3.2. In order to achieve this goal, a quantity termed "time constant" will be derived from the basic definition of thermal conductivity and estimated for our potential samples. At the outset, we consider a few quantities related to heat transfer:

Thermal conductivity The intensive property of a material that indicates its ability to conduct heat, defined as the quantity of heat Q, transmitted in time t, through a thickness L, in a direction normal to a surface area (A), due to a temperature difference $\Delta\Theta$, under steady state conditions and when the heat transfer is dependent only on the temperature gradient.

$$\begin{aligned}\text{Thermal Conductivity} = k &= \frac{Q}{t} \times \frac{L}{A \times \Delta\Theta} \\ &= \text{Heat flow rate} \times \frac{\text{Distance}}{\text{Area} \times \text{Temperature gradient}} \\ &= [Js^{-1}] \times [m] \times [m^2K^{-1}]^{-1} \qquad = [Js^{-1}m^{-1}K^{-1}]\end{aligned} \tag{5.2}$$

Specific heat capacity and heat capacity Amount of heat energy required to achieve temperature difference of 1 K in 1 m^3 of a material. Heat capacity = $c_P \times \rho$ = Specific heat capacity $\times$ Density = $[Jm^{-3}K^{-1}]$

Thermal diffusivity

$$\begin{aligned}\text{Thermal diffusivity} &= \frac{k}{\rho \times c_P} \qquad = \frac{\text{Thermal conductivity}}{\text{Density} \times \text{Specific heat capacity}} \\ &= [Js^{-1}m^{-1}K^{-1}][kgm^{-3}Jkg^{-1}K^{-1}]^{-1} \qquad = [m^2s^{-1}]\end{aligned} \tag{5.3}$$

Time constant (T) This quantity will be defined as the minimum time required for the whole sample to change a single degree, or equivalently a single Kelvin. The derivation and mathematical expression of this entity will be displayed in the following. To derive the "Time constant": From the definition of thermal conductivity (cf. Eq 5.2 and diffusivity (cf. Eq 5.3):

$$\begin{aligned}k &= \frac{Q}{t} \times \frac{L}{A \times \Delta\Theta} \qquad = [Js^{-1}m^{-1}K^{-1}] \\ &= \text{Energy conducted per second per m per K}\end{aligned}$$

$$\begin{aligned}\Rightarrow \quad \text{Time constant} &= \text{Time taken for 1 K change} \\ \Rightarrow \quad T &= \frac{QL}{A\Delta\Theta} \times \frac{1}{k} \\ &= \frac{\text{Heat energy conducted} \times \text{Thickness}}{\text{Surface area} \times \text{Temperature difference} \times \text{Thermal conductivity}}\end{aligned}$$

However, from the definition of heat capacity:

$$
\begin{aligned}
Q &= \text{Quantity of heat energy conducted} \\
&= \text{amount of heat required to accomplish certain temperature change} \\
&= \text{Heat capacity} \times \text{Volume} \times \text{Temperature difference} \\
&= c_P \rho A L \Delta\Theta \\
\therefore T &= \frac{(c_P \rho A t \Delta\Theta)\, t}{A\Delta\Theta} \times \frac{1}{k} \qquad = \frac{c_P \rho t^2}{k} \\
&= t^2 \times \frac{1}{\text{Thermal diffusivity}}
\end{aligned}
\tag{5.4}
$$

Evaluation of time constants for our composites We now calculate the time constant (T) for the largest of samples, which should tell us whether the maximum heating rate used (two °C per minute) is viable or not. Although our samples do not consist of a single material, it is still possible to use "Time constant" to estimate the minimum time (τ) the sample requires for the whole sample to attain 1 K of change in temperature. With our sample configurations in mind, the logic dictates that with the assumption of constant $\Delta\Theta$, this minimum value will lie somewhere between the maximum time constant of all the layers and the sum of all layers' time constants. Therefore, if our heating rate has a time constant (amount of time required for a degree of temperature change) much larger than the sum of all the time constants from each layer, then we can safely assume that the heating rate does not exceed the limit posed by the effective thermal conductivity of the whole sample.

Therefore, for a laminate structure with three layers (namely layers 1, 2, and 3):
$Max(T_1, T_2, T_3) < \tau < T_1 + T_2 + T_3$ where T_i is the time constant for layer i

This means if the time constant of our heating rate is larger than $T_1+T_2+T_3$, it should be larger than τ, and hence PY coef measurement of the sample should not be affected by the heating rate. Typical values used for our sample time constant calculation:

- Thermal diffusivity of Stainless steel = 4.05 $\times 10^{-6} m^2 s^{-1}$
- ${}^{PT}c_p$ = Specific heat capacity of PZT = 420 $Jkg^{-1}K6{-}1$
- ${}^{PT}\rho$ = Density of PZT = 7.8 $\times 10^3 kgm^{-3}$
- ${}^{PT}k$ = Thermal conductivity of PZT = 1.25 $Js^{-1}m^{-1}K^{-1}$

For 2 degrees a minute heating rate, the time needed for 1 K temperature change is 30 seconds. Meanwhile, our largest sample has dimensions:

- Layer 1 : Stainless steel of thickness ${}^{St}t = 250\mu m$
- Layer 2 : PZT of thickness ${}^{PT}t = 267\mu m$
- Layer 3 : Stainless steel of thickness ${}^{St}t = 250\mu m$

$$
\begin{aligned}
T_1 = T_3 &= \frac{{}^{St}t^2}{\text{Thermal diffusivity of St}} \\
&= \frac{(250 \times 10^{-6})^2}{4.05 \times 10^{-6}} \approx 1.54 \times 10^{-4} s \\
T_2 &= \frac{{}^{PT}c_p \, {}^{PT}\rho \, {}^{PT}t^2}{{}^{PT}k} \\
&= \frac{420 \times 7.8 \times 10^3 \times (267 \times 10^{-6})^2}{1.25} \approx 1.87 \times 10^{-1} s \\
&\therefore \text{Time constant for our largest sample} \\
&= T_1 + T_2 + T_3 \quad \approx 1.87 \times 10^{-1} s \qquad \ll 30 s
\end{aligned}
$$

Therefore, the use of heating rates up to 2 degrees a minute should definitely not affect the measurements.

Consequences of various heating rates and high temperature treatment on pyroelectric coefficient

In order to corroborate the thermal diffusivity calculation results of 2 °Cmin^{-1} being low enough heating rate for the sample structures concerned and the adequacy of the pyro-rig for measuring the PY coef with such heating rates, various heating rates (0.5, 1.0, and 2.0 degrees a minute) were used on randomly selected samples to establish the indifference in PY coef measurements. Although the 'heating' rate could attain even higher values, the maximum 'cooling' rate the pyro-rig can accommodate consistently was experimentally verified to be 2.0 degrees a minute, dependent on atmospheric temperatures evidently, and therefore the heating/cooling rates higher than this were not considered.

Furthermore, it was suggested that bonding and/or testing temperatures of 80-90 degrees may de-pole the PZTs being investigated. Therefore, again on randomly selected samples, effects of reaching such temperatures were examined by measuring PY coef before and after such heat treatments.

The pre-bonded PY materials, i.e. PZT, from the samples VII_3 and VI_3 were employed to investigate the effect of heating rates, whilst that from VII_6, VI_3, and IX11 were probed for the effect of high temperature (80-90 °C) treatment:

Heating rate study As an initial pilot experiment, sample VII_3 was tested at 42-46 degrees range with two different heating rates of 0.5 and 2.0 degrees a minute, findings of which are represented in Figure 5.5(a).

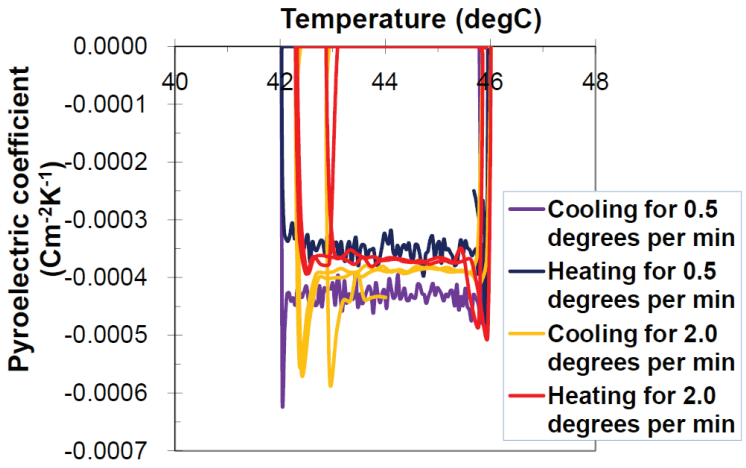

(a) PY coef of VII_3 for 0.5 and 2.0 degrees per min heating rates at 42-46 range

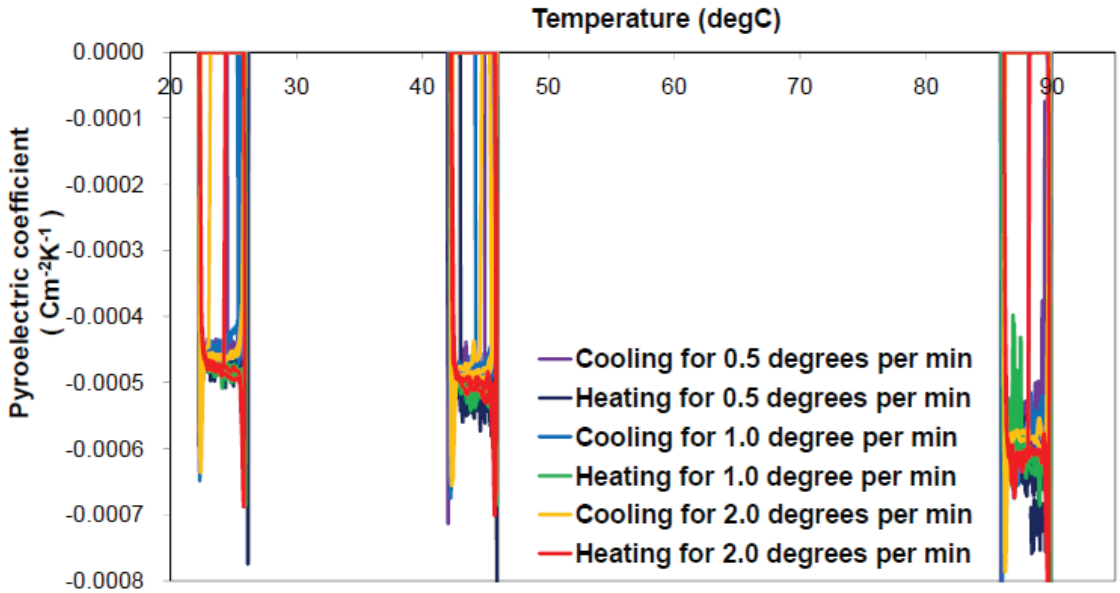

(b) PY coef of VI_3 for different heating rates at various temperature ranges

Figure 5.5: Pyroelectric coefficient enhancement in PZT/St laminates

The same overall PY coef of $-4.0 \times 10^{-4}\ Cm^{-2}K^{-1}$ was observed for both heating and cooling, although for the lower heating rate, namely 0.5 degrees a minute, the difference between heating and cooling seemed to be amplified. The exact reasons behind this phenomenon is unknown at present, but as the magnitude of this discrepancy is negligible in comparison to the scale of the total coefficient, the PY coef can be presumed to be unaltered for both heating rates.

As anticipated, the lower heating rate of 0.5 degrees a minute revealed more noise on the readings (represented on the graph as small peaks and troughs), since lower heating rate results in higher temperature resolution, leading to larger sampling rate in relation to temperature axis.

Since the testing of VII_3 (cf. Figure 5.5(a)) revealed independence of PY coef from the heating rate at a certain measuring temperature (Op. temp) range, namely 42-46 degrees, it was deemed appropriate to expand on this result and conduct further experimentation on different Op. temp ranges and heating rates. Therefore, a more comprehensive study on the heating rate and PY coef relationship was performed on VI_3.

With the purpose of concluding and summarising the findings so far on PY coef of PZTs from samples VII_3 and VI_3, and heating rates, VI_3 was subjected to an experiment with three different heating rates, i.e. 0.5, 1.0, and 2.0 degrees a minute, and three different temperature ranges, i.e. 22-26, 42-46, and 86-90 degrees. The result of this experiment is shown in Figure 5.5(b). When each temperature range is compared for different heating rates, it is clear that the range of heating rates investigated do not affect the magnitude of PY coef. For 0.5, 1.0, and 2.0 degrees a minute, the magnitude of PY coef remains unchanged at $-4.5 \times 10^{-4}\ Cm^{-2}K^{-1}$ for 22-26, $-5.0 \times 10^{-4}\ Cm^{-2}K^{-1}$ for 42-46, and $-6.0 \times 10^{-4}\ Cm^{-2}K^{-1}$ for 86-90 degrees Op. temp ranges.

After observing the apparent independence of PY coef measurements from the heating rates under 2.0 degrees a minute, it was logical to investigate the same parameters for thicker samples than just PZTs, or at least samples which have the same layered laminate structures as the aimed assembly. Hence, such samples were measured, confirming above stated independence again for samples with even higher thermal mass.

In conclusion, it was found to be safe to assume that the heating rates of up to 2.0 degrees a minute will not affect our PY coef measurements as it was first anticipated by our time constant calculations in Subsubsection 5.3.3. Therefore, 2.0 degrees a minute will be employed wherever possible in our experimentation phase, saving valuable time

without the introduction of any undesired inconsistency into our experiments.

Effect of reaching 90 degrees during PY coef measurements With the intention of scrutinising the possibility of PZT depolarisation after high temperature measurements at 86-90 degrees range, samples VII_6 and VI_3 were assessed before and after 86-90 degrees measurement. As both displayed similar behaviour, the results of this thermal fatigue assessment for sample VII_6 only are exhibited.

PY coef before and after 86-90 degrees measurement for VII_6's PZT resulted in Figure 5.6.

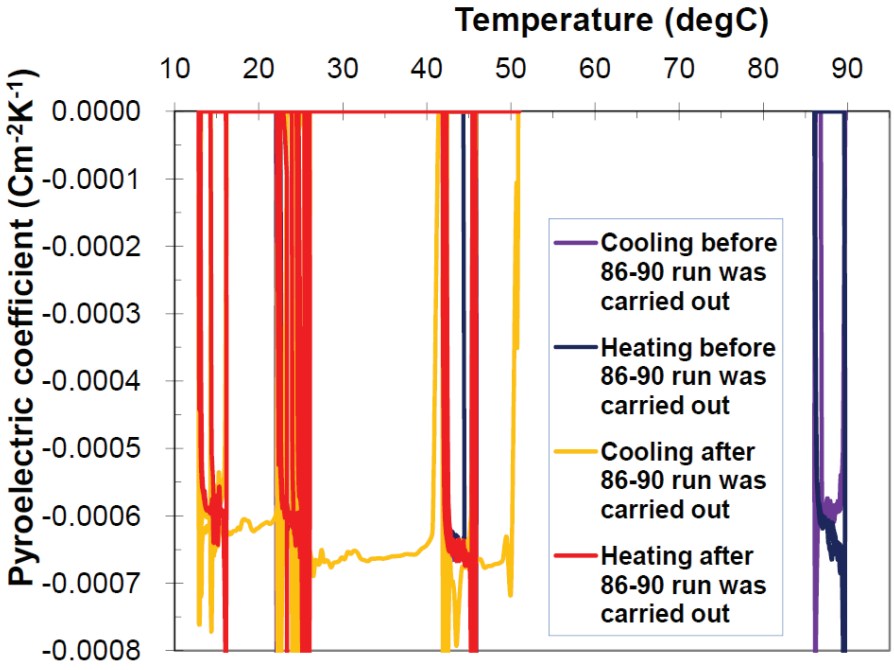

Figure 5.6: PY coef of VII_6 before and after the run on 86-90 degrees Op. temp range

From Figure 5.6, it is evident that reaching 90 degrees and testing the sample at such high temperatures do not affect the pyroelectric performance of the sample. The same PY coef was recorded for both before and after 86-90 degrees run for all investigated temperature ranges of 22-26 and 42-46 degrees at approximately $-6.0 \times 10^{-4}\ Cm^{-2}K^{-1}$ and $-6.5 \times 10^{-4}\ Cm^{-2}K^{-1}$, respectively.

In conclusion, it was found to be safe to assume that the PZT samples do not, and will not, get de-poled during the experimental runs at 86-90 degrees provided that the experiments at such temperatures do not exceed one hour. This one hour limit was imposed since all the test runs at 86-90 degrees for the experiment above were conducted

for one hour only. The effects of any such heat treatments for longer hours are not investigated since all the measurements at such temperature ranges never exceeded one hour. However, from the results of the investigation into the effects of bonding at high temperature (cf. Figure 5.7), it seems reasonable to assume that this conclusion will hold up to at least five hours. Please refer to the next section of this dissertation for further details.

Effect of bonding at high temperatures Since temperatures of around 80-90 degrees were used for bonding the samples, it could be argued that prolonged exposure, around 5 hours required for bonding for example, to such high temperatures may lead to de-poling of a PZT. Therefore, an experiment was conducted on a PZT sample, namely IX11, to validate this hypothesis one way or the other.

This experiment was conducted by:

1. Measure the PY coef of a PZT
2. Place the same exact PZT inside an oven with temperatures of 80-90 degrees Celsius with typical bonding dead weights on top
3. Measure the PY coef of the same PZT after 5 hours in the oven, henceforth referred to as "heat treatment"

The outcome of this experiment is displayed in Figure 5.7.

It is quite clear that the PZTs were not de-polarised when they underwent the heating during their bonding procedure. For both "heating" and "cooling" phase of the PY coef measurement, the PY coef remained exactly the same at around $6.0 \times 10^{-4}\ Cm^{-2}K^{-1}$ whether the measurement took place before or after prolonged heat treatment inside the oven.

Sine wave

In 1972, Hartley et al.[73] suggested a new measurement technique for PY coef using sine heating/cooling function. As our particular experimental rig permits the use of both sine and triangular function, the investigation into these two types of thermal stimuli and their effect on the measurements seemed necessary.

In order to verify whether the use of sine wave function offers any advantage over the triangular one, a sample was tested with the usual triangular wave and then with the sine

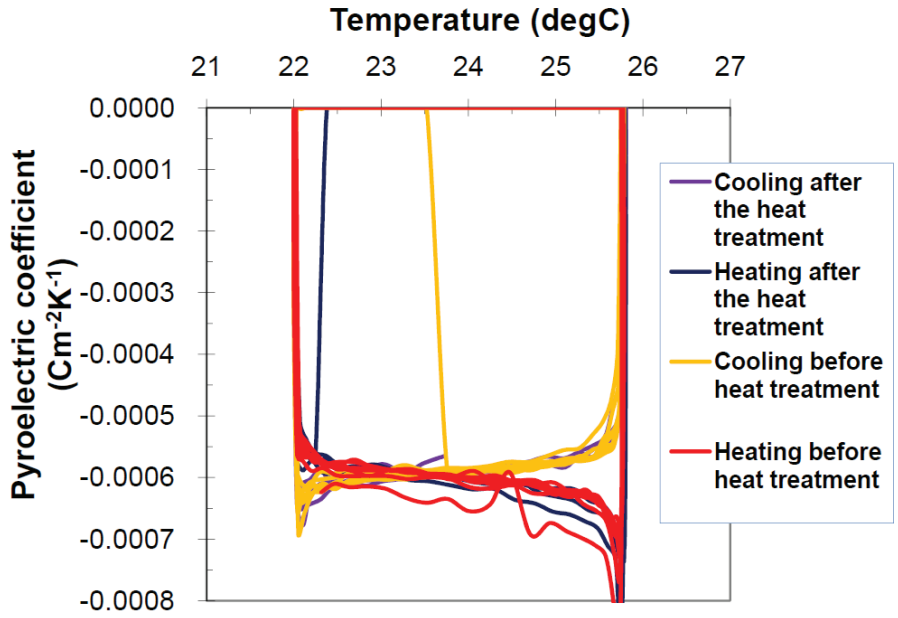

Figure 5.7: PY coef of IX11 before and after the heat treatment in the oven

wave. The investigated temperature ranges were 12-16 and 22-26 degrees for heating rate of 0.5, 1.0, and 2.0 degrees per minute. As the observation from theses tests were very similar for all these heating rates employed, only 2.0 degrees a minute will be presented in this dissertation.

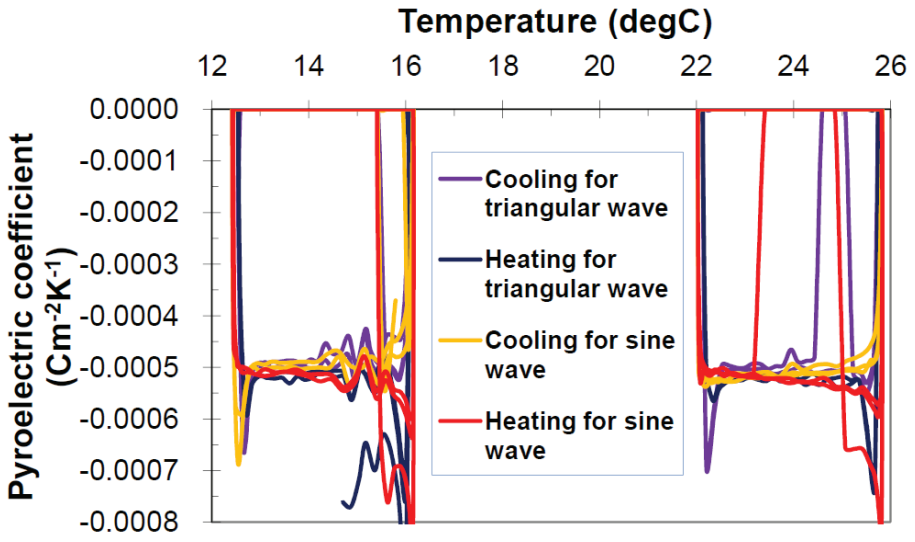

Figure 5.8: PY coef measurement with sine and triangular waves for heating rate 2.0 degrees a minute

From Figure 5.8, it is evident that although the magnitude of PY coef itself does not depend on the heating function, the trend of the coef over the given temperature range

was slightly smoother, i.e. less noise was picked up, for the case with sine wave function. However, in relation to the overall magnitude of PY current measurement, these observed discrepancies were deemed insignificant as we are mainly interested in the magnitude of the PY coef. Hence, in most cases triangular wave was used in the main experimentation phase with a number of random repetition experiments with sine waves being conducted for comparison and re-affirmation purposes.

Effect of having stainless steel, electrode or thermal paste

With and without stainless steel Prior to assuming that PY coef before and after bonding can be contrasted by comparing values between just PZT and PZT with stainless steel substrates bonded (cf. Section 5.2), it must be confirmed that having, but without being mechanically bonded, stainless steel below and above the PZT does not influence the measurements. In order to substantiate this, PZT samples VI_3, VII_3 and VII_6 were measured with and without stainless steel substrates placed, but not bonded, below and above them.

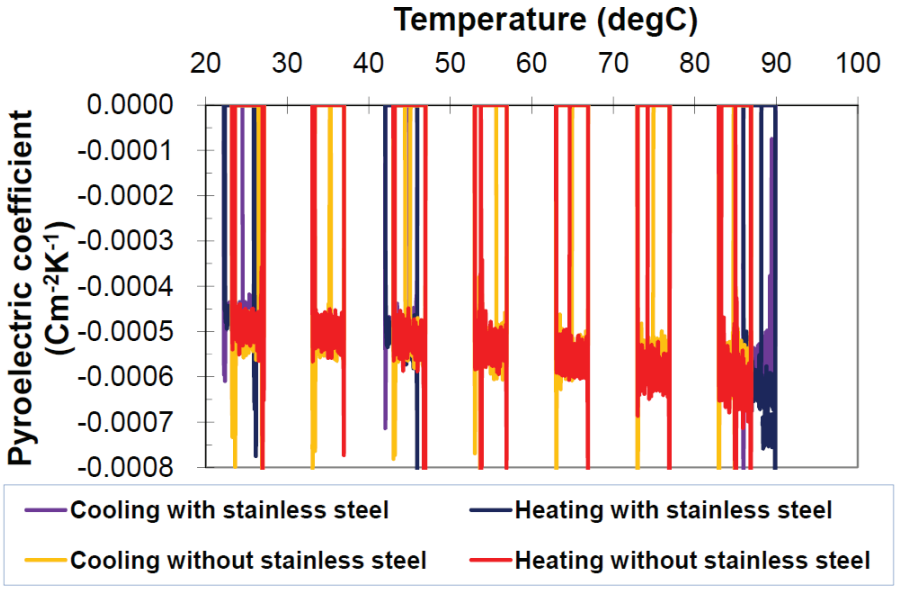

Figure 5.9: PY coef measurements of VI_3's PZT with and without stainless steel substrate

Figure 5.9, representing the PY coef measurement of VI_3's PZT with and without stainless steel, exhibits a very typical PY coef graph for all the PZT samples that were tested. PY coef, measured to be approximately $-5.0 \times 10^{-4}\ Cm^{-2}K^{-1}$ at 22-26 degrees range, increases with temperature and "cooling" leads to larger values at lower

temperature ranges than "heating" and vice versa for the higher temperature ranges.

It is clear from Figure 5.9 that having stainless steel placed, but not bonded, on top and bottom of the PZT does not significantly affect the PY coef measurements at temperature ranges 22-26, 42-46, and 86-90 degrees, which are the main ranges used for the experimentation.

In conclusion, even though the introduction of stainless steel substrates do seem to decrease the PY coef by a very small amount owing to increased thermal mass, the magnitude of this reduction suggests it can be perceived as being insignificant, less than 5 % of the overall PY coef in fact, when compared to the total value of PY coef. Therefore, it was deemed reasonable to assume that having stainless steel on PZTs' surface, again not bonded of course, does not affect the PY coef measurements significantly.

With and without electrodes attached and thermally conductive pastes used
After bonding, it was found that attaching electrodes and utilising thermally conductive, but electrically non-conductive, paste is necessary for the establishment of reasonably sufficient enough electrical and thermal contacts for two layer samples. The reason behind this is due to the curvature on their contact surface resulting from the thermal expansion coefficient mismatch, as observed in Thunder^{TM} samples.

Due to this reason, grounds for the investigation of the consequences of attaching electrodes and utilising thermally conductive pastes on PY coef measurements of three layer samples became apparent. Figure 5.10 represents measurements on a three layer structure bonded at 50 degrees, namely VII_3, before and after using electrodes and thermally conductive pastes.

Attaching electrodes and using thermally conductive paste did not change the magnitude of PY coef for three layer samples. With the use of the electrodes and thermal paste only being able to improve the PY coef measurement of our samples, it is safe to assume that for three layer samples at least not using electrodes and thermal pastes still result in sufficiently accurate values of PY coef enhancement. In addition, the lack of discrepancy between the measurements with and without thermally conductive paste demonstrates that the tertiary pyroelectric effect is not an issue in our measurement of three layer 2-2 connectivity laminate composites (cf. Subsubsection 5.3.2). This is on the contrary to two layer samples, where electrodes and thermal pastes are observed to significantly improve the PY coef measurement of such samples through establishment of better thermal and electrical contact.

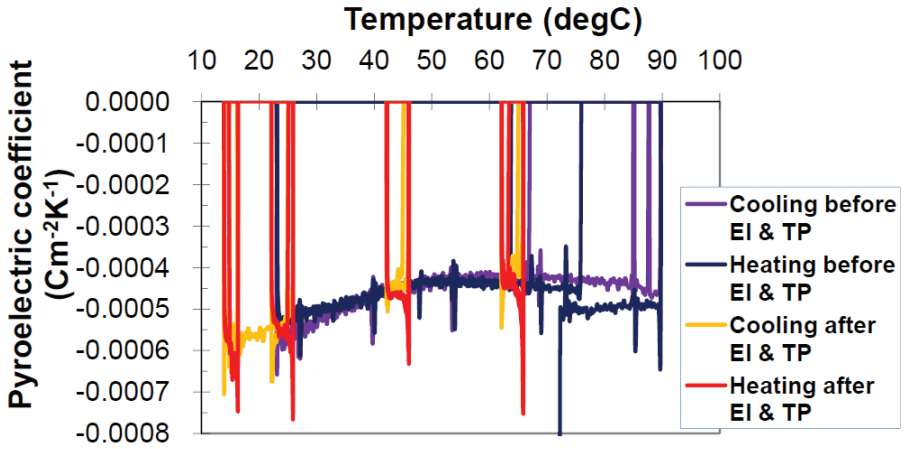

Figure 5.10: A three layer structure based on VII_3 PZT measured before and after using electrodes (El) and thermally conductive pastes (TP)

A three layer sample bonded at 50 degrees that was de-laminated after the electrodes were installed, i.e. VI_4, was tested for three different conditions, specifically before bonding, bonded but without electrodes, and bonded with electrodes but partially de-laminated. Figure 5.11 exhibits our observation on the effects of bonding, electrodes, and de-lamination on PY coef measurement.

It is clear from Figure 5.11 that quite a significant PY coef gain was achieved by bonding. Maximum gain was around $2.5 \times 10^{-4}\ Cm^{-2}K^{-1}$ (from $-5.0 \times 10^{-4}\ Cm^{-2}K^{-1}$ to $-7.5 \times 10^{-4}\ Cm^{-2}K^{-1}$). In particular, at lower temperature range, cooling produced even higher PY current than that at the highest temperature range, contrary to typical PY current trend.

Despite its extremely poor quality of bonding, illustrated by its de-lamination later on, it still achieved this enhancement which was a very promising result for us. The reasons behind this particularly good enhancement at lower temperature range may lie with its poor bonding. This lack of mechanical coupling means the strain transfer between PY and NP layers is very inefficient. However at lower temperature ranges (lower the temperature, larger the difference from curing temperature) the pre-stress (owing to strain differences) present between PY and NP layers is increased, resulting in bonding layer experiencing larger stresses which in turn increases the mechanical coupling between PY and NP layers.

Although the data collected was not entirely reliable enough due to the partial de-lamination of the sample, similar PY coef values as before the bonding were observed for

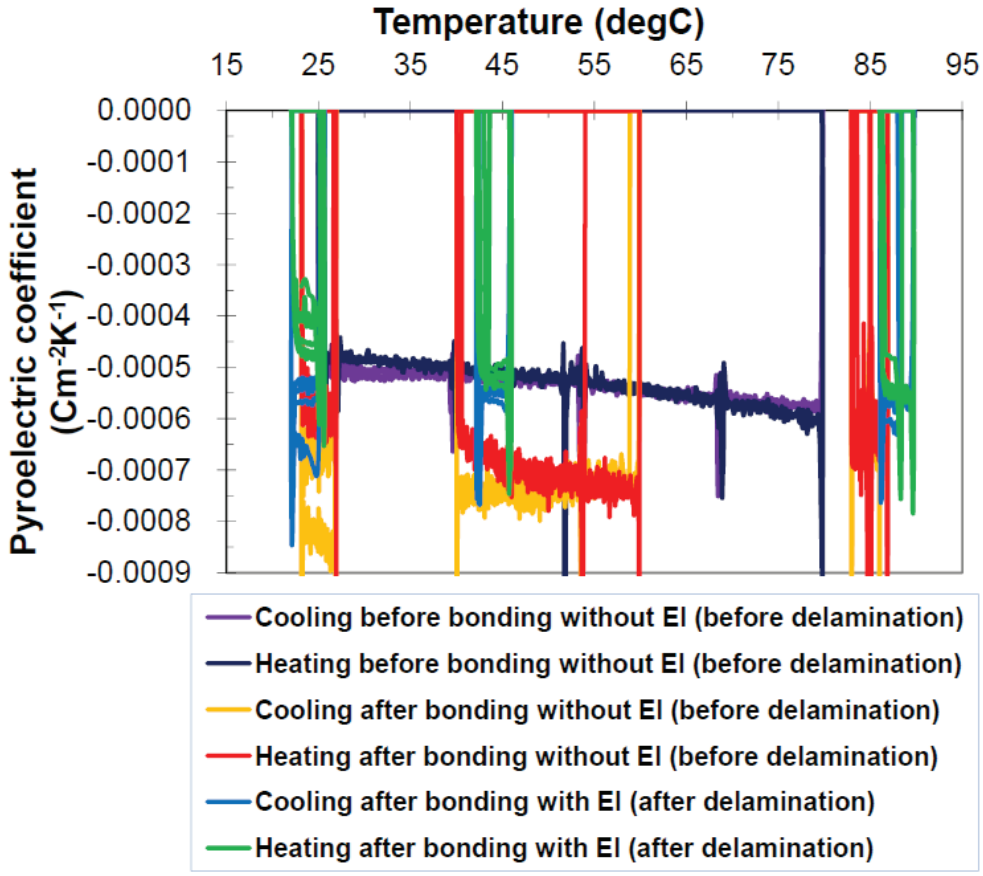

Figure 5.11: A three layer structure based on VI_4 PZT measured before and after using electrodes (El) and thermally conductive pastes (TP) and de-lamination

the delaminated sample. This also is an indicator stating that it is indeed the mechanical bonding of stainless steel onto PZT that is causing the enhancement in PY coef.

To conclude, although it was not possible to check if the PY coef of two layer laminates did alter with the attachment of electrodes and utilization of thermal paste, due to the lack of sufficient thermal and electrical contact, the experiments on three layer structures confirm that the introduction electrodes and thermal pastes do not influence the reading of PY coef in 2-2 connectivity laminate composites. Moreover, the results from partially de-laminated sample, namely VI_4, suggest that PY coef enhancement is indeed due to the mechanical bonding of PZT to a material with much higher thermal expansion coef, i.e. stainless steel substrate, since the enhancement disappears once the sample has been delaminated.

PY coef measurement of various samples and their enhancement through product property

Typical PY coef measurement results from a PZT A PZT sample, namely VI_3, has been characterised completely with repeated experiments. As expected, the difference in heating rate (between 2.0 and 0.5 degrees per minute) was not found to affect the magnitude of PY coef. Subsequent graph, namely Figure 5.12, illustrates very typical PY coef graph trends for all the PZT samples tested, albeit the magnitude of PY coef did vary between one PZT sample to another. For this particular sample, PY coef at room temperature was approximately $5.0 \times 10^{-4}\ Cm^{-2}K^{-1}$, increasing with temperature and "cooling" producing slightly larger values at lower temperature range than "heating" and vice versa for the higher temperatures.

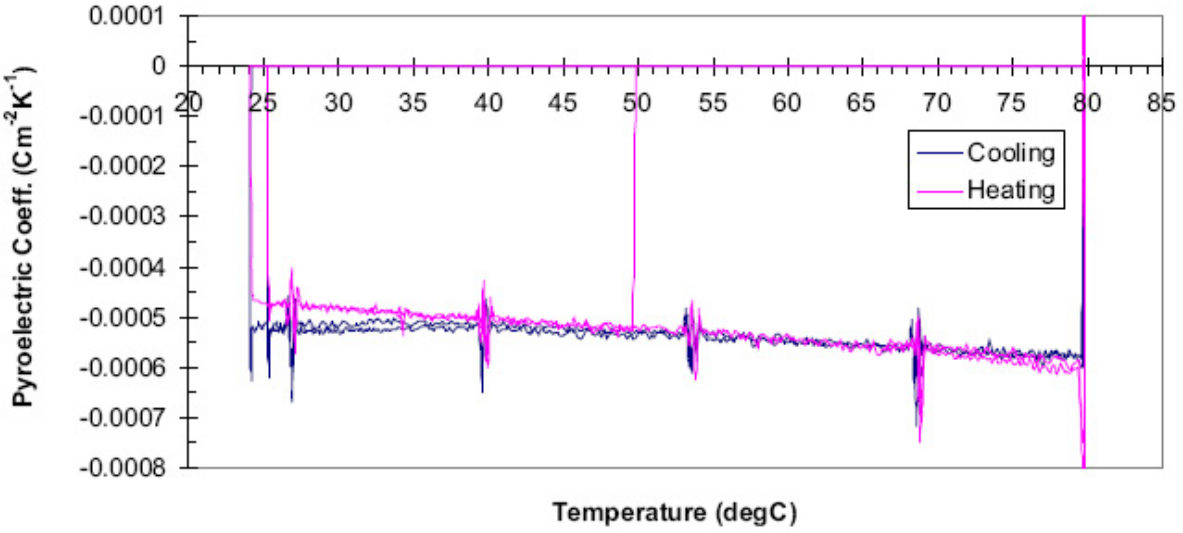

Figure 5.12: PY coef of VI_3 between 22-80 °C (Typical PY coef measurement of a PZT sample)

Comparison between before and after bonding for various samples - PZT thickness and bonding layer thickness varied Now we move on to comparing the PY coefs before and after bonding the samples. Please note that from the study on the effect of having not-bonded stainless steel substrates placed on the PZTs, it was shown that the PZT sample's performance is slightly better when no stainless steel is used in the test, although the difference is deemed to be insignificant when compared to the total PY coef. Hence, to confirm an improvement only the measurements between just PZT and the bonded sample needs to be considered. For this reason, the experimentation consisted

of more than 20 PZT samples being tested and bonded then tested again. However, only 11 of these 20 samples resulted in successful, if not partially successful, bonding and hence meaningful comparisons during the preliminary experimentation phase. Following summarizes the findings from these experiments:

VI_4 is a three layer sample bonded at 50 °C that was the first specimen to successfully demonstrate the PY coef enhancement. Quite a significant PY coef gain was achieved by bonding with maximum gain of approximately 2.5 $\times$ 10^{-4} $Cm^{-2}K^{-1}$, equivalent to around 50 % increase, at room temperature.

In order to investigate the effect of using thicker PZT, i.e. 267 μm, in a three layer structure, IX5 was fabricated by sandwiching a 267 micron PZT between two 50 μm stainless steels with Epotek 301-2 using bonding temperatures of 80-90 °C. Please note that this is exactly the same configuration as VII_6 except the thickness of PZT being larger.

Table 5.6: Comparison between VII_6 and IX5 for determining the effect of PZT thickness

Name	PY material thickness	PY coef gain for the temperature range		
		22-26 °C	42-46 °C	86-90 °C
VII_6	127 μm PZT-5H	1.75 (+41.2%)	2.1 (+47.7%)	0.7 (+13.2%)
IX5	267 μm PZT-5H	1.8 (+41.9%)	1.8 (+38.3%)	0.4 (+7.1%)

Units: $\times$ 10^{-4} $Cm^{-2}K^{-1}$

When the data in Table 5.6 are compared without considering the bonding temperature (i.e. the best comparison can be made at the bonding temperature when there should not be any residual stress present), it is easy to see that although the numerical values of the enhancement do not match, both the theory and experimental data agree that the PY coef enhancement is smaller for thicker PZT samples, i.e. in IX5. This is because less strain is experienced by the PY material if it is thicker, and the enhancement in secondary PY coef depends on this strain as it is essentially a piezoelectric effect.

As the residual stress is increased, i.e. temperature was lowered away from the bonding temperature, the enhancement improves for both thin and thick samples. This may be due to the damping effect of thick layer of adhesive (Epotek 301-2) being overcome by large strain produced by stainless steel (which in effect leads to thinner bonding layer) or the residual stresses affecting the pyroelectric and piezoelectric performance of the PZT.

Further experiments are conducted on this issue as demonstrated in Section 6.1.

IX6 sample has the exact same configuration as IX5 but instead of Epotek 301-2, WLK30 epoxy was used to investigate the effect of thick adhesive layer (Please note that WLK30 has much higher viscosity than Epotek 301-2, resulting in thicker bonding layer when applied).

Table 5.7: Comparison between IX5 and IX6 with different adhesives and bonding layer thicknesses

Name	Epoxy used	PY coefficient gain for the temperature range				
		12-16 °C	22-26 °C	42-46 °C	62-66 °C	86-90 °C
IX5	Epotek 301-2 (Thinner bonding layer)	1.75 (+41.2%)	1.8 (+41.9%)	1.8 (+38.3%)	1.75 (+35.0%)	0.4 (+7.1%)
IX6	WLK30 (Thicker bonding layer)	1.5 (+33.3%)	0.8 (+17.0%)	0.3 (+6.0%)	0.45 (+8.5%)	0.4 (+6.7%)

Units: $\times 10^{-4}\ Cm^{-2}K^{-1}$

Table 5.7 compares the two samples with different epoxies, i.e. thickness of bonding layers. As expected, IX6 with thicker bonding layer experienced much less PY coef enhancement until very low temperatures are reached. At such low temperature range, due to large temperature, and hence thermal expansion, difference from the bonding/curing temperature (around 80-90 °C), the strain produced by stainless steel start to overcome the damping effect of the thick interface, leading to amply large improvement in PY coef. Therefore it would be reasonable to hypothesize that if the thinnest possible bonding layer is achieved, one should expect to observe the maximum enhancement by reducing such damping effects. One method of obtaining such interface would be to use optimal conditions of epoxy bonding process quoted in Subsubsection 5.1.1.

Chapter 6

Results and discussion - Pyroelectric coefficient enhancement

Two sections make up this chapter. Section 6.1 presents the experimental results from the Curing temperature study and the derivation/analysis of the mathematical expression for pre-stresses parallel to all three axes. The outcomes from this section determined Cur and Op. temps to be employed in the Enhancement study, the results of which are presented in Section 6.2. Pyroelectric coefficient enhancement potentials of various PY-NP pairs will be also discussed and analyzed in this section.

6.1 Curing and operating temperature variation and the effect of pre-stress

6.1.1 Curing temperature study results

After the comparison between PY coef enhancements in IX5 and IX6 samples in Subsubsection 5.3.3, it was clear that the potential impact of the epoxy layer's thickness and the temperature difference between the operating and curing temperatures on the overall PY coef enhancement must be assessed. Hence, various samples with the same thickness ratio of R = 0.254 (127 μm PZT-5H sandwiched between two 250 μm St) were created using various curing temperatures while all the other bonding conditions were kept the same (cf. Subsubsection 5.1.1 for other bonding conditions and Subsection 5.2.1 for the experiment methodology). Figure 6.1 displays the findings of this investigation.

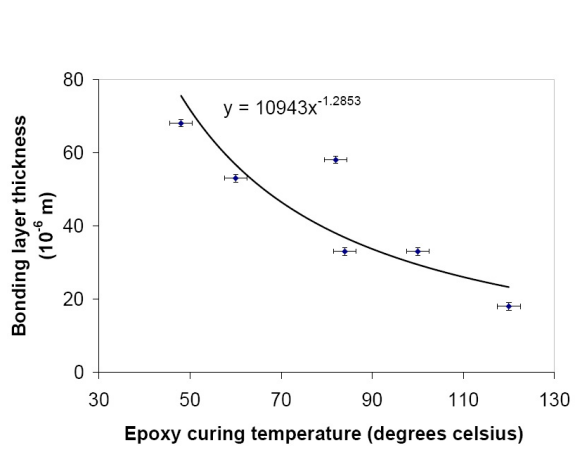

(a) Epoxy curing temperature and bonding layer thickness achieved

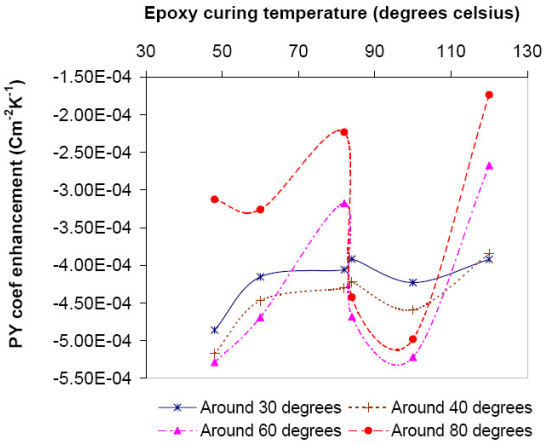

(b) Curing temperature and its affect on PY coef enhancements

Figure 6.1: Epoxy curing temperatures and their effect on the bonding layer thickness and PY coef enhancements

It must be noted that it seems quite plausible that the two parameters, epoxy layer thickness and curing temperature, may well not be independent of each other provided the same epoxy and all the other bonding conditions are used for the curing process. Hence the created samples' bonding layer thicknesses were measured at room temperature (25 °C) with a micro-meter, the summary of which is depicted in Figure 6.1(a). All the bonding layer thicknesses in Figure 6.1(a), except the one cured at 82 °C, supports the idea that there is an inversely proportional relationship between the epoxy curing temperature and bonding layer thickness achieved after the curing process. This complements well with us attributing the IX5 and IX6 samples' PY coef exhibiting higher enhancement at lower measuring temperature range, i.e. ranges with larger difference between the curing and Op. temp, to the increased residual stress (pre-stress) reducing the damping effects from the thick epoxy layer by effectively decreasing its thickness (cf. Subsubsection 5.3.3).

Figure 6.1(b) demonstrates the measured PY coef enhancement for the samples created at various curing temperatures, with the measurement taking place at around 30, 40, 60, and 80 °C. It is rather difficult to see any trend from this figure due to the unexpectedly low enhancement from the sample cured at 82 °C resulting from its uncharacteristically thick bonding layer. Therefore, the bonding achieved by curing the epoxy at 82 °C was deemed an anomaly and henceforth the result from this sample is ignored.

6.1.2 Mathematical model for Pre-stress

Before analyzing the results from the Curing temperature study in more detail, the author would first like to derive an expression for the Pre-stress our samples are expected to experience due to the temperature difference between the Op. and Cur temps. By evaluating this stress value for samples, created at 120 °C being measured at Op. temp of around 30 °C, should give us an indication of what kind of pre-stress levels these samples undergo when they are fabricated and then measured.

Please note that following derivation process can be used for evaluating stresses under OC as well, although some of the assumed symmetry, such as ${}^{PY}\alpha = {}^{PY}\alpha_j \qquad \forall j = 1..3$, can not hold for j=3 under OC due to highly anisotropic behaviour of thermal expansion coefficients under OC as illustrated in Chapter 8. As the author intends to use this stress expression for assessing our experimental samples, only the derivation for SC will be provided in this treatise.

Now to the derivation. From Eq 3.7:

$$\begin{aligned}
\Rightarrow \quad dS_{ij} &= \left(\frac{\partial S_{ij}}{\partial T_{kl}}\right)_{E,\Theta} dT_{kl} + \left(\frac{\partial S_{ij}}{\partial \Theta}\right)_{T,E} d\Theta \\
\Rightarrow \quad dT_{kl} &= \left(\frac{\partial S_{ij}}{\partial T_{kl}}\right)^{-1}_{E,\Theta} \left[dS_{ij} - \left(\frac{\partial S_{ij}}{\partial \Theta}\right)_{T,E} d\Theta\right] \\
&= (s^{E,\Theta}_{ijkl})^{-1} \left\{dS_{ij} - \alpha^{T,E}_{ij} d\Theta\right\} \\
&= c^{E,\Theta}_{ijkl} \left\{dS_{ij} - \alpha^{T,E}_{ij} d\Theta\right\} \qquad \forall i,j,k,l = 1..3 \\
\therefore \quad dT_k &= c^{E,\Theta}_{ik} \left\{dS_i - \alpha^{T,E}_{i} d\Theta\right\} \qquad \forall i,k = 1..6
\end{aligned} \tag{6.1}$$

From PZT's symmetry (cf. Subsubsection 3.4.1) and Eqs 3.26 and 3.27; ${}^{PY}S_1 = {}^{PY}S_2$ and ${}^{PY}S_3 = 2\Lambda\,{}^{PY}S_1$ where $\Lambda = \dfrac{s_{13}\left(c_{11}+c_{12}\right)}{1-2s_{13}c_{13}}$. But from Eq 3.24 we know that (let $c^{E,\Theta}_{ik} = c_{ik}$ and $\alpha^{T,E}_i = \alpha_i$):

$$\begin{aligned}
dS_i &= \left({}^{PY}S_i + 1\right)\left(1 + {}^{PY}\alpha_i d\Theta\right) - 1 \\
&= {}^{PY}S_i\left(1 + {}^{PY}\alpha_i d\Theta\right) + {}^{PY}\alpha_i d\Theta \qquad \forall i = 1..2
\end{aligned}$$

and

$$\begin{aligned}
dS_3 &= \left({}^{PY}S_3 + 1\right)\left(1 + {}^{PY}\alpha_3 d\Theta\right) - 1 \quad = \left(2\Lambda\,{}^{PY}S_1 + 1\right)\left(1 + {}^{PY}\alpha_3 d\Theta\right) - 1 \\
&= 2\Lambda\,{}^{PY}S_1\left(1 + {}^{PY}\alpha_3 d\Theta\right) + {}^{PY}\alpha_3 d\Theta
\end{aligned} \tag{6.2}$$

Since $dT_m = 0$ and $dS_m = 0\ \forall m = 4..6$ under the plane stress condition with negligible shear stress, and from Eqs 6.1 and 6.2 (let ${}^{PY}S_i = S_i$):

$$\begin{aligned}
\Rightarrow \qquad dT_k &= \sum_{i=1}^{3} c_{ik} \left\{ dS_i - {}^{PY}\alpha_i d\Theta \right\} \qquad \forall k = 1..3 \\
&= (c_{1k} + c_{2k}) \left\{ dS_1 - {}^{PY}\alpha_1 d\Theta \right\} + c_{3k} \left\{ dS_3 - {}^{PY}\alpha_3 d\Theta \right\} \\
&\qquad\qquad \because {}^{PY}\alpha_1 = {}^{PY}\alpha_2 \text{ and } dS_1 = dS_2 \\
&= (c_{1k} + c_{2k})\, S_1 \left(1 + {}^{PY}\alpha_1 d\Theta\right) + c_{3k} 2\Lambda S_1 \left(1 + {}^{PY}\alpha_3 d\Theta\right) \\
&= S_1 \left\{ (c_{1k} + c_{2k}) \left(1 + {}^{PY}\alpha_1 d\Theta\right) + 2\Lambda c_{3k} \left(1 + {}^{PY}\alpha_3 d\Theta\right) \right\} \qquad \text{where } k = 1..3
\end{aligned} \tag{6.3}$$

Assuming $c_{11} = c_{22}$, $c_{12} = c_{21}$, and $c_{13} = c_{31} = c_{23} = c_{32}$ from PZT's symmetry and noting the strain expression in Eq 3.27, for $k = 1..2$:

$$\begin{aligned}
\Rightarrow \qquad dT_k &= S_1 \left\{ (c_{11} + c_{12}) \left(1 + {}^{PY}\alpha_1 d\Theta\right) + \frac{2s_{13}\,(c_{11} + c_1 2)}{1 - 2s_{13}c_{13}} c_{13} \left(1 + {}^{PY}\alpha_3 d\Theta\right) \right\} \\
&= S_1\,(c_{11} + c_{12}) \left[\left(1 + {}^{PY}\alpha_1 d\Theta\right) + \frac{2s_{13}c_{13} \left(1 + {}^{PY}\alpha_3 d\Theta\right)}{1 - 2s_{13}c_{13}} \right] \\
&= (c_{11} + c_{12}) \left(1 + {}^{PY}\alpha d\Theta\right) \left[1 + \frac{2s_{13}c_{13}}{1 - 2s_{13}c_{13}} \right] S_1 \\
&\qquad\qquad \text{provided for PZT under SC } {}^{PY}\alpha_1 = {}^{PY}\alpha_3 = {}^{PY}\alpha \\
&= \frac{c_{11} + c_{12}}{1 - 2s_{13}c_{13}} \left(1 + {}^{PY}\alpha d\Theta\right) S_1 \\
&= \frac{c_{11} + c_{12}}{1 - 2s_{13}c_{13}} \left(1 + {}^{PY}\alpha d\Theta\right) \\
&\qquad \times \frac{Y\,(1 - 2s_{13}c_{13}) \left({}^{NP}\alpha - {}^{PY}\alpha\right) d\Theta}{(1 - \nu)\,(c_{11} + c_{12})\,(1 + {}^{NP}\alpha d\Theta)\,R + Y\,(1 - 2s_{13}c_{13})\,(1 + {}^{PY}\alpha d\Theta)} \\
&= \frac{Y\,(c_{11} + c_{12}) \left(1 + {}^{PY}\alpha d\Theta\right) \left({}^{NP}\alpha - {}^{PY}\alpha\right) d\Theta}{(1 - \nu)\,(c_{11} + c_{12})\,(1 + {}^{NP}\alpha d\Theta)\,R + Y\,(1 - 2s_{13}c_{13})\,(1 + {}^{PY}\alpha d\Theta)}
\end{aligned} \tag{6.4}$$

In addition, from Eq 6.3:

$$
\begin{aligned}
\Rightarrow \qquad dT_3 &= S_1 \left\{ (c_{13} + c_{23}) \left(1 + {}^{PY}\alpha d\Theta\right) + 2\Lambda c_{33} \left(1 + {}^{PY}\alpha d\Theta\right) \right\} \\
&= S_1 \left\{ 2c_{13} \left(1 + {}^{PY}\alpha d\Theta\right) + \frac{2c_{33}s_{13}\left(c_{11} + c_{12}\right)}{1 - 2s_{13}c_{13}} \left(1 + {}^{PY}\alpha d\Theta\right) \right\} \\
&= 2\left(1 + {}^{PY}\alpha d\Theta\right) \left\{ c_{13} + \frac{c_{33}s_{13}\left(c_{11} + c_{12}\right)}{1 - 2s_{13}c_{13}} \right\} S_1 \\
&= 2\left(1 + {}^{PY}\alpha d\Theta\right) \left[\frac{c_{13} - s_{13}\left\{2c_{13}^2 - c_{33}\left(c_{11} + c_{12}\right)\right\}}{1 - 2s_{13}c_{13}} \right] S_1 \\
&= \frac{2Y\left[c_{13} - s_{13}\left\{2c_{13}^2 - c_{33}\left(c_{11} + c_{12}\right)\right\}\right]\left(1 + {}^{PY}\alpha d\Theta\right)\left({}^{NP}\alpha - {}^{PY}\alpha\right) d\Theta}{\left(1 - \nu\right)\left(c_{11} + c_{12}\right)\left(1 + {}^{NP}\alpha d\Theta\right) R + Y\left(1 - 2s_{13}c_{13}\right)\left(1 + {}^{PY}\alpha d\Theta\right)}
\end{aligned}
\tag{6.5}
$$

Using expressions in Eqs 6.4 and 6.5, one can estimate the amount of pre-stress a sample might experience when it is brought down from Cur temp to Op. temp or atmospheric temperature by setting $d\Theta$ = Op. temp - Cur temp. Figure 6.2 exhibits these pre-stress values. For example, "-90 degrees" graph represents the pre-stress levels of a sample fabricated at Cur temp of 120 °C that is being measured at Op. temp of 25-35, i.e. ≈ 30 °C.

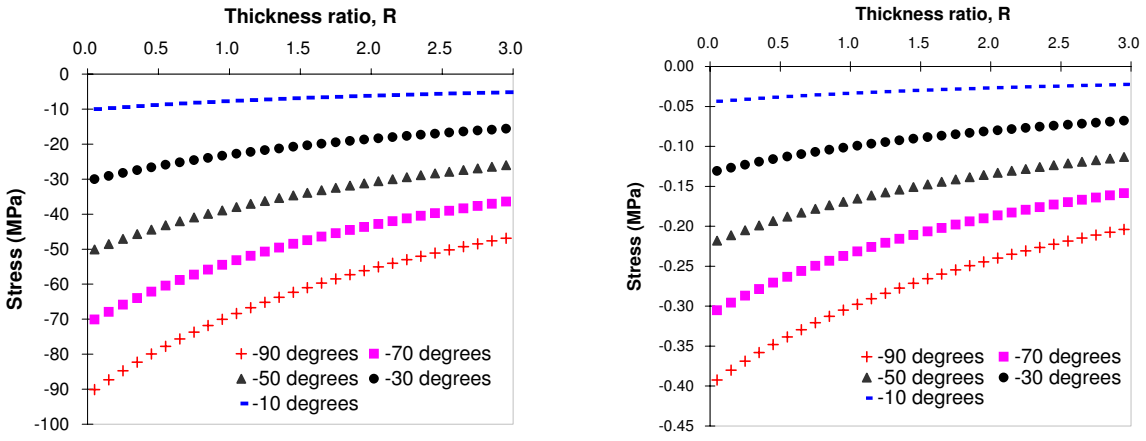

(a) Pre-stress parallel to 1 & 2 axes with Op.-Cur temp difference of -10, -30, -50, -70, and -90 °C

(b) Pre-stress parallel to 3 axis with Op.-Cur temp difference of -10, -30, -50, -70, and -90 °C

Figure 6.2: Pre-stress estimates for various 2-2 connectivity laminate composites

As one would expect, increasing thickness ratio (R) leads to reduced pre-stress since thicker PZTs bonded to thinner St will result in less stress/strain being experted/experienced on/by the PZTs. The Planar pre-stresses (pre-stress parallel to 1 and 2 axes) are found

to be over two orders of magnitude larger than the Normal pre-stress (pre-stress parallel to 3 axis), which may be due to the fact that it is these Planar stresses that causes the Normal pre-stress via Poisson effect.

The samples bonded at 120 °C being measured at 25-35 °C temperature range with $R = 0.254$ have estimated Planar pre-stress of -85 MPa and Normal pre-stress of -0.37 MPa. Although the former is well above 25-30 MPa uniaxial compressive stress range quoted by Zhou et al.[201], the latter is well below it. This may suggest that the effect of Normal pre-stress on the piezoelectric activity, i.e. secondary pyroelectric effect, would be very limited. However, despite it not being an uniaxial stress, there is a very good chance that Planar pre-stress may also reduce the secondary pyroelectric effect in samples bonded at very high Cur temps. In fact, Figure 6.3 seems to support this. Hence, there is a balance to be struck, between high Cur temps achieving thin bonding layers as seen in Figure 6.1(a), which should improve the interfacial transfer of stress St produces, and lower Cur temps reducing the potential impairment of our PZT's piezoelectric ability by creating large Planar pre-stress.

6.1.3 Curing temperature study revisited

Armed with pre-stress evaluations from before, the author will now attempt to draw some conclusions from the Curing temperature study results in Subsection 6.1.1, which should help with the choice of Cur and Op. temps to be used in the Enhancement study, minimising potential impact on enhancement measurements from pre-stress. Figure 6.3 displays the Curing temperature study results with anomaly removed.

With the "anomaly" removed from Figure 6.1, the PY coef enhancement and epoxy curing temperature and Op. temp can be plotted against, which resulted in Figure 6.3. Please note that the error bars have been removed as PY coef enhancement values have very small error owing to Keithley's excellent accuracy and the temperature values have the same error margin as those presented in Figure 6.1.

It is very difficult to draw any conclusion from Figures 6.3(a) and 6.3(b) except that samples cured at 120 °C shows the lowest PY coef enhancement for all Op. temps, which is even more prominently visible in Figure 6.3(c). Most of the samples, however, demonstrated minimum PY coef enhancement when their estimated Planar pre-stress was higher than that at maximum PY coef enhancement, insinuating that Planar pre-stress indeed plays a role in determining the effectiveness of the secondary PY effect.

On the other hand, Figures 6.3(c) and 6.3(d) depict a much clearer picture. Samples with Cur temp of 48/60, 84/100, and 120 °C behave all differently to increasing Op. temp. 48/60 pair both have maximum PY coef enhancement at Op. temp of around 55 °C, i.e. when pre-stress introduced is around 5-10 MPa, while 80 °C Op. temp (around 20-30 MPa Planar stress) reduces the enhancement quite drastically. Similar, but slightly shifted, trend is visible with 84/100 pair as well, with maximum enhancement at around 60 °C corresponding to about 20-40MPa (although the author suspects that had the Op. temp of 70 °C investigated, this would have shown even higher value) and minimum enhancement expected to occur at Op. temps above 80 °C, which is outside our experimental kit's range. However, 84/100 pair also had a minimum at Op. temp of 30 °C, which corresponds to about 50-70 MPa of Planar pre-stress.

However, the samples fabricated at 120 °C behaved very differently from these two pairs. Its PY coef enhancement peaked at Op. temp of 30 °C, which corresponds to around 90 MPa of Planar pre-stress, and decreased drastically as the Op. temp is increased, i.e. Planar pre-stress is decreased. This is the opposite effect of Planar pre-stress from the other two pairs and at present the author does not have a definitive explanation

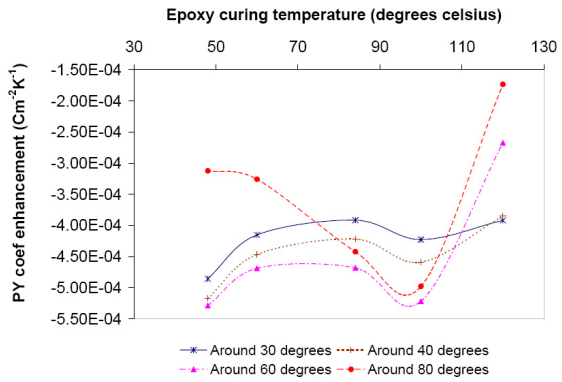

(a) Curing temperatures and their effect on PY coef enhancement for measurements taken at various temperature

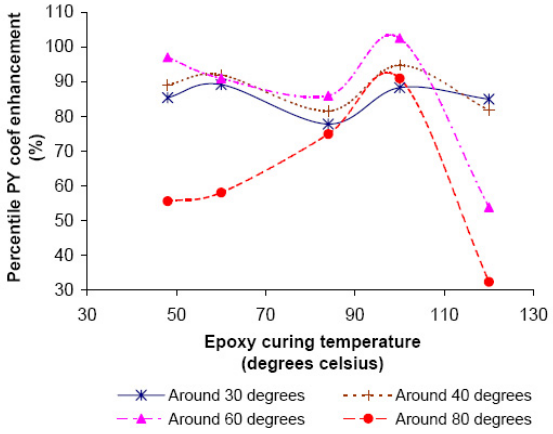

(b) Curing temperatures and their effect on Percentile PY coef enhancement for measurements taken at various temperatures

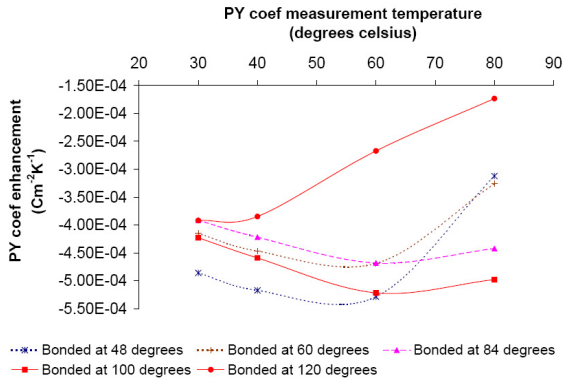

(c) The effect of PY coef Op. temp ranges on its enhancement for samples created at various curing temperatures

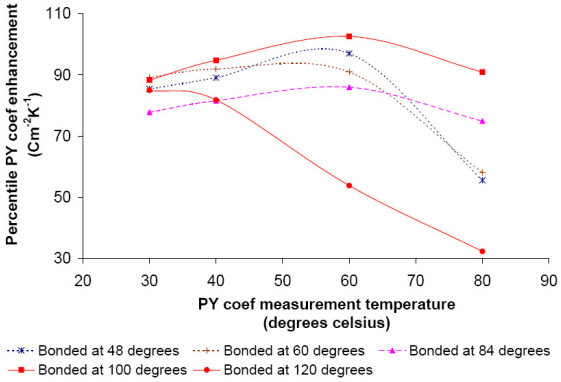

(d) The effect of PY coef Op. temp ranges on its Percentile enhancement for samples created at various curing temperatures

Figure 6.3: PY coef Op. temp ranges and its effect on PY coef enhancement for various samples fabricated at different curing temperatures

for this. It may well be that both samples created at 120 °C having such thin bonding layer (cf. Figure 6.1(a)) lead to partial bonding failures at later measurements at high Op. temps, which was supported by later repeated experiments showing reduced PY coef enhancement at lower Op. temp ranges. However, the PY coef enhancement observed in the repeated experiment was as high as that observed at high Op. temp measurements in the initial experiment, which seems to suggest that there is something more than just bonding layer failure/re-adjustment going on.

In addition, Figure 6.2 suggests samples bonded at 100 °C being measured at 25-35 °C temperature range with $R = 0.254$ have estimated Planar pre-stress of around -66 MPa and Normal pre-stress of about -0.29 MPa. However, from Figures 6.3(a) and 6.3(b) it is clear that Op. temp of 30 and 40 °C resulted in the most stable PY coef enhancement values for all the samples cured at temperatures between 48-120 °C. Hence this Op. temp will be used for the planned Enhancement study outlined in Subsection 5.2.2, i.e. Op. temp of 25-35 °C, while bonding temperature of around 100 °C will also be used since Figures 6.3(c) and 6.3(d) hints to the samples cured at this temperature as being the most consistent performer for the various Op. temps considered, i.e. most promising at being independent of the effects of pre-stress. The large temperature difference between the curing and Op. temps means we can also minimize the effect of the epoxy layer's thickness. Employing these conditions should ensure the uniqueness of our Enhancement study's dependence on the thickness ratios of our samples.

6.2 Pyroelectric coefficient enhancement study

The results from the preliminary experiments and Section 6.1 means we can now investigate the effect of the thickness ratio ($R = \frac{^{PY}t}{^{NP}t}$) on PY coef enhancement with all possible discrepancies from the other potential sources of error assumed negligible. This section will first comment on the enhancement potentials of various pyroelectric-non-pyroelectric pairs, followed by the presentation of the Enhancement study experimental results, comparing those with the theoretical expectations from the mathematical models developed in Chapter 3.

6.2.1 Enhancement potentials of various pyroelectric and non-pyroelectric pairs

The theoretical models developed in Sections 3.2 and 3.4 are used to evaluate the PY coef enhancement potentials of the 2-2 connectivity laminate composites of various PY-NP pairs. Although the author has investigated all thirty-six possible pairs of PY-NP laminate composites, in this dissertation only the ones with the most promising results in PY coef enhancement are presented. PY materials such as LTO and LNO both have dc1, dc2, and dc3 of the same sign (cf. Table B.3), implying that the enhancement available in these materials would be rather limited due to the cancellation owing to conflicting alteration in the strains corresponding to 1- and 2- axes and 3-axis from Poisson effect. In fact, LTO and LNO displayed relatively small enhancement with similar trends to that of BTO, and hence the results of LTO and LNO are omitted. In addition, similar argument also applies to PZT-5A, which exhibited similar enhancement behavior to that of PZT-5H. Where NP materials are concerned, in almost all the simulations Zn outperformed Al when it comes to the enhancement. However, since their difference is quite consistent throughout our investigative thickness range, the pairs with Al are only presented where appropriate. Some of the more interesting theoretical PY coefs of 2-2 connectivity PY-NP laminate composites are depicted in Figure 6.4.

PZT-5H

PZT-5H's PY coef enhancement potential with various NP materials are presented in Figure 6.4(a). It portrays the extreme PY coef enhancement of PZT-5H with CPVC at low R values (R<0.15), while at higher R values Al out-performs CPVC largely due to the much smaller Young's modulus of CPVC. However, it is quite clear that with Al or CPVC,

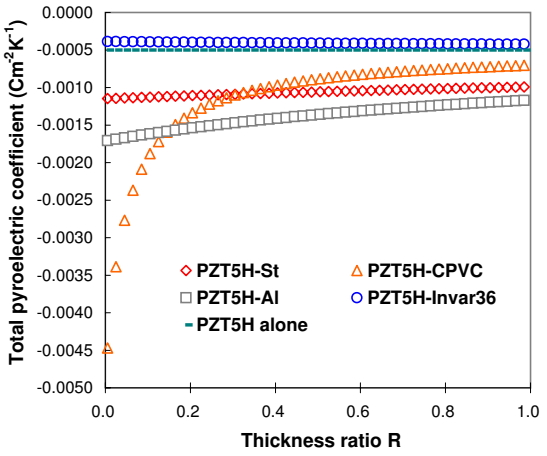

(a) Total pyroelectric coefficient versus R for PZT-5H pairs

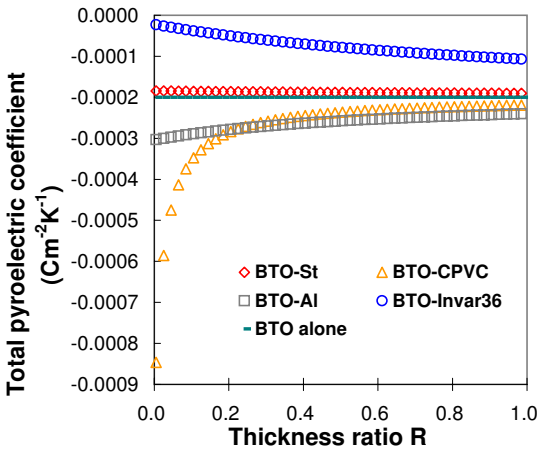

(b) Total PY coef vs R for BTO pairs

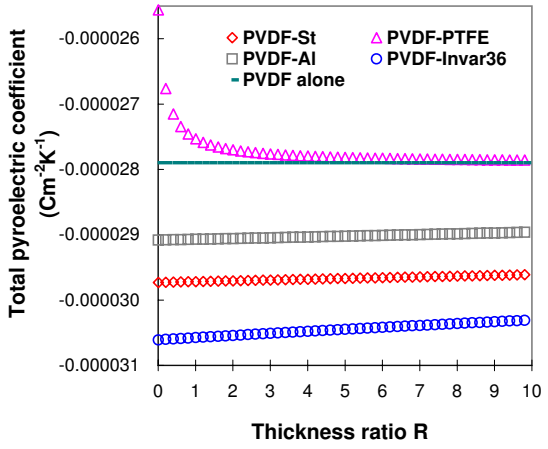

(c) Total PY coef vs R for PVDF pairs

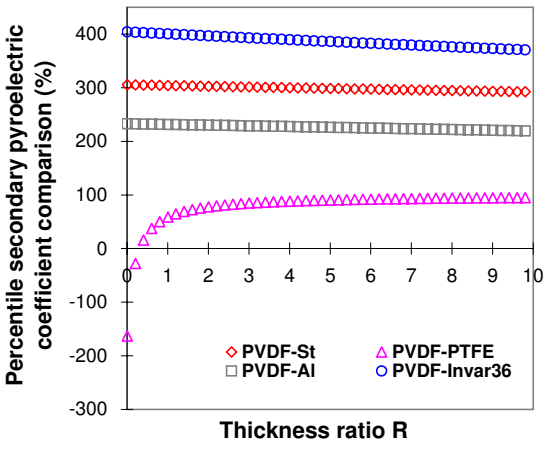

(d) Percentile secondary contribution from NP material versus R for PVDF pairs

Figure 6.4: Pyroelectric coefficient enhancements under short circuit condition in 2-2 connectivity PY-NP laminate composites vs thickness ratios (R)

one should expect to see much higher PY coef enhancement than the one we observed with St (cf. Eq 3.29) owing to their superior thermal expansion coefficients as illustrated in Table A.4. PZT5H-Al pair has the PY coef of $-0.5\times10^{-3}-\frac{66\times10^5}{55\times10^8+(45\times10^8)\times R}\ Cm^{-2}K^{-1}$ and PZT5H-CPVC's is $-0.5\times10^{-3}-\frac{94\times10^4}{22\times10^7+(45\times10^8)\times R}\ Cm^{-2}K^{-1}$. At R=0.15, the PY coef is approximately $-16\times10^{-4}\ Cm^{-2}K^{-1}$ for both pairs while at R=0.005 PZT5H-CPVC pair exhibits the maximum PY coef of $-45\times10^{-4}\ Cm^{-2}K^{-1}$. This value at R=0.005 is for the ideal case where there exists no loss at the interfacial layer, which in

reality is difficult to achieve. This is the reason behind the development of PY coef with k-factors (cf. Subsubsection 3.4.2), the results of which will be presented in relation to the experimental data with PZT5H-St pair in Subsection 6.2.2. However, this enhancement at R=0.005 for PZT5H-CPVC pair demonstrates the magnitude of enhancement potential in PZT-5H since its PY coef without enhancement is only $-5.0 \times 10^{-4}\ Cm^{-2}K^{-1}$ as illustrated in Table A.1, in other words theoretically around 800% increase in PY coef is possible.

BTO

Figure 6.4(b) describes largely subdued enhancement for BTO due to relatively small dc1, dc2, and dc3 values when compared to that of PZT-5H. However, BTO-CPVC displays rather high enhancement for small thickness ratios of R<0.1 with a peak of $-8.5 \times 10^{-4}\ Cm^{-2}K^{-1}$ at R=0.005, which is a gain of 325%. Then it settles to around $-3.0 \times 10^{-4} \sim -2.5 \times 10^{-4}\ Cm^{-2}K^{-1}$ for R>0.1.

PVDF

As PVDF is a polymer with rather high thermal expansion coefficient with dc1, dc2, and dc3 values of opposite signs from the rest of PY materials investigated so far, it is expected to behave rather differently from others. It is evident from Figure 6.4(c) that the total magnitude of the enhancement is rather small for PVDF. However, Figure 6.4(d) demonstrates how much of an improvement the introduction of NP elastic layer has had on the secondary PY coef of PVDF with PVDF-Invar36 pair presenting the greatest gain of $260 \sim 300\%$ as expected, and PVDF-St pair also performing well at about 200% increase. This method of comparison may be better suited since the secondary contribution of PVDF's PY coef varies quite significantly from a sample of PVDF to another, owing largely to their preparation process. The material data used for our simulation was for a PVDF with secondary contribution of only 3.25% of the overall PY coef. Hence if we can achieve high percentile secondary PY coef enhancement (a percentile comparison between the secondary PY coefs only), for PVDF samples with higher proportion of secondary contribution such as those presented by Kepler and Anderson[90], one could expect to achieve similar percentage of enhancement, which could be a significantly large magnitude enhancement. Noticeably, Figure 6.4(d) portrays the maximum of 300% enhancement in the secondary PY coef for PVDF-Invar36 pair, which potentially could

lead to extremely large enhancement in other PVDF samples with higher proportion of secondary contribution.

Best performing pairs

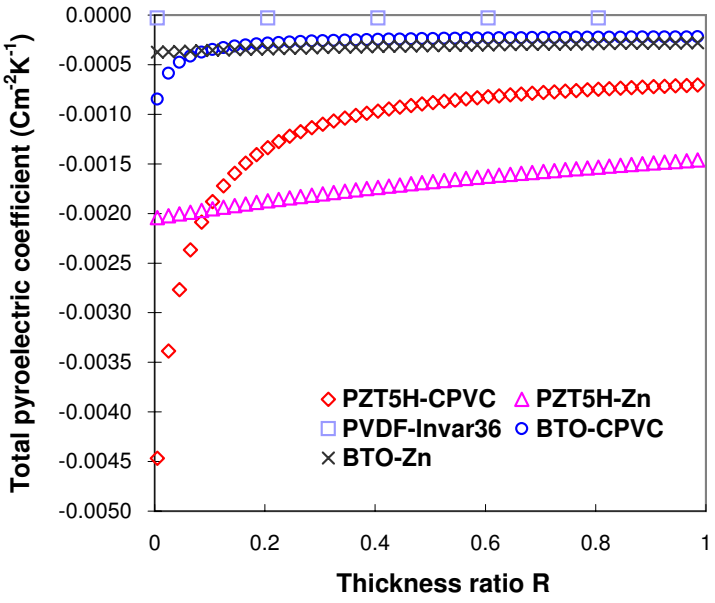

Figure 6.5: Pyroelectric coefficient enhancements under short circuit condition of the best performing 2-2 connectivity PY-NP laminate composites vs thickness ratios (R)

In general, PZT5H-Zn's secondary PY coef (demonstrated in Figure 6.5) is around 25-45% higher than that of Al depicted in Figure 6.4(a), with the difference getting greater steadily with increasing R. For BTO, Zn's secondary PY coef is around 35-45% higher than that of Al, with the difference getting steadily less with increasing R as evident from Figures 6.4(b) and 6.5. It is evident from Figure 6.5 that PZT-5H is by far the best performing material, with CPVC and Zn providing maximum enhancements at R<0.09 and R>0.09, respectively, while at R=0.09 the value for both pairs coincide at approximately $-20 \times 10^{-4}\ Cm^{-2}K^{-1}$. It would be very interesting to experimentally verify the extreme PY coef enhancement of PZT5H-CPVC pair at very low R values. Although the enhancement for BTO and PVDF were relatively very small, BTO's enhancement was still up to 325% at very low R range with CPVC and around 65% for high R range with Zn. In addition, PVDF showed the best enhancement with Invar36, as expected.

6.2.2 Experimental results and validity of the analytical model

Although the analytical model from Chapter 3 predicts high PY coef enhancement in various PY-NP 2-2 connectivity laminate composites, as illustrated in Subsection 6.2.1, and the observation of the enhancement in PZT5H-St pairs in the preliminary experiments (cf. Section 5.3) have been made, the accuracy of the analytical model has not been evaluated. This part of the dissertation will attempt to do exactly that by presenting the results of the Enhancement study planned in Subsection 5.2.2, where PY coef enhancement and its dependence on thickness ratio (R) were experimentally investigated.

At this point, the author would like to introduce the readers to a typical PY coef enhancement measurement. Using the quoted measurement procedure in Subsection 5.2.2, Figure 6.6 was produced.

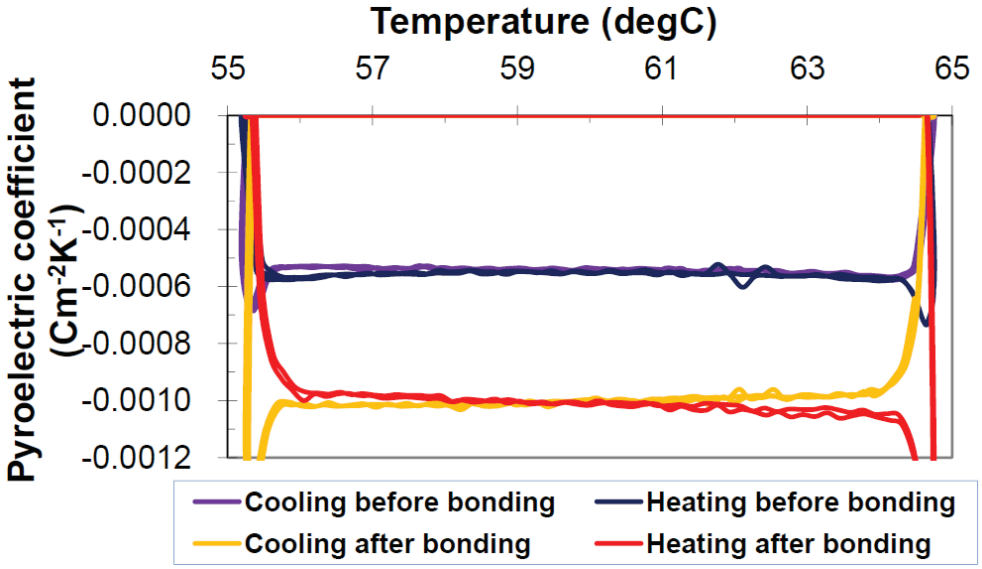

Figure 6.6: A typical PY coef enhancement measurement under SC during cooling and heating cycles before and after bonding the sample

It is quite evident from Figure 6.6 that this particular sample achieved up to approximately 80-90% enhancement. In fact, as illustrated by Table 6.1 a sample with thickness ratio (R) of 2.67 (267 μm PZT-5H with two 50 μm St) was observed to show enhanced PY coef of approximately -6.7×10^{-4} compared to -4.1×10^{-4} $Cm^{-2}K^{-1}$ before the introduction of bonding with St. When R=0.254 (127 μm PZT-5H with two 250 μm St), this was observed to rise to -9.0×10^{-4} from -4.8×10^{-4} $Cm^{-2}K^{-1}$. This represents a PY coef enhancement of approximately 4.2×10^{-4} $Cm^{-2}K^{-1}$ (around 90%). In addition, although the author did not explore the whole range of R values as with PZT-5H, when the PZT was exchanged to PZT-5A, for the same R=0.254 the bonded stack exhibited

PY coef enhancement of 105% ($3.9 \times 10^{-4}\ Cm^{-2}K^{-1}$ gain), an increase from -3.7×10^{-4} to $-7.6 \times 10^{-4}\ Cm^{-2}K^{-1}$ [43].

Table 6.1: Experimental results from the Enhancement study

Sample name	${}^{PY}t$	${}^{NP}t$	R	p_{before}	p_{after}	Δp	Percentile Δp
XI3	127	250	0.254	-5.01	-9.18	-4.17	83.1
XII4	127	250	0.254	-4.79	-9.02	-4.23	88.3
XI5	191	250	0.382	-5.23	-9.22	-3.99	76.3
XIR5	191	250	0.382	-4.25	-7.37	-3.12	73.6
XI8=X3	267	250	0.534	-4.36	-7.95	-3.59	82.4
XI7	267	125	1.068	-4.64	-8.56	-3.92	84.4
XIR7C	267	125	1.068	-4.80	-8.68	-3.88	80.8
XIR7	267	125	1.068	-4.79	-8.74	-3.95	82.6
XI1	127	50	1.270	-5.17	-7.96	-2.79	54.0
XIR1	127	50	1.270	-4.80	-7.55	-2.75	57.3
XI4	191	50	1.910	-5.41	-7.49	-2.08	38.4
XIR4	191	50	1.910	-4.53	-7.14	-2.61	57.5
XIR4C	191	50	1.910	-4.39	-7.17	-2.78	63.1
XI6=X2	267	50	2.670	-4.10	-6.72	-2.62	63.8

Units: - ${}^{PY}t$ = Thickness of PY material ; μm
- ${}^{NP}t$ = Thickness of each NP material ; μm
- $R = \frac{{}^{PY}t}{{}^{NP}t}$ = Thickness ratio ; No unit
- p_{before} = PY coef before bonding with NP ; $\times\ 10^{-4}\ Cm^{-2}K^{-1}$
- p_{after} = PY coef after bonding with NP ; $\times\ 10^{-4}\ Cm^{-2}K^{-1}$
- $\Delta p = p_{after} - p_{before}$ = Magnitude of PY coef enhancement ; $\times\ 10^{-4}\ Cm^{-2}K^{-1}$
- Percentile $\Delta p = \left(\frac{p_{after} - p_{before}}{p_{before}}\right) \times 100$ = Percentile PY coef enhancement ; %

(Note: - L (Average length) $\approx 2\ cm$ - W (Average width) $\approx 1\ cm$)

Two types of interfacial factors, namely k-factors, were introduced in 3.4.2 in an attempt to describe the effects of the bonding layer. The need for such factors was quite apparent from our FEA results in Section 3.3. Their influence on the analytical model's prediction of PY coef was illustrated in Figure 3.6. As the k-factor values decrease, since k_1 also includes the description for the other force losses during its transmission through

the epoxy layer, it depicts a more dramatic reduction in the PY coef enhancement than k_2, which is intended to portray only the deformation of the epoxy layer. Figure 6.7 illustrates suitability of the analytical models with k-factors for describing the experimental results of the Enhancement study, and hence the PY coef enhancement effect in 2-2 connectivity laminate composites.

From Figures 6.7(a) and 6.7(b), it is quite clear that k-factor values of around 0.75 fits our experimental data the best, while Figures 6.7(c) and 6.7(d) seem to suggest that k_1 may be a better fit than k_2, insinuating the presence of other effects than just the elastic deformation of the bonding layer.

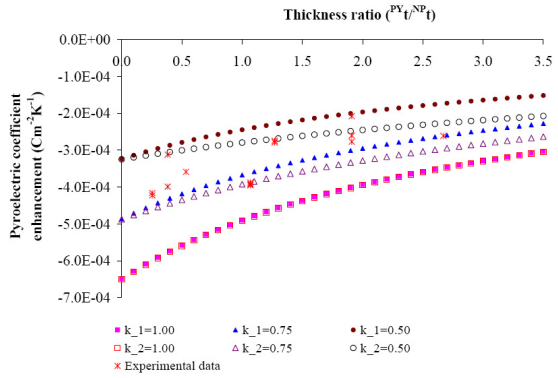

(a) PY coef enhancement from the experiment (Exp) and analytical models with k-factors vs R

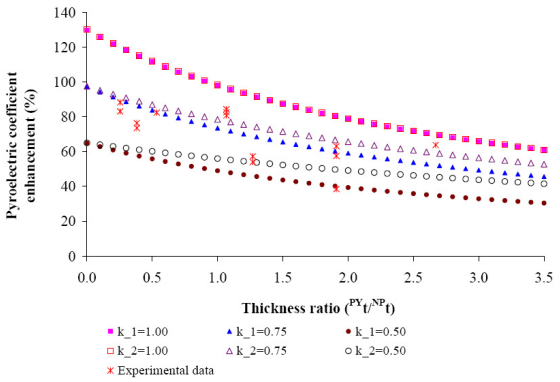

(b) Percentile PY coef enhancement from the experiment (Exp) and analytical models with k-factors vs R

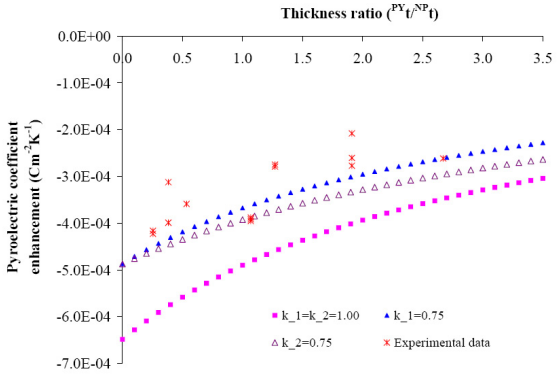

(c) PY coef enhancement from the experiment (Exp) and analytical models with best fitting k-factor values vs R

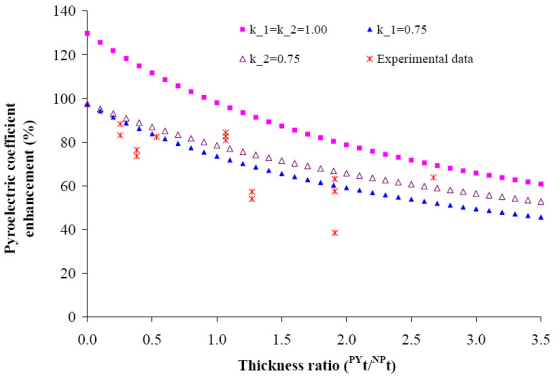

(d) Percentile PY coef enhancement from the experiment (Exp) and analytical models with best fitting k-factor values vs R

Figure 6.7: Pyroelectric coefficient enhancement under SC in St/PZT/St laminates measured in the Enhancement study experimentation (Exp) and predicted by the analytical models with k-factors from Subsubsections 3.4.1 and 3.4.2

Figure 6.8 summarises our experimental data with theoretical model under SC using k_1 factor. As conducting experiments under open circuit condition is extremely difficult, it requires a very good vacuum which our pyro-rig can not deliver for starters, the author was not able to repeat the same experiment under OC (cf. Chapter 8). The observation of this enhancement under OC could be a very interesting future work (cf. Section 16.5).

Noting that the PY coef of a PZT-5H under free body condition is around -5.0×10^{-4} $Cm^{-2}K^{-1}$, Figure 6.8(a) clearly illustrates that as we approach the perfect bonding case of $k = 1.0$ the magnitude of the enhancement exceeds this value for thickness ratios (R) below around 1. This implies that for such small R and near perfect bonding, one could expect to achieve more than double the overall PY coef by just introducing the NP layers, namely stainless steel in this case. $K = 0.75$ appearing to provide the best fit for the experimental results for various R values, insinuates that the loss due to the epoxy layer seems to be approximately 25% in the Enhancement study.

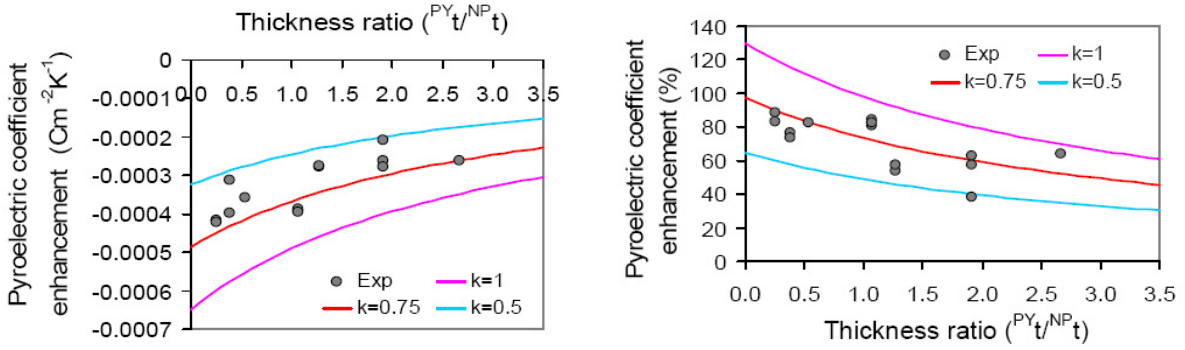

(a) Magnitude of PY coef enhancement vs R for different k_ 1 values

(b) Percentile PY coef enhancement vs R for different k_ 1 values

Figure 6.8: Pyroelectric coefficient enhancement under SC in St/PZT/St laminates measured in the Enhancement study and predicted by the k_ 1 factors

The reason for presenting the PY coef enhancement as a percentile of the PY coef of PZT-5H at free body condition (as in Figures 6.7(b), 6.7(d), and 6.8(b)) is to obtain better representation of the enhancements observed in the experimental sample. As all PZT-5H samples go through manufacturing processes with slightly varying conditions, they are bound to possess some discrepancies in their polarisation states, leading to slight variations among their PY coefs. Under a very simple assumption that the polarisation state of a PZT sample is linearly proportional with PY coef, these discrepancies and their impact on the comparison of PY coef enhancements of various PZT-5H samples could be reduced by comparing these percentiles. Figure 6.8(b) demonstrates that for near perfect bonding case with small R, PY coef enhancements of up to approximately 130%

is theoretically viable.

To summarise, we have observed nearly or more than 100% enhancement in PY coefs of 2-2 connectivity laminate St/PZT/St structures with Figure 6.8 evidently demonstrating that there is a good agreement between the theoretical and experimental values when $k = 0.75$. This insinuates that the average loss of strain due to the interfacial coupling is around 25%, which leads to the hypothesis that there still is a substantial improvement that can be made for our already large enhancement by further perfecting the interfacial bonding.

Chapter 7

Conclusions - Pyroelectric coefficient enhancement

Objectives 1-1c from Section 1.2 have been achieved.

Starting from the definition of pyroelectricity and using thermodynamic principles, we have analytically modelled 2-2 connectivity composites of PY and NP materials and evaluated the potential enhancement in PY coefs of thirty-six such composites, identifying the best possible partnership among these PY and NP materials. This potentially large PY coef enhancement was attributed to dissimilar signs of the piezoelectric coefs of the PY material (dc1, dc2, and dc3 in Table B.3 from Appendix B.2) and the exploitation of this particular symmetry through the deployment of 2-2 connectivity configuration, where externally exerted stress/strain by NP elastic layer results in cumulative piezoelectricity arising from three separate axes owing to Poisson effect. In doing so, we have also discovered and confirmed that the sum terms, dc1, dc2, and dc3 are the most viable indicators for determining the feasibility and potential for PY coef enhancement (cf. Section 4.3). The choice of NP material was also found to be dependent on these sum terms, as demonstrated by PVDF-Invar36 pair's theoretical enhancement. With the importance the connectivity concept plays in other application areas such as thermal imaging[17], this analysis on 2-2 connectivity composites could find use in many other diverse areas of research such as Infra-Red detectors and thin-film technologies.

PZT-5H and PZT-5A exhibited very large PY coef enhancement with theoretical possibility of 800% increase at $R = 0.005$ for PZT5H-CPVC and a more moderate gain of 220% at $R = 0.15$. BTO's enhancement potential was much less than PZT's, but BTO-CPVC still managed to display quite high theoretical enhancement for small thickness

ratios of $R < 0.1$ with a gain of 325% at $R = 0.005$.

Due to the opposite signs of dc1, dc2, and dc3 of PVDF, when compare to that of the rest of PY materials, NP material with smaller thermal expansion coef than PVDF, namely Invar36, exhibited the highest theoretical enhancement. Although its total PY coef enhancement magnitude was miniscule, due to this particular uni-axially orientated PVDF having secondary contribution to the overall PY coef of only about 3.25%, PVDF-Invar36 demonstrated the maximum of 300% growth in the secondary PY coef, which potentially could lead to extremely large enhancements in other PVDF samples with higher proportion of the secondary contribution.

The best performing partnership out of the thirty-six PY-NP pairs were PZT5H-CPVC for $R < 0.09$ and PZT5H-Zn for $R > 0.09$ with both demonstrating theoretical total PY coef of approximately $-20 \times 10^{-4}\ Cm^{-2}K^{-1}$ at $R = 0.09$, which corresponds to approximately 300% increase. As mentioned earlier, PZT5H-CPVC also showed maximum of 800% gain in theoretical PY coef.

In order to measure this enhancement and verify its dependence on thickness ratio (R), we have also paid due attention to various factors and issues that may also affect the PY coef enhancement measurements when pyro-rig is used; heating rates, type of epoxy used for bonding, thickness of the bonding layer, and the presence of pre-stress, to list a few. Techniques such as Finite Element Analysis and analytical modelling were employed to assess these factors/issues followed by preliminary experimentation. Various preliminary PY coef measurements were undertaken to find ways to eliminate such undesirable factors/issues, the main example of which would be Curing temperature study, which revealed some of the effects of pre-stress on the PY coef measurement. From this study we were able to identify the Cur and Op. temps for the Enhancement study, minimising the potential errors pre-stress might introduce in the PY coef enhancement measurements.

The Enhancement study has enabled us to observe more than 100% PY coef enhancement in 2-2 connectivity laminate composites of St/PZT/St experimentally, as evident from Figure 6.8, demonstrating that there is a good agreement between the theoretical and experimental values when $k = 0.75$ with k_1 seeming being a better interfacial factor than k_2. This also insinuated that the average loss of strain due to the interfacial coupling is around 25% and it is not entirely from the elastic deformation of the bonding layer, which lead to the hypothesis that there still is a substantial improvement to be made for this already large enhancement via further perfecting of the interfacial bonding.

Chapter 8

Theoretical analysis - Boundary conditions and thermal mass

Derivation of the pyroelectric coefficient under open circuit condition for 2-2 connectivity laminate composites (including that of St/PZT-5H/St) and comparison with that under short circuit condition will be presented in Section 8.1, with Subsection 8.1.2 providing comparison of various material properties under these two boundary conditions. Section 8.2 will introduce the readers to the concept of the thermal-to-electrical conversion efficiency (Eff) followed by its derivation process and its use in Figure of merit for efficiencies.

8.1 Pyroelectric coefficient expression under OC

8.1.1 Open circuit pyroelectric coefficient

Having established the findings depicted in Section 3.1, in this subsection we derive the PY coef under OC that is analogous to that under SC (cf. Eq 3.10), derived in Subsubsection 3.2.1.

We know from Subsubsection 3.2.1 that $P_{Si} = D_i - \varepsilon_0(\varepsilon_r)_i E_i$ [44]. Therefore for open circuit condition, $dD_i = 0$ (cf. subsection 3.1.1);

$$p_i = \frac{dP_{Si}}{d\Theta} = -\varepsilon_0(\varepsilon_r)_i \frac{dE_i}{d\Theta} \tag{8.1}$$

where $\boldsymbol{P_S}$ = Spontaneous polarisation

$\boldsymbol{D}$ = Electric displacement (Electric flux density)

$\boldsymbol{E}$ = Electric field (intensity)

ε_0 = Permittivity of free space

$\boldsymbol{\varepsilon_r}$ = Relative dielectric constant (Relative permittivity)

(Note that for the purpose of our studies, as in practice most measurements are taken under constant stress condition, where they are not mechanically clamped and free to deform, we can safely assume that $((\varepsilon_r)_i = (\varepsilon_r^T)_i$, i.e. relative dielectric constants are evaluated under constant stress.)

For OC, we assume constant electric displacement, i.e. $dD_n = 0 \forall n$ (cf. subsection 3.1.1), and define the temperature (Θ), stress (T_{ij}), and electric displacement (D_m) as the independent variables (cf. 3.2.1) of the Gibbs free energy function to make the constitutive equations resulting from Gibbs free energy function (Eq 3.5) solvable. With that in mind, we move on to deriving the expression for $\frac{dE_i}{d\Theta}$ by considering thermodynamics, which will then be used to develop the PY coef expression under OC[109,124,133]. By considering the conventional nine components of the second order strain and stress tensors, while the magnetic effect is ignored as usual, we have:

$$G = G(T_{ij}, D_m, \Theta)$$

$$\Rightarrow \quad dS_{ij} = \sum_k \sum_l \left(\frac{\partial S_{ij}}{\partial T_{kl}}\right)_{D,\Theta} dT_{kl} + \sum_n \left(\frac{\partial S_{ij}}{\partial D_n}\right)_{T,\Theta} dD_n + \left(\frac{\partial S_{ij}}{\partial \Theta}\right)_{T,D} d\Theta$$

and

$$dE_m = \sum_k \sum_l \left(\frac{\partial E_m}{\partial T_{kl}}\right)_{D,\Theta} dT_{kl} + \sum_n \left(\frac{\partial E_m}{\partial D_n}\right)_{T,\Theta} dD_n + \left(\frac{\partial E_m}{\partial \Theta}\right)_{T,D} d\Theta \tag{8.2}$$

Assuming constant electric displacement (i.e. $dD_n = 0 \forall n$ for OC) and using Einstein's summation indexing method:

$$\text{Eq 8.2} \qquad \Rightarrow \quad dS_{ij} = \left(\frac{\partial S_{ij}}{\partial T_{kl}}\right)_{D,\Theta} dT_{kl} + \left(\frac{\partial S_{ij}}{\partial \Theta}\right)_{T,D} d\Theta$$

and

$$dE_m = \left(\frac{\partial E_m}{\partial T_{kl}}\right)_{D,\Theta} dT_{kl} + \left(\frac{\partial E_m}{\partial \Theta}\right)_{T,D} d\Theta \tag{8.3}$$

From Eq 8.3 with $(\partial S_{ij}/\partial T_{kl})^{-1}_{D,\Theta}$ denoting the inverse tensor of $(\partial S_{ij}/\partial T_{kl})_{D,\Theta}$, which is assumed to exist as $(\partial S_{ij}/\partial T_{kl})_{D,\Theta} = s^{D,\Theta}_{ijkl}$:

$$\Rightarrow \quad dT_{kl} = \left(\frac{\partial S_{ij}}{\partial T_{kl}}\right)^{-1}_{D,\Theta}\left[dS_{ij} - \left(\frac{\partial S_{ij}}{\partial \Theta}\right)_{T,D} d\Theta\right] \tag{8.4}$$

While also noting the following relations:

$$\begin{aligned}\left(\frac{\partial E_m}{\partial \Theta}\right)_{T,D} &= \left.\frac{dE_m}{d\Theta}\right|_{T,D} - \left.\left(\frac{\partial E_m}{\partial D_n}\frac{dD_n}{d\Theta}\right)\right|_{T,D} - \left.\left(\frac{\partial E_m}{\partial T_{kl}}\frac{dT_{kl}}{d\Theta}\right)\right|_{T,D} \\ &= \left.\frac{dE_m}{d\Theta}\right|_{T,D} = \left.\left(\frac{dE_m}{dD_n}\frac{dD_n}{d\Theta}\right)\right|_{T,D} = \left(\frac{\partial E_m}{\partial D_n}\right)_{T,\Theta}\left(\frac{\partial D_n}{\partial \Theta}\right)_{T,D}\end{aligned}$$

since similarly, $\left.\frac{dE_m}{dD_n}\right|_{T,D} = \left(\frac{\partial E_m}{\partial D_n}\right)_{T,\Theta}$ and $\left.\frac{dD_n}{d\Theta}\right|_{T,D} = \left(\frac{\partial D_n}{\partial \Theta}\right)_{T,D}$

Also, correspondingly;

$$\begin{aligned}\left(\frac{\partial E_m}{\partial T_{kl}}\right)_{D,\Theta} &= \left.\frac{dE_m}{dT_{kl}}\right|_{D,\Theta} - \left.\left(\frac{\partial E_m}{\partial D_n}\frac{dD_n}{dT_{kl}}\right)\right|_{D,\Theta} - \left.\left(\frac{\partial E_m}{\partial \Theta}\frac{d\Theta}{dT_{kl}}\right)\right|_{D,\Theta} \\ &= \left.\frac{dE_m}{dT_{kl}}\right|_{D,\Theta} = \left.\left(\frac{dE_m}{dD_n}\frac{dD_n}{dT_{kl}}\right)\right|_{D,\Theta} = \left(\frac{\partial E_m}{\partial D_n}\right)_{T,\Theta}\left(\frac{\partial D_n}{\partial T_{kl}}\right)_{D,\Theta}\end{aligned}$$

Equipped with above relations, substitute Eq 8.4 into the change in electric field expression in Eq 8.3:

$$\begin{aligned}
\Rightarrow \quad dE_m &= \left(\frac{\partial E_m}{\partial T_{kl}}\right)_{D,\Theta}\left(\frac{\partial S_{ij}}{\partial T_{kl}}\right)^{-1}_{D,\Theta}\left[dS_{ij} - \left(\frac{\partial S_{ij}}{\partial \Theta}\right)_{T,D} d\Theta\right] + \left(\frac{\partial E_m}{\partial \Theta}\right)_{T,D} d\Theta \\
\Rightarrow \quad \left(\frac{\partial E_m}{\partial \Theta}\right)_{T,D} &= \frac{dE_m}{d\Theta} + \left(\frac{\partial E_m}{\partial T_{kl}}\right)_{D,\Theta}\left(\frac{\partial S_{ij}}{\partial T_{kl}}\right)^{-1}_{D,\Theta}\left[\left(\frac{\partial S_{ij}}{\partial \Theta}\right)_{T,D} - \frac{dS_{ij}}{d\Theta}\right] \\
\Rightarrow \quad \frac{dE_m}{d\Theta} &= \left(\frac{\partial E_m}{\partial \Theta}\right)_{T,D} - \left(\frac{\partial E_m}{\partial T_{kl}}\right)_{D,\Theta}\left(\frac{\partial S_{ij}}{\partial T_{kl}}\right)^{-1}_{D,\Theta}\left[\left(\frac{\partial S_{ij}}{\partial \Theta}\right)_{T,D} - \frac{dS_{ij}}{d\Theta}\right] \\
&= \left(\frac{\partial E_m}{\partial D_n}\right)_{T,\Theta}\left(\frac{\partial D_n}{\partial \Theta}\right)_{T,D} \\
&\quad - \left(\frac{\partial E_m}{\partial D_n}\right)_{T,\Theta}\left(\frac{\partial D_n}{\partial T_{kl}}\right)_{D,\Theta}\left(\frac{\partial S_{ij}}{\partial T_{kl}}\right)^{-1}_{D,\Theta}\left[\left(\frac{\partial S_{ij}}{\partial \Theta}\right)_{T,D} - \frac{dS_{ij}}{d\Theta}\right] \\
&= \left(\frac{\partial E_m}{\partial D_n}\right)_{T,\Theta}\left[\left(\frac{\partial D_n}{\partial \Theta}\right)_{T,D}\right. \\
&\qquad \left. - \left(\frac{\partial D_n}{\partial T_{kl}}\right)_{D,\Theta}\left(\frac{\partial S_{ij}}{\partial T_{kl}}\right)^{-1}_{D,\Theta}\left[\left(\frac{\partial S_{ij}}{\partial \Theta}\right)_{T,D} - \frac{dS_{ij}}{d\Theta}\right]\right]
\end{aligned} \tag{8.5}$$

Substituting Eq 8.5 into Eq 8.1:

$$
\begin{aligned}
\therefore \quad p_m^{OC} &= -\varepsilon_0(\varepsilon_r)_m \frac{dE_m}{d\Theta} \\
&= -\varepsilon_0(\varepsilon_r)_m \left(\frac{\partial E_m}{\partial D_n}\right)_{T,\Theta} \\
&\quad \times \left[\left(\frac{\partial D_n}{\partial \Theta}\right)_{T,D} - \left(\frac{\partial D_n}{\partial T_{kl}}\right)_{D,\Theta} \left(\frac{\partial S_{ij}}{\partial T_{kl}}\right)_{D,\Theta}^{-1} \left[\left(\frac{\partial S_{ij}}{\partial \Theta}\right)_{T,D} - \frac{dS_{ij}}{d\Theta}\right]\right] \\
&= -\left(\varepsilon_0(\varepsilon_r)_m\right) \left(\frac{1}{\varepsilon_0 \left(\varepsilon_r^T\right)_m}\right) \\
&\quad \times \left[\left(\frac{\partial D_n}{\partial \Theta}\right)_{T,D} - \left(\frac{\partial D_n}{\partial T_{kl}}\right)_{D,\Theta} \left(\frac{\partial S_{ij}}{\partial T_{kl}}\right)_{D,\Theta}^{-1} \left[\left(\frac{\partial S_{ij}}{\partial \Theta}\right)_{T,D} - \frac{dS_{ij}}{d\Theta}\right]\right] \\
&= -\left(\frac{\partial D_n}{\partial \Theta}\right)_{T,D} + \left(\frac{\partial D_n}{\partial T_{kl}}\right)_{D,\Theta} \left(\frac{\partial S_{ij}}{\partial T_{kl}}\right)_{D,\Theta}^{-1} \left[\left(\frac{\partial S_{ij}}{\partial \Theta}\right)_{T,D} - \frac{dS_{ij}}{d\Theta}\right] \\
&= p_m^{T,D} + d_{mkl}^{D,\Theta} (s_{ijkl}^{D,\Theta})^{-1} \left[\alpha_{ij}^{T,D} - \frac{dS_{ij}}{d\Theta}\right] \\
&= p_m^{T,D} + d_{mkl}^{D,\Theta} c_{ijkl}^{D,\Theta} \left[\alpha_{ij}^{T,D} - \frac{dS_{ij}}{d\Theta}\right]
\end{aligned}
\tag{8.6}
$$

where p_m^{OC} = Total pyroelectric coefficient under OC

$\frac{dE_m}{d\Theta}$ = Change in electric field per temperature change

$\left(\frac{\partial E_m}{\partial D_n}\right)_{T,\Theta}$ = $\beta_{mn}^{T,\Theta}$ = Inverse of permittivity tensor, which can be replaced by $\beta_m^{T,\Theta} = \left(\frac{\partial E_m}{\partial D_m}\right)_{T,\Theta}$ or $\frac{1}{\varepsilon_m^{T,\Theta}} = \frac{1}{\varepsilon_0(\varepsilon_r^T)_m}$ since the permittivity tensor is a diagonal matrix

$p_m^{T,D}$ = Pyroelectric coefficient at constant stress (free boundary condition) and electric displacement

$d_{mkl}^{D,\Theta}$ = Piezoelectric constant at constant temperature and electric displacement

$s_{ijkl}^{D,\Theta}$ = Elastic compliance at constant temperature and electric displacement

$c_{ijkl}^{D,\Theta} = (s_{ijkl}^{D,\Theta})^{-1}$ = Elastic stiffness at constant temperature and electric displacement

$\alpha_{ij}^{T,D}$ = Thermal expansion coefficient at constant stress and electric displacement

dS_{ij} = Total strain experienced by the pyroelectric material

i,j,k,l,m = 1..3

(Please compare this expression with the expression from the literature, Eq 3.1, and Eq 3.9 for better understanding of the difference.)

Notice the change in the sign of the secondary PY from that of SC (Eq 3.9). This indicates that PY coef under OC can vary greatly from that under SC, since where the secondary effect is an enhancement will lead to reduction and vice versa for these two differing conditions provided the same amount of strain is applied. Indeed, our analysis illustrates that the enhancement under SC leads to reduction under OC, but due to the sheer magnitude of the secondary effect it can lead to change of sign in the PY coef itself where very large alteration of the PY coef is achieved at very low thickness ratios (R) for PY materials that demonstrated relatively large enhancements under SC such as PZT and BTO.

It is evident from Eq 8.6 that larger the strain the NP component can exert on PY component and greater the piezoelectric coef of the PY material, bigger the change in secondary contribution. This leads to the conclusion that stiffer NP material with greater disparity in thermal expansion coef (α) with that of PY and more compliant PY material with high piezoelectric coefs would lead to largest PY coef alteration.

In addition, since primary PY coef $p^{S,D}$ is measured when $dS_{ij} = 0$;

$$p_m^{S,D} = p_m^{T,D} + d_{mkl}^{D,\Theta} c_{ijkl}^{D,\Theta} \alpha_{ij}^{T,D} \tag{8.7}$$

(cf. Eq 3.10 for SC)

8.1.2 Comparison between various material properties under SC and OC

Although the use of PY coef expression under SC (p_m^{SC} cf. Eq 3.9) is quite common in general, and hence it is easy to evaluate for various PY materials, the use of that under OC (p_m^{OC} cf. Eq 8.6) is not so. This creates difficulties when the evaluation of p_m^{OC} is required. Hence, in this subsection we shall review the literature that enables us to compare the two expressions and draw parallels between them, facilitating for the evaluation of material properties necessary for p_m^{OC} calculation from that of p_m^{SC}.

The information on the material properties required for the evaluation of Eq 3.9 is largely available from various sources such as the manufacturers[3,4,9,12,15]. However, that of Eq 8.6 poses significantly more difficult challenge due to the lack of availability of material properties evaluated under necessary conditions. Therefore, efforts will be made to establish the relations between these two sets of parameters from various literatures[109,124,133,194], which will then be employed to evaluate various material properties under OC as illustrated in Tables B.1 and B.2 in Appendix B.1.

- Primary pyroelectric coefficients under SC and OC

The author has yet to come across a definitive literature which explicitly deals with this issue. However, as the primary PY coef is a fundamental intrinsic property of the material, for the purpose of this project we shall assume the following equality relationship between the primary PY coef under SC and OC, namely $p_m^{S,E}$ and $p_m^{S,D}$ respectively;

$$p_m^{S,E} = p_m^{S,D}$$

Hence, from Eq 3.10 and 8.7:

$$\begin{aligned} \Rightarrow \quad & p_m^{T,E} - d_{mkl}^{E,\Theta} c_{ijkl}^{E,\Theta} \alpha_{ij}^{T,E} = p_m^{T,D} + d_{mkl}^{D,\Theta} c_{ijkl}^{D,\Theta} \alpha_{ij}^{T,D} \\ \Rightarrow \quad & \therefore \\ & p_m^{T,D} = p_m^{T,E} - d_{mkl}^{E,\Theta} c_{ijkl}^{E,\Theta} \alpha_{ij}^{T,E} - d_{mkl}^{D,\Theta} c_{ijkl}^{D,\Theta} \alpha_{ij}^{T,D} \end{aligned} \tag{8.8}$$

The fact that there is no distinction between the primary coefs under SC and OC in Grout et al.'s work[68] and the same value for the PY coef was used for both SC and OC cases of the PY coef expressions derived by Ploss et al.[145], further reinforces the validity

of this equality assumption.

- Piezoelectric constants under SC and OC

As the piezoelectric constants are measured under SC in general, $d_{mkl}^{E,\Theta}$ is the only available data. Conventionally, the piezoelectric constants are assumed to be the same under both SC and OC since the elastic coefficients, which will be multiplied to the piezoelectric constant to describe the overall piezoelectric effect, will reflect the consequences of this electrical condition on the overall piezoelectric effect. Hence;

$$d_{mkl}^{E,\Theta} = d_{mkl}^{D,\Theta}$$

- Elastic compliances under SC and OC[109,122,133]

The relation between the elastic compliances under SC and OC can be used to derive that of elastic stiffness, namely $c_{ijkl}^{D,\Theta}$ and $c_{ijkl}^{E,\Theta}$, which are the elastic compliances' inverse tensors. This should help with the evaluation of the secondary PY coef under OC since $c_{ijkl}^{D,\Theta}$ is a necessary parameter for such calculation. From the literature it is clear that;

$$s_{ijkl}^{D,\Theta} - s_{ijkl}^{E,\Theta} = -d_{mij}^{E,\Theta} d_{nkl}^{E,\Theta} \beta_{mn}^{T,\Theta}$$

and

$$c_{ijkl}^{D,\Theta} - c_{ijkl}^{E,\Theta} = e_{ijm}^{\Theta} e_{klw}^{\Theta} \beta_{mw}^{S,\Theta}$$

where $\beta_{mn}^{T,\Theta}$ = A component from the inverse of the permittivity tensor, which is equal to $\dfrac{1}{\varepsilon_0(\varepsilon_r^T)_m}$ due to the symmetry of the permittivity matrix

$\beta_{mn}^{S,\Theta}$ = A component from the inverse of the permittivity tensor, which is equal to $\dfrac{1}{\varepsilon_0(\varepsilon_r^S)_m}$ due to the symmetry of the permittivity matrix

$e_{ijm}^{\Theta} = c_{ijkl}^{E,\Theta} d_{klm}^{E,\Theta}$ = Piezoelectric constant (stress/electric field)

- Thermal expansion coefficients under SC and OC[122,133]

Similarly, Nye's book[133] also contains the following relationship for the thermal expansion coefs. Once more this is useful for the calculation of the secondary PY coef under

OC. In particular, it is essential for the evaluation of the strain experienced by the PY material upon thermal stimulation.

$$\alpha_{ij}^{T,D} - \alpha_{ij}^{T,E} = -d_{kij}^{E,\Theta}\beta_{kl}^{T,\Theta}p_{l}^{T,E} \tag{8.9}$$

Comparison between short and open circuit condition

With PY coef expression under OC derived, one can now compare it with that under SC in Subsection 3.2.1. In this Subsubsection, only a brief comparison between the expressions will be presented, since the results on different PY-NP pairings will be provided in Chapter 9.

To begin with, let us first look at the two expressions for the general PY coefs under SC and OC:

$$\begin{aligned}
&\text{For PY coef under SC, from Eq 3.9;} \qquad p_m^{SC} = p_m^{T,E} - d_{mkl}^{E,\Theta}c_{ijkl}^{E,\Theta}\left[\alpha_{ij}^{T,E} - \frac{dS_{ij}}{d\Theta}\right] \\
&\text{For PY coef under OC, from Eq 8.6;} \qquad p_m^{OC} = p_m^{T,D} + d_{mkl}^{D,\Theta}c_{ijkl}^{D,\Theta}\left[\alpha_{ij}^{T,D} - \frac{dS_{ij}}{d\Theta}\right]
\end{aligned} \tag{8.10}$$

Using the previously stated four relations between the parameters under SC and OC from Subsection 8.1.2, it is also possible to evaluate Eq 8.6 in terms of the parameters used in Eq 3.9. For the purpose of this dissertation, as the elastic stiffness under OC for the PY material is also provided by the manufacturer[3], following expression for the PY coef under OC will be used as the general form, but it should also be noted that other forms are also easily derivable from the four relations in Subsection 8.1.2:

From Eq 8.10 and the four relations (cf. Subsection 8.1.2), Eq 8.8 in particular;

$$\begin{aligned}
p_m^{OC} &= p_m^{T,D} + d_{mkl}^{D,\Theta}c_{ijkl}^{D,\Theta}\left[\alpha_{ij}^{T,D} - \frac{dS_{ij}}{d\Theta}\right] \\
&= p_m^{T,E} - d_{mkl}^{E,\Theta}c_{ijkl}^{E,\Theta}\alpha_{ij}^{T,E} - d_{mkl}^{D,\Theta}c_{ijkl}^{D,\Theta}\alpha_{ij}^{T,D} + d_{mkl}^{D,\Theta}c_{ijkl}^{D,\Theta}\left[\alpha_{ij}^{T,D} - \frac{dS_{ij}}{d\Theta}\right] \\
&= p_m^{T,E} - d_{mkl}^{E,\Theta}c_{ijkl}^{E,\Theta}\alpha_{ij}^{T,E} - d_{mkl}^{D,\Theta}c_{ijkl}^{D,\Theta}\left[\frac{dS_{ij}}{d\Theta}\right] \qquad \text{where} \quad \text{i,j,k,l,m} = 1..3
\end{aligned} \tag{8.11}$$

As expected, this expression in Eq 8.11 agrees perfectly with our equality assumption between the primary PY coefs used in the derivation of Eq 8.8. When $\frac{dS_{ij}}{d\Theta} = \alpha_{ij}^{T,D}$, Eq 8.11 becomes Eq 8.8. Note, that when Eq 8.11 is employed as a measure of our enhancement in the secondary PY coef under OC, the expression for $\frac{dS_{ij}}{d\Theta}$ will be a function of $\alpha_{ij}^{T,D}$, necessitating the utilisation of Eq 8.9.

Pyroelectric coefficients under OC for PZT

We can also simplify Eq 8.11 even further by considering the crystal symmetry of PZT and all the other PY materials considered in this dissertation excluding PVDF. This will results in the PY coef expression under OC that is analogous to Eq 3.25 for SC in Subsubsection 3.4.1.

With PZT's symmetry (cf. PZT symmetry table in Subsubsection 3.4.1 and matrices in Appendix A.1) and relation $d_{mkl}^{E,\Theta} = d_{mkl}^{D,\Theta}$ from Subsection 8.1.2 in mind[78,103,133,192] (cf. Subsubsection 3.4.1), from Eq 8.11:

$$\begin{aligned} p_3^{OC} &= p_3^{T,E} - \sum_{i,j} \left[d_{3i}^{E,\Theta} c_{ij}^{E,\Theta} \alpha_j^{T,E} + d_{3i}^{D,\Theta} c_{ij}^{D,\Theta} \left\{ \frac{dS_{ij}}{d\Theta} \right\} \right] \qquad \text{for } i,j = 1..6 \\ &= p_3^{T,E} - d_{31}^{E,\Theta} \sum_{j=1}^{3} \left[\left(c_{1j}^{E,\Theta} + c_{2j}^{E,\Theta} \right) \alpha_j^{T,E} + \left(c_{1j}^{D,\Theta} + c_{2j}^{D,\Theta} \right) \frac{dS_{ij}}{d\Theta} \right] \\ &\quad - d_{33}^{E,\Theta} \sum_{j=1}^{3} \left[c_{3j}^{E,\Theta} \alpha_j^{T,E} + c_{3j}^{D,\Theta} \frac{dS_j}{d\Theta} \right] \end{aligned} \tag{8.12}$$

This expression, Eq 8.12, along with the strain expression Eq 3.28 derived in Subsubsection 3.4.1 evaluated with OC material properties, enables us to calculate the PY coef under OC for our St/PZT-5H/St samples with Eq 3.29 as its SC counterpart. dc1, dc2, and dc3 values under OC have also been evaluated and are presented in Table B.4, demonstrating significantly different behaviour from their SC counterparts in Table B.3 for some of the PY materials. Please note that again PVDF does not satisfy ${}^{PY}\alpha = {}^{PY}\alpha_j \quad \forall j = 1..2$, and hence the full solution to the force balance equation was used when evaluating the strain expressions from Eqs 3.26 and 3.27 for its laminate composites.

8.2 Thermal mass and thermal-to-electrical conversion efficiencies

Definition of, and derivation process for, the thermal-to-electrical conversion efficiency (Eff) will be presented in Section 8.2. This "Efficiency" expression is an extended version of Figure of merit F_i, which should enable one to assess a particular material/composite's potential thermal-to-electrical conversion performance.

Despite having a large impact on the feasibilities of any PY material/composite in practical applications, thermal mass is one of the main issues that was not addressed so far in this dissertation. Although it may not be a major concern when there is an abundant heat energy source nearby the pyroelectricity application, such as energy harvesting from industrial heat, for others this could play an integral part in the measure of performance whereby the feasibility of pyroelectric effect in that particular application may be decided by it[108]. Therefore, we define a measure termed "Efficiency (Eff)" based on the thermal mass calculations and use it as a measure of how efficiently our PY structures convert heat energy into an electrical one.

8.2.1 Definition of efficiency

There already exists a vast quantity of research conducted on the thermal analysis of various PY and other applications[95,108]. However, as we do not require such sophisticated measures for considering the thermal mass of our devices at present stage, we defined a simple quantity termed "Efficiency (Eff)" as:

$$\begin{aligned} Eff &= \frac{\text{Polarisation change due to PY effect}}{\text{Thermal energy input}} \\ &= \frac{\Delta P_S}{Vol \times c_{vol} \times \Delta\Theta} = \frac{p_3 \Delta\Theta}{Vol \times c_{vol} \times \Delta\Theta} = \frac{p_3}{Vol \times c_{vol}} \end{aligned} \tag{8.13}$$

measured in $Cm^{-2}J^{-1}$, where ΔP_S is the polarisation change, Vol is the volume, c_{vol} is the volumetric heat capacity, $\Delta\Theta$ is the change in temperature, and p_3 is the PY coef.

For the purpose of simplification, following definition will be used when composites are concerned[134]:

Total thermal energy input of the whole composite

= Arithmetic sum of each constituent's Vol $\times c_{vol} \times \Delta\Theta$

$$\Rightarrow \quad {}^{Com}Eff = \text{Efficiency of a composite} = \frac{{}^{Com}(\Delta P_S)}{\text{Total thermal energy input}} = \frac{{}^{Com}p_3 \Delta\Theta}{[\sum_i \{(Vol)_i \times (c_{vol})_i\}] \times \Delta\Theta} = \frac{{}^{Com}p_3}{\sum_i \{(Vol)_i \times (c_{vol})_i\}} \tag{8.14}$$

where ^{Com} denotes "composite" and $()_i$ stands for "of the i-th constituent".

With this "Eff", we can now quantify the ratio of electrical energy a material or composite can produce given a standard unit of thermal energy. This in effect states the quality or the efficiency of our structures where the thermal mass is of a major importance.

8.2.2 Figure of merit for efficiency expressions

In order to make useful efficiency comparisons between different materials before and after the enhancement, we first decide on which parameters are independent and which are not. Since we only consider 2-2 connectivity structures, we assume all constituents of the structure to have the same length L and width W. As the PY coef is dependent on the thickness ratio between PY and NP materials (R), it would make sense to have R as the independent variable. In order to derive the efficiency comparison expression, let $t_3 = {}^{PY}t + {}^{NP}t$ be the total thickness of all the constituents (also assume that we only have two constituents, namely PY and NP, for simpler derivation process although expansion into larger number of constituents is possible) added together: $t_3 = {}^{PY}t + {}^{NP}t$ and $R = \frac{{}^{PY}t}{{}^{NP}t} \quad \Rightarrow \quad {}^{PY}t = \frac{t_3 R}{R+1}$ and ${}^{NP}t = \frac{t_3}{R+1}$. Substituting these relations into Eq 8.14:

$$\begin{aligned} {}^{Com}Eff &= \frac{{}^{Com}p_3}{\sum_i \{(Vol)_i \times (c_{vol})_i\}} = \frac{p(R)}{LW\left[\frac{{}^{PY}c_{vol}t_3 R}{R+1} + \frac{{}^{NP}c_{vol}t_3}{R+1}\right]} \\ &= \frac{p(R)}{\frac{t_3 LW}{R+1}\left[{}^{PY}c_{vol}R + {}^{NP}c_{vol}\right]} \end{aligned} \tag{8.15}$$

where ${}^{PY}t$ is the thickness of PY, ${}^{NP}t$ is the thickness of NP, $p(R)$ is PY coef as a function of R, and ${}^{PY}c_{vol}$ or ${}^{NP}c_{vol}$ is the volumetric heat capacity of PY or NP. Please note that $p(R)$ could also be a function with k-factors included as well, if required.

What we are really interested in is not just how efficient our structures are, but also how they compare with just a PY material alone. Does it give an improvement or does it actually worsen the issues with additional thermal mass? A good way of making such comparison between just the PY material and our composite of PY/NP material would be to define a ratio between the efficiencies of the two. This ratio should demonstrate to us the amount by which the overall thermal mass or efficiency of our structures have been altered by our modification. One can then make a comparison between a PY material by itself and its 2-2 connectivity composite. Hence, we define a "Figure of merit for efficiency" by: $F_{eff} = \frac{^{Com}Eff}{^{PY}Eff}$, where ^{PY}Eff denotes the efficiency of the pure PY material. Depending on the application, we have derived two different expressions for F_{eff}:

Figure of merit for efficiency type a (F^a_{eff})

First is the ratio between the same total volume of PY material and 2-2 connectivity composite, namely F^a_{eff}, which will result in the ratio between a 2-2 connectivity composite and a PY material with the same thickness as the total thickness of the composite (this means the thickness of the PY material used in the composite is thinner than the stand alone PY material). Assume the total volume for both cases to be $Vol = t3LW$:

$$F^a_{eff} = \frac{^{Com}Eff}{^{PY}Eff} = \frac{\frac{^{Com}p_3}{\frac{t_3LW}{R+1}\left[^{PY}c_{vol}R + ^{NP}c_{vol}\right]}}{\frac{^{PY}p_3}{t_3LW^{PY}c_{vol}}} = \frac{^{Com}p_3{}^{PY}c_{vol}\left[R+1\right]}{^{PY}p_3\left[^{PY}c_{vol}R + ^{NP}c_{vol}\right]} \tag{8.16}$$

where $^{PY}p_3$ is PY coef of PY material.

If $F^a_{eff} > 1$, then this denotes an improvement in the thermal-to-electrical conversion efficiency compared with that of pure PY material, while $F^a_{eff} < 1$ implies an inferior conversion performance. Since both the composite and the PY material are of the same volume, this ratio will indicate an improvement as long as $^{PY}c_{vol} > ^{NP}c_{vol}$ and $^{Com}p_3 > ^{PY}p_3$.

Figure of merit for efficiency type b (F^b_{eff})

Another ratio is between a PY material and a composite with the PY material of the same thickness. Since ${}^{PY}t = \dfrac{t_3 R}{R+1}$, we have:

$$F^b_{eff} = \frac{{}^{Com}Eff}{{}^{PY}Eff} = \frac{\dfrac{{}^{Com}p_3}{\dfrac{t_3 LW}{R+1}\left[{}^{PY}c_{vol}R + {}^{NP}c_{vol}\right]}}{\dfrac{{}^{PY}p_3}{{}^{PY}tLW{}^{PY}c_{vol}}} = \frac{\dfrac{{}^{Com}p_3}{\dfrac{t_3 LW}{R+1}\left[{}^{PY}c_{vol}R + {}^{NP}c_{vol}\right]}}{\dfrac{R+1}{t_3 R}\dfrac{{}^{PY}p_3}{LW{}^{PY}c_{vol}}}$$
$$= \frac{{}^{Com}p_3\,{}^{PY}c_{vol}R}{{}^{PY}p_3\left[{}^{PY}c_{vol}R + {}^{NP}c_{vol}\right]} \tag{8.17}$$

Once more, $F^b_{eff} > 1$ signifies raised efficiency. However, in this case the enhanced PY coef and augmented thermal mass due to the additional mass of NP material means there is a trade-off between the increased efficiency from the enhanced PY coef and the decrease from the additional thermal mass.

8.2.3 Figure of merit for efficiency evaluations

Here are some simple instructions on how to evaluate efficiency expressions, and hence ultimately the Figures of merit for efficiency expression.

Efficiency expressions under SC

It is quite straightforward to evaluate these expressions. One just has to substitute following relations into Eq 8.15 and Eqs 8.16 and 8.17 for corresponding Figure of merit for efficiency.

- ${}^{Com}p_3 = p(R,k) = p^{SC}_m$ from Eq 8.10
- ${}^{PY}c_{vol} = {}^{PY}c^{T,E}_{vol}$ = Heat capacity of PY material at constant stress and electric field
- ${}^{PY}p_3 = p^{T,E}_m$ = PY coef at constant stress (free boundary condition) and electric field

Efficiency expressions under OC

This is not as straightforward as the SC case. Although the data on heat capacity for SC case, ${}^{PY}c^{T,E}_{vol}$, is readily available, the same can not be said with regards to ${}^{PY}c^{T,D}_{vol}$.

Hence we require another relation[122,133] similar to those presented in Subsection 8.1.2;

$${}^{PY}c_{vol}^{T,D} - {}^{PY}c_{vol}^{T,E} = -\Theta(p_i^{T,E})(p_j^{T,E})(\beta_{ij}^{T,\Theta})$$

where $\beta_{ij}^{T,\Theta}$ = A component from the inverse of the permittivity tensor, $\boldsymbol{\varepsilon}^{T,\Theta}$

$p_i^{T,E}$ = PY coef at constant stress (free boundary condition) and electric field

Θ = Thermodynamic/Absolute temperature measured in Kelvin

${}^{PY}c_{vol}^{T,D}$ = Heat capacity of PY material at constant stress and electric displacement

${}^{PY}c_{vol}^{T,E}$ = Heat capacity of PY material at constant stress and electric field

With this relation in mind, one just needs to make following substitutions for the efficiency and Figure of merit for efficiency expressions under OC.

- ${}^{Com}p_3 = p(R,k) = p_m^{OC}$ from Eq 8.10
- ${}^{PY}c_{vol} = {}^{PY}c_{vol}^{T,D}$ = Heat capacity of PY material at constant stress and electric displacement
- ${}^{PY}p_3 = p_m^{T,D}$ = PY coef at constant stress (free boundary condition) and electric displacement

Note that with $p_i^{T,E}$ being non-zero only at $i = 3$ and having relatively small magnitude, this difference between heat capacities under SC and OC is expected to be very small for our case. In fact, Nye's book[133] puts the order of magnitude of relative difference between the two at 10^{-5}. Therefore the heat capacities are assumed to be the same for both SC and OC for the analysis.

Chapter 9

Results and discussion - Boundary conditions and thermal mass

This chapter will analyze the SC and OC PY coef enhancement and thermal-to-electrical conversion efficiencies for the laminate composites as R varies. In Section 9.1, the author will comment on and compare the enhancement potentials of various PY-NP pairs under two electrical boundary conditions. The differences between PY coefs measured under short and open circuit conditions will be highlighted and discussed. Section 9.2, will deal with the thermal-to-electrical conversion efficiencies of PY-NP pairs under both electrical boundary conditions, namely SC and OC. Evaluation procedures introduced in 8.2.3 and 8.2.3 will be followed to calculate the Figures of merit for efficiency for the pairs under SC and OC, respectively.

9.1 Pyroelectric coefficient under two conditions

9.1.1 Enhancement potentials of various pyroelectric and non-pyroelectric pairs under OC

The enhancement potentials of various PY-NP pairs under two electrical boundary conditions will be compared. The differences between PY coefs measured under short and open circuit conditions will be highlighted and discussed. Six different PY and NP materials were paired and analyzed for their open circuit PY coef alteration credentials. Although all the thirty-six pairs were examined, the conclusions of only selected few with the most interesting results are presented in Figures 9.1, 9.2, and 9.3.

Note the stand alone PY coefs of various PY materials and the difference between them and their SC counterparts. Tables B.1 and B.2 in Appendix B.1 elucidate the difference between the material properties under SC and OC. In particular, materials with high $p_m^{T,E}$ such as PZT, BTO, and LTO show the largest change in their thermal expansion coefs due to the relation stated in Eq 8.9. This significant change in their thermal expansion behaviour also leads to substantial change in their secondary contribution to the overall PY coef under OC, $p_m^{T,D}$. For PZT, LTO, and LNO the magnitude of PY coef is greater under OC, while the opposite is true for others as illustrated in Table B.2. This suggests that where secondary PY coef is concerned, it is rather difficult to anticipate its contribution to overall PY coef under both SC and OC conditions until all the components, such as the thermal expansion coefs and the signs of the secondary part, are all identified and their interactions assessed for its overall input. Table B.4 further reinforces this view as the signs of the secondary PY coefs are only different from that of under SC in materials such as LTO, LNO, and PVDF despite the expected change of sign from Eq 8.10, owing largely to significant change in the thermal expansion coefs as displayed in Table B.1. For instance, although Eq 8.10 suggests PZT-5H's secondary PY coef under OC might have the opposite sign from that under SC, valued at -0.473×10^{-4} $Cm^{-2}K^{-1}$, it actually evaluates to -18.593×10^{-4} $Cm^{-2}K^{-1}$ since its thermal expansion coefs are altered so drastically under OC as apparent from Table B.1. Meanwhile, LTO's secondary PY coef under OC valued at -0.195×10^{-4} $Cm^{-2}K^{-1}$ has the opposite sign from that under SC, 0.103×10^{-4} $Cm^{-2}K^{-1}$ as the thermal expansion coefs of LTO are not changed as severely from the transition of electrical conditions.

PZT-5H

The behaviour of PZT-5A is very similar to that of PZT-5H, and hence only the results of PZT-5H are provided. It is evident from Tables B.1 and B.2 that PZT-5H is the main beneficiary of the increased PY coef under OC owing to substantial changes in its thermal expansion coefs as consequences of high PY coef under SC. Its PY coef under OC is -23.1×10^{-4} $Cm^{-2}K^{-1}$, whereas under SC this is only -5.0×10^{-4} $Cm^{-2}K^{-1}$. In addition, its dc1, dc2, and dc3 values under OC is also about 5.4 times larger than that under SC, leading to larger contribution from the secondary effect to the overall PY coef, as depicted in Figure 9.2(a).

It is evident from Figures 9.2(a) and 9.1 that what was an enhancement under SC

at low thickness ratios (R) is a reduction under OC due to the sign for secondary effect demonstrated in Eq 8.10 and the secondary contribution can be so large that at very low R values it actually switches the sign of the overall PY coef to the positive region peaking at huge PY coef of $97 \times 10^{-4}\ Cm^{-2}K^{-1}$ at $R = 0.005$ (minimum R value evaluated, namely R_{min}) for PZT5H-CPVC pair and around $40 \times 10^{-4}\ Cm^{-2}K^{-1}$ at $R = R_{min}$ for PZT5H-Zn pair. The R value at which the sign change in the total PY coef occurs is smaller for NP materials with lower Young's modulus and thermal expansion coefs as expected. Figure 9.1 illustrates how the secondary contribution varies in some of PZT-5H's pairs when R is small, i.e. when NP material's influence is very large, demonstrating some extreme PY coefs at very low R.

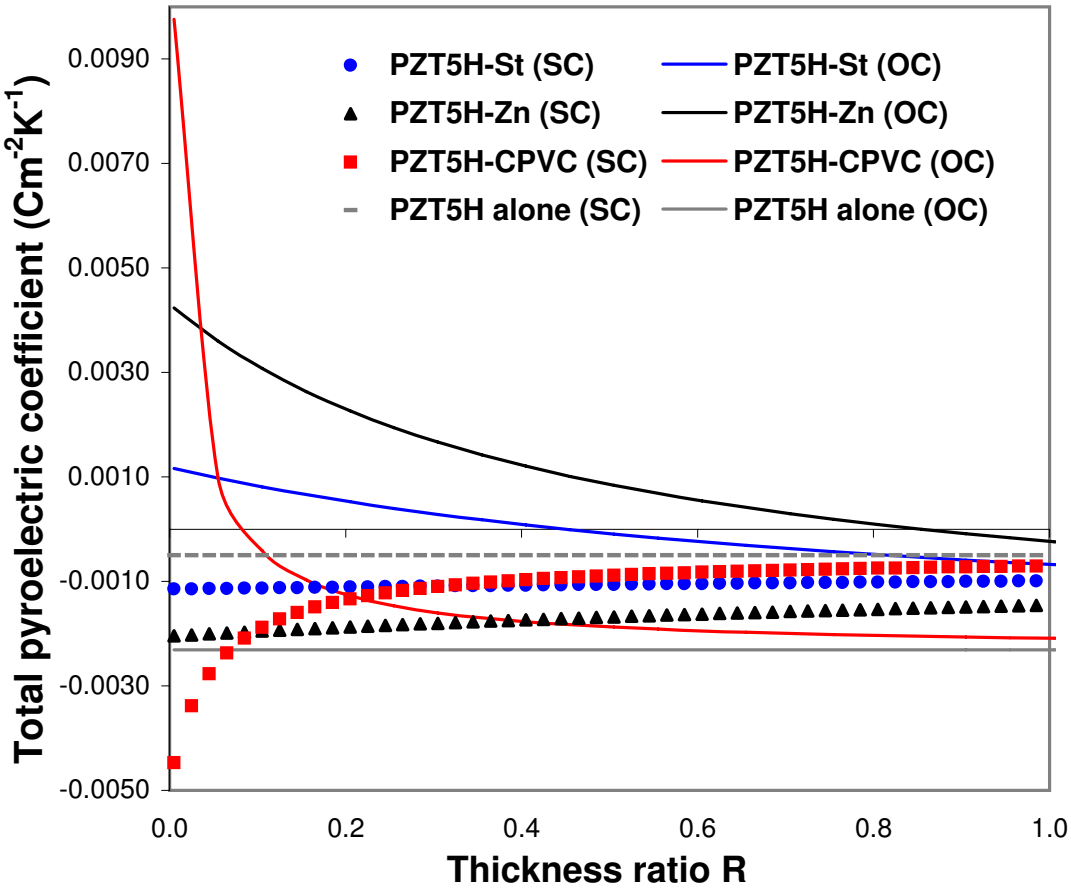

Figure 9.1: Total pyroelectric coefficients of various pairs under SC and OC for very small thickness ratio

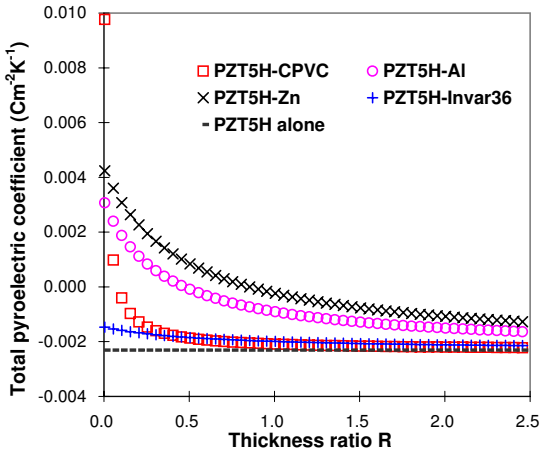

(a) Total PY coef vs R for PZT-5H pairs under OC

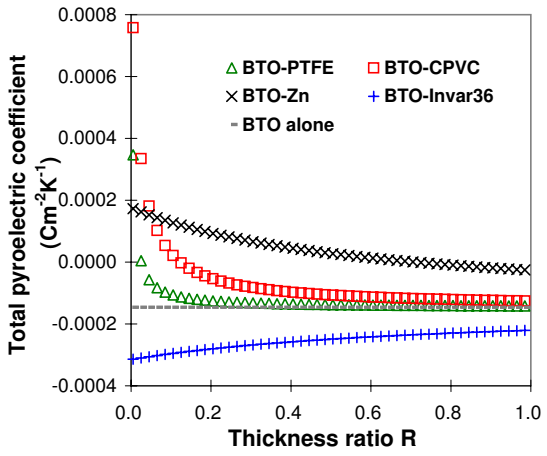

(b) Total PY coef vs R for BTO pairs under OC

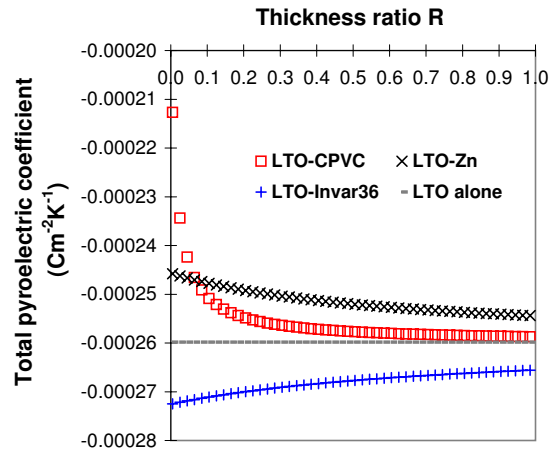

(c) Total PY coef vs R for LTO pairs under OC

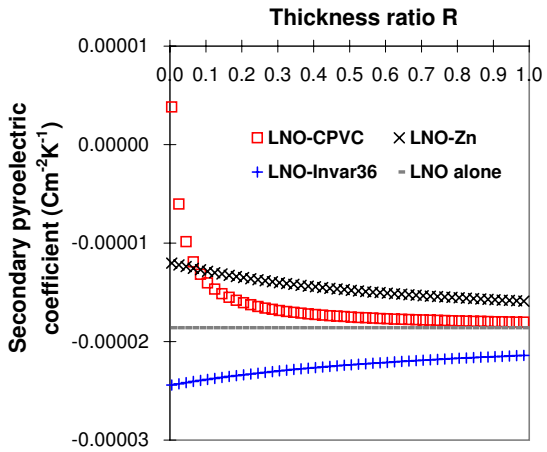

(d) Total PY coef vs R for LNO pairs under OC

Figure 9.2: Total pyroelectric coefficients for various PY-NP pairs under OC

BTO

BTO and PVDF were the only PY materials that experienced reduced PY coef under OC when compared to that evaluated under SC. Although BTO's thermal expansion coefs also experienced quite a large change, α_3^D in particular as exhibited in Table B.1, the change in its dc1, dc2, and dc3 meant that the overall secondary effect under OC is drastically reduced to approximately $-0.079 \times 10^{-4}\ Cm^{-2}K^{-1}$, which is only about one eighth of that under SC.

As is evident from Figure 9.2(b), BTO-CPVC attains the highest total PY coef of $7.6 \times 10^{-4}\ Cm^{-2}K^{-1}$ at $R = R_{min}$ and maintains its superiority till $R = 0.05$ at which

point BTO-Zn takes over as the dominant pair. However, BTO-Invar36 is the only pair that consistently outperforms BTO's own PY coef as it is the only pair that has PY coef more negative than $-1.461 \times 10^{-4}\ Cm^{-2}K^{-1}$, the PY coef of BTO under OC, with maximum value of approximately $-3.14 \times 10^{-4}\ Cm^{-2}K^{-1}$ at R_{min}, owing to Invar36's unusually small thermal expansion coef.

LTO

Figure 9.2(c) displays the PY coefs for LTO pairs. All the pairs except LTO-Invar36 show reduction in the PY coef with LTO-CPVC reaching minimum of -2.127×10^{-4} $Cm^{-2}K^{-1}$ and LTO-Invar36 maximum of $-2.725 \times 10^{-4}\ Cm^{-2}K^{-1}$ at R_{min}. All in all, LTO behaves similar to BTO with the exception of sign change in the PY coefs owing to the limited secondary effect contribution to the overall PY coef.

LNO

The behaviors of the PY coefs of LNO pairs are very similar to that of LTO pairs. Figure 9.2(d) demonstrates how similar they are by displaying the secondary PY effect contributions to the overall PY coef arising from the introduction of the NP materials. LNO-Invar36 is again the only pair that exhibits enhancement in the secondary PY coef, and hence the overall PY coef, while LNO-Zn shows reduction but falls short of changing the sign of the secondary effect. LNO-CPVC, however, displays both reduction and change of sign in the secondary PY coef. The maximum secondary PY coef observed is $-0.244 \times 10^{-4}\ Cm^{-2}K^{-1}$ at R_{min} by LNO-Invar36 pair, which corresponds to around 31% increase in the secondary PY coef by the introduction of Invar36 to LNO.

PVDF

PVDF experienced reduced PY coef under OC as illustrated in Table B.2. Although the difference in the magnitude of the overall PY coef is quite small, the introduction of NP materials does affect the PY coef of PVDF as depicted in Figure 9.3(a). Introduction of PTFE or CPVC leads to enhancement while others results in reduction with both PVDF-PTFE and PVDF-CPVC reaching their maximum values of approximately $-0.28 \times 10^{-4}\ Cm^{-2}K^{-1}$ at R_{min}.

Another measure for the performance of NP elastic layers is shown in Figure 9.3(b). It demonstrates how much of an alteration potential the introduction of NP material

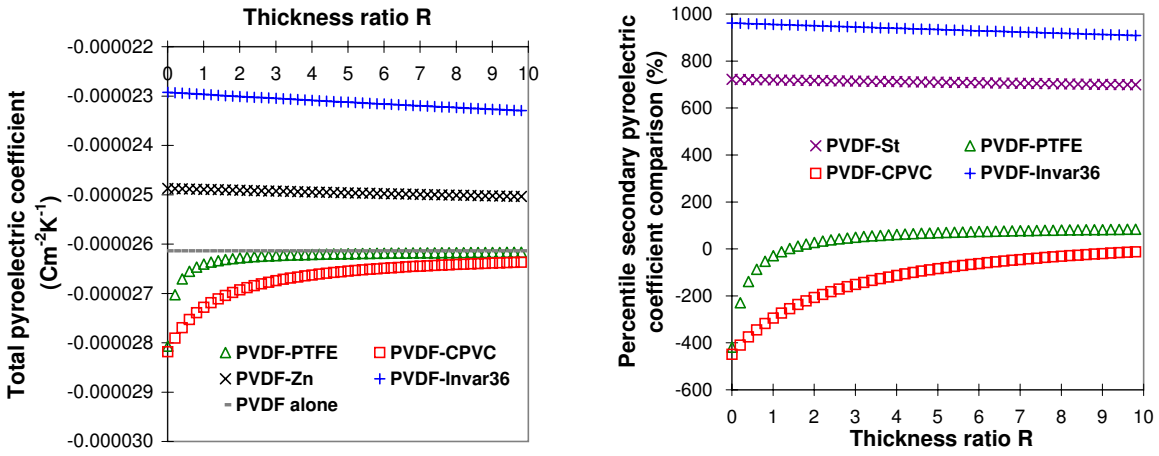

(a) Total PY coef vs R

(b) Percentile secondary contribution from NP material vs R

Figure 9.3: Pyroelectric coefficient enhancements in PVDF pairs under OC

has on the secondary PY coef of PVDF in percentage terms. The reason why using this method of comparison might be better than the one utilized in Figure B.2 is presented in Section 4.2. At R_{min}, PVDF-Invar36 pair presents the greatest change of 960% and PVDF-St about 720%, with St outperforming both Al and Zn, unlike with other PY material pairs. Since the overall PY coef is negative while the secondary PY coef of PVDF alone under OC is positive, both Invar36 and St results in the reduction of the overall PY coef's magnitude. However, with negative percentile secondary contributions PTFE and CPVC lead to enhancement. At R_{min}, PVDF-PTFE peaks at -420% while PVDF-CPVC reaches -450%, both indicating over 300% increase in the secondary PY coef of the PVDF composites, which potentially points to extremely large enhancement in other PVDF samples with greater proportion of secondary contribution.

Best performing pairs

In terms of the pure magnitude of the PY coef under OC, PZT-5H is the best performing PY material as illustrated in Figure 9.2(a). PZT-5H-CPVC pair's huge PY coef of 97 $\times$ 10^{-4} $Cm^{-2}K^{-1}$ at R_{min} and around 40 $\times$ 10^{-4} $Cm^{-2}K^{-1}$ at $R = 0.022$ after which PZT-5H-Zn takes over as the optimum PY coef pair are unrivaled by all of the PY material investigated.

9.2 Figure of merit for efficiency types a and b under two conditions

In this section, the author would like to comment on and compare the thermal-to-electric conversion efficiencies of PY-NP pairs under both electrical boundary conditions, namely SC and OC. Evaluation procedures introduced in 8.2.3 and 8.2.3 will be followed to calculate the Figures of merit for efficiency for the pairs under SC and OC, respectively.

9.2.1 Figures of merit for efficiency of various pyroelectric and non-pyroelectric pairs under SC

Figures of merit for efficiency under SC for various PY-NP pairs are considered. As with PY coef enhancement potential under SC assessment in Subsection 6.2.1, the results from only pairs of PZT-5H, BTO, and PVDF will be presented.

PZT-5H

Figure 6.4(a) portrayed the extreme PY coef enhancement with CPVC at low R values ($R < 0.15$). Owing to this enhancement, the efficiency increase illustrated in Figure 9.4(a) is also very large when the same volume of PY material and composites are considered (F^a_{eff}). At extremely low R of 0.005, F^a_{eff} peaks at 20 for PZT5H-CPVC pair, indicating a twenty fold increase in its efficiency. PZT5H-Al overtakes PZT5H-CPVC pair at $R = 0.35$ with F^a_{eff} of 3.5 and continues to outperform the latter at higher R values. This could be important in applications such as PY sensors[188,189]. In particular, the large efficiency increases at extremely low R values suggests a thin PZT-5H on CPVC substrate may find potential application in PY sensors. Even for the Figure of merit for efficiency between PY material alone and NP material added on top (F^b_{eff}), as illustrated in Figure 9.4(b), PZT-5H attains values above 1.0, i.e. an improvement, for PTFE, CPVC, Al, and Zn. This denotes PZT-5H to be very promising for applications where large amount of steady heat energy is readily available, for example in PY energy harvesting[70,138] which utilizes industrial residual heat.

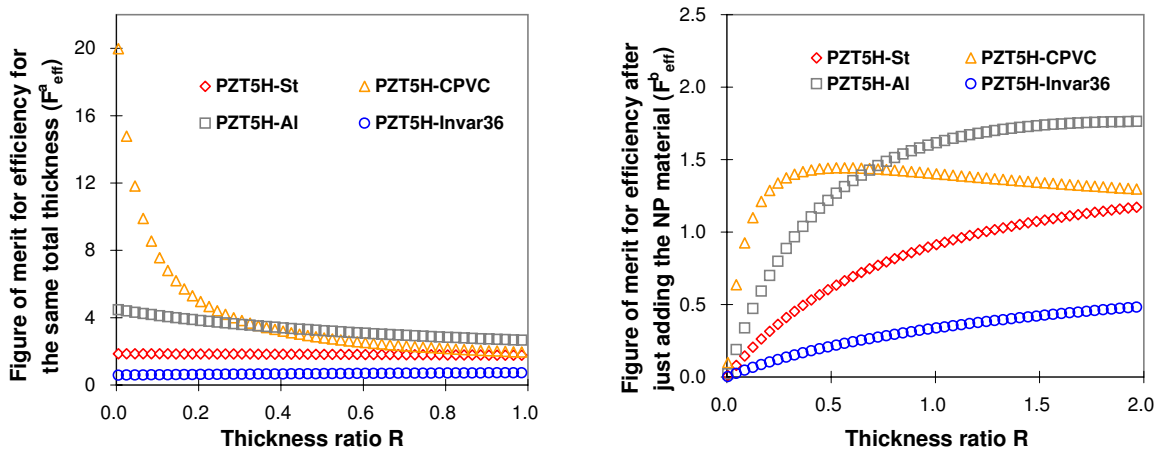

(a) F^a_{eff} vs R for PZT-5H pairs under SC (b) F^b_{eff} vs R for PZT-5H pairs under SC

Figure 9.4: Figure of merit for efficiency of PZT-5H pairs under SC

BTO

Figure 6.4(b) described largely subdued enhancement for BTO due to relatively small dc values when compared to PZT-5H. However, BTO-CPVC displayed rather high enhancement for small thickness ratios of $R < 0.1$. As far as F^a_{eff} is concerned, Figure 9.5(a) denotes PTFE (Teflon) displaying the most promising Figure of merit for efficiency at low R values with Al performing the best of the rest, excluding CPVC, which performed only slightly worse than PTFE with similar trends of high values at low R. When F^b_{eff} of BTO pairs is considered, BTO-PTFE pair has Figure of merit for efficiency larger than one as illustrated in Figure 9.5(b), signifying that the efficiency improvement is a possibility with F^b_{eff} approaching 1.11, i.e. 11% increase. This seems to indicate that a thin coating of PTFE on BTO can lead to higher efficiency.

PVDF

PVDF is a polymer with rather high thermal expansion coef with dc values of opposite signs from the rest of PY materials investigated so far, and hence it is expected to behave rather differently from other PY materials. In Figure 6.4(d), a maximum of 300% enhancement in the secondary PY coef for PVDF-Invar36 pair was predicted, which could potentially lead to extremely large enhancement in other PVDF samples with higher proportion of secondary contribution. Where F^a_{eff} is concerned, Figure 9.6(a) shows PVDF-PTFE demonstrating relatively good values, nearly approaching 3 at very

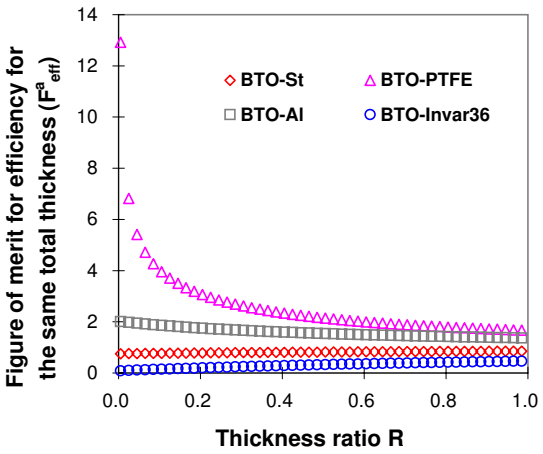

(a) F^a_{eff} vs R for BTO pairs under SC

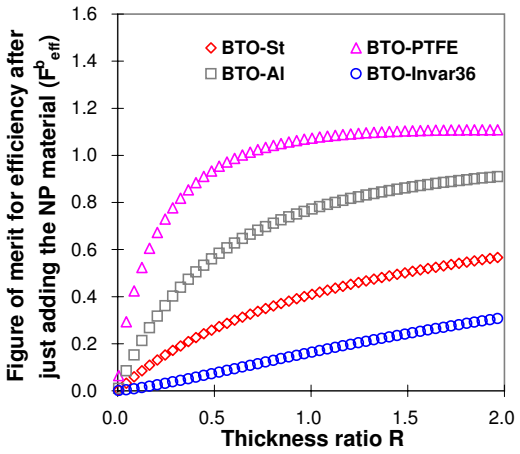

(b) F^b_{eff} vs R for BTO pairs under SC

Figure 9.5: Figure of merit for efficiency of BTO pairs under SC

low R, suggesting an improvement in efficiency owing almost entirely to very small heat capacity of PTFE (cf. Table A.4). However, other pairs struggle to approach 1 due to already rather low heat capacity of PVDF and very small magnitude of enhancement in comparison. All F^b_{eff} values for PVDF pairs struggle to achieve values higher than one with none of the NP materials actually managing to achieve $F^b_{eff} = 1$ within the range of $0 < R < 2$, as illustrated by Figure 9.6(b). Therefore, among all the PY materials analyzed PVDF pairs are the worst performers when it comes to efficiencies, which is not too surprising since the overall magnitude of enhancement was rather small.

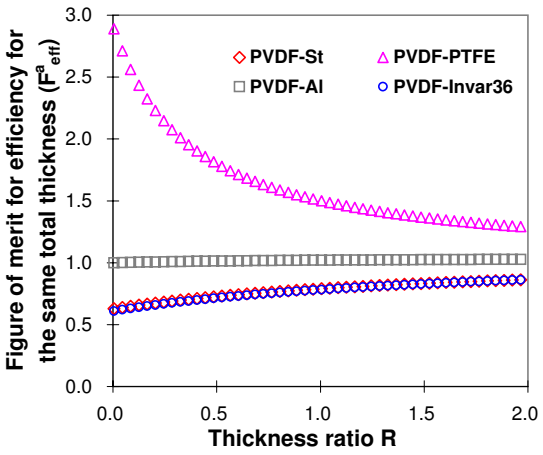

(a) F^a_{eff} vs R for PVDF pairs under SC

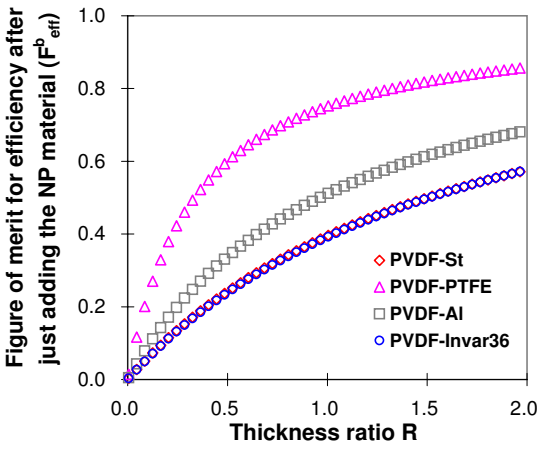

(b) F^b_{eff} vs R for PVDF pairs under SC

Figure 9.6: Figure of merit for efficiency of PVDF pairs under SC

Best performing pairs

PZT5H-CPVC's F^a_{eff} peaked to 20 and F^b_{eff} to 1.5. For PZT5H-Zn F^a_{eff} reached maximum of 4.6 and F^b_{eff} of 2.1, while PZT5H-Al showed very similar trends with maximum F^a_{eff} of 4.5 and F^b_{eff} of 1.7. All these improvements in efficiencies of PZT-5H insinuates a potential for increased use of PZTs in areas such as PY sensors[188,189] and PY energy harvesting[70,138]. As far as BTO pairs' F^a_{eff} is concerned, PTFE (Teflon) showed the most promising Figure of merit for efficiency of 13 at low R values, while their F^b_{eff} became larger than one at $R > 0.605$. For PVDF, only PVDF-PTFE's F^a_{eff} approaches 3 at very low R while F^b_{eff} for all the pairs investigated was smaller than 1.

9.2.2 Figures of merit for efficiency of various pyroelectric and non-pyroelectric pairs under OC

Figures of merit for efficiency under OC are considered. PZT-5A's results have similar trend to that of PZT-5H, so only that of the latter will presented. Unlike in SC case, the results of LTO and LNO will also be presented for OC as they are PY single crystals widely employed in OC applications such as PY X-ray generation[35,63]. Only the figures of merit for efficiency demonstrating interesting findings will be dealt with in this subsection.

PZT-5H

Figure 9.7(a) describes the figure of merit for efficiency belonging to the same volume of PZT-5H and its composites (F^a_{eff}). They all reach the value of zero at certain values of R owing to the PY coef switching between negative and positive signs at low R values. PZT-5H-CPVC pair peaks at around 9.4 at R_{min} while PZT-5H-PTFE reaches its maximum of approximately 7.0 at the same R_{min}. It is apparent from Figure 9.7(a) that both pairs mentioned above have reasonably high F^a_{eff}, between 2.6 and 1.3, for the whole of the R range considered, insinuating improvement in the efficiencies of PZT-5H when CPVC or PTFE is attached. Zn and Al pairs fail to reach figure of merit for efficiency of higher than one except at $R < 0.230$ and $R < 0.110$ respectively, and this trend is expected to continue at R values higher than one as increasing R means less volume of NP material attached and hence the overall PY coef converging to that of PZT-5H alone. Where F^b_{eff} is concerned, all pairs depict values lower than one, hence worse efficiency than PZT-5H alone, within range $0 < R < 2$ except PZT5H-PTFE which exceeds one for

$R > 1.125$. In fact, PZT5H-PTFE pair demonstrated maximum F^b_{eff} of 1.7 near $R = 3$ region as illustrated in Figure 9.7(b) with larger R range.

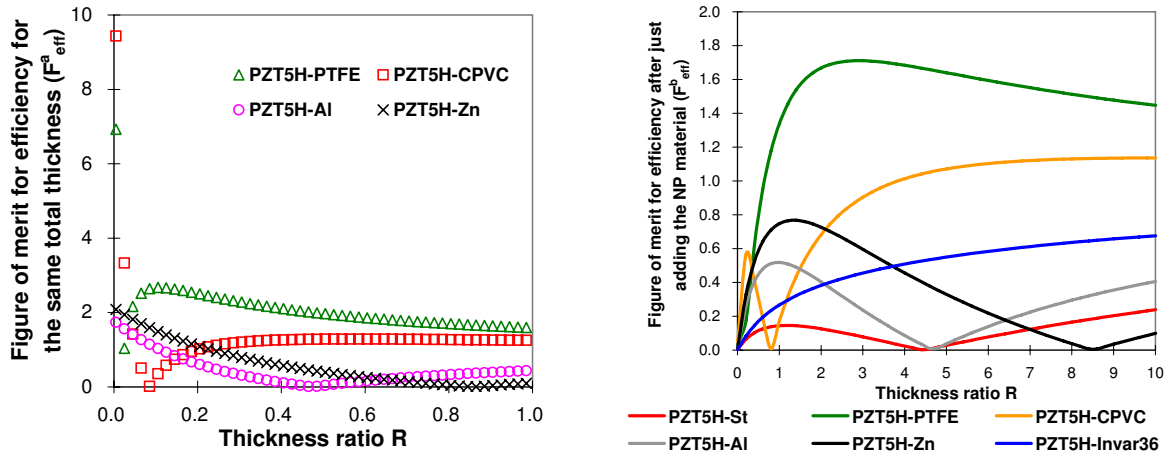

(a) F^a_{eff} vs R for PZT-5H pairs under OC

(b) F^b_{eff} vs R for PZT-5H pairs under OC

Figure 9.7: Figure of merit for efficiency of PZT-5H pairs under OC

BTO

Figure of merit for efficiency when NP materials are added to BTO, leading to increased volume, are presented in Figure 9.8. Where F^a_{eff} is concerned,BTO-PTFE and BTO-CPVC pairs demonstrated maximum of 10 and 12 respectively at R_{min}, while the only other pair to have value larger than one is BTO-Invar36 pair with consistent above one values throughout the range of R investigated in Figure 9.8(a). This suggests that where BTO applications are concerned, a layer of Invar36 on its surface may improve its thermal-to-electrical conversion efficiency slightly while where very thin BTO is employed on very thick substrates of PTFE or CPVC, a large improvement could be expected. As evident from Figure 9.8(b), although some enhancement on the magnitude of the PY coef is achieved, it is not enough to drive F^b_{eff} to higher than one in all the pairs except one. BTO-PTFE pair is the only one which possesses $F^b_{eff} > 1$ reaching maximum of 1.05 at $R = 2.00$, while all the others indicate reduction in efficiency due to increased thermal mass. BTO-Invar36 is the second best performing pair for BTO, which is quite surprising considering Invar36's rather high volumetric heat capacity of $5.15 \times 10^6\ Jm^{-3}K^{-1}$, the highest among all NP and PY materials considered.

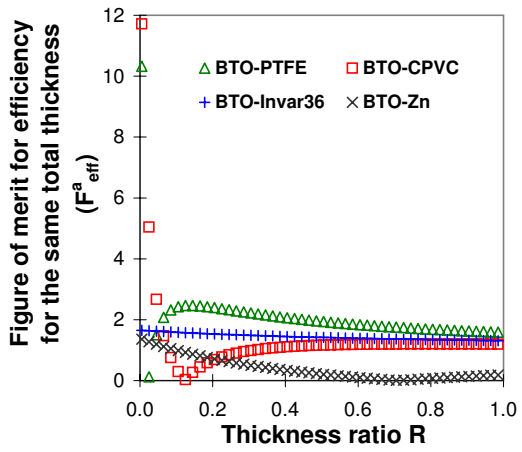

(a) F^a_{eff} vs R for BTO pairs under OC

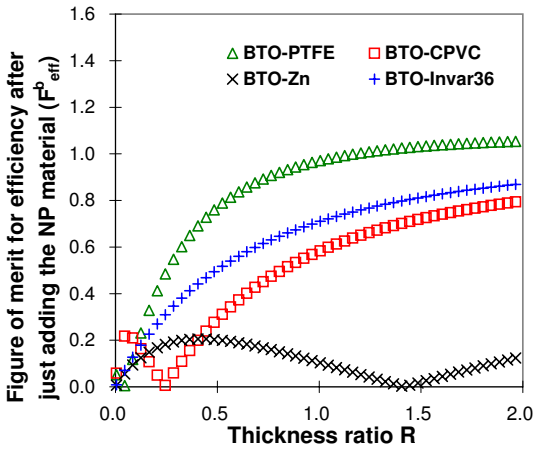

(b) F^b_{eff} vs R for BTO pairs under OC

Figure 9.8: Figure of merit for efficiency of BTO pairs under OC

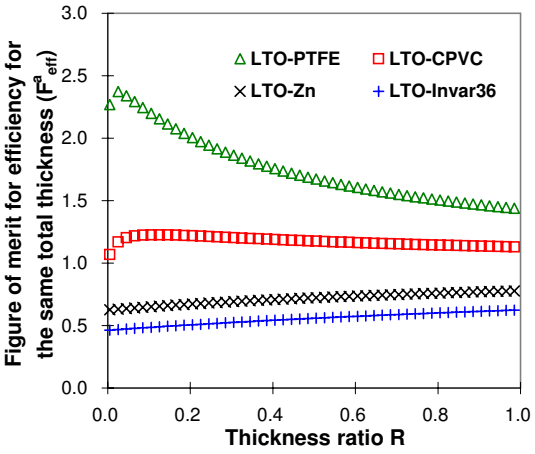

(a) F^a_{eff} vs R for LTO pairs under OC

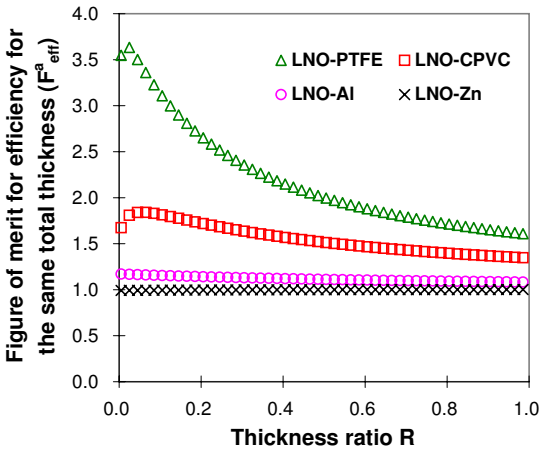

(b) F^a_{eff} vs R for LNO pairs under OC

Figure 9.9: Figure of merit for efficiency of LTO and LNO pairs under OC

LTO

Although most of the pairs show reduction in the PY coef magnitude, some manage to show improvement in efficiency where the same volume of the composites are concerned (F^a_{eff}) as illustrated in Figure 9.9(a). LTO-PTFE pair exhibits peak of approximately 2.4 at $R = 0.025$ and maintains $F^a_{eff} > 1$ throughout the R range investigated with the minimum of 1.4 at $R = 1.005$. LTO-CPVC also manages $F^a_{eff} > 1$ throughout the R range albeit at much smaller values of $1.1 < F^a_{eff} < 1.2$. The reasons behind these improvements are the exceptionally low volumetric heat capacities of PTFE and CPVC,

again leading to good F^a_{eff} values.

LNO

As evident from Figure 9.9(b), where F^a_{eff} is concerned LNO-PTFE performs the best with the optimum F^a_{eff} value of 3.63 at $R = 0.025$ due to PTFE's lowest volumetric heat capacity among all the materials investigated. LNO-CPVC pair does not fare too badly either with optimum of 1.84 at $R = 0.065$, while other pairs exhibiting improvement in the efficiency also include LNO-Al and LNO-Zn, whose F^a_{eff} lie very near to one.

PVDF

Figure 9.10 depicts F^a_{eff} behavior of PVDF pairs. Only PTFE and CPVC exhibits improvement in efficiency while Al and Zn nearly approaches $F^a_{eff} = 1$ mark, which St and Invar36 fails to do. At R_{min}, maximum F^a_{eff} of 3.4 is attained by PVDF-PTFE, while PVDF-CPVC pair reaches 1.8, both indicating significant improvement in efficiency.

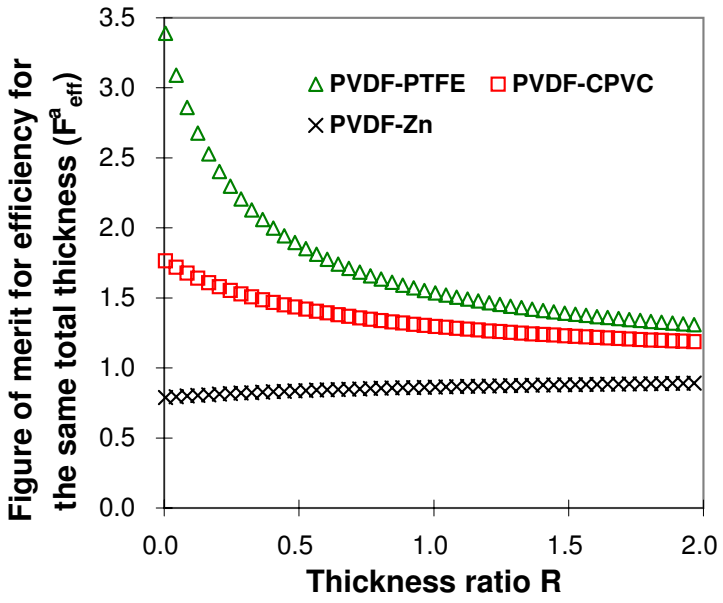

Figure 9.10: Figure of merit for efficiency F^a_{eff} of PVDF pairs under OC

Best performing pairs

In order to illustrate the best performer in the figure of merit for efficiency values, Figure 9.11 has been presented despite it displaying PZT-5A pairs. As evident from

Figure 9.11 and others, as far as F^a_{eff} is concerned, PZT5A-PTFE achieves maximum of 24, PZT5H-CPVC 9.4, BTO-CPVC 12, and PVDF-PTFE obtains 3.4 at R_{min}, while LTO-PTFE and LNO-PTFE attains 2.4 and 3.63 respectively at $R = 0.025$. PZT5A, LTO, and PVDF all fail to register any pair that exhibited improvement in the efficiency with F^b_{eff}. However, PZT5H-PTFE reaches $F^b_{eff} \approx 1.7$ at $R \approx 3.0$, while F^b_{eff} reaches values higher than one for BTO-PTFE at $R > 1.1$ and LNO-PTFE at $R > 0.95$.

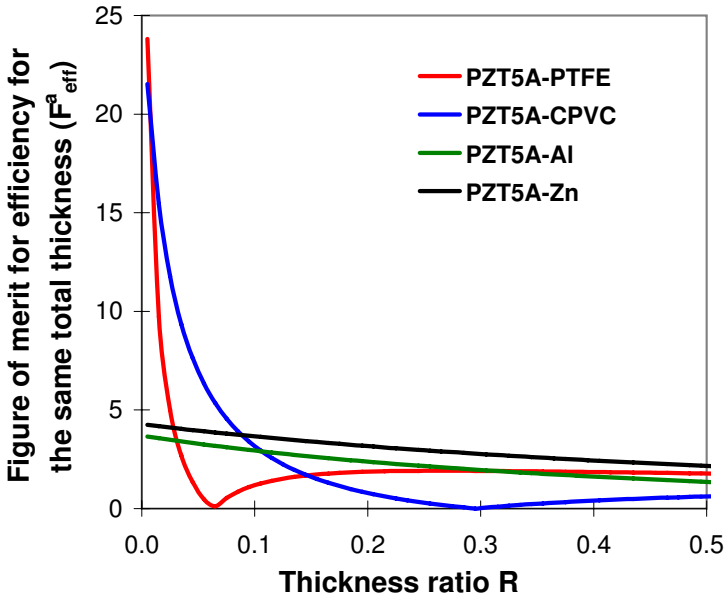

Figure 9.11: Figure of merit for efficiency F^a_{eff} of PZT-5A pairs under OC displaying extreme values

Chapter 10

Conclusions - Boundary conditions and thermal mass

After considering PY X-ray generation (cf. Section 11.2), which should be under OC, as a potential application for the PY coef enhancement achieved earlier, it was discovered that the enhancement in the secondary PY coef behaves rather differently under OC when compared to that under SC. This difference for various materials and their 2-2 connectivity laminate composites have been presented while the difference between these two boundary conditions were also highlighted. We achieved this by first considering the definition of the two electrical boundary conditions, namely SC and OC, and the relationship between various material properties under these two conditions. The PY coef expression under OC was also derived and compared with that under SC from Part I. By defining a quantity termed "efficiency", a measure for the laminate composites' thermal-to-electrical conversion efficiency was proposed, while Figures of merit for efficiency (F^a_{eff} and F^b_{eff}) were derived as a ratio between the efficiencies of stand alone PY material and its laminate composite for the purpose of comparing the efficiencies between them. Using these figures of merit for efficiency, various PY-NP pairs and their potential efficiency improvements were analyzed.

On the whole, in terms of the magnitude of the PY coef change, Zn was found to outperform Al/St and CPVC to outperform PTFE in most of the pairings with PY materials except PVDF, in which case it was the opposite due to PVDF's extremely high thermal expansion coef. This is due to Zn and CPVC having higher thermal expansion coef and Young's modulus than Al and CPVC, respectively. However, where the figures of merit for efficiency is concerned, this did not always hold since PTFE and Al possess lower

volumetric heat capacity than CPVC and Zn, respectively. Following sections provide further details on the outcomes of these analyses.

10.1 Thermal mass considerations under short circuit condition

Investigation into the thermal mass issue of the laminate composites from Part I have taken place using Figure of merit for efficiency with two different cases considered (F^a_{eff} and F^b_{eff}) and examined for all thirty-six PY-NP pairs of interest. With PZT-5H and PZT-5A exhibiting very large PY coef enhancement with theoretical possibility of 800% increase at R_{min} for PZT5H-CPVC, high Figure of merit for efficiency with the maximum of twenty fold increase was predicted by F^a_{eff}, while F^b_{eff} predicted improvements in the thermal-to-electrical conversion efficiencies for pairs with PTFE, CPVC, Al, and Zn. All these improvements in efficiencies of PZT-5H insinuates a potential for increased use of PZTs in areas such as PY sensors[188,189] and PY energy harvesting[70,138].

BTO's PY coef enhancement potential was much less than PZT's, but as far as F^a_{eff} and F^b_{eff} are concerned, BTO-PTFE showed the most promising Figure of merit for efficiency at low R values, insinuating that a thin layer of BTO on thick PTFE could lead to higher efficiency. Only PVDF-PTFE and PVDF-CPVC displayed an improvement in F^a_{eff} while F^b_{eff} was smaller than one for all PVDF pairs, due to the minute magnitude of the overall PY coef enhancement.

10.2 Pyroelectric coefficient, its enhancement, and thermal mass considerations under open circuit condition

For OC, extraordinarily large PY coef of $97 \times 10^{-4}\ Cm^{-2}K^{-1}$ at minimum thickness ratio R_{min} is expected for PZT-5H-CPVC pair, while PVDF-CPVC could show increase in the secondary PY coef of up to 350%. In addition, where the figures of merit for efficiency are concerned, for the same volume of the composite (F^a_{eff}) PZT-5A-PTFE pair reaches 24, a twenty-four fold increase in efficiency at R_{min}, while F^b_{eff} indicates most pairings under OC will struggle to achieve the same level of efficiency when additional NP

materials, and hence additional thermal mass, are introduced for the PY coef alteration.

The best performing pairs for F^a_{eff} are; PZT5A-PTFE at 24, PZT5H-CPVC 9.4, BTO-CPVC 12, and PVDF-PTFE at 3.4 when $R = R_{min}$, while LTO-PTFE and LNO-PTFE attains 2.4 and 3.63 respectively at $R = 0.025$. PZT5A, LTO, and PVDF all fail to register any pair that exhibited improvement in the efficiency with F^b_{eff}. However, PZT5H-PTFE reaches $F^b_{eff} \approx 1.7$ at $R \approx 3.0$, while F^b_{eff} reaches values higher than one for BTO-PTFE at $R > 1.1$ and LNO-PTFE at $R > 0.95$.

Note that the assumptions made in the thermal expansion coefs under SC (cf. Table A.2), for example PZT manufacturer's data on coefs in all three axes being the same, which are used to evaluate the thermal expansion coefs under OC (cf. Table B.1), makes the numerical values of the secondary PY coefs under OC somewhat questionable. However, it is clear from the analyses that there indeed is a substantial dissimilarity between the PY coefs and figures of merit for efficiency for various PY-NP pairs under SC and OC. In fact, the effect these electrical boundary conditions have on the ferroelectric domain structures of Lead titanate thin films have already been investigated by Li et al.[106] with interesting results. The author believes this implies that there should be a greater distinction made between the PY coefs under SC and OC than previously thought. The analysis techniques used here provide a methodology for assessing the potentials of particular PY material and its 2-2 laminate composites for applications under OC. For instance, appraising employment credentials of LTO or LNO in applications such as PY X-ray generation, electron accelerator, and nuclear fusion (cf. Chapter 11).

Part II

Potential applications

Various applications where pyroelectric coefficient enhancement may find use in will be considered. In particular, its applicability in pyroelectric energy harvesting will be analyzed via analytical modelling of a hypothetical pyroelectric energy harvesting system. How the enhancement affects the system's performance will be assessed while the parameters that play a significant role in this assessment will be identified. The energy harvesting potentials of thirty-six 2-2 connectivity laminate composites and the experimental samples of Enhancement study from Part I will also be assessed.

Chapter 11

Literature review - Potential applications

This literature review will provide an overview of the potential applications of the enhanced pyroelectric effect described in Part I. Although some of the applications listed here are not discussed in great detail, the author believes they are areas where this enhancement could have an impact.

At the outset, the application of most interest for this project was PY X-ray generation presented in Section 11.2. However, as the project progressed it became apparent that evaluating the potential impact the enhancement can have on this particular application would be rather difficult. Even theoretical approximation would not be possible at this stage as the definite theoretical description behind this particular X-ray generation phenomenon is not yet known to the author's knowledge. With experimental verification out of the question due to time and equipment constraints, it was decided that we will make the energy harvesting application (cf. Section 11.1) the key area of interest.

Note that although Subsection 11.1.1 describes energy harvesting method that is not pyroelectric, with the enhancement described in this dissertation being piezoelectric effect based, and rather large amount of research having been conducted on piezoelectric energy harvesting methods by others already, the author felt it would be useful to introduce the readers to this field as well. In fact, the author uses one of the techniques proposed in this area of research to evaluate the performance of the enhanced laminate composites in pyroelectric energy harvesting application (cf. Chapters 12 and 13).

11.1 Pyroelectric energy harvesting

Recent developments in mobile devices have lead to increased use of wireless technology, which suffers from design and portability constraints owing to the use of batteries and their limited capacity/lifetime and miniaturisation issues. Therefore there has been a large increase in research being conducted on self-powering systems and energy harvesting applications form an integral part of this. Although there are many different miniature energy harvesting technologies being considered at present, solar cells, thermoelectricity, Micro fuel cells, and Micro engines to name a few, this section details two particular examples of energy harvesting methods that are of interest to this project, namely pyroelectric and piezoelectric methods. It should be noted that various hybrids of these and other methods of energy harvesting also exist, such as the hybrid between magnetostriction and piezoelectricity in Magnetoelectric[146,147] devices.

11.1.1 Piezoelectric method

As the PY coef enhancement is in the secondary (piezoelectric) part of PY effect, it would be a good idea to look into piezoelectric energy harvesting methods first. In addition, much more research has been already conducted in piezoelectric energy harvesting application, which could benefit the PY one, more efficient energy harvesting electronic circuit for example.

Most research in piezoelectricity generally concerns actuation, control or self-sensing technology. However, recent need for miniature energy harvesting technology has resulted in significant research being conducted on piezoelectric energy harvesting technologies. For example, in 1984 researchers implanted PVDF patch onto the rib cage of a mongrel dog to harvest energy during respiration[74] with peak voltage of 18 V, which corresponds to around 17 μW of power. Other experiments followed with many successfully harvesting several μW to mW of usable power. More recent research include energy harvesting from the ambient vibration[172] or vibrational sources[23,168] for recharging a discharged battery[169,170]. Some other examples of piezoelectric energy harvesting applications are listed below while selected four's schematics are provided in Figure 11.1.

- Ren et al.[148]

Using 1-3 composites of Lead magnesium niobate-Lead titanate (PMN-PT) single crystals in a soft epoxy matrix, they have achieved 22.1 $mWcm^{-3}$ power density under a

mechanical stress of 40.4 MPa.

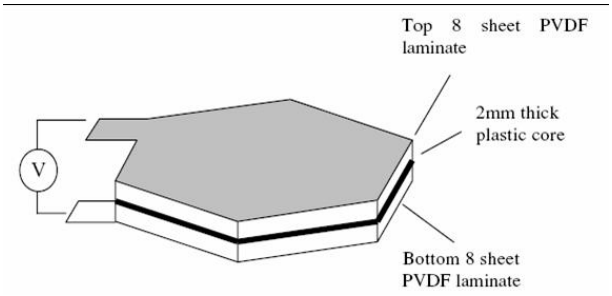

(a) PVDF/plastic laminate sheets by Kymissis et al.[97]

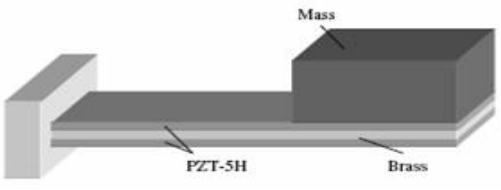

(b) Cantilever based system by Roundy et al.[154]

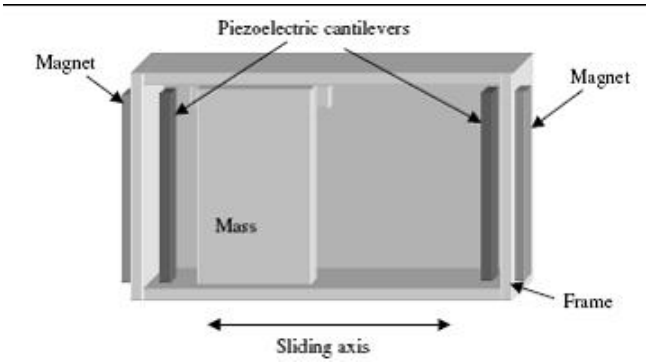

(c) Bi-stable impact based transducer by Renaud et al.[149]

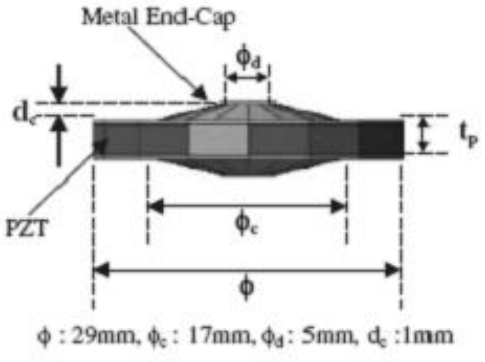

(d) Cymbal transducer by Kim et al.[92]

Figure 11.1: Various piezoelectric energy harvesting systems

- Umeda et al. at Niigata Polytech., Japan[180]

An impact based piezo-generator that transforms mechanical impact energy to electrical one using a steel ball impacting a PZT disc, was reported to produce 88.9 $\mu W cm^{-3}$.

- Kymissis et al. at MIT[97]

A PVDF/plastic laminate sheets in Figure 11.1(a) generated 81 $\mu W cm^{-3}$ of power when driven at 0.9 Hz frequency.

- Shenck et al. at MIT[164]

A PZT bimorph located in the heal of shoe that is being driven by a person walking, is reported to produce around 340 $\mu W cm^{-3}$.

- Roundy et al. at Berkeley[154]

A Brass/PZT cantilever with a Tungsten mass produced 375 $\mu W cm^{-3}$ when driven at 120 Hz frequency with 2.5 ms^{-2} acceleration using 9.2 g mass (cf. Figure 11.1(b)).

- Renaud et al. at IMEC, Belgium[149]

A configuration of permanent magnets and piezoelectric cantilevers, which are impacted by sliding inertial mass in a bi-stable state, the system in Figure 11.1(c) generated 40 $\mu W cm^{-3}$ power at 1 Hz frequency with 10 cm amplitude, i.e. 0.1 ms^{-2}.

- Kim et al. at ICAT, Penn. State Uni.[92]

Using a "cymbal" piezoelectric transducer design (a metal-ceramic/PZT composite in Figure 11.1(d)), at 100 Hz frequency they produced 39 mW of power. The power density was calculated to be 60 $mW cm^{-3}$. Use of cymbal structure resulted in stress amplification, enabling bigger contribution from d_{31} piezoelectric coef. In effect, this cymbal structure "actively" promotes the contribution from d_{31} based piezoelectric effect, which is analogous to the 2-2 connectivity laminate composites producing higher PY coef owing to Poisson effect driven contribution from d_{33}, which can be described as "passive".

11.1.2 Pyroelectric method

When considering energy conversion from heat, it is necessary to compare efficiencies with Carnot cycle efficiency ($\eta_{Carnot} = \frac{\Theta_H - \Theta_L}{\Theta_L}$), which is the maximum energy that can be converted from a given temperature variation. Seebeck effect based thermoelectric energy conversion has efficiency expressed as[117];

$$\eta_{therm} = \frac{\Theta_H - \Theta_L}{\Theta_L} \times \frac{\sqrt{ZT+1}-1}{\sqrt{ZT+1}+\frac{\Theta_H}{\Theta_L}} \tag{11.1}$$

where Θ_H, Θ_L, and ZT are the hot, cold temperature and figure of merit respectively. It is also theoretically possible to describe a Carnot cycle with a PY material. However, due to difficulty in controlling successive adiabatic and isothermal conditions and the need for excessive electric fields, Carnot cycle for PY energy conversion is not realistic. As a consequence, other cycles are considered, such as Stirling cycle (two constant electric induction paths and two isotheral paths) or Ericsson cycle (two constant electric field paths and two isothermal paths)[161].

It must be noted that at present thermoelectric modules are the method of choice when it comes to energy harvesting from temperature. Their operational principles are based on spatial temperature gradients leading to heat flow through the thermoelectric generator with a small percentage of that heat flow being converted into electric energy. They have commercially been shown to be capable of generating power output from μW

to kW of electrical energy. Material properties, such as Seebeck coefficient and figure of merit, are the key parameter for improving both the output power and the efficiency of these modules. However, difficulty in maintaining the spatial temperature gradient despite increasing thermal heat flow, and hence heat diffusion, for higher power limits their output power. Typical thermoelectric generators have efficiencies that are around 5%[150].

PY materials may also be used for thermal to electrical energy conversion. As they require temporal temperature gradient, their application fields are where spatial temperature gradients are not possible and temperature is not static. For example, small scale micro-generators with dimensions smaller than the spatial temperature fluctuation length may find it not possible to be subjected to temperature gradients. On the other hand, natural temporal temperature variations do occur due to convection process, which can quite easily be exploited by PY energy harvesting process. It is also possible to transform a spatial temperature gradient into a temporal one via a caloric fluid pumping between hot and cold reservoirs. The pumping unit may require much less energy than the total produced energy, depending on the scale of the device of course, and may produce temperature variations of 1 to 20 °C at 2 Hz, for example. Recognising such wide ranging potentially applicable fields, there are a number of research groups, such as Xie et al.[19], Vanderpool et al.[182], and Sebald et al.[70,160], working on PY energy harvesting at present.

- Xie et al.[19]

Experimenting with the use of PZT-5A in PY energy harvesting, they observed 0.23 $\mu W cm^{-2}$ of power for a maximum heating rate of 15 °Cs^{-1} using 150 μm thick PZT-5A samples. This corresponds to around 15.3 $\mu W cm^{-3}$ of power density.

- Vanderpool et al.[182]

Largely based on Olsen et al.'s work on PY energy conversion[135,137,138], while numerically simulating a prototypical PY converter (assembled by Olsen et al.[135]) they established that up to 40 % of Carnot efficiency, namely 3.4 % efficiency at $f = 0.062Hz$, is possible while Lead zirconate stannate titanate (PZST) can achieve power density of 24 $mW cm^{-3}$ at $f = 0.2Hz$. However, it must be noted that Olsen et al. also considered PZST as well, but due to its high cost they used 30-70 μm thick PVDF films instead[136].

- Sebald et al.[70,91,160,161]

This group's work is largely based on PY energy harvesting techniques using high PY

activities at phase transitions. Energy harvesting based on ferroelectric-paraelectric (FE-PA) and FE-FE transitions using Ericsson and Stirling cycles are among those investigated[70,161]. Guyomar et al. also looked at the feasibility of heat energy harvesting using the PY effect on PVDF films[71]. Using Ericsson thermodynamic cycle they claim to achieve efficiencies (in relation to that of Carnot cycle) of 100 times higher than direct PY energy harvesting's.

11.1.3 Optimisation methods

In order to optimise any energy harvesting technique, the first step would be the optimisation of the energy conversion process, such as consideration of different mechanisms (piezoelectric, direct pyroelectric, or phase transition based pyroelectric) and thermodynamic cycles (as presented above). Then, the problems of electric loading from the energy harvesting circuit/storage should be addressed. Present methods for optimising this part of energy conversion vary greatly depending on whether what type of energy harvesting mechanism and thermodynamic cycle is used. Some examples of these are provided below.

- Resistive or standard interface[105]

This is the standard resistive load connecting circuit with a diode rectifier bridge and a filter capacitor (AC-DC converter). This is the simplest circuit for rectifying and smoothing an AC voltage.

- Use of step-Down converter in discontinuous conduction mode[139]

Using an adaptive step down DC-DC converter, the power output from a piezoelectric device was maximised with increase of up to 325 % at high levels of excitation. However, the additional circuitry required quite a high open circuit voltage for increased power to be supplied to the load.

- Synchronised electric charge extraction (SECE)[104]

This works by periodically removing the electric charge accumulated on the blocking capacitor of a piezoelectric element, transferring the corresponding amount of electrical energy to the load or to the energy storage element. The extraction phases are synchronised with the mechanical vibration, while piezoelectric element is allowed to be under open circuit condition most of the time.

- Synchronised switch damping on inductor (SSDI)[69]

Designed for mechanical vibration damping, this technique dissipates the mechanical en-

ergy of vibrating structures with piezoelectric inserts, damping the structural resonance modes. This vibration suppression technique works by switching the voltage of the ferroelectric material on an inductor at every peak and trough of the temperature variation, allowing for the electric field polarity to be quasi-instantaneously reversed. The main difference compare to SECE is that the electric field is not reduced to zero, but nearly the same magnitude of the opposite sign. The inductor enables for this to happen with minimised energy cost.

- Synchronised switch harvesting on inductor (SSHI) [20]

Based on SSDI, this was designed specifically for energy harvesting application. As SSDI is much more efficient than SECE, SSHI is also very efficient, but by removing the number of diodes required for its operation Makihara et al. [113] improved its efficiency even further.

11.2 Pyroelectric X-ray/Neutron generation

11.2.1 Pyroelectric X-rays

Although this was the originally aimed application of the PY coef enhancement, the proposed mechanisms behind PY X-ray generation meant the use of PY coef enhancement in PZTs would not be possible in this application. According to this mechanism, materials with high dielectric constant such as PZT, which is the main beneficiary of the PY coef enhancement, will not be able to generate X-rays since the voltage they generate will not be large enough. As the author was unable to theoretically and experimentally investigate this application further due to time constraint, the main focus of the author's research was diverted to PY energy generation. However, the mechanisms behind various ferroelectric and PY electron emission cathodes [153,166] suggest that in fact high dielectric constant is desirable for certain types of electron emission and should PY X-ray generation be an outcome of this electron emission mechanism, which is possible, there is no doubt in the author's mind that PY coef enhancement achieved in this research can also find application in this field.

PY X-ray generation utilises a PY accelerator and a target to produce X-rays. In a PY crystal held below a critical temperature (Curie temperature), heating or cooling causes distortions in the lattice of atoms which in turn creates strong electric fields at the surface of the crystal (PY effect). James Brownridge of the State University of New York

at Binghamton used these electric fields to create stable, self-focused electron beams with energies as high as 170 keV. The energy conversion is not particularly efficient, inputting watts of heating energy produces only μWs of output electron beam energy, but this is not of major significance. PY crystals (such as those made of $LiNbO_3$) are already widely used as detectors for infrared and THz radiation, but the discovery by Brownridge that they can also be used to produce energetic electron beams, if heated or cooled in dilute gas atmospheres, means that they can be employed to produce X-ray fluorescence for elemental analysis of complex materials. Portable economical X-ray fluorescence was now a real possibility and this lead to the development of Cool-X, a miniature X-ray generator with PY crystal that has the maximum Bremsstrahlung energy of about 35 keV, by Amptek Inc.[5].

Major achievements, besides the first reporting of a PY X-ray generator, of James D. Brownridge are numerous publishing of many new phenomena that can be observed when a crystal of $LiNbO_3$ or $LiTaO_3$ is heated and cooled in a dilute gas. These are[38]:

- A self-focusing electron beam going away from the crystal
- A self-focusing electron beam coming towards the crystal
- A self-focusing positive ion beam going away from the crystal
- A "believed to be but never observed" self-focusing positive ion beam going towards the crystal
- The source of the electrons and the positive ions is the field ionisation via tunnelling in the residual gas molecules in the vicinity of the crystal
- Energies of electron beams can be optimised by controlling the pressure of the gas in the chamber (Gas-Amplification effect)
- There is no corresponding increase in positive ion beam's energies when the pressure is varied
- Electrons that are accelerated away from the vicinity of the crystal are nearly mono-energetic
- Given the right conditions, a crystal will continue to accelerate electrons nearly mono-energetically for more than 15 days following a heating cycle
- Self-focused beams observed can remain stable for more than 16 hours
- It is possible to produce characteristic X-rays of elements with Z as high as Pb (i.e. Atomic number of 82)

In 1992, James D. Brownridge reported the first PY X-ray generator in Nature[35]. He produced an X-ray generator capable of creating photons with energies of around 20 keV. This generator consisted of a PY crystal, namely $CsNO_3$, with a gold foil fixed closely to it acting as a target for the accelerated electrons to bombard into, hence generating X-rays. Prior to his work, it had been reported that certain PY crystals emit electrons[18,30,32,51,75,94,96]; in case of $LiNbO_3$ single crystal it had been observed to emit electrons with energies of up to 100 keV and electric fields as high as 1 $MVcm^{-1}$, and it is this high electric field that Brownridge used to accelerate the electrons. It must be noted that in his system these electrons are thought to have originated mainly from the ionization of molecules of the residual gases in the system. To produce X-rays, his device had a heater that turned on and off, thermally cycling the crystal between approximately 77 and 273 K with cycle time of about 5 min that lead to around 1 min of X-ray production[35].

Brownridge then started investigating ways of enhancing this device in collaboration with other researcher such as S. Raboy of the State University of New York at Binghamton and S. M. Shafroth of the University of North Carolina. He first studied the influences of the environment external to PY crystals to the PY generation of X-rays with $LiTaO_3$, $LiNbO_3$ and $CsNO_3$ crystals, publishing a more comprehensive report in 1999[36]. In this report, he attempts to find explanations for the maximum energy of the electrons, the circumstances for the production of the electrons, the sources of the causes behind the lack of reproducibility from one thermal cycle to the next and the source of light that was observed by Brownrdige and others in the vacuum system. Some of the parameters he explored to investigate these issues include; the orientation of the PY crystals (+z or −z base towards the detector), method of temperature change (warming or cooling), application of epoxy on the surface of the PY crystals and pressure of the gas in the vacuum. Please refer to Figure 11.2 for further clarification.

The crystal orientation and mode of temperature change (warming up or cooling down) were observed to show symmetrical behaviour (i.e. crystal with +z base facing the detector that was warming up, Figure 11.2 (a), resulted in similar X-ray generation as the one with −z base facing the detector that was cooling down, Figure 11.2 (d), and vice versa) whereas the application of epoxy had resulted in either little reduction (in terms of energy of X-ray produced) or total prevention of X-ray generation depending on the mode. When the crystal itself was used as the target for X-ray generation, epoxy

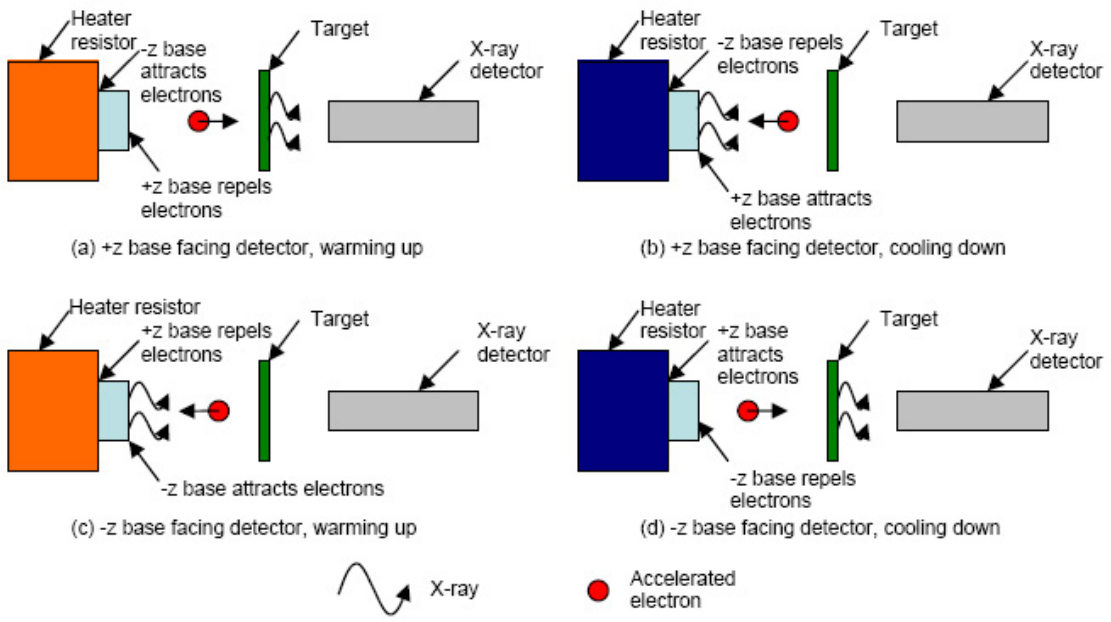

Figure 11.2: Various orientation and modes of X-ray generation investigated by Brownridge

layer blocked the penetration of attracted electrons trying to enter the crystal, hence preventing any characteristic X-ray production by some of the constituent atoms of the crystal, however with copper as the target the epoxy was also polarised by the crystal's polarisation which in turn lead to electrons being accelerated towards the target, resulting in X-rays. With regards to the pressure, they observed that the maximum rate of X-ray generation with a separate target occurred at about 33 $mTorr$ whereas the case with the crystal itself as the target showed maximum occurrence at somewhere between 44 and 56 $mTorr$. However, they also noted that the values of the pressures at which maximum X-ray generation occurs depended on the experimental arrangement of the target with respect to the PY crystal, which was then expanded to also depend on shape, size and type of the vacuum chamber housing the crystal[37]. Finally, they attributed the light observed, also associated with the PY effect, to the recombination process of positive molecular ions and electrons of the gases in the vacuum chamber.

In light of Brownridge et al.'s research a few other researchers have also attempted to create an X-ray generation device using PY effect. One major group consists of J. A. Geuther and Y. Danon, both from Rensselaer Polytechnic Institute, New York. Also employing $LiTaO_3$ and $LiNbO_3$ as their PY crystals, they managed to verify some of the observations that Brownridge et al. had made with their own experiments[62], for

example the "bunched / clustered" electron emission effect observed by Brownridge et al.[39]. However their major achievement lies with a system of X-ray generating crystals they refer to as "Paired-crystal PY source". Using this system they managed to produce electron beams with double the energies (X-ray yield was also approximately doubled) resulting in X-rays with end point energies of up to 215 keV [62–65]. This is high enough to fluoresce the K-shell of any element up to Thorium ($Z = 90$), which is a significant improvement from Brownridge et al.'s limit of Lead ($Z = 82$). "Paired-crystal PY source" has the following schematics:

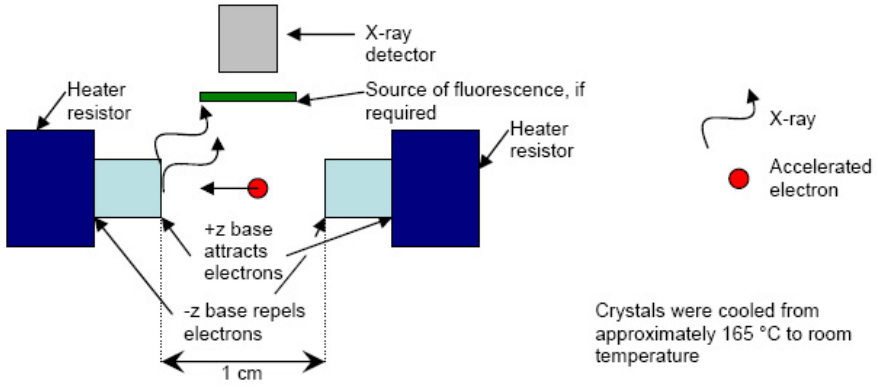

Figure 11.3: Paired-crystal pyroelectric source schematics

11.2.2 Pyroelectric neutron generation via nuclear fusion

This is a relatively new application of PY effect. First report of this application was published in 2005 on Nature by S. Putterman and Naranjo[127]. In this review, two main groups that investigated this application will be introduced:

- S. Putterman and B. Naranjo of University of California Los Angeles (UCLA) [127,128,191]
- J. A. Geuther and Y. Danon of Rensselaer Polytechnic Institute[61,66]

Upon learning Brownridge et al.'s observation that it was possible to produce electron / ion beams with energies exceeding 100 keV using PY crystals, in 2002, Putterman et al. realised that these energy levels are indeed high enough to cause fusion between deuterium nuclei and started proposing a fusion system from deuterated PY / ferroelectric crystals[128]. In 2005, they reported the first apparatus that uses PY effect to accelerate deuterium positive ions on to a deuterium target causing a nuclear fusion, leading to

neutron emissions[127,191].

By gently heating a $LiTaO_3$ crystal from 240 to 265 K in a vacuum chamber with a small deuterium pressure of 0.7 Pa, they generated a potential of 100 kV on the crystal's surface. Then by attaching a sharp Tungsten (W) probe on to the crystal's surface, they managed to concentrate the field at the probe tip with field strengths reaching the values of around 25 Vnm^{-1}. As this field is strong enough to ionise all the passing deuterium molecules, they were able to ionise the deuterium molecules and accelerate the resulting deuterium ions (with beam energies of over 100 keV), eventually hitting the deuterated target. This lead to a neutron emission with a peak flux of 800 neutrons (each with 2.45 MeV) per second[127,191]. Although their system required cryogenic temperatures and did not prove to be useful in the power-producing sense, it was deemed to be a good starting point for the development of palm-sized/compact neutron generator.

Following Putterman et al.'s success, Geuther et al. also started investigating their Paired-crystal PY source's potential as a neutron generator[61], and in 2006 they managed to induce nuclear reactions using their Paired-crystal system without cryogenic cooling. With low-power thermoelectric heaters (that are attached onto copper heat sinks), they heated $LiTaO_3$ discs up to 130 °C then let them cool down to room temperatures, during which they were able to induce the nuclear fusion reactions. Best result of approximately 138 ± 7 net neutron counts per heating cycle, with average emission time of 120 seconds, was obtained when the chamber base pressure of 1 $\mu Torr$ was used, which was then raised to the final pressure of 1.2 $mTorr$ by the introduction of deuterium gas[66].

11.3 Other applications of pyroelectricity

Some of the other applications of pyroelectricity are presented below. PY coef enhancement under OC should find applications in these fields.

11.3.1 High Voltage generation

Fundamentally very similar to X-ray/Neutron generation application, this application makes use of the PY materials being a dielectric, and hence having the ability to generated high potential difference across their opposing faces. Many applications require a source of high voltage pulses. These include drivers for piezoelectric devices, ion tubes, gas tubes, liquid polarizing cells, beam steering applications, the generation of electric fields

in aqueous solutions, and time-of-flight mass spectrometry measurements, for example. Although the author is not aware of high voltage generation using PY effect at present, following application of piezoelectricity means it could well be possible.

Since 2000, Keawboonchuay and Engel have been working on a piezoelectric pulse generator[54,87–89]. They have developed a high power piezoelectric pulse generator based on a piezoelectric element producing a transient voltage pulse when it is mechanically compressed.

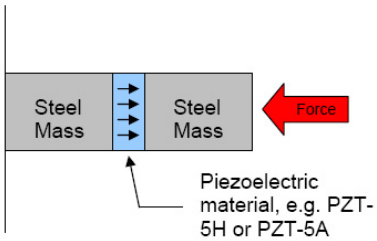

Figure 11.4: Mechanism behind piezoelectric high voltage pulse generation[41].

It essentially consists of a piezoelectric material located between two steel masses that conduct current to a suitable load as illustrated by Figure 11.4. When a significantly large enough force is applied, the piezoelectric element is compressed, generating the voltage with which a pulse is formed. Using this arrangement, they were able to produce voltages of up to 3.0 kV with 7 kN impact force and PZT-5H as the piezoelectric element (note PZT-5H is also PY material used in Part I). The theoretical results showed that the generated voltage is linearly proportional to the thickness-to-cross-sectional area ratio of the piezoelectric material (thickness of PZT/surface area of PZT) and the impact force, whilst the current is actually maximised when the minimum thickness-to-cross-sectional area ratio is utilised. Although Keawboonchuay and Engel used piezoelectric effect to generate high voltage pulse, the same principal could also be employed with PY effect as long as large enough charge can be built up on the PY material.

11.3.2 Pyroelectric lithography

In 2001 and 2002, a group from Samsung Advance Institute of Technology, lead by I. K. Yoo and C. W. Moon, investigated potential use of the PY emission in lithography application[198]. They fabricated patterned electron emitters using $LiNbO_3$ single crystals[118]. By noting that pyroelectrically induced electron emission can be suppressed by coating Platinum (Pt) or Titanium (Ti) thin films, hence the potential as the blocking

layer, and that SiO_2 layer had no effect on the electron emission behaviours, hence the potential as the emission layer, a system for patterned emitters was suggested with respective films and layers as the corresponding functional layers for the system. Using 1:1 electron beam projection system, 100 and 5 μm dots on the exposed resist were obtained from 300 μm and 30 μm dots on emitters.

Chapter 12

Theoretical analysis - Potential applications

In this chapter, theoretical analysis and formulation of pyroelectric energy harvesting application using 2-2 connectivity laminate composites will be presented. Section 12.1 will illustrate a simple energy harvesting arrangement which can turn a typical spatial temperature gradient into a temporal one, and hence enabling the use of pyroelectric materials in applications where thermoelectric routes would normally have been taken. For the analysis/formulation in Section 12.2, we will only consider the energy harvesting potentials of the 2-2 connectivity laminate composites under short circuit condition since the experimental measurements taken in Section 6.2 were under this condition. As the author has already demonstrated the differences between the short and open circuit conditions in Chapter 8, it should pose no problem for the readers to derive the analogous expressions for the open circuit condition by themselves.

12.1 Schematics of simple pyroelectric energy harvesting device

The author would first like to introduce the readers to a schematic diagram of a PY energy harvesting device he would like to consider in this Chapter. The simplest structure with the conventional steel and SMA springs displayed in Figure 12.1 should suffice. One-way SMA springs with steel ones for returning SMA springs into their original shape is employed.

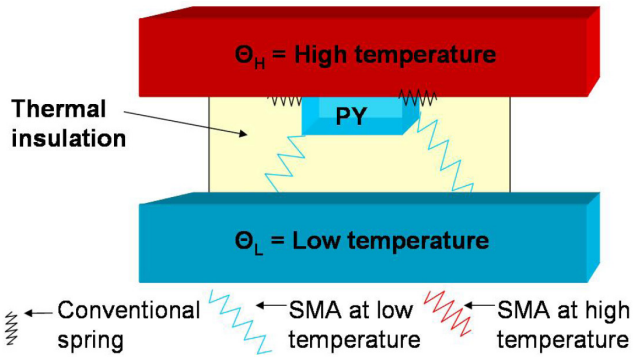

(a) $\Theta_{PY} = \Theta_{SMA} = \Theta_L$ (SMA springs are in martensite phase, enabling steel springs to contract and force PY element onto Θ_H surface)

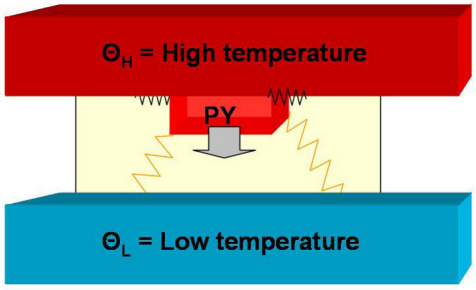

(b) $\Theta_{PY} = \Theta_H$ and $\Theta_L < \Theta_{SMA} < \Theta_H$ (SMA springs start to change into austenite phase, overcoming steel springs' forces and pulling PY towards Θ_L surface)

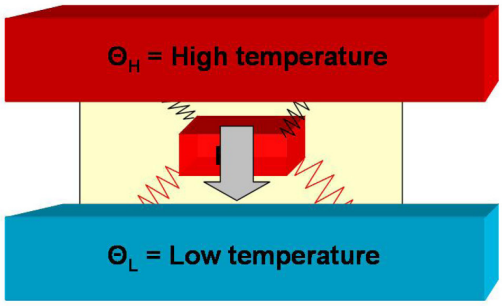

(c) $\Theta_{PY} = \Theta_{SMA} = \Theta_H$ (SMA springs are in austenite phase and pull PY towards Θ_L surface)

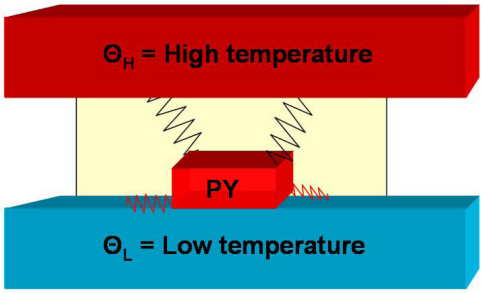

(d) $\Theta_{PY} = \Theta_{SMA} = \Theta_H$ (SMA springs are in austenite phase, stretching steel springs and forcing PY element onto Θ_L surface)

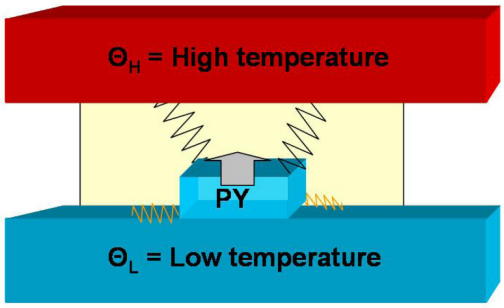

(e) $\Theta_{PY} = \Theta_L$ and $\Theta_L < \Theta_{SMA} < \Theta_H$ (SMA springs start to change into martensite phase, and hence steel springs overcome SMA's forces pulling PY towards Θ_H surface)

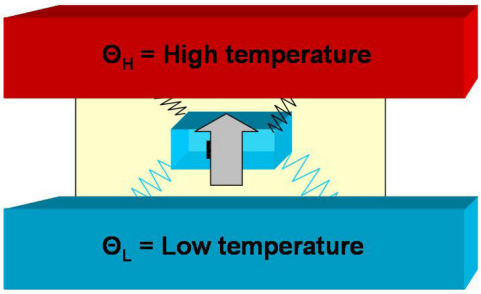

(f) $\Theta_{PY} = \Theta_{SMA} = \Theta_L$ (SMA springs are in martensite phase and the steel springs pull PY towards Θ_H surface)

Figure 12.1: Schematics of a simple pyroelectric energy harvesting device where Θ_{PY} and Θ_{SMA} are the temperatures of PY element and SMA, respectively

Cyclic behaviour from Figures 12.1(a) to 12.1(f) then back to 12.1(a) transforms the spatial temperature gradient between the Θ_H and Θ_L surfaces into a temporal one. Although the existence of the thermal insulation layer is not essential, it does enable a much simpler phenomenological view of the overall operation while enhancing the actuation behaviour of SMA springs. Spring arrangements illustrated in Figure 12.2 should maximise the surface contact between the PY element and temperature surfaces, aiding thermal conduction.

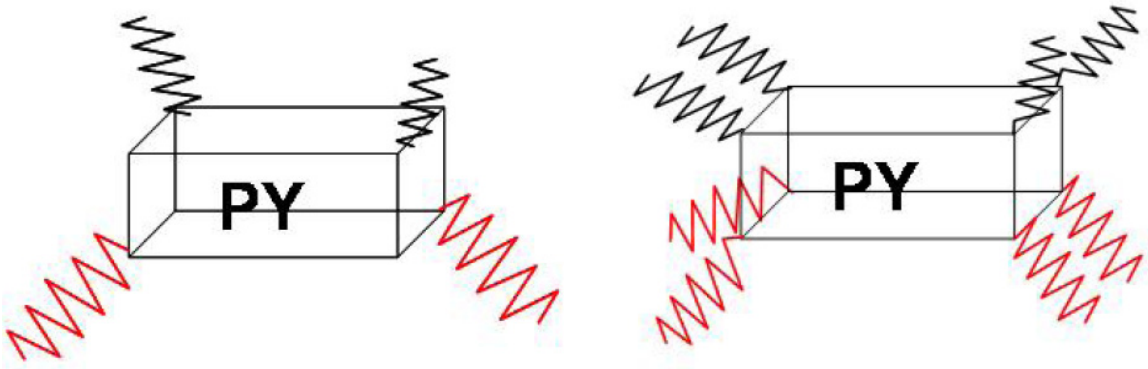

(a) Two SMA and steel springs on adjacent corners

(b) Four SMA and steel springs attached to each corner for additional stability

Figure 12.2: Spring positions for maximising the contact surface between pyroelectric element and temperature surfaces

It must be noted that the use of SMA means frequency achievable from such arrangements would be rather limited despite this improved thermal conductivity. This is one of the main reasons why the frequency range considered in Chapter 13 is constrained to those below or equal to 1 Hz, dampening the potential energy output available. One way of overcoming this may be the use of ferromagnetic SMA[116], which can produce actuation frequency ranges of 200 Hz or more, although the use of magnetic stimuli means more design complications.

12.2 Mathematical treatment of the potential energy output

In order to derive the expression for potential power output from the device depicted in Figure 12.1, the author will use similar technique to that employed by Ren et al.[148] and Shu and Lien[165] in the piezoelectric energy harvesting application. A simple resistive cycle case in Sebald et al.'s work[160] and standard interface in Lefeuvre et al.'s work[105] correspond to this. First consider Eq 3.6 from Subsubsection 3.2.1.

$$\begin{aligned} dD_m &= \sum_k \sum_l \left(\frac{\partial D_m}{\partial T_{kl}}\right)_{E,\Theta} dT_{kl} + \sum_n \left(\frac{\partial D_m}{\partial E_n}\right)_{T,\Theta} dE_n + \left(\frac{\partial D_m}{\partial \Theta}\right)_{T,E} d\Theta \\ &= d_{mkl}^{E,\Theta} dT_{kl} + \varepsilon_{mn}^{T} dE_n + p_m^{T,E} d\Theta \end{aligned} \tag{12.1}$$

Assuming the PY element is free to deform and even 2-2 connectivity laminate composites behave in a homogeneous manner in this freedom ($dT_{kl} = 0$), Eq 12.1 can be simplified.

$$dD_m = \varepsilon_{mn}^{T} dE_n + p_m^{T,E} d\Theta \tag{12.2}$$

Let thermal stimulus, namely temperature variation inside PY element, be Θ, f frequency ($\omega = 2\pi f$), t time, and Θ_0 amplitude of temperature variation ($\Theta_0 = \dfrac{\Theta_H - \Theta_L}{2}$).

$$\begin{aligned} \Rightarrow \qquad \Theta &= \Theta_0 \exp(i\omega t) + \frac{\Theta_L + \Theta_H}{2} \\ \therefore \frac{d\Theta}{dt} &= i\omega\Theta_0 \exp(i\omega t) \qquad \text{with thermal variation assumed to be sinusoidal} \end{aligned} \tag{12.3}$$

Now, $dQ_m = A dD_m$ and $dE_n = \dfrac{dV_n}{{}^{PY}t}$ where Q_m is the charge on the surface, A surface area, V_n potential difference across the thickness of PY element, and ${}^{PY}t$ the thickness of PY element.

From Eq 12.2:

$$\Rightarrow \qquad dQ_m = A dD_m = A\left(\varepsilon_{mn}^{T} dE_n + p_m^{T,E} d\Theta\right) = \frac{A}{{}^{PY}t}\varepsilon_{mn}^{T} dV_n + A p_m^{T,E} d\Theta \tag{12.4}$$

From Eq 12.3:

$$\begin{aligned}\Rightarrow \qquad I_m &= \frac{dQ_m}{dt} = \frac{A}{{}_{PY}t}\varepsilon^T_{mn}\frac{dV_n}{dt} + Ap^{T,E}_m\frac{d\Theta}{dt} \\ &= \frac{A}{{}_{PY}t}\varepsilon^T_{mn}\frac{d\left\{V_0\exp(i(\omega t+\theta))\right\}}{dt} + Ap^{T,E}_m\left(i\omega\Theta_0\exp(i\omega t)\right) \\ &= \frac{A}{{}_{PY}t}\varepsilon^T_{mn}\left\{i\omega V_0\exp(i(\omega t+\theta))\right\} + i\omega\Theta_0 Ap^{T,E}_m\exp(i\omega t)\end{aligned} \tag{12.5}$$

where I_m = Current generated from PY element

V_0 = Amplitude of the potential difference generated across PY element

θ = Phase difference between the sinusoidal thermal variation and the potential difference across PY element

Eq 12.5 implies the generated potential difference or voltage across a resistor R_0 (total external load resistor) will be:

$$\begin{aligned}V = dV_n = V_0\exp(i(\omega t+\theta)) = R_0 I_m = R_0\left[\frac{i\omega A\varepsilon^T_{mn}}{{}_{PY}t}V_0\exp(i\theta) + i\omega\Theta_0 Ap^{T,E}_m\right]\exp(i\omega t) \\ \Rightarrow \qquad V_0\exp(i\theta) = \frac{i\omega R_0\Theta_0 Ap^{T,E}_m}{1 - i\omega\dfrac{R_0 A\varepsilon^T_{mn}}{{}_{PY}t}}\end{aligned} \tag{12.6}$$

Hence power dissipation averaged over time in the load resistor R_0 is:

$$\text{Power } = P = \frac{V_0^2}{2R_0} = \frac{\omega^2 R_0\Theta_0^2 A^2\left(p^{T,E}_m\right)^2}{2\left[1 + \dfrac{\omega^2 R_0^2 A^2\left(\varepsilon^T_{mn}\right)^2}{{}_{PY}t^2}\right]} = \frac{\omega^2 R_0\Theta_0^2 A^2\left(p^{T,E}_m\right)^2}{2\left[1+\omega^2 R_0^2 C_0^2\right]} \tag{12.7}$$

where C_0 = Capacitance of PY element = $\dfrac{\varepsilon^T_{mn}A}{{}_{PY}t}$

Note that this power dissipation in Eq 12.7 is the power generated from PY element, which in turn gets dissipated by the external load resistor R_0. This expression reaches its

maximum when $R_0 = \dfrac{1}{\omega C_0}$, i.e. when R_0 matches the impedance of the voltage source.

$$\begin{aligned}\Rightarrow \qquad P_{max} &= \frac{\omega\Theta_0^2 A^2 \left(p_m^{T,E}\right)^2}{4C_0} \\ &= \frac{\omega\Theta_0^2 A \left(p_m^{T,E}\right)^2}{4\dfrac{\varepsilon_{mn}^T}{{}^{PY}t}} = \frac{{}^{PY}t\omega\Theta_0^2 A \left(p_m^{T,E}\right)^2}{4\varepsilon_{mn}^T}\end{aligned} \tag{12.8}$$

Also from Eq 12.7:

$$\begin{aligned}\Rightarrow \qquad \text{Power density} = P_{den} &= \frac{\text{Power}}{\text{Volume}} = \frac{\omega^2 R_0\Theta_0^2 A^2 \left(p_m^{T,E}\right)^2}{2\left[1+\omega^2 R_0^2 C_0^2\right] \times A\left({}^{NP}t + {}^{PY}t\right)} \\ &= \frac{\omega^2 R_0\Theta_0^2 A \left(p_m^{T,E}\right)^2}{2\left[1+\omega^2 R_0^2 C_0^2\right]\left({}^{NP}t + {}^{PY}t\right)} \\ \Rightarrow \qquad \text{Maximum power density} = P_{denMax} &= \frac{\omega\Theta_0^2 A \left(p_m^{T,E}\right)^2}{4C_0\left({}^{NP}t + {}^{PY}t\right)} \\ &= \frac{\omega A\Theta_0^2 \left(p_m^{T,E}\right)^2}{4\dfrac{\varepsilon_{mn}^T A}{{}^{PY}t}\left({}^{NP}t + {}^{PY}t\right)} = \frac{\omega\Theta_0^2 \left(p_m^{T,E}\right)^2}{4\varepsilon_{mn}^T\left(\dfrac{{}^{NP}t}{{}^{PY}t}+1\right)} \\ &= \frac{2\pi f\Theta_0^2 \left(p_m^{T,E}\right)^2}{4\varepsilon_{mn}^T\left(\dfrac{1}{R}+1\right)} = \frac{\pi f\Theta_0^2 \left(p_m^{T,E}\right)^2}{2\varepsilon_{mn}^T\left(\dfrac{1}{R}+1\right)} \\ &= \frac{\pi f \left(p_m^{T,E}\right)^2 \left(\Theta_H-\Theta_L\right)^2}{2\varepsilon_{mn}^T\left(\dfrac{1}{R}+1\right)\times 4} = \frac{\pi f \left(p_m^{T,E}\right)^2 \left(\Theta_H-\Theta_L\right)^2}{8\varepsilon_{mn}^T\left(\dfrac{1}{R}+1\right)}\end{aligned} \tag{12.9}$$

where $R = \dfrac{{}^{PY}t}{{}^{NP}t}$ is the thickness ratio, $\omega = 2\pi f$ with f being frequency in Hz, and the unit of Power density being $Watts m^{-3}$ or Wm^{-3}.

$$\begin{aligned}\Rightarrow \qquad \text{Maximum electrical energy output} = W &= P_{denMax} \times \tau_{H\_L} \times Vol \\ &= \frac{\pi \left(p_m^{T,E}\right)^2 \left(\Theta_H-\Theta_L\right)^2}{8\varepsilon_{mn}^T\left(\dfrac{1}{R}+1\right)} \times \left(f \times \tau_{H\_L}\right) \times Vol \\ &= \frac{\pi \left(p_m^{T,E}\right)^2 \left(\Theta_H-\Theta_L\right)^2}{16\varepsilon_{mn}^T\left(\dfrac{1}{R}+1\right)} \times Vol\end{aligned} \tag{12.10}$$

where $\tau_{H\_L} = \dfrac{1}{2f}$ is the time taken for Θ_{PY} to vary from Θ_H to Θ_L (this would be half of the period of this sinusoidal wave), Vol is the volume, and W is measured in $Watts$.

Note that W is evaluated over a period of half a thermal variation cycle, i.e. from Figures 12.1(b) to 12.1(e), since the next half cycle will have exactly the same electrical characteristics except the direction of polarisation/current/voltage being reversed, which can be taken care of using AC-DC converter circuit incorporating rectifier bridge.

In order to make comparisons with various other PY energy harvesting arrangements, techniques employed in Sebald et al.'s work[160], namely evaluation and comparison of the "Efficiency (η)" and "Electrothermal coupling factor (k^2)", will need to be carried out. η is a more application specific version of the author's "Eff" expression in Eq 8.14 from Subsection 8.2.1, so the distinction between the two "Efficiencies" must be made.

For the time period of $\tau_{H\_L} = \dfrac{1}{2f}$ one can also calculate the amount of thermal energy input used for bring about the temperature change of PY element from Θ_H to Θ_L.

$$\begin{aligned}\text{Thermal energy input} = \text{Heat taken from hot reservoir} = Q_h \\ &= Vol \times \bar{c_E} \int_0^{\tau_{H\_L}} \left(\frac{d\Theta}{dt}\right) dt \\ &= Vol \times \bar{c_E} \left[\Theta\right]_{t=0}^{t=\tau_{H\_L}} = Vol \times \bar{c_E} \times 2\Theta_0 \\ &= \frac{R^{PY}c_E + {}^{NP}c_E}{R+1} \times (\Theta_H - \Theta_L) \times Vol\end{aligned} \tag{12.11}$$

where $\bar{c_E} = \dfrac{A\left({}^{PY}c_E\,{}^{PY}t + {}^{NP}c_E\,{}^{NP}t\right)}{A\left({}^{PY}t + {}^{NP}t\right)} = \dfrac{R^{PY}c_E + {}^{NP}c_E}{R+1}$ is the volumetric heat capacity of the whole PY element and $c_E = c_{vol}$ volumetric heat capacity of each constituent.

Eqs 12.10 and 12.11 leads to optimal η (Efficiency) expression for simple resistive load PY energy harvesting case, namely η_{Res}.

$$\begin{aligned}\Rightarrow \qquad \eta_{Res} = \frac{W}{Q_h} &= \frac{\dfrac{\pi\left(p_m^{T,E}\right)^2(\Theta_H - \Theta_L)^2}{16\varepsilon_{mn}^T\left(\dfrac{1}{R}+1\right)} \times Vol}{\dfrac{R^{PY}c_E + {}^{NP}c_E}{R+1} \times (\Theta_H - \Theta_L) \times Vol} \\ &= \frac{\pi\left(p_m^{T,E}\right)^2(\Theta_H - \Theta_L)}{16\varepsilon_{mn}^T\left(\dfrac{R+1}{R}\right)\left(\dfrac{R^{PY}c_E + {}^{NP}c_E}{R+1}\right)} = \frac{\pi\left(p_m^{T,E}\right)^2(\Theta_H - \Theta_L)}{16\varepsilon_{mn}^T\left({}^{PY}c_E + \dfrac{{}^{NP}c_E}{R}\right)}\end{aligned} \tag{12.12}$$

It is apparent from Eq 12.12 that where η_{Res} is concerned there is a trade off between increased PY coef and denominator of η_{Res} expression as R gets smaller. Hence for every 2-2 connectivity laminate composite, there will be an optimal R which maximises the efficiency (η_{Res}). In addition it also suggests that enhancing PY coef is a very effective route for improving PY energy harvesting efficiency since η_{Res} is proportional to $\left(p_m^{T,E}\right)^2$.

In the literature[160] "Electrothermal coupling factor (k^2)" is defined as:

$$\begin{aligned}\text{Electrothermal coupling factor at } \Theta_H = k^2 &= \frac{\left(p_m^{T,E}\right)^2 \Theta_H}{\varepsilon_{mn}^T \bar{c_E}} \\ &= \frac{\left(p_m^{T,E}\right)^2 \Theta_H \left(R+1\right)}{\varepsilon_{mn}^T \left(R^{PY}c_E + {}^{NP}c_E\right)}\end{aligned} \tag{12.13}$$

Using Eq 12.13 and noting the Carnot efficiency is defined as[70,160]; $\eta_{Carnot} = 1 - \dfrac{\Theta_L}{\Theta_H} = \dfrac{\Theta_H - \Theta_L}{\Theta_H}$ with temperatures measured in absolute temperature scale, i.e. $Kelvin$, one can also make comparison between η_{Carnot} and η_{Res} (Eq 12.12), ideally optimised energy harvesting cycle (Carnot cycle)'s efficiency and that of simple resistive load case respectively.

$$\begin{aligned}\Rightarrow \qquad \eta_{Res} &= \frac{\pi \left(p_m^{T,E}\right)^2 \left(\Theta_H - \Theta_L\right)}{16\varepsilon_{mn}^T \left({}^{PY}c_E + \dfrac{{}^{NP}c_E}{R}\right)} \\ &= \frac{\pi}{16} \times \frac{\left(p_m^{T,E}\right)^2 \Theta_H \left(R+1\right)}{\varepsilon_{mn}^T \left(R^{PY}c_E + {}^{NP}c_E\right)} \times \frac{\Theta_H - \Theta_L}{\Theta_H} \times \frac{\left(R^{PY}c_E + {}^{NP}c_E\right)}{R+1} \times \frac{1}{{}^{PY}c_E + \dfrac{{}^{NP}c_E}{R}} \\ &= \frac{\pi}{16} \times k^2 \eta_{Carnot} \times \frac{\left(R^{PY}c_E + {}^{NP}c_E\right) R}{\left(R+1\right)\left(R^{PY}c_E + {}^{NP}c_E\right)} \\ &= \frac{\pi}{16} \left[\frac{R}{R+1}\right] k^2 \eta_{Carnot}\end{aligned} \tag{12.14}$$

Comparison in Eq 12.14 is useful as this allows comparison between various PY energy harvesting systems operating in the same environment, namely defined available temperature gradient or hot/cold reservoirs and evaluated maximum possible energy conversion efficiency (Carnot efficiency).

It should also be noted that all expressions, Eqs 12.9 $\sim$ 12.14 converges to that of non-composite PY material only case as $R \to \infty$.

Chapter 13

Results and discussion - Potential applications

Section 13.1 of this chapter will present the findings from the analysis performed on the thirty-six PY-NP 2-2 connectivity laminate composites using techniques from Chapter 12 with regards to PY energy harvesting application. With resistive cycle case assumed, Maximum power density (P_{denMax} from Eq 12.9), Efficiency (η_{Res} from Eq 12.12), and Electrothermal coupling factor (k^2 from Eq 12.13) will be evaluated for each pair for comparison purposes. New electrothermal coupling factor (k^2_{New} from Eq 13.1) will also be derived for laminate composites, with its ability to describe PY energy harvesting potentials vindicated. This will then be followed by Section 13.2, where the author will focus the readers' attention on PZT5H-St pair, demonstrating the energy harvesting potentials of the experimentally measured samples from Section 6.2. During the analyses of these composites, recommendations will also be made on how to improve PY energy harvesting efficiency and output.

It must be noted that in Figure 12.1, although Θ_H and Θ_L are shown as the temperatures of hot and cold reservoirs/heat sources/drains respectively, as long as the resultant force from steel and SMA springs changes direction at these temperatures owing to SMA springs temperature dependent spring constant (Elastic stiffness), the actual temperatures of the hot and cold reservoirs (Θ_{hot} and Θ_{cold}) can be anything as long as they satisfy $\Theta_{hot} > \Theta_H$ and $\Theta_{cold} < \Theta_L$. This facilitates the possibility of having potentially huge spatial temperature gradient when PY element is in contact with the surfaces of hot and cold reservoirs, which can improve the thermal conductivity even further leading to higher available frequency (f), and hence ultimately greater Maximum power density

(P_{denMax}).

13.1 Pyroelectric energy harvesting potentials of 2-2 connectivity laminate composites

As in previous chapters, although PZT-5A's energy harvesting credentials were also considered, the trend was very similar to that of PZT-5H with smaller numerical values. Hence only the outcomes of the latter will be presented as an example of perovskite materials' energy harvesting potential. Meanwhile, LNO behaved very similarly to LTO with only smaller numerical values. Hence only LTO's results are presented.

13.1.1 PZT-5H pairs

From Figures 13.1(a) and 13.1(b), it is evident that despite PTFE and CPVC introducing extreme PY coef enhancements, owing to their high thermal expansion coefs, and possessing very low volumetric heat capacities, it is in fact Zn, Al, and St with their reasonably high thermal expansion coefs and middle-range volumetric heat capacities that demonstrate the most promise in PY energy harvesting (cf. Table A.4). This is traced back to their high Young's moduli, which provides for sufficient enhancement even at relatively high R values, i.e. even when only small mass of NP material attached. This is a very good example of a case where pure enhancement in PY coef alone is not enough for good performance in a particular application of PY effect. Energy harvesting characteristics of PZT5H-Zn, PZT5H-Al, and PZT5H-St pairs indicate their great potential in PY energy harvesting applications. In particular, noting that all these values are evaluated for the simplest resistive cycle case means should much better energy harvesting circuits and storage technologies be used, there indeed is great potential in these 2-2 connectivity laminate composites to be exploited in PY energy harvesting application.

Figures 13.1(c) and 13.1(d) are presented as a guideline since Sebald et al.[160] uses k^2 to assess each PY materials potentials. In fact, this measure of potential in PY energy harvesting turns out to be insufficient for 2-2 connectivity laminate composites, which will be dealt with in more detail in Subsection 13.1.5.

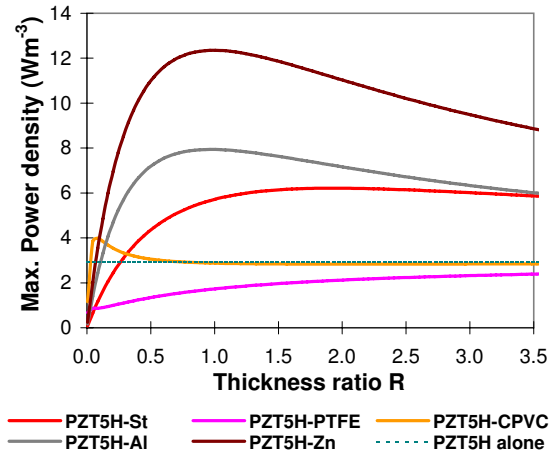

(a) Maximum power density (Wm^{-3} or μWcm^{-3}) vs R

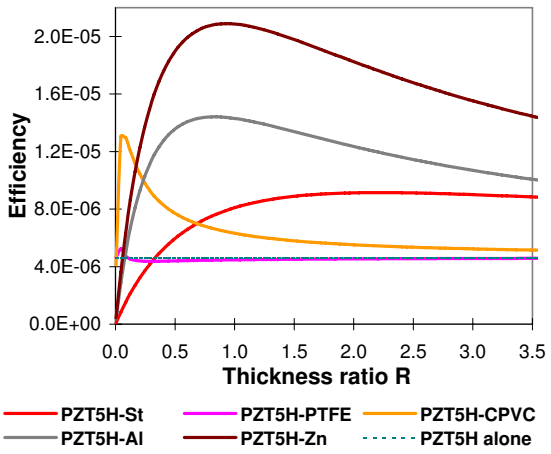

(b) Efficiency (η_{Res}) vs R

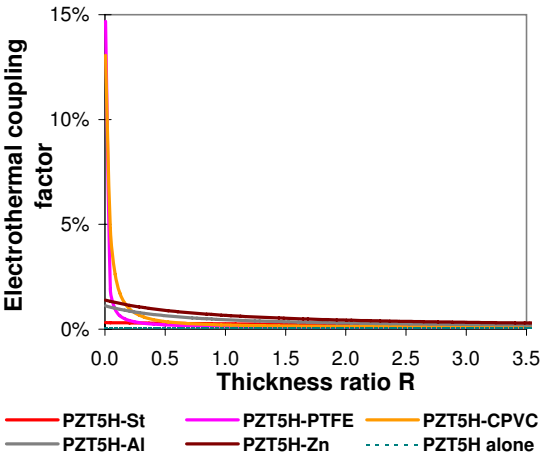

(c) Electrothermal coupling factor (k^2) vs R

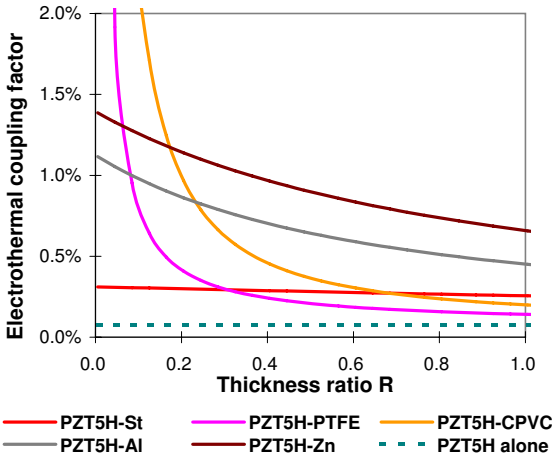

(d) Zoomed in view of Electrothermal coupling factor (k^2) vs R

Figure 13.1: Pyroelectric energy harvesting potentials of PZT5H pairs with ideal interfacial bonding layer, $\Theta_L = 300K$, $\Theta_H = 310K$, and $f = 0.01Hz$ assumed

13.1.2 BTO pairs

As evident from Figure 13.2, only BTO-Zn pair manages to improve P_{denMax} and η_{Res} at relatively high R values of around 0.85-1.20 and above, again Zn's high Young's modulus seemingly playing an important role.

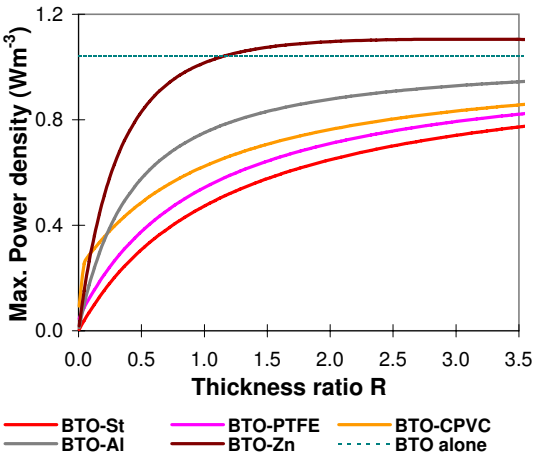

(a) Maximum power density (Wm^{-3} or μWcm^{-3}) vs R

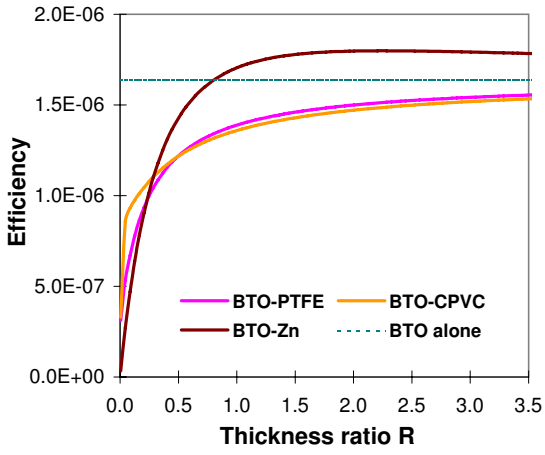

(b) Efficiency (η_{Res}) vs R

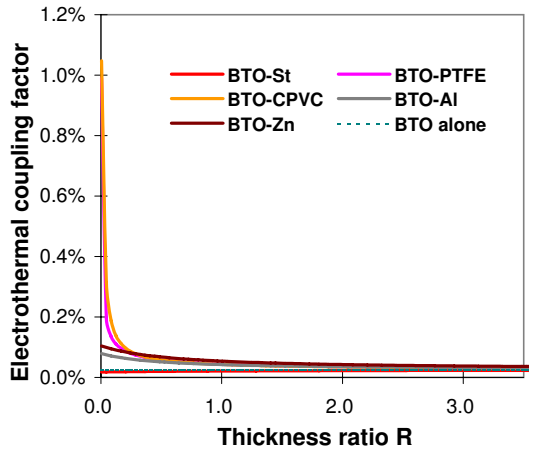

(c) Electrothermal coupling factor (k^2) vs R

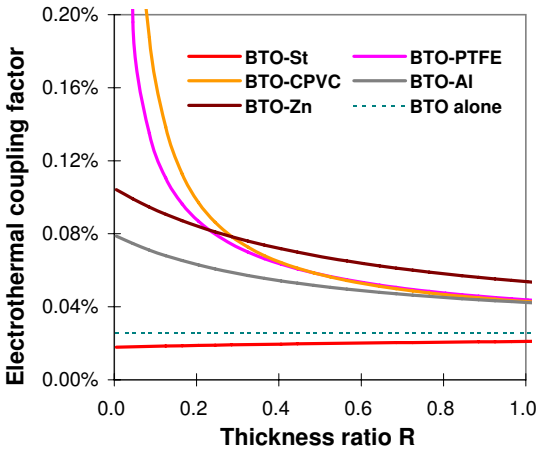

(d) Zoomed in view of Electrothermal coupling factor (k^2) vs R

Figure 13.2: Pyroelectric energy harvesting potentials of BTO pairs with ideal interfacial bonding layer, $\Theta_L = 300K$, $\Theta_H = 310K$, and $f = 0.01Hz$ assumed

13.1.3 LTO pairs

LNO and LTO's small PY coef enhancement meant that their 2-2 connectivity laminate composites actually reduced their PY energy harvesting abilities as illustrated by Figures 13.3(a) and 13.3(b). However, LTO and LNO single crystals by themselves are expected to show the highest P_{denMax} of all the materials and composites considered in this dissertation, implying to its potential employment in energy harvesting applications. The reason for this is their relatively high PY coefs coupled with low dielectric constants resulting in high voltage response.

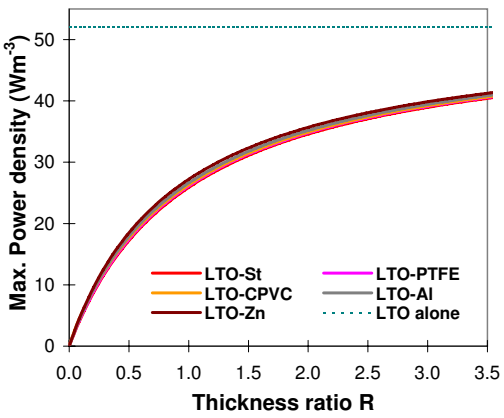

(a) Maximum power density (Wm^{-3} or μWcm^{-3}) vs R

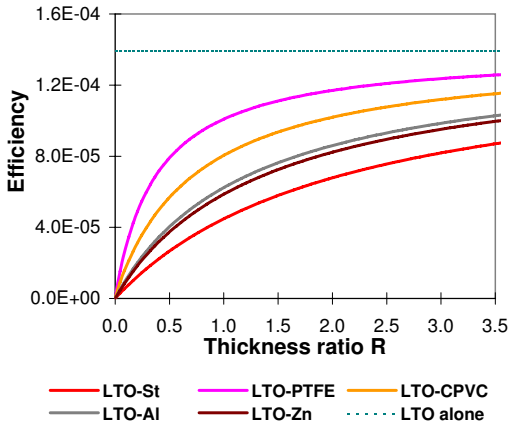

(b) Efficiency (η_{Res}) vs R

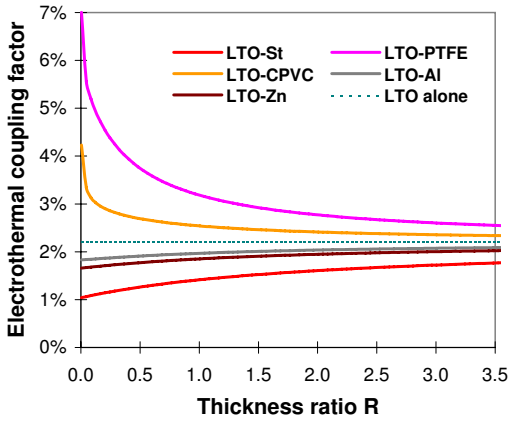

(c) Electrothermal coupling factor (k^2) vs R

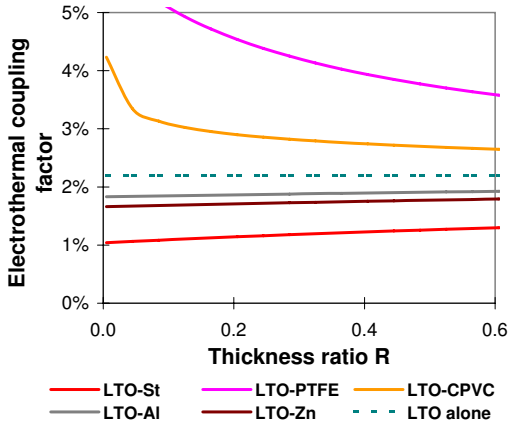

(d) Zoomed in view of Electrothermal coupling factor (k^2) vs R

Figure 13.3: Pyroelectric energy harvesting potentials of LTO pairs with ideal interfacial bonding layer, $\Theta_L = 300K$, $\Theta_H = 310K$, and $f = 0.01Hz$ assumed

13.1.4 PVDF pairs

Figures 13.4(a) and 13.4(b) insinuates that although PVDF pairs also fared rather badly when it comes to PY energy harvesting abilities, at higher R values some actually showed slight improvement, PVDF-Invar36 and PVDF-St in particular. This suggests that where PY energy harvesting application is concerned, thin coating of Invar36 or St on PVDF (even to act as electrodes) can improve electrical energy output (P_{denMax} and η_{Res}) of PVDF PY element.

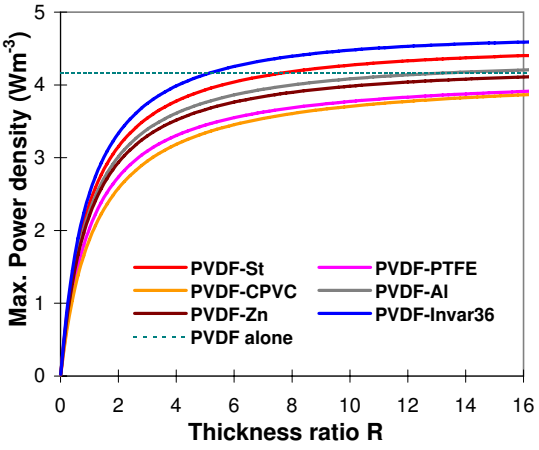

(a) Maximum power density (Wm^{-3} or μWcm^{-3}) vs R

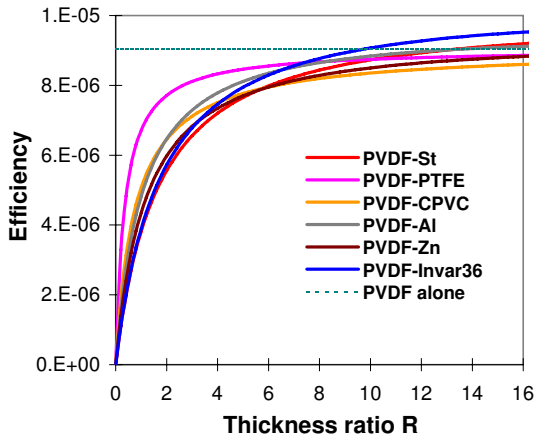

(b) Efficiency (η_{Res}) vs R

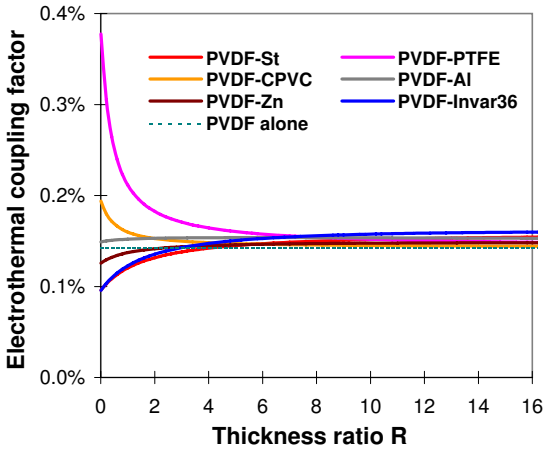

(c) Electrothermal coupling factor (k^2) vs R

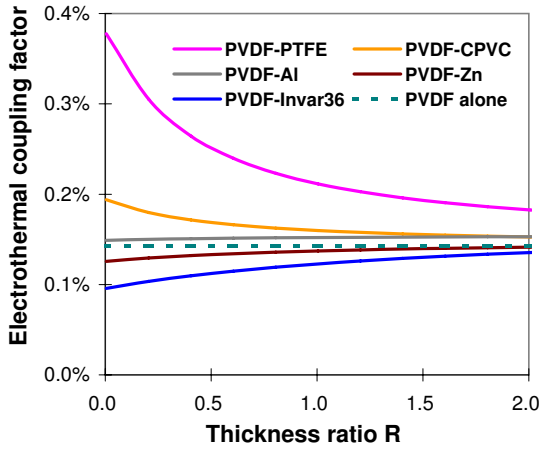

(d) Zoomed in view of Electrothermal coupling factor (k^2) vs R

Figure 13.4: Pyroelectric energy harvesting potentials of PVDF pairs with ideal interfacial bonding layer, $\Theta_L = 300K$, $\Theta_H = 310K$, and $f = 0.01Hz$ assumed

13.1.5 Comparison with other pyroelectric materials

In order to make comparison between PY materials and laminate composites considered in this dissertation and various PY elements assessed by Sebald et al.[160], Table 13.1 was created with materials such as PMN-PT = Lead magnesium niobate-Lead titanate single crystals, PLZT = Lead-lanthanum-zirconate-titanate, and PVDF-HFP = Poly(vinylidene fluoride-hexafluoropropylene) copolymer.

Table 13.1: Comparison between enhanced 2-2 connectivity laminate composites and pyroelectric elements considered by Sebald et al.[160] for energy harvesting application

PY element	p	ε_{33}^{T}	P_{denMax}	η_{Res}	k^2	$\frac{R}{R+1}k^2$
Selected PY elements from the literature[160]						
111 PMN-0,25PT	-17.90	961	N/A	N/A	4.79	N/A
PZT	-5.33	1116	N/A	N/A	0.37	N/A
PLZT 0.5/53/47	-3.60	854	N/A	N/A	0.22	N/A
PVDF	-0.33	9	N/A	N/A	0.14	N/A
PZT/PVDF-HFP 50/50	-4.50	85	N/A	N/A	4.28	N/A
PY materials considered						
PZT5H	-5.00	2874	2.92	4.63	0.073	N/A
PZT5A	-3.00	1803	2.22	3.52	0.056	N/A
BTO	-2.00	168	1.04	1.64	0.026	N/A
LTO	-2.30	45	52.14	139.41	2.20	N/A
LNO	-0.83	30	10.18	17.44	0.28	N/A
PVDF	-0.274	7.75	4.16	9.05	0.14	N/A
Selected 2-2 connectivity laminate composites						
PZT5H-CPVC ($R = 0.005$)	-44.68	2874	1.16	4.11	13.06	0.065
PZT5H-Zn ($R = 1.005$)	-14.53	2874	12.35	20.86	0.66	0.33
PZT5H-CPVC ($R = 0.045$)	-27.68	2874	3.85	13.05	4.78	0.21
PZT5H-PTFE ($R = 0.005$)	-34.16	2874	0.68	4.63	14.69	0.073

Units: - p (PY coef); $\times\ 10^{-4}\ Cm^{-2}K^{-1}$ - ε_{33}^{T}; No unit - η_{Res}; $\times\ 10^{-6}$ (No unit)
- P_{denMax}; Wm^{-3} or μWcm^{-3} (evaluated at $f = 0.01Hz$) - k^2; %

Note that our PZTs have much lower k^2 since the literature used much smaller ε_{33}^T and $c_E = c_{vol}$ values than ours. In case k^2 was not fully representative of potential P_{denMax} particular PY element might be capable of, $k_{New}^2 = \dfrac{R}{R+1}k^2$ from Eq 12.14 were also evaluated as illustrated by Table 13.1. Eq 12.13 can be used to derive an expression for k_{New}^2.

$$k_{New}^2 = \frac{R}{R+1}k^2 = \left(\frac{R}{R+1}\right)\frac{\left(p_m^{T,E}\right)^2\Theta_H\left(R+1\right)}{\varepsilon_{mn}^T\left(R^{PY}c_E + {}^{NP}c_E\right)} = \frac{\left(p_m^{T,E}\right)^2\Theta_H R}{\varepsilon_{mn}^T\left(R^{PY}c_E + {}^{NP}c_E\right)} = \frac{\left(p_m^{T,E}\right)^2\Theta_H}{\varepsilon_{mn}^T\left({}^{PY}c_E + \dfrac{{}^{NP}c_E}{R}\right)} \tag{13.1}$$

This new electrothermal coupling factor for composites (k_{New}^2) should be used when assessing PY energy harvesting potentials of 2-2 connectivity laminate composites, which suggests that when considering various composites for their energy harvesting credentials, as suggested by Sebald et al.[160], their particular connectivity symmetry must be taken into account before carrying out comparisons with their material counterparts. Figure 13.5 illustrates this point very well by closely approximating the trends depicted in Figure 13.1(a).

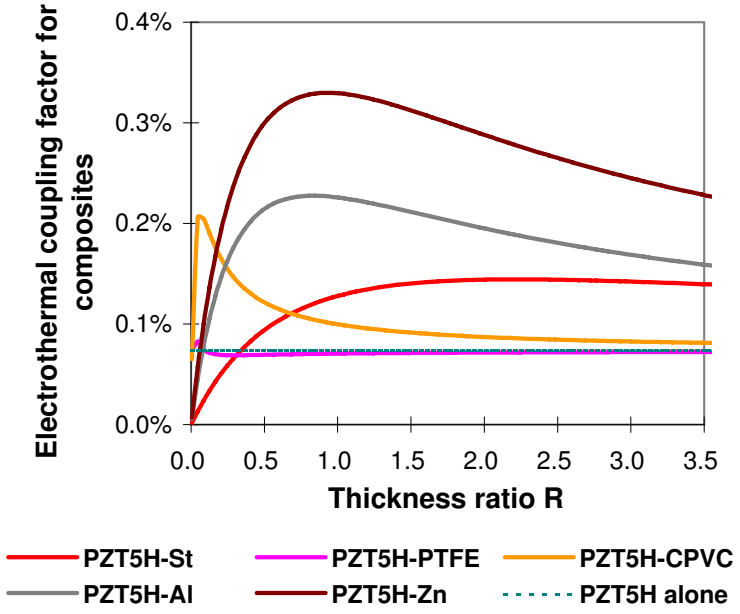

Figure 13.5: New electrothermal coupling factor ($k_{New}^2 = \dfrac{R}{R+1}k^2$) for PZT5H pairs with ideal interfacial bonding layer, $\Theta_L = 300K$, $\Theta_H = 310K$, and $f = 0.01Hz$ assumed

Good k^2_{New} values predicted for PZT5H-Zn, PZT5H-Al, and to a less extent PZT5H-St in Figure 13.5 owes largely to NP materials' ability to generate significantly large enough PY coef enhancement even at quite high R values while having relatively low c_{vol}, leading to less additional thermal mass. PTFE and CPVC pairs do have a peak at low R due to their extreme PY coef enhancements at such R values and their extremely low c_{vol}. (cf. Table A.4)

It is also evident from Table 13.1 that LTO single crystal is a very promising PY material for energy harvesting application. Although PMN-PT single crystal from literature exhibits the highest k^2 it is expensive and fragile, while PZT/PVDF-HFP composite, another PY element from literature with great promise, has k^2 evaluated from electrothermal coupling factor expression not yet adapted for composites. With that in mind, LTO single crystal, PZT5H-Zn ($R = 1.005$), and PZT5H-CPVC ($R = 0.045$) 2-2 connectivity laminate composites show extreme promise in PY energy harvesting application. In particular, PZT5H-Zn ($R = 1.005$) composite's P_{denMax} of 12.35 Wm^{-3} at $\Theta_L = 300K$, $\Theta_H = 310K$, and $f = 0.01Hz$, is very respectable, which can easily be further improved by increasing $\Theta_H - \Theta_L$ and f, when compared to that of a typical thermoelectric module, i.e. 30 Wm^{-3} [160].

Considering the important role the frequency plays in determining the maximum power density (cf. Eq 12.9), it must be noted that the choice of $0.01Hz$ frequency was not entirely arbitrary. In Subsubsection 5.3.3, "Time constant" expression in Eq 5.4 was used for the largest sample experimentally investigated (a 267 μm PZT5H and two 250 μm St), with the maximum time constant being evaluated to be approximately $1.87 \times 10^{-1}s$, giving maximum thermal variational frequency of $f_{max} = \frac{1}{\text{Maximum time constant}} \approx 5.35Hz$ for $1K$ temperature variation. However, for $\Theta_H = 310K$ and $\Theta_L = 300K$ considered in this part of dissertation, total temperature change of PY element during one full thermal variation cycle in Figure 12.1 is $\Delta\Theta = 2 \times 2\Theta_0 = 2 \times (\Theta_H - \Theta_L) = 20K$. In addition, the movement of PY element from one surface to another is not instantaneous. The time taken for this translation from Figures 12.1(a) to 12.1(d) would depend on the exact configurations of the SMA and Steel springs. It would be a very much conservative estimate to assume that this can take place within one second, considering some of SMA's actuation applications [81,171] such as spectacles frames that recover their original shape, blood clot filters that open up at body temperature to arrest clots, Braille characters that pop up when moved by SMA actuators that can be "rewritten", actuators for vanes

controlling the flow of air through jet engines, and devices to control the sag of electrical power transmission lines, among others.

Hence for a given thermal cycle, the total time it takes for the translation to take place would be $\tau_{tran} = 1 \times 2 = 2s$. For $\Delta\Theta = 20K$ temperature variation, the time used for changing Θ_{PY} would be $\tau_{PY} = 0.187 \times 20 = 3.74s$, assuming that SMA and Steel springs' temperature changing times are a lot less than PY element's due to their volume being much smaller. Hence a single thermal cycle process should take a maximum of $\tau_{total} = \tau_{trans} + \tau_{PY} = 5.74s$. This means the maximum thermal variational frequency a 2-2 connectivity laminate composite of PZT5H-St can achieve is at least $f_{Max} = \dfrac{1}{\tau_{total}} = 0.175Hz$, which is much larger than $0.01Hz$ used for our analysis. The fact that Xie et al.[19] uses heating rate of 15 °Cs^{-1}, effectively $0.75Hz$ frequency for $\Delta\Theta = 20K$ cycles, on a 150 μm thick PZT-5A demonstrates that this should be achievable, implying $0.01Hz$ is a very conservative and reasonable choice.

13.2 Pyroelectric energy harvesting potentials of experimentally measured samples

Here the author would like to present the results of similar analyses to those performed in Section 13.1.5 on the experimental samples whose PY coefs were measured for the Enhancement study in Subsection 6.2.2. Should the same samples be measured for their power output with impedance matching circuitry, following outcomes in Tables 13.2 $\sim$ 13.6 are expected.

The frequencies investigated in these tables are; $f = 0.0017Hz$ representing 2 °Cmin^{-1} heating rate (used in Enhancement study experimentation for testing the samples, cf. Subsection 6.2.2) applied to a $\Delta\Theta = 20K$ thermal cycle, and $f = 0.07$ for being the frequency at which some of the tested experimental samples start to achieve maximum power densities (P_{denMax}) larger than that of a typical thermoelectric module, i.e. 30 Wm^{-3}. Where the efficiencies are concerned, $\eta_{Carnot} = 0.0323$ for $\Theta_H = 310$, while $\eta_{Carnot} = 0.0625$ for $\Theta_H = 320$.

Table 13.2 illustrates the kinds of energy harvesting parameters bonded 2-2 connectivity laminate composites of PZT5H-St can produce. Even after taking the differences in frequencies investigated into account, the composites in Table 13.2 that possess $R > 1$ outperform the typical PZT5H's parameters presented in Section 13.1. Although smaller R leads to higher PY coef enhancement, it also means larger additional thermal mass from NP layer, resulting in larger $\bar{c_E}$ which in turn has a negative effect on all the energy harvesting parameters, P_{denMax}, η_{Res}, and k^2_{New}. This suggests maximising the PY coef alone is not enough to optimise the energy harvesting system. As one would expect, other issues such as the additional thermal mass needs to be considered.

Where the new electrothermal coupling factor (k^2_{New}) is concerned Sample XIR7 with $R = 1.068$ has the highest value, leading to highest maximum power densities of 32.2 and 129.0 Wm^{-3} at $f = 0.07Hz$ for $\Theta_H = 310$ and $\Theta_H = 320$ respectively. All the samples with $R > 1$ depict a rather large P_{denMax}, larger than 100 Wm^{-3} at $f = 0.07Hz$ for $\Theta_H = 320$, insinuating their potential deployment in energy harvesting application. Bearing in mind that the frequency and temperature variations used for these calculations are all viewed as reasonably conservative values, the author believes there is a good chance that these composites, or similar composites with different PY or NP materials such as Zn, Al, or CPVC (cf. Figure 13.5) could well find their use in PY energy harvesting.

Table 13.2: Energy harvesting potentials of experimental samples after enhancement

Name	R	p	Θ_H	$P_{denMax}^{0.07}$	$P_{denMax}^{0.0017}$	η_{Res}	k_{New}^2
XI3	0.254	-9.18	310	13.9	0.33	2.65	0.042
			320	55.7	1.33	5.30	0.043
XII4		-9.02	310	13.5	0.32	2.56	0.040
			320	53.8	1.28	5.12	0.042
XI5	0.382	-9.22	310	19.2	0.46	3.71	0.059
			320	76.8	1.83	7.41	0.060
XIR5		-7.37	310	12.3	0.29	2.37	0.037
			320	49.1	1.17	4.74	0.039
XI8=X3	0.534	-7.95	310	18.0	0.43	3.52	0.056
			320	71.8	1.71	7.04	0.057
XI7	1.068	-8.56	310	30.9	0.74	6.28	0.099
			320	123.7	2.94	12.56	0.102
XIR7C		-8.68	310	31.8	0.76	6.46	0.102
			320	127.2	3.03	12.91	0.105
XIR7		-8.74	310	32.2	0.77	6.55	0.103
			320	129.0	3.07	13.09	0.107
XI1	1.270	-7.96	310	29.0	0.69	5.94	0.094
			320	116.0	2.76	11.88	0.097
XIR1		-7.55	310	26.1	0.62	5.34	0.084
			320	104.2	2.48	10.68	0.087
XI4	1.910	-7.49	310	30.1	0.72	6.31	0.100
			320	120.5	2.87	12.62	0.103
XIR4		-7.14	310	27.3	0.65	5.72	0.090
			320	109.4	2.60	11.45	0.093
XIR4C		-7.17	310	27.5	0.66	5.77	0.091
			320	110.2	2.62	11.54	0.094
XI6=X2	2.670	-6.72	310	26.8	0.64	5.71	0.090
			320	107.4	2.56	11.43	0.093

Units: - R ; No unit - p = PY coef ; $\times 10^{-4}\ Cm^{-2}K^{-1}$ - Θ_H ; K $(\Theta_L = 300K)$

- $P_{denMax}^{0.07}$ = Maximum power density at $f = 0.07$; Wm^{-3} (or μWcm^{-3})
- $P_{denMax}^{0.0017}$ = Maximum power density at $f = 0.0017$ ($2°\mathrm{C}min^{-1}$) ; Wm^{-3}
- η_{Res} = Efficiency in resistive cycle case ; $\times 10^{-6}$ (No unit)
- k_{New}^2 = New electrothermal coupling factor for laminate composites ; %

Figures 13.6, 13.7, and 13.8 summarizes the findings from Table 13.2 and compares them with the predictions of the analytical model developed in Section 3.4. k_1 factors are employed to describe the effect of imperfect boding layer. It is clear from these figures that as long as the thickness ratio (R) is larger than certain value and the bonding quality is reasonably good, 2-2 connectivity laminate composites of PZT-5H will outperform stand alone PZT-5H in the energy harvesting application.

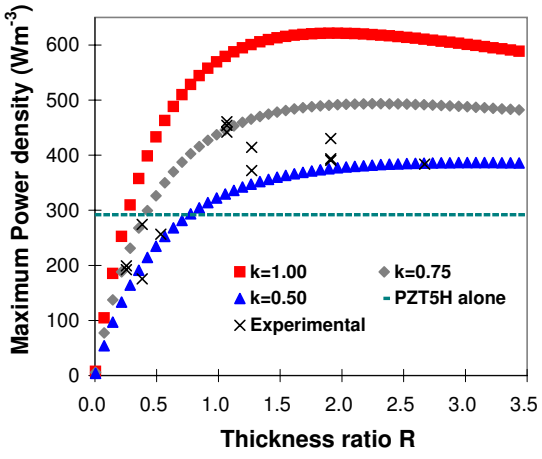

(a) $\Theta_L = 300K$, $\Theta_H = 310K$, and $f = 1Hz$

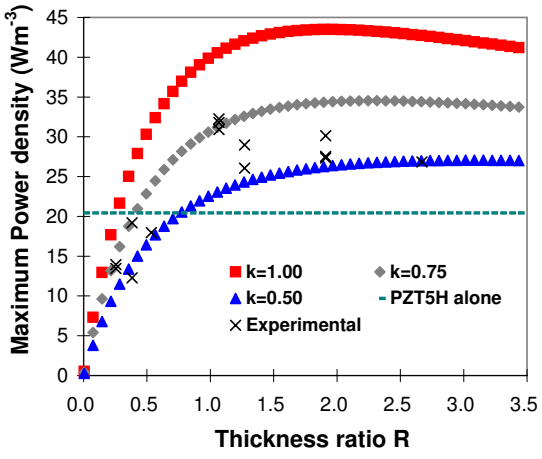

(b) $\Theta_L = 300K$, $\Theta_H = 310K$, and $f = 0.07Hz$ for around 30 μWcm^{-3} or Wm^{-3}

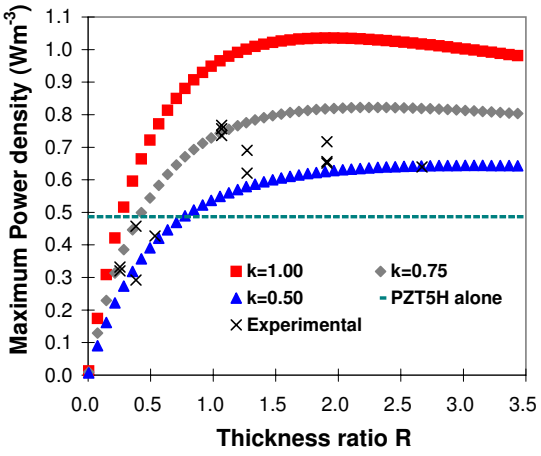

(c) $\Theta_L = 300K$, $\Theta_H = 310K$, and $f = 0.0017Hz$ (Experimental frequency)

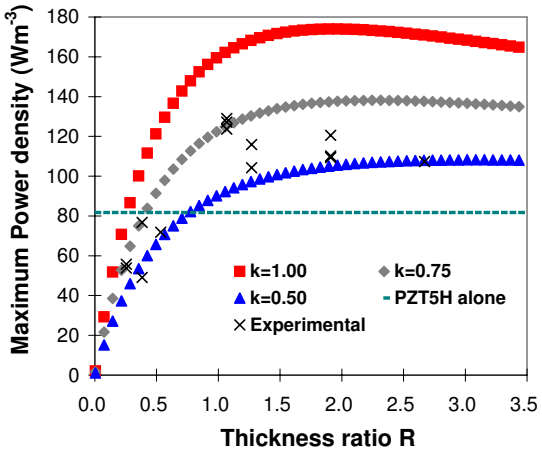

(d) $\Theta_L = 300K$, $\Theta_H = 320K$, and $f = 0.07Hz$ (Increasing temperature variation amplitude)

Figure 13.6: Maximum power density for PZT5H-St pairs and the samples from the experiment in Section 6.2 (with k_1 factor)

In Figure 13.6(a), a theoretical P_{denMax} should $f = 1Hz$ be possible is displayed.

With PY coef enhancement of over 100 % predicted, theoretically over 500 Wm^{-3} or 0.5 $mWcm^{-3}$ is shown to be possible. Considering the fact that phase transition independent PY effect (direct PY effect)'s energy harvesting credentials were previously assumed to be rather limited, this is certainly a respectable value. In particular, with PZT5H-St pair not being the best performing 2-2 connectivity laminate composite pair in PY coef enhancement, there is a good chance that even this value can be exceeded by substituting the NP or PY materials.

Figures 13.6(b) $\sim$ 13.6(d) demonstrate more realistic cases where the frequency and temperature variations are well within the value the previously described PY energy harvesting system in Figure 12.1 can deliver. P_{denMax} of over 160 $mWcm^{-3}$ is predicted to be possible at $f = 0.07Hz$ and $\Theta_H = 320K$ with the best performing experimental sample exhibiting about 130 Wm^{-3} under the same condition. This again is a considerable amount of power. For example, a 1 cm^3 PY element of this composite should be able to provide the maximum of 130 μW of power, which is enough to power a Radio Frequency IDentification (RFID) tag or a hearing aid[160].

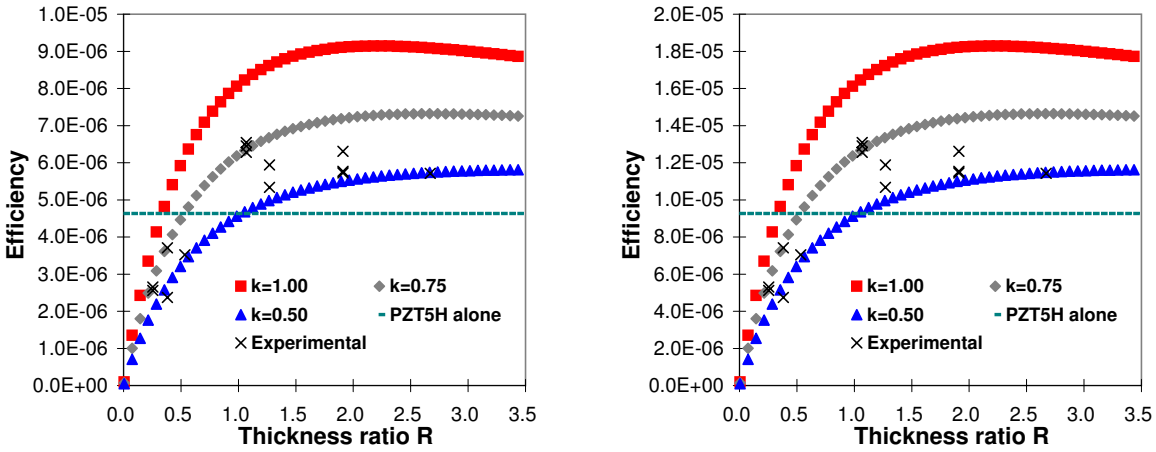

(a) $\Theta_L = 300K$, $\Theta_H = 310K$, $f = 0.07Hz$, and $\eta_{Carnot} = 0.0323$

(b) $\Theta_L = 300K$, $\Theta_H = 320K$, $f = 0.07Hz$, and $\eta_{Carnot} = 0.0625$ (Increasing temperature variation amplitude)

Figure 13.7: Efficiency (η_{Res}) for PZT5H-St pairs and the samples from the experiment in Section 6.2 (with k_1 factor)

In Subsection 9.2.1, where Figure of merit for efficiency under SC were discussed, Figure 9.4 displayed the outcomes of the analysis on two Figures of merit, namely F^a_{eff} and F^b_{eff}. Figure 9.4(b) 's F^b_{eff} describes a similar trend to the efficiency figures in Figure 13.7

with both predicting an improvement in the efficiency at around $R > 1$ or $R > 1.5$. This demonstrates that the Figures of merit for efficiency are indeed a good initial indicator for describing a general conversion efficiency of any PY material/composite. Maximum of near doubling of the efficiency (η_{Res}) are predicted via PY coef enhancement, although experimental samples were only able to demonstrate up to around 40 % improvement. It should be noted that η_{Res} is independent of frequency, as the expression in Eq 12.12 suggests.

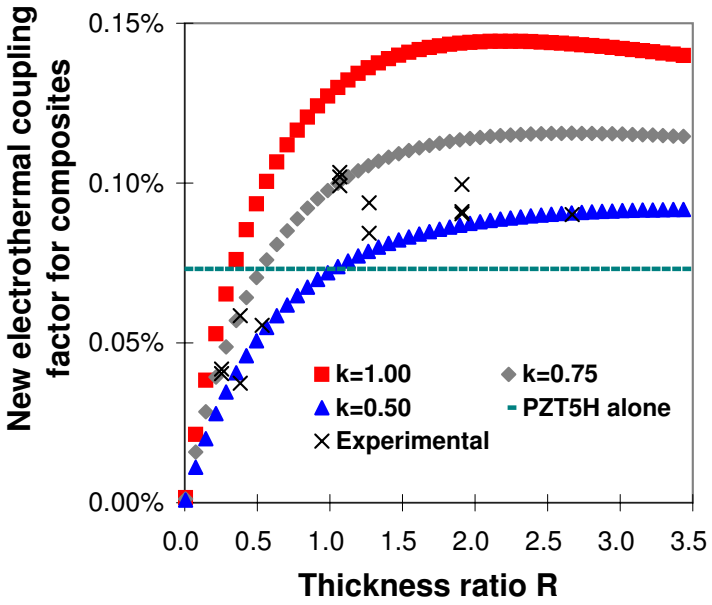

Figure 13.8: New electrothermal coupling factor for composites (k^2_{New}) evaluated for PZT5H-St pairs and the samples from the experiment in Section 6.2 (with k_1 factor)

New electrothermal coupling factor (k^2_{New}) and its relationship with R is depicted in Figure 13.8. This measure for PY energy harvesting credentials was developed to assess a PY material or composite's potential in PY energy harvesting application. As such, it is independent of frequency and temperature variation amplitude (cf. Eq 13.1). It is evident from Figure 13.8 that it predicts PZT5H-St laminate composite's performance in both P_{denMax} and η_{Res} quite well, with up to doubling of k^2_{New} under optimal conditions.

Figure 13.9 is based on values from Tables 13.2, 13.3, and 13.4. It describes how the percentile change in energy harvesting application specific parameters (P_{denMax}, η_{Res}, and k^2_{New}) vary with the percentile PY coef enhancement. By comparing the percentile improvements in these parameters between stand alone PZT-5H and PZT5H-St composite (with additional NP layer bonded, and hence with larger volume), one can investigate

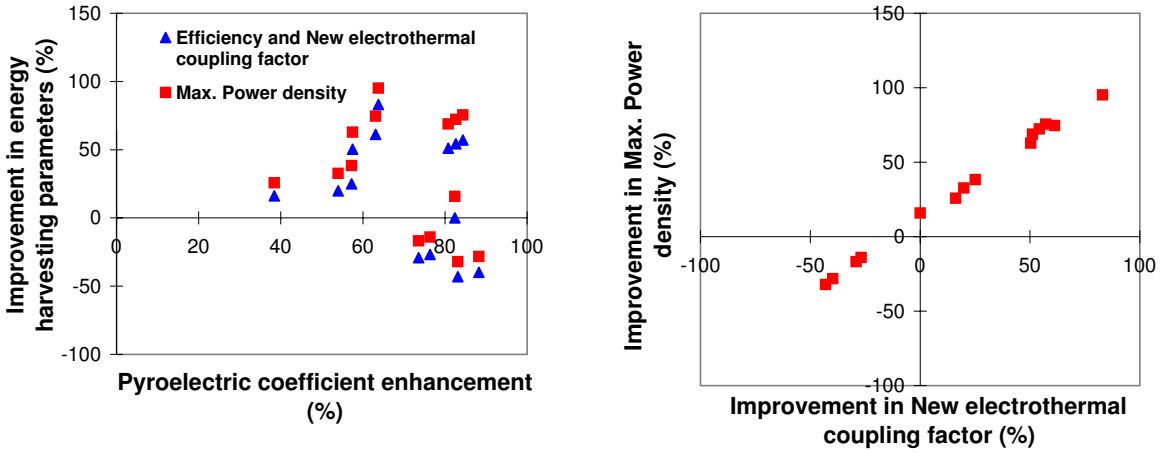

(a) Percentile PY coef enhancement vs improvements in P_{denMax}, η_{Res}, and k^2_{New} in percentage

(b) Percentile improvement in k^2_{New} vs Percentile improvement in P_{denMax}

Figure 13.9: Percentile improvements in P_{denMax}, η_{Res}, and k^2_{New} (from Table 13.4)

the effect of trade-off between the enhanced PY coef and increased thermal mass. Indeed the comparison conditions are identical to that of F^b_{eff}. Figure 13.9(a) depicts a somewhat confusing picture where rather unexpectedly high PY coef enhancement leads to a reduction, which can be attributed to increased thermal mass from NP overtaking the improvement from the enhanced PY coef. However, Figure 13.9(b) describes a proportional correlation between Percentile Δk^2_{New} and Percentile ΔP_{denMax}, demonstrating the suitability of k^2_{New} as potential indicators for PY energy harvesting performance.

Table 13.3 illustrates the kind of energy harvesting parameters one can expect from the exact stand alone PZT-5H PY materials that are later used for fabricating the experimental samples. It is evident from Table 13.3 that even before the PY coef enhancement, PZT-5H alone are quite capable of producing relatively high maximum power densities of up to around 90 Wm^{-3} at $f = 0.07$ and $\Delta\Theta = 40K$. Note that XI4's unusually high PY coef before attaching NP materials, which results in very high $P^{0.07}_{denMax}$ of 95.8 Wm^{-3}, meant its enhancement in PY coef was calculated to be rather small, and hence it was considered to be an anomaly in Subsection 6.2.2. As expected, η_{Res} and k^2_{New} values are very similar to that of a typical PZT5H in Table 13.1, although for $\Theta_H = 320K$ η_{Res} values are doubled due to η_{Res}'s dependency on $(\Theta_H - \Theta_L)$ (cf. Eq 12.12). Again, it is quite clear that the independence of k^2_{New} from $(\Theta_H - \Theta_L)$ and f makes it an ideal parameter for judging the energy harvesting credentials of PY materials or composites provided Θ_H is sufficiently large enough (cf. Eq 13.1).

Table 13.3: Energy harvesting potentials of experimental samples' PY material (PZT-5H) only before enhancement, i.e. bonding

Name	R	p	Θ_H	$P_{denMax}^{0.07}$	$P_{denMax}^{0.0017}$	η_{Res}	k_{New}^2
XI3	0.254	-5.01	310	20.5	0.49	4.65	0.074
			320	82.1	1.95	9.31	0.076
XII4		-4.79	310	18.7	0.45	4.25	0.067
			320	75.0	1.79	8.50	0.069
XI5	0.382	-5.23	310	22.3	0.53	5.07	0.080
			320	89.4	2.13	10.13	0.083
XIR5		-4.25	310	14.7	0.35	3.34	0.053
			320	59.0	1.40	6.69	0.055
XI8=X3	0.534	-4.36	310	15.5	0.37	3.52	0.056
			320	62.0	1.48	7.03	0.057
XI7	1.068	-4.64	310	17.6	0.42	3.99	0.063
			320	70.5	1.68	7.99	0.065
XIR7C		-4.80	310	18.8	0.45	4.27	0.067
			320	75.3	1.79	8.54	0.070
XIR7		-4.79	310	18.7	0.45	4.24	0.067
			320	74.9	1.78	8.49	0.069
XI1	1.270	-5.17	310	21.9	0.52	4.96	0.078
			320	87.4	2.08	9.91	0.081
XIR1		-4.80	310	18.8	0.45	4.27	0.067
			320	75.3	1.79	8.54	0.070
XI4	1.910	-5.41	310	23.9	0.57	5.43	0.086
			320	95.8	2.28	10.86	0.089
XIR4		-4.53	310	16.8	0.40	3.81	0.060
			320	67.2	1.60	7.61	0.062
XIR4C		-4.39	310	15.8	0.38	3.58	0.057
			320	63.1	1.50	7.16	0.058
XI6=X2	2.670	-4.10	310	13.8	0.33	3.12	0.049
			320	55.0	1.31	6.24	0.051

Units: - R ; No unit - p = PY coef ; $\times 10^{-4}\ Cm^{-2}K^{-1}$ - Θ_H ; K $(\Theta_L = 300K)$

- $P_{denMax}^{0.07}$ = Maximum power density at $f = 0.07$; Wm^{-3} (or μWcm^{-3})
- $P_{denMax}^{0.0017}$ = Maximum power density at $f = 0.0017$ ($2°\text{C}min^{-1}$) ; Wm^{-3}
- η_{Res} = Efficiency in resistive cycle case ; $\times 10^{-6}$ (No unit)
- k_{New}^2 = New electrothermal coupling factor for laminate composites ; %

Table 13.4: Experimental samples from the Enhancement study before (without NP layer) and after (with NP) bonding (analogous to F_{eff}^{b}, Table 13.3 → 13.2)

Sample name	R	Percentile Δp	Percentile ΔP_{denMax}	Percentile $\Delta \eta_{Res}$	Percentile Δk_{New}^{2}
XI3	0.254	83.1	-32.1		-43.0
XII4	0.254	88.3	-28.2		-39.8
XI5	0.382	76.3	-14.0		-26.8
XIR5	0.382	73.6	-16.7		-29.1
XI8=X3	0.534	82.4	15.8		0.08
XI7	1.068	84.4	75.5		57.2
XIR7C	1.068	80.8	68.8		51.2
XIR7	1.068	82.6	72.3		54.3
XI1	1.270	54.0	32.6		19.9
XIR1	1.270	57.3	38.4		25.1
XI4	1.910	38.4	25.8		16.2
XIR4	1.910	57.5	62.8		50.4
XIR4C	1.910	63.1	74.6		61.2
XI6=X2	2.670	63.8	95.1		83.1

Units: - $R = \frac{PY_t}{NP_t}$ = thickness ratio ; No unit
- Percentile Δp = Percentile PY coef enhancement after bonding ; %
- Percentile ΔP_{denMax} = Percentile maximum power density (P_{denMax}) change after enhancement ; %
- Percentile $\Delta \eta_{Res}$ = Percentile efficiency (η_{Res}) change after enhancement ; %
- Percentile Δk_{New}^{2} = Percentile new electrothermal coupling factor (k_{New}^{2}) change after enhancement ; %

Changes in energy harvesting parameters as a PZT-5H is measured (cf. Table 13.3), then attached to St forming a laminate composite (cf. Table 13.2), are displayed in Table 13.4. This is analogous to F_{eff}^{b} where ratio between efficiencies of stand alone PY material and its laminate composite (with larger volume) is considered. Samples up to $R < 0.534$ show reduction in their parameters despite large Percentile Δp of up to 88.3 % owing to increased thermal mass from the introduction of NP layer. XI6 ($R = 2.670$) showed the best improvement in all the parameters despite its relatively low Percentile

Δp of 63.8 %. In fact, near doubling of P_{denMax} (95.1 % increase), and both η_{Res} and k^2_{New} (83.1 % increase) indicates that attaching a thin layer of St may be the best route for improving PY energy harvesting with PZT-5H. One of the main reasons behind this is St's large c_{vol} ($3.91 \times 10^6\ Jm^{-3}K^{-1}$), which is even larger than that of PZT-5H ($3.15 \times 10^6\ Jm^{-3}K^{-1}$). Use of other NP materials such as Al ($c_{vol} = 2.40 \times 10^6\ Jm^{-3}K^{-1}$), or even PTFE and CPVC with 0.72 and $1.40 \times 10^6\ Jm^{-3}K^{-1}$ respectively, should aid in reducing this hinderance to improvement. Table 13.4 formed the basis for Figure 13.9.

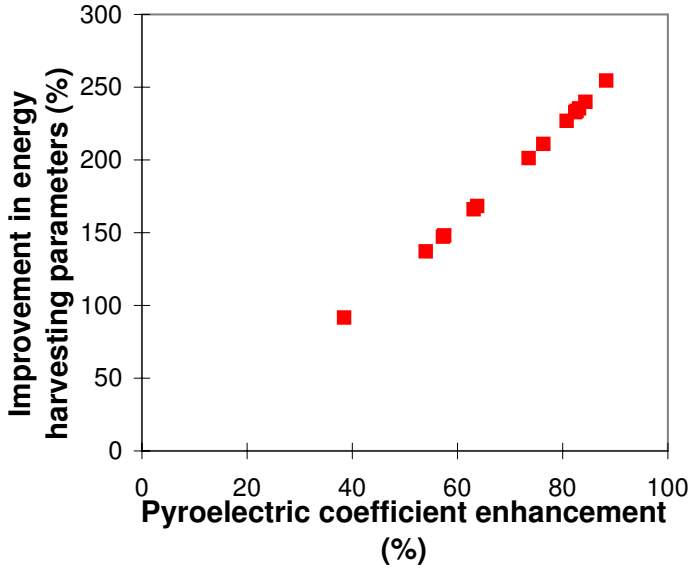

Figure 13.10: Percentile pyroelectric coefficient enhancement versus improvements in P_{denMax}, η_{Res}, and k^2_{New} in percentage (from Table 13.6)

Based on Tables 13.2, 13.5, and 13.6, Figure 13.10 depicts the proportional correlation between Percentile Δp and Percentile ΔP_{denMax}, $\Delta \eta_{Res}$, and Δk^2_{New}. Being analogous to F^a_{eff}, this comparison between results from Tables 13.2 and 13.5 represents a case where both PZT-5H and St were assumed present when considering both before and after bonding. Hence this represents the case where the overall volume of initial materials (as PY and NP are not yet bonded, they are not a composite) is equal to the volume of resultant laminate composite after bonding. As there is no additional thermal mass after the bonding (it was added beforehand leading to values in Table 13.5 being much smaller than those in Table 13.3), the only quantity that affects the energy harvesting parameters is the enhanced PY coef. This correlation between Percentile Δp and the improvements in all three energy harvesting parameters is also present in Table 13.6, which formed the basis for Figure 13.10.

Table 13.5: Energy harvesting potentials of experimental samples (PY-NP together) before enhancement, i.e. bonding

Name	R	p	Θ_H	$P_{denMax}^{0.07}$	$P_{denMax}^{0.0017}$	η_{Res}	k_{New}^2
XI3	0.254	-5.01	310	4.16	0.10	0.79	0.012
			320	16.63	0.40	1.58	0.013
XII4		-4.79	310	3.80	0.09	0.72	0.011
			320	15.19	0.36	1.44	0.012
XI5	0.382	-5.23	310	6.18	0.15	1.19	0.019
			320	24.70	0.59	2.38	0.019
XIR5		-4.25	310	4.08	0.10	0.79	0.012
			320	16.30	0.39	1.57	0.013
XI8=X3	0.534	-4.36	310	5.40	0.13	1.06	0.017
			320	21.58	0.51	2.11	0.017
XI7	1.068	-4.64	310	9.10	0.22	1.85	0.029
			320	36.39	0.87	3.69	0.030
XIR7C		-4.80	310	9.73	0.23	1.98	0.031
			320	38.90	0.93	3.95	0.032
XIR7		-4.79	310	9.67	0.23	1.96	0.031
			320	38.66	0.92	3.93	0.032
XI1	1.270	-5.17	310	12.23	0.29	2.51	0.040
			320	48.91	1.16	5.01	0.041
XIR1		-4.80	310	10.53	0.25	2.16	0.034
			320	42.14	1.00	4.32	0.035
XI4	1.910	-5.41	310	15.72	0.37	3.29	0.052
			320	62.86	1.50	6.58	0.054
XIR4		-4.53	310	11.02	0.26	2.31	0.036
			320	44.08	1.05	4.61	0.038
XIR4C		-4.39	310	10.36	0.25	2.17	0.034
			320	41.43	0.99	4.34	0.035
XI6=X2	2.670	-4.10	310	10.01	0.24	2.13	0.034
			320	40.04	0.95	4.26	0.035

Units: - R ; No unit - p = PY coef ; $\times 10^{-4}\ Cm^{-2}K^{-1}$ - Θ_H ; K $(\Theta_L = 300K)$

- $P_{denMax}^{0.07}$ = Maximum power density at $f = 0.07$; Wm^{-3} (or μWcm^{-3})
- $P_{denMax}^{0.0017}$ = Maximum power density at $f = 0.0017$ ($2°\text{C}min^{-1}$) ; Wm^{-3}
- η_{Res} = Efficiency in resistive cycle case ; $\times 10^{-6}$ (No unit)
- k_{New}^2 = New electrothermal coupling factor for laminate composites ; %

Table 13.6: Experimental samples from the Enhancement study before and after the bonding (PY and NP layers are present for both measurements, analogous to F^a_{eff}, Table 13.5 $\rightarrow$ 13.2)

Sample name	R	Percentile Δp	ΔP_{denMax}, $\Delta\eta_{Res}$, and Δk^2_{New} (Percentile)
XI3	0.254	83.1	235.3
XII4	0.254	88.3	254.4
XI5	0.382	76.3	211.0
XIR5	0.382	73.6	201.2
XI8=X3	0.534	82.4	232.7
XI7	1.068	84.4	239.9
XIR7C	1.068	80.8	226.8
XIR7	1.068	82.6	233.6
XI1	1.270	54.0	137.1
XIR1	1.270	57.3	147.3
XI4	1.910	38.4	91.7
XIR4	1.910	57.5	148.1
XIR4C	1.910	63.1	166.0
XI6=X2	2.670	63.8	168.2

Units: - $R = \frac{PY_t}{NP_t}$ = thickness ratio ; No unit
- Percentile Δp = Percentile PY coef enhancement after bonding ; %
- Percentile ΔP_{denMax} = Percentile maximum power density (P_{denMax}) change after enhancement ; %
- Percentile $\Delta\eta_{Res}$ = Percentile efficiency (η_{Res}) change after enhancement ; %
- Percentile Δk^2_{New} = Percentile new electrothermal coupling factor (k^2_{New}) change after enhancement ; %

As one would expect, in the case of Table 13.6 and Figure 13.10, larger the PY coef enhancement larger the improvement in the energy harvesting parameters. It must be noted that all three parameters demonstrated the same amount of percentile improvement since the only reason Percentile ΔP_{denMax} behaved differently from the other two parameters in Table 13.4 was due to its dependence on the overall volume, which was not constant between Tables 13.2 and 13.3, whereas in Table 13.6 it remains constant between

Tables 13.2 and 13.5. Sample XI7 ($R = 1.068$) is expected to show up to 240 % increase in P_{denMax}, η_{Res}, and k^2_{New} from PY coef enhancement of only 84.4 %, which suggests that thin PZT-5H with thick St attached could improve the overall energy harvesting performance quite drastically for the same volume of PY material and 2-2 connectivity laminate composite. This indicates that the use of thin-films, or at least the thinnest possible bulk material, in the PY energy harvesting applications will be a good idea despite the scaling behaviour of thin films, as this leads to reduction in the significantly negative role played by the additional thermal mass. In addition, use of other NP materials with lower c_{vol} values than that of PZT-5H, such as Al, Zn, PTFE or CPVC, should lead to even larger improvements as this will lead to reduced thermal mass. This reduced thermal mass should also enable the use of higher f values, potentially resulting in very high P_{denMax}, η_{Res}, and k^2_{New}.

Chapter 14

Conclusions - Potential applications

Objective 2 from Section 1.2 has been achieved.

After briefly describing various applications of pyroelectricity that may benefit from this research, the author has derived mathematical expressions/parameters that are important in judging the energy harvesting credentials of any PY material or PY-NP 2-2 connectivity laminate composites, namely Maximum power density (P_{denMax} from Eq 12.9), Efficiency (η_{Res} from Eq 12.12), and Electrothermal coupling factor (k^2 from Eq 12.13). In doing so, he has discovered that while Electrothermal coupling factor (k^2) quoted in the literature[160] is fine for stand alone PY materials, for laminate composites its more general counterpart in New electrothermal coupling factor (k^2_{New} from Eq 13.1) should be used. It seems quite possible that for other connectivity configurations of composites, various different electrothermal coupling factor expressions may be needed. It was found that main application parameters that affect P_{denMax} are $\Theta_H - \Theta_L$ and f, while η_{Res} was independent of f, and k^2_{New} of both. The independence of k^2_{New} from $(\Theta_H - \Theta_L)$ and f made it an ideal parameter for judging the energy harvesting credentials of PY materials or composites, provided Θ_H is sufficiently large enough. In order to investigate these parameters, PY energy harvesting system in Figure 12.1 was designed as a hypothetical application of pyroelectricity and PY coef enhanced 2-2 connectivity laminate composites, while impedance matching and resistive load cycle were assumed in its energy harvesting/storage circuitry.

From considering the resistive cycle energy harvesting credentials of the thirty-six PY-NP 2-2 connectivity laminate composites in Section 13.1, it was found that LTO single crystal show immense promise as a prime PY material candidate for energy harvesting application, although its 2-2 connectivity laminate composite counterparts' performances

were rather disappointing due to small PY coef enhancement, if not a reduction. The author believes this situation can be changed should a more suitable NP material for PY coef enhancement found for LTO using the criteria laid out in Part I.

PZT5H-Zn ($R = 1.005$) and PZT5H-CPVC ($R = 0.045$) 2-2 connectivity laminate composites also show extreme promise in PY energy harvesting application. In particular, PZT5H-Zn ($R = 1.005$) composite's P_{denMax} of 12.35 Wm^{-3} at $\Theta_L = 300K$, $\Theta_H = 310K$, and $f = 0.01Hz$, is very respectable, which can easily be further improved by increasing $\Theta_H - \Theta_L$ and f, when compared to that of a typical thermoelectric module, i.e. 30 Wm^{-3} [160]. Considering the important role the frequency plays in determining P_{denMax}, these P_{denMax} values where evaluated after careful consideration was given to estimating practically possible f values. By employing "Time constant" expression (Eq 5.4) from Subsubsection 5.3.3, maximum thermal variational frequency was estimated to be at least $f_{Max} = 0.175Hz$, vindicating the use of $f = 0.01Hz$ in the analyses. The possibility of further improvements were noted by facilitating potentially huge spatial temperature gradient when PY element is in contact with the surfaces of hot and cold reservoirs, which can improve the thermal conductivity even further leading to higher available frequency (f), and hence ultimately greater P_{denMax}.

In Section 13.2, the author focussed his attention to PZT5H-St pairs, demonstrating the energy harvesting potentials of the experimentally measured samples from PY coef enhancement study in Section 6.2. Numerous tables, each representing a particular state of the composite (stand alone PY material, PY material surrounded by NP materials, and bonded laminate composite of NP/PY/NP for example), were created with frequencies of: $f = 0.0017Hz$ representing 2 °Cmin^{-1} heating rate (used in Enhancement study experimentation for testing the samples, cf. Subsection 6.2.2) applied to a $\Delta\Theta = 20K$ thermal cycle, and $f = 0.07$ for being the frequency at which some of the tested experimental samples start to achieve maximum power densities (P_{denMax}) larger than that of a typical thermoelectric module, i.e. 30 Wm^{-3}. Although respectable, P_{denMax} achievable using $f = 0.0017Hz$ was rather small, whereas $f = 0.07$ demonstrated quite high values.

When bonded laminate composites of PZT-5H and St were considered, the composites with $R > 1$ outperformed the typical PZT5H's energy harvesting parameters. Although smaller R leads to higher PY coef enhancement, it also means larger additional thermal mass from NP layer, resulting in larger effective volumetric heat capacity ($\bar{c_E}$) which in turn has a negative effect on all the energy harvesting parameters, P_{denMax}, η_{Res},

and k^2_{New}. This suggests maximising the PY coef alone is not enough to optimise the energy harvesting system. As one would expect, other issues such as the additional thermal mass needs to be considered. The best performing experimental sample was deemed to be XIR7 ($R = 1.068$) with its largest k^2_{New}, resulting in highest P_{denMax} of 32.2 and 129.0 Wm^{-3} at $f = 0.07Hz$ for $\Theta_H = 310$ and $\Theta_H = 320$ respectively. This is a considerable amount of power. For example, a 1 cm^3 PY element of this composite should be able to provide maximum of 129 μW of power, which is enough to power a Radio Frequency IDentification (RFID) tag or a hearing aid[160]. All the samples with $R > 1$ depicted a rather large P_{denMax}, larger than 100 Wm^{-3} at $f = 0.07Hz$ for $\Theta_H = 320$, insinuating their potential deployment in energy harvesting application. Bearing in mind that the frequency and temperature variations used for these calculations are all viewed as reasonably conservative values, the author believes there is a good chance that these composites, or similar composites with different PY or NP materials such as Zn, Al, or CPVC could well find their use in PY energy harvesting.

A purely theoretical P_{denMax} was also simulated for $f = 1Hz$, a value which might be achievable should a very thin PZT-5H be used. With PY coef enhancement of over 100 % predicted, theoretically over 500 Wm^{-3} or 0.5 $mWcm^{-3}$ is shown to be possible. Considering the fact that phase transition independent PY effect (direct PY effect)'s energy harvesting credentials were previously assumed to be rather limited, this is certainly a respectable value. In particular, with PZT5H-St pair not being the best performing 2-2 connectivity laminate composite pair in PY coef enhancement, there is a good chance that even this value can be exceeded by substituting the NP or PY materials.

Validation of the new electrothermal coupling factor (k^2_{New}) as the main indicator for predicting laminate composites' energy harvesting credentials have also taken place by comparing two different cases that are analogous to two Figures of merit for efficiency under SC discussed in Subsection 9.2.1, namely F^a_{eff} (Same overall volume) and F^b_{eff}. Indeed it was found that percentile improvement in k^2_{New} (Percentile Δk^2_{New}) was able to demonstrate a proportional correlation with the percentile improvement in P_{denMax} (Percentile ΔP_{denMax}) in both cases, which percentile PY coef enhancement (Percentile Δp) failed to do in the case that is analogous to F^b_{eff} due to the introduction of additional thermal mass in the form of NP layer leading to dissimilar volume expression before and after the bonding of the laminate composite. This means k^2_{New} indeed is the parameter for judging PY energy harvesting credentials of 2-2 connectivity laminate composites of

PY-NP pairs, as dc1, dc2, and dc3 are to PY coef enhancement.

When the effects of PY coef enhancement on the energy harvesting parameters is considered, from the analysis that is analogous to F^b_{eff} (where ratio between efficiencies of stand alone PY material and its laminate composite, with larger volume, is considered), samples up to $R < 0.534$ demonstrated reduction in their parameters despite large Percentile Δp of up to 88.3 % owing to increased thermal mass from the introduction of NP layer. Sample XI6 ($R = 2.670$) showed the best improvement in all the parameters despite its relatively low Percentile Δp of 63.8 %. In fact, near doubling of P_{denMax} (95.1 % improvement), and both η_{Res} and k^2_{New} (83.1 % improvement) indicates that when it comes to improvements in PY energy harvesting with PZT-5H, it may well be the best to attach a thin layer of St or NP layer with larger thermal expansion coef. One of the main reasons behind this is attributed to St's large c_{vol} of $3.91 \times 10^6\ Jm^{-3}K^{-1}$, which is even larger than that of PZT-5H ($3.15 \times 10^6\ Jm^{-3}K^{-1}$). Use of other NP materials such as Al with c_{vol} value of $2.40 \times 10^6\ Jm^{-3}K^{-1}$, or even PTFE and CPVC with 0.72 and 1.40 $\times 10^6\ Jm^{-3}K^{-1}$ respectively, should aid in reducing this hinderance to improvement.

From the analysis analogous to F^a_{eff}, Sample XI7 ($R = 1.068$) is expected to show up to 240 % increase in P_{denMax}, η_{Res}, and k^2_{New} from PY coef enhancement of only 84.4 %, which suggests that thin PZT-5H with thick St attached could improve the overall energy harvesting performance quite drastically for the same volume of PY material and 2-2 connectivity laminate composite. This suggests that the use of thin-films, or at least the thinnest possible bulk material, in the PY energy harvesting applications will be a good idea despite the scaling behaviour of thin films, as this leads to reduction in the significantly negative role played by the additional thermal mass. In addition, use of other NP materials with lower c_{vol} values than that of PZT-5H, such as Al, Zn, PTFE or CPVC, should lead to even larger improvements as this will lead to reduced thermal mass. This reduced thermal mass should also enable the use of higher f values, potentially resulting in very high P_{denMax}, η_{Res}, and k^2_{New}.

It must be noted that all the analyses performed concern a simple resistive loading case. Use of more efficient energy harvesting circuitry such as SSHI should improve the PY energy harvesting parameters even further, improving the likelihood of the employment of 2-2 connectivity laminate composites of PZT-5H in PY energy harvesting application.

To summarize, the parameters for assessing a material or laminate composite's PY energy harvesting credentials have been identified, while a brief comparison with Figures

of merit for efficiency (F^a_{eff} and F^b_{eff}) derived in previous part of the dissertation has been made. The use of New electrothermal coupling factor for composites (k^2_{New}) for such assessment has been vindicated while the experimental samples are demonstrated to show significant improvement in their pyroelectric energy harvesting performance via pyroelectric coefficient enhancement. Finally, some recommendations have been made to improve the performance of 2-2 connectivity laminate composites in this application.

Chapter 15

Summary

To summarize, all the objectives listed in Section 1.2 have been achieved resulting in a number of journal publications[43–45] and interesting suggestions for future work to be undertaken (cf. Chapter 16).

Starting from the definition of pyroelectricity and using thermodynamic principles, analytical model for 2-2 connectivity laminate composites of PY and NP materials have been developed. This model was then applied to the potential PY coef enhancements in thirty-six such composites, identifying the best possible partnership among these composites. This potentially large theoretical PY coef enhancement was attributed to dissimilar signs of the piezoelectric coefs of the PY material (dc1, dc2, and dc3) and the exploitation of this particular symmetry through the deployment of 2-2 connectivity configuration. The sum terms dc1, dc2, and dc3 are identified as the most viable indicators for determining the feasibility and potential for PY coef enhancement. With the importance the connectivity concept plays in other application areas such as thermal imaging[17], this analysis on 2-2 connectivity composites could find use in many other diverse areas of research such as Infra-Red detectors and thin-film technologies. The best performing partnership out of the thirty-six PY-NP pairs was PZT5H-CPVC demonstrating maximum of 800 % increase in theoretical PY coef at $R = R_{min}$. Experimental verification of stated enhancements in PZT5H-St has also been conducted with observed PY coef enhancements of more than 100 %. Various factors involved in making such measurement have also been identified and explored, main examples being the effects of pre-stress and interfacial bonding quality.

With potential applications of PY coef enhancement in mind, both electrical boundary conditions SC and OC, have been investigated. Theoretical differences between them

have been highlighted with significant dissimilarities in PY coef enhancement being predicted. In addition, by defining a quantity termed "efficiency" a measure for the laminate composites' thermal-to-electrical conversion efficiency has been proposed which can also consider the effects of thermal mass variation arising from dissimilar volumetric heat capacities of PY and NP materials. Figures of merit for efficiency (F^a_{eff} and F^b_{eff}) were also derived as a ratio between these efficiencies of stand alone PY material and its laminate composite for the purpose of assessing the potential conversion performance of these composites. Using these Figures of merit for efficiency, various PY-NP pairs and their potential efficiency improvements were also analysed. PZT5H-CPVC laminate composites are simulated to have high Figures of merit for efficiency with the maximum of twenty fold increase in efficiency predicted by F^a_{eff} under SC, insinuating a potential for increased employment of PZTs in areas such as PY sensors[188,189] and PY energy harvesting[70,138].

For OC, very large PY coef is shown to be expected for PZT-5H-CPVC while Figures of merit for efficiency also showed improved efficiencies in laminate composites. It was also noted that the assumptions made in the thermal expansion coefs under SC makes the numerical values of the secondary PY coefs under OC somewhat questionable although this does not dispute the findings that there indeed is a substantial dissimilarity between the PY coefs and Figures of merit for efficiency for various PY-NP pairs under SC and OC. The author believes this implies that there should be a greater distinction made between the PY coefs under SC and OC than previously thought. The analysis techniques used in this dissertation provide a methodology for assessing the potentials of particular PY material and its 2-2 laminate composites for applications under OC. For instance, appraising employment credentials of LTO or LNO in applications such as PY X-ray generation, electron accelerator, and nuclear fusion.

After considering various applications of pyroelectricity, PY energy harvesting was chosen as a suitable application of PY coef enhancement observed in this research that constitutes further investigation. In order to investigate this application further, PY energy harvesting system in Section 12.1 was designed as a hypothetical application of pyroelectricity and PY coef enhanced 2-2 connectivity laminate composites. Numerous parameters for assessing a material or laminate composite's PY energy harvesting credentials have been identified and evaluated, while a brief comparison with Figures of merit for efficiency (F^a_{eff} and F^b_{eff}) derived in previous part of the dissertation has also been made. The use of New electrothermal coupling factor for composites (k^2_{New}) for such as-

sessment has been vindicated while the experimental samples were demonstrated to show significant improvement in their PY energy harvesting performance via PY coef enhancement. Finally, some recommendations have also been made to improve the performance of 2-2 connectivity laminate composites in this particular application.

In essence, PY coef enhancement via product property in its secondary part has been theoretically modelled and experimentally verified. Two electrical boundary conditions under which this enhancement might be employed have been investigated with their effect on the enhancement itself analytically modelled. Consideration into the enhancement's applicability in a number of applications of pyroelectricity has been conducted with PY energy harvesting application being demonstrated as a potential beneficiary of this enhancement. Theoretical analysis confirms that large improvement in PY energy harvesting performance can be expected in PZTs by converting them into 2-2 connectivity laminate composites.

Chapter 16

Future work

16.1 Potential advancements in the theoretical modelling techniques

16.1.1 Laminate structures and related strains

In Subsection 3.2.2, we attempted to describe the interaction between PY and NP materials using simple beam theory under plane stress and negligible shear stress conditions. However, as illustrated in Sections 3.3 and 3.4, although this simplification is sufficient to approximate our experimental PY coef enhancements, it may well be that a more elaborate model that takes into account of more phenomena that accompany our enhancement would be more desirable for the future. The author would like to suggest following works by other researchers that may pave the way to achieve this:

At the outset, the brief review by Suhir[174] should provide a good foundation and provide insight into some of the published work in the analytical modelling of the thermally induced stresses and displacements, which forms the basis for describing the interaction between our PY and NP materials.

In order to apply a more realistic boundary condition than the plane stress and negligible shear stress conditions and also introduce shear stresses into our model, research conducted by Tsai[178,179], Horton and Tupholme[80], Pinarbasi et al.[144], and Kapuria et al.[86] should help. While the former three teams developed analytical models for describing an elastic medium placed between two rigid plates, which is essentially our 2-2

connectivity laminate composite as long as NP is much stiffer than PY material, the latter developed a layer-wise theory for analysing piezoelectric sandwich beams, which again should fit very well with our own objectives with some modifications.

Meanwhile, work by Suhir[173] and Gaudette et al.[59] should provide good analytical techniques for modelling thermal expansion coefficient mismatch induced stresses in our composites with former characterising the presence of the adhesive (epoxy) layer and the latter presenting a method for accounting any fatigue issue that may arise from prolonged application of our composites.

16.1.2 Finite Element Analysis

Although we were unable to use FEA package ANSYS® to model pyroelectric effect (cf. Section 3.3), there is a group in Germany, Drescher et al. namely, who has managed to do this by including the pyroelectric part of the constitutive law as body loads[52]. Although our enhancement means the pyroelectric part of the constitutive law has now changed, it may well be possible to model our effect with ANSYS® using similar techniques. It would be very interesting to see how ANSYS® or any other FEA package describes our enhancement. In addition, incorporating Lee and Saravanos'[102] thermopiezoelectric layer-wise finite element formulations that takes the temperature dependencies of the material properties into account could also lead to FEA models that is valid over a wide temperature range.

16.1.3 Investigation into the effect of pre-stress exerted by the thermal expansion coefficient mismatch

As curing temperatures can be varied for the adhesive used, namely Epotek 301-2, it would be interesting to see how curing temperature affects the enhancement. Despite the author's attempts at measuring this phenomena (cf. Section 6.1), the outcome from the Curing temperature study has been inconclusive so far. Using wider range of Cur and Op. temps should reveal some insight into this issue. There is no doubt that pre-stress can affect the piezoelectric and dielectric properties of PZT[197,199–201] (cf. Subsubsection 2.2.2), and how this affects pyroelectric effect and domain switching could be an interesting subject to look into. Landau-Devonshire's phenomenological theory based thermodynamic models, such as those proposed by Bell et al.[24,25] and Kanno et al.[85], should be able to

describe such effects. It may well be that there is even more room for improvement in our enhancement through this route. The presence of pre-stress could also affect the curie temperature and phase transitions of PY materials, which may potentially find use in PY energy harvesting applications where cycles utilising high PY activities at ferroelectric transitions are employed[70,91] to generate electricity.

16.2 SMA for potentially higher enhancement

As mentioned in Subsection 4.1.1, once an analytical or computational model is developed to successfully describe the interaction between PY and SMA layer in a 2-2 connectivity configuration, it may well be possible to improve on our already rather impressive enhancement in PY coef using SMA. The author believes that perhaps Lee and Saravanos' work[102] could be beneficial where the computational modelling is concerned as SMA has variable material properties depending on its state. It remains to be seen whether the fatigue (potential requirement for re-training after an extensive use) and fabrication technique issues can be resolved to achieve this.

16.3 Experimental verification of extremely large PY coef enhancements

Extremely large PY coef enhancements have been predicted for some of the PY-NP pairs investigated in Subsection 6.2.1. In particular, around 800% increase in PY coef has been predicted for PZT5H-CPVC pair at R=0.005. By employing very thick CPVC laminates and thin PZT-5H, it should be possible to demonstrate at least a portion of this enhancement experimentally, which could pave the way for the development of a new type of laminate composites with extreme PY coefs. In addition, experimental verification of huge PY coefs under OC should also lead to further understanding of the PY coef enhancement under OC.

16.4 Potential further enhancement in polymers such as PVDF

Work by researchers like Grima et al.[67] on structures with negative thermal expansion coefs and Poisson's ratio could pave the way for large PY coef enhancements in polymer based PY materials such as PVDF, which demonstrated its enhancement potential with Invar36 in Subsection 6.2.1. Materials such as these have relatively low curie temperatures, which may suit certain types of PY energy harvesting applications, and extremely good flexibility compared to other PY materials. By sacrificing some of this flexibility, it may be possible to introduce very high PY coef enhancements in these materials, improving their PY performance.

16.5 True open circuit measurement

How to achieve PY coef enhancement measurements under such electrical conditions and their potential applications is something that deserve some further research. Although single crystals theoretically investigated in this project did not show ample enough PY coef enhancement to be feasible in PY X-ray application, the large enhancement exhibited by ceramic PZTs mean that there is room for potential application of our enhancement in this application as well. As we expect this application to take place under OC, it would be interesting to see if our enhanced composites of ceramics, perhaps with another PZT possessing lower dielectric constant leading to high potential difference across the composite, can provide improvement in this area.

16.6 Some of the potential applications of this work

16.6.1 High voltage electric field generation

This application concerns the use of huge open circuit condition PY coef to create high voltage electric field via PY effect. Although the PZTs considered in this dissertation, which were the most promising PY materials for PY coef enhancement, have rather high dielectric constants limiting the magnitude of potential difference available across the PY material and its laminate composites, there are other PZTs such as Pz35 ($\varepsilon = 220$ and $d_{33} = 100\ pCN^{-1}$)[3] or Pz46 ($\varepsilon = 120$ and $d_{33} = 18\ pCN^{-1}$)[3] that possess quite low

dielectric constants as well which may well be good enough to create quite high potential difference across its laminate composites generating extreme electric fields via enhanced PY coef. Use of composites such as 0-3 PZT/PVDF-HFP composite as PY material in 2-2 laminate composite with its low dielectric constant (50/50 vol % : $\varepsilon = 85$, $p = 4.5 \times 10^{-4}\ Cm^{-2}K^{-1}$, and $d_{33} = 24\ pCN^{-1}$)[114] will also demonstrate similar possibility via creation of a double connectivity composite with synergy effect. Research conducted by Sandomirsky et al.[155,156] suggests that potentially there may be a way around high dielectric constant problem of these ceramics, although the author is not yet entirely convinced of the accuracy behind their analysis.

16.6.2 Pyroelectric X-rays

The PY materials mentioned in Subsection 16.6.1 can also find use in this application, while huge open circuit PY coef should also prove useful. In addition, as mentioned earlier the phenomenological description of PY X-ray generating mechanism proposed by Brownridge et al.[35–37] may not be the whole story behind this application. With so many other mechanisms behind PY/ferroelctric electron emissions proposed by other researchers[18,32,46,94,96,153,166] their argument of all the electrons/ions being generated from the ionisation of gas molecules caused solely by strong electric field seems to necessitate a more comprehensive experimental verification than an employment of adhesive layer on the single crystal surface as an attempt to block any electron emission. In particular, Yoo et al.'s work on PY lithography[118,198] indicates only certain types of materials are able to block these electron emissions, casting further doubts to their attempted experimental verification. Hence it may well be possible to utilise the large PY coef enhancement in PZTs demonstrated in this dissertation in PY X-ray generation application to improve X-ray beam intensity. Similar argument can also be made in PY ion or neutron beam application, and even PY nuclear fusion application could potentially benefit from this enhanced PY coef.

16.6.3 Improved pyroelectric energy harvesting application

As demonstrated in this dissertation, the improved PY coef can lead to significant increase in electrical energy harvestable via direct PY effect route. As all the PY energy harvesting parameters are proportional to $\left(p_m^{T,E}\right)^2$, very large improvements in PY energy harvesting systems could be achieved by utilising these 2-2 connectivity laminate com-

posites. In addition, the effect of pre-stress on phase transitions of these PY composites could also lead to better performance in other phase transition based PY energy harvesting applications that uses cycles such as Stirling or Ericsson cycles as proposed by Sebald et al.[70,71,91,160,161] and Olsen et al.[135–138] among others. It should also noted that LTO's great potential in PY energy harvesting is another area of great interest. Experimental verification of these promises and realisation of full potential could be a research field of immense interest and importance given the current political will towards decreasing the concentrations of CO_2 in the atmosphere as illustrated by The United Nations Framework Convention on Climate Change (UN 1992, article 2) calling for:

> "...stabilization of greenhouse gas concentrations in the atmosphere at a level that would prevent dangerous anthropogenic interference with the climate system..."

Part III

Appendices

Appendix A

Material properties

This chapter will present the material data used with our model. Numerous sources were searched and considered before the decision to use this particular set of data was made.

A.1 Material properties of pyroelectric materials

A.1.1 Pyroelectric and thermal coefficients and dielectric constants

All the data quoted in this section are evaluated at the room temperature unless stated otherwise.

Table A.1: Pyroelectric coefficients of various pyroelectric materials

	PZT-5H [4]	PZT-5A [4]	BTO [49]	LTO [12]	LNO [12]	PVDF [77]
$P_1^{T,E}$	0	0	0	0	0	0
$P_2^{T,E}$	0	0	0	0	0	0
$P_3^{T,E}$	-5.0	-3.0	-2.0	-2.3	-0.83	-0.274

Units: $\times 10^{-4}$ $Cm^{-2}K^{-1}$

Table A.2: Thermal coefficients of various pyroelectric materials

	PZT-5H	PZT-5A	BTO[1]	LTO[12]	LNO[12]	PVDF
$\alpha_1{}^{\mathrm{E}}$	3.0[4]	4.0[4]	15.7	16	15	13[77,90]
$\alpha_2{}^{\mathrm{E}}$	3.0[4]	4.0[4]	15.7	16	15	145[77,90]
$\alpha_3{}^{\mathrm{E}}$	3.0[4]	4.0[4]	6.2	4	7.5	80[157]
c_{vol}	3.15[3,26]	3.15[3,26]	3.19	1.87	2.92	2.3[124]

Units: - α ; $\times 10^{-6}$ $\mathrm{mm^{-1}K^{-1}}$ - c_{vol} ; $\times 10^{6}$ $\mathrm{Jm^{-3}K^{-1}}$

Table A.3: Dielectric constants of various pyroelectric materials

	PZT-5H[3]	PZT-5A[3]	BTO[13,76]	LTO[185]	LNO[185]	PVDF[152]
$\varepsilon_{11}{}^{\mathrm{T}}$	2438	1796	2920	51	84	7.35
$\varepsilon_{22}{}^{\mathrm{T}}$	2438	1796	2920	51	84	9.27
$\varepsilon_{33}{}^{\mathrm{T}}$	2874	1803	168	45	30	7.75

No units

A.1.2 Piezoelectric coefficients

Units: $\times 10^{-12}$ $\mathrm{CN^{-1}}$

Lead Zirconate Titanate (PZT)
(Tetragonal, 4mm)

■ PZT-5H[3,4]

$$\mathbf{d}^E = \begin{pmatrix} 0 & 0 & 0 & 0 & d_{15} & 0 \\ 0 & 0 & 0 & d_{15} & 0 & 0 \\ d_{31} & d_{31} & d_{33} & 0 & 0 & 0 \end{pmatrix} = \begin{pmatrix} 0 & 0 & 0 & 0 & 724 & 0 \\ 0 & 0 & 0 & 724 & 0 & 0 \\ -320 & -320 & 650 & 0 & 0 & 0 \end{pmatrix}$$

■ PZT-5A[3,4]

$$\mathbf{d}^E = \begin{pmatrix} 0 & 0 & 0 & 0 & d_{15} & 0 \\ 0 & 0 & 0 & d_{15} & 0 & 0 \\ d_{31} & d_{31} & d_{33} & 0 & 0 & 0 \end{pmatrix} = \begin{pmatrix} 0 & 0 & 0 & 0 & 506 & 0 \\ 0 & 0 & 0 & 506 & 0 & 0 \\ -190 & -190 & 390 & 0 & 0 & 0 \end{pmatrix}$$

Barium Titanate (BTO) [13,76]
(Tetragonal, 4mm)

$$\mathbf{d}^E = \begin{pmatrix} 0 & 0 & 0 & 0 & d_{15} & 0 \\ 0 & 0 & 0 & d_{15} & 0 & 0 \\ d_{31} & d_{31} & d_{33} & 0 & 0 & 0 \end{pmatrix} = \begin{pmatrix} 0 & 0 & 0 & 0 & 392 & 0 \\ 0 & 0 & 0 & 392 & 0 & 0 \\ -34.5 & -34.5 & 85.6 & 0 & 0 & 0 \end{pmatrix}$$

Lithium Tantalate (LTO) [185]
(Trigonal, 3m)

$$\mathbf{d}^E = \begin{pmatrix} 0 & 0 & 0 & 0 & d_{15} & -2d_{22} \\ -d_{22} & d_{22} & 0 & d_{15} & 0 & 0 \\ d_{31} & d_{31} & d_{33} & 0 & 0 & 0 \end{pmatrix} = \begin{pmatrix} 0 & 0 & 0 & 0 & 26 & -14 \\ -7 & 7 & 0 & 26 & 0 & 0 \\ -2 & -2 & 8 & 0 & 0 & 0 \end{pmatrix}$$

Lithium Niobate (LNO) [185]
(Trigonal, 3m)

$$\mathbf{d}^E = \begin{pmatrix} 0 & 0 & 0 & 0 & d_{15} & -2d_{22} \\ -d_{22} & d_{22} & 0 & d_{15} & 0 & 0 \\ d_{31} & d_{31} & d_{33} & 0 & 0 & 0 \end{pmatrix} = \begin{pmatrix} 0 & 0 & 0 & 0 & 68 & -42 \\ -21 & 21 & 0 & 68 & 0 & 0 \\ -1 & -1 & 6 & 0 & 0 & 0 \end{pmatrix}$$

Poly-vinylidene Fluoride (PVDF) [90,100]
(Orthorhombic, 2mm)

$$\mathbf{d}^E = \begin{pmatrix} 0 & 0 & 0 & 0 & d_{15} & 0 \\ 0 & 0 & 0 & d_{24} & 0 & 0 \\ d_{31} & d_{32} & d_{33} & 0 & 0 & 0 \end{pmatrix} = \begin{pmatrix} 0 & 0 & 0 & 0 & -15.7 & 0 \\ 0 & 0 & 0 & d_{24} & 0 & 0 \\ 21.4 & 2.3 & -31.5 & 0 & 0 & 0 \end{pmatrix}$$

Please note that it was not possible to find the value of one of the coefficients. However, as this coefficient is involved with shear strain/stress, which is an effect our analytical models exclude, it should not affect the numerical values from our calculations.

A.1.3 Elastic constants

Units: - c^E; $\times 10^9$ Nm^{-2} - c^D; $\times 10^9$ Nm^{-2}

Lead Zirconate Titanate (PZT)
(Tetragonal, 4mm)

■ PZT-5H[3]

$$\mathbf{c}^E = \begin{pmatrix} c_{11}^E & c_{12}^E & c_{13}^E & 0 & 0 & 0 \\ c_{12}^E & c_{11}^E & c_{13}^E & 0 & 0 & 0 \\ c_{13}^E & c_{13}^E & c_{33}^E & 0 & 0 & 0 \\ 0 & 0 & 0 & c_{44}^E & 0 & 0 \\ 0 & 0 & 0 & 0 & c_{44}^E & 0 \\ 0 & 0 & 0 & 0 & 0 & c_{66}^E \end{pmatrix} = \begin{pmatrix} 134 & 89.7 & 85.7 & 0 & 0 & 0 \\ 89.7 & 134 & 85.7 & 0 & 0 & 0 \\ 85.7 & 85.7 & 109 & 0 & 0 & 0 \\ 0 & 0 & 0 & 18.5 & 0 & 0 \\ 0 & 0 & 0 & 0 & 18.5 & 0 \\ 0 & 0 & 0 & 0 & 0 & 22 \end{pmatrix}$$

■ PZT-5A[3]

$$\mathbf{c}^E = \begin{pmatrix} c_{11}^E & c_{12}^E & c_{13}^E & 0 & 0 & 0 \\ c_{12}^E & c_{11}^E & c_{13}^E & 0 & 0 & 0 \\ c_{13}^E & c_{13}^E & c_{33}^E & 0 & 0 & 0 \\ 0 & 0 & 0 & c_{44}^E & 0 & 0 \\ 0 & 0 & 0 & 0 & c_{44}^E & 0 \\ 0 & 0 & 0 & 0 & 0 & c_{66}^E \end{pmatrix} = \begin{pmatrix} 147 & 105 & 93.7 & 0 & 0 & 0 \\ 105 & 147 & 93.7 & 0 & 0 & 0 \\ 93.7 & 93.7 & 113 & 0 & 0 & 0 \\ 0 & 0 & 0 & 23 & 0 & 0 \\ 0 & 0 & 0 & 0 & 23 & 0 \\ 0 & 0 & 0 & 0 & 0 & 21.2 \end{pmatrix}$$

Barium Titanate (BTO)[13,76]
(Tetragonal, 4mm)

$$\mathbf{c}^E = \begin{pmatrix} c_{11}^E & c_{12}^E & c_{13}^E & 0 & 0 & 0 \\ c_{12}^E & c_{11}^E & c_{13}^E & 0 & 0 & 0 \\ c_{13}^E & c_{13}^E & c_{33}^E & 0 & 0 & 0 \\ 0 & 0 & 0 & c_{44}^E & 0 & 0 \\ 0 & 0 & 0 & 0 & c_{44}^E & 0 \\ 0 & 0 & 0 & 0 & 0 & c_{66}^E \end{pmatrix} = \begin{pmatrix} 275.1 & 179 & 151.6 & 0 & 0 & 0 \\ 179 & 275.1 & 151.6 & 0 & 0 & 0 \\ 151.6 & 151.6 & 164.9 & 0 & 0 & 0 \\ 0 & 0 & 0 & 54.34 & 0 & 0 \\ 0 & 0 & 0 & 0 & 54.34 & 0 \\ 0 & 0 & 0 & 0 & 0 & 113.1 \end{pmatrix}$$

Lithium Tantalate (LTO)[185]
(Trigonal, 3m)

$$\mathbf{c}^E = \begin{pmatrix} c_{11}^E & c_{12}^E & c_{13}^E & c_{14}^E & 0 & 0 \\ c_{12}^E & c_{11}^E & c_{13}^E & -c_{14}^E & 0 & 0 \\ c_{13}^E & c_{13}^E & c_{33}^E & 0 & 0 & 0 \\ c_{14}^E & -c_{14}^E & 0 & c_{44}^E & 0 & 0 \\ 0 & 0 & 0 & 0 & c_{44}^E & c_{14}^E \\ 0 & 0 & 0 & 0 & c_{14}^E & \frac{1}{2}(c_{11}^E - c_{12}^E) \end{pmatrix} = \begin{pmatrix} 233 & 47 & 81 & -11 & 0 & 0 \\ 47 & 233 & 81 & 11 & 0 & 0 \\ 81 & 81 & 275 & 0 & 0 & 0 \\ -11 & 11 & 0 & 94 & 0 & 0 \\ 0 & 0 & 0 & 0 & 94 & -11 \\ 0 & 0 & 0 & 0 & -11 & 93 \end{pmatrix}$$

Lithium Niobate (LNO) [185]

(Trigonal, 3m)

$$\mathbf{c}^E = \begin{pmatrix} c_{11}^E & c_{12}^E & c_{13}^E & c_{14}^E & 0 & 0 \\ c_{12}^E & c_{11}^E & c_{13}^E & -c_{14}^E & 0 & 0 \\ c_{13}^E & c_{13}^E & c_{33}^E & 0 & 0 & 0 \\ c_{14}^E & -c_{14}^E & 0 & c_{44}^E & 0 & 0 \\ 0 & 0 & 0 & 0 & c_{44}^E & c_{14}^E \\ 0 & 0 & 0 & 0 & c_{14}^E & \frac{1}{2}(c_{11}^E - c_{12}^E) \end{pmatrix} = \begin{pmatrix} 203 & 53 & 75 & 9 & 0 & 0 \\ 53 & 203 & 75 & -9 & 0 & 0 \\ 75 & 75 & 245 & 0 & 0 & 0 \\ 9 & -9 & 0 & 60 & 0 & 0 \\ 0 & 0 & 0 & 0 & 60 & 9 \\ 0 & 0 & 0 & 0 & 9 & 75 \end{pmatrix}$$

Poly-vinylidene Fluoride (PVDF) [152]

(Orthorhombic, 2mm)

$$\mathbf{c}^D = \begin{pmatrix} c_{11}^D & c_{12}^D & c_{13}^D & 0 & 0 & 0 \\ c_{12}^D & c_{22}^D & c_{23}^D & 0 & 0 & 0 \\ c_{13}^D & c_{23}^D & c_{33}^D & 0 & 0 & 0 \\ 0 & 0 & 0 & c_{44}^D & 0 & 0 \\ 0 & 0 & 0 & 0 & c_{55}^D & 0 \\ 0 & 0 & 0 & 0 & 0 & c_{66}^D \end{pmatrix} = \begin{pmatrix} 3.61 & 1.61 & 1.42 & 0 & 0 & 0 \\ 1.61 & 3.13 & 1.31 & 0 & 0 & 0 \\ 1.42 & 1.31 & 1.63 & 0 & 0 & 0 \\ 0 & 0 & 0 & 0.55 & 0 & 0 \\ 0 & 0 & 0 & 0 & 0.59 & 0 \\ 0 & 0 & 0 & 0 & 0 & 0.69 \end{pmatrix}$$

PVDF proved to be the most difficult material to gather the required data for. Unfortunately, only open circuit condition measurement of the elastic constants ($\mathbf{c}^D$) were found, and hence for evaluating models under short circuit condition the inverted relations to those presented in Subsection 8.1.2 were used to evaluate the required short circuit condition constants, $\mathbf{c}^E$.

A.2 Material properties of non-pyroelectric materials

A.2.1 Non-pyroelectric materials investigated and their material properties

Table A.4: Material properties of non-pyroelectric materials

	St[9]	PTFE[15]	CPVC[14]	Al[2,13,14]	Zn[9,14]	Invar36[141,142]
α	14.4	79.0	80.0	24.3	30.2	1.0
c_{vol}	3.91	0.72	1.40	2.40	2.77	5.15
Young's modulus (Y)	193	0.5	3.15[14,115]	73.1	108	141
Poisson's ratio (ν)	0.30	0.46	0.27[159]	0.33	0.25	0.26

Units: - α ; $\times 10^{-6}$ $mm^{-1}K^{-1}$ - c_{vol} ; $\times 10^{6}$ $Jm^{-3}K^{-1}$ - Y ; $\times 10^{9}$ Nm^{-2} - ν ; No unit

Appendix B

Materials Assessment

All the data quoted in this chapter are evaluated at the room temperature unless stated otherwise.

B.1 Material properties under short and open circuit conditions

Appendix B.1 presents tables with material properties evaluated for both SC and OC for comparison purposes. Theoretical relationship between these two sets of material properties can be found in Subsection 8.1.2.

Table B.1: Thermal coefficients of various pyroelectric materials under SC and OC[44]

	PZT-5H	PZT-5A	BTO[1]	LTO[12]	LNO[12]	PVDF
$\alpha_1{}^E$	3.0[4]	4.0[4]	15.7	16	15	13[77,90]
$\alpha_2{}^E$	3.0[4]	4.0[4]	15.7	16	15	145[77,90]
$\alpha_3{}^E$	3.0[4]	4.0[4]	6.2	4	7.5	80[157]
$\alpha_1{}^D$	-3.3	0.4	11.1	14.8	14.7	21.5
$\alpha_2{}^D$	-3.3	0.4	11.1	14.8	14.7	145.9
$\alpha_3{}^D$	15.8	11.3	17.7	8.6	9.4	67.4
c_{vol}	3.15[3,26]	3.15[3,26]	3.19	1.87	2.92	2.3[124]

Units: - α^E and α^D ; $\times 10^{-6}$ $mm^{-1}K^{-1}$ - c_{vol} ; $\times 10^6$ $Jm^{-3}K^{-1}$

Table B.2: Pyroelectric coefficients of various pyroelectric materials under SC and OC[44]

	PZT-5H[4]	PZT-5A[4]	BTO[49]	LTO[12]	LNO[12]	PVDF[77]
$P_3^{T,E}$	-5.0	-3.0	-2.0	-2.3	-0.83	-0.274
$P_3^{T,D}$	-23.120	-4.078	-1.461	-2.598	-1.173	-0.261

Units: $\times 10^{-4}$ $Cm^{-2}K^{-1}$

B.2 Pyroelectric materials assessment

Following Tables B.3 and B.4 display potential PY coef enhancement credentials of various PY materials considered in this dissertation.

Table B.3: Pyroelectric materials assessment for SC[45]

	PZT-5H	PZT-5A	BTO	LTO	LNO	PVDF
Young's modulus $\approx c_{11}$ ($\times 10^9 Nm^{-2}$)	134.0	147.0	275.1	233.0	203.0	3.6
dc1 (Cm^{-2})	-15.879	-11.337	-2.690	0.088	0.194	0.0355
dc2 (Cm^{-2})	-15.879	-11.337	-2.690	0.088	0.194	0.0004
dc3 (Cm^{-2})	16.002	8.464	3.660	1.876	1.320	-0.0176
Primary PY coef ($\times 10^{-4} Cm^{-2}K^{-1}$)	-4.527	-2.432	-1.382	-2.403	-0.982	-0.265
Secondary PY coef ($\times 10^{-4} Cm^{-2}K^{-1}$)	-0.473	-0.568	-0.618	0.103	0.152	-0.009
PY coef before enhancement ($\times 10^{-4} Cm^{-2}K^{-1}$)	-5.000	-3.000	-2.000	-2.300	-0.830	-0.274
Largest PY coef after enhancement at R=0.2 ($\times 10^{-4} Cm^{-2}K^{-1}$)	-18.7	-11.5	-3.40	-2.40	-0.878	-0.301

Table B.4: Pyroelectric materials assessment for OC[44]

	PZT-5H	PZT-5A	BTO	LTO	LNO	PVDF
Young's modulus $\approx c_{11}$ ($\times 10^9 Nm^{-2}$)	185.6	162.0	282.4	240.0	219.9	3.6
dc1 (Cm^{-2})	-82.749	-21.662	-4.045	0.091	0.200	0.0362
dc2 (Cm^{-2})	-82.749	-21.662	-4.045	0.091	0.200	0.0004
dc3 (Cm^{-2})	83.390	16.172	5.497	1.948	1.359	-0.0179
Primary PY coef ($\times 10^{-4} Cm^{-2} K^{-1}$)	-4.527	-2.432	-1.382	-2.403	-0.987	-0.265
SC secondary PY coef ($\times 10^{-4} Cm^{-2} K^{-1}$)	-0.473	-0.568	-0.618	0.103	0.152	-0.009
OC secondary PY coef ($\times 10^{-4} Cm^{-2} K^{-1}$)	-18.593	-1.646	-0.079	-0.195	-0.186	0.004
PY coef before enhancement ($\times 10^{-4} Cm^{-2} K^{-1}$)	-23.120	-4.078	-1.461	-2.598	-1.173	-0.261
Largest PY coef after enhancement at R=0.2 ($\times 10^{-4} Cm^{-2} K^{-1}$)	22.648	11.551	-2.801	-2.700	-1.174	-0.270

Appendix C

Abstracts from the author's journal articles

The author's journal publications to date:

1. H. H. S. Chang, R. W. Whatmore, and Z. Huang, "Pyroelectric effect enhancement in laminate composites under short circuit condition", Journal of Applied Physics, 106 (11), 114110 (2009).[45]

2. H. H. S. Chang and Z. Huang, "Pyroelectric effect enhancement through product property under open circuit condition", Journal of Applied Physics, 106 (1), 014101 (2009).[44]

3. H. H. S. Chang and Z. Huang, "Substantial pyroelectric effect enhancement in laminated composites", Applied Physics Letters, 92 (15), 152903 (2008).[43]

4. C. Popov, H. Chang, P. M. Record, E. Abraham, R. W. Whatmore, and Z. Huang, "Direct and converse magnetoelectric effect at resonant frequency in laminated piezoelectric-magnetostrictive composite", Journal of Electroceramics, 20 (1), 53-58 (2007).[146]

5. P. Record, C. Popov, J. Fletcher, E. Abraham, Z. Huang, H. Chang, and R. W. Whatmore, "Direct and converse magnetoelectric effect in laminate bonded Terfenol-D-PZT composites", Sensors and Actuators B: Chemical, 126 (1), 344-349 (2007).[147]

C.1 Article on Journal of Applied Physics - SC (2009)

JOURNAL OF APPLIED PHYSICS **106**, 114110 (2009)

Pyroelectric effect enhancement in laminate composites under short circuit condition

H. H. S. Chang,[1,a)] R. W. Whatmore,[2] and Z. Huang[1]
[1]*Department of Materials, Cranfield University, Bedfordshire, MK43 0AL, United Kingdom*
[2]*Tyndall National Institute, Lee Maltings, Prospect Row, Cork, Ireland*

(Received 16 January 2009; accepted 24 October 2009; published online 9 December 2009)

The pyroelectric coefficients of laminate composites under short circuit condition have been investigated by analytical modeling and numerical simulations. Indicators for various pyroelectric/non-pyroelectric material pairs that can be utilized to determine their pyroelectric coefficient enhancement credentials have been identified. Six pyroelectric materials were paired with six non-pyroelectric/elastic materials and their pyroelectric coefficient enhancement potential and figure of merit for efficiency were investigated. The best performing partnership out of the 36 pairs was lead zirconate titanate (PZT5H)-chlorinated polyvinyl chloride thermoplastic (CPVC) for thickness ratios (R) below 0.09 and PZT5H-zinc for R larger than 0.09 with both demonstrating total pyroelectric coefficient of approximately -20×10^{-4} C m^{-2} K^{-1} at R=0.09, which corresponds to approximately 300% increase in the coefficient. PZT5H-CPVC also showed maximum of 800% rise in the pyroelectric coefficient while figure of merit for efficiency indicated up to twentyfold increase in its electrical response output per given thermal stimuli when compared to that of PZT5H by itself. © *2009 American Institute of Physics*. [doi:10.1063/1.3264623]

I. INTRODUCTION

The pyroelectric (PY) effect describes a change in the charge density of a material upon thermal stimulus, which can occur in any material with a polar symmetry. Its applications range from thermal radiation detection to fire alarms, intruder detection, and thermal imaging. The pyroelectric coefficient (PY coef.), usually measured at constant stress $p^{T,E}$, consists of the primary PY coef. at the constant strain $p^{S,E}$ and the secondary PY coef. arising from strain,[1]

$$p_m^{T,E} = p_m^{S,E} + d_{mkl}^{E,\Theta} c_{ijkl}^{E,\Theta} \alpha_{ij}^{T,E}. \quad (1)$$

Here, $d_{mkl}^{E,\Theta}$ is the piezoelectric constant, $c_{ijkl}^{E,\Theta}$ is the elastic stiffness, $\alpha_{ij}^{T,E}$ is the thermal expansion coefficient, E is the electric field, and Θ is the temperature. Notice the use of Einstein summation convention which is used throughout this article along with Voigt notation.

A number of researches on the secondary PY coef. can be found in the literature.[2,3] For instance, the effect of a substrate on PY thin films, arising from thermal expansion mismatch, has been investigated extensively by various researchers.[3–7] Generally speaking, for perovskite-based ferroelectric materials the product term $d_{mkl}^{E,\Theta}\, c_{ijkl}^{E,\Theta}\, \alpha_{ij}^{T,E}$ is much smaller than the primary term $p^{S,E}$ and hence the effect of this mismatch is expected to be rather limited.[4,7] The possibility of utilizing secondary PY effect to enhance the total PY coef. was researched by Newnham *et al.*[8] and Nan.[9] Their works led to the development of various composites with superior mechanical flexibility accompanied by good PY performances.[10–14] They concluded that in most cases due to the small hydrostatic piezoelectric effect, arising from cancellation between coefficients of opposite signs, the enhancement available through the secondary contribution is rather limited.

In our previous communication, we reported a substantial PY coef. enhancement in laminar stainless steel/lead zirconate titanate (PZT)/stainless steel structures.[15] With both experimental observation and theoretical prediction demonstrating PY coef. enhancements of more than 100%, we attributed this large enhancement to dissimilar signs of the piezoelectric coefficients of PZT and the exploitation of this particular symmetry through deployment of 2–2 connectivity configuration, where externally exerted strains by the non-pyroelectric (NP) elastic layer, namely, stainless steel, are transferred through in two axes resulting in cumulative piezoelectricity arising from three separate axes owing to Poisson effect.

This dissimilarity in piezoelectric coefficient signs also results in small hydrostatic piezoelectric effect, which in turn lead to the previously held belief that for materials such as PZT the expected gain in PY coef. through its secondary effect would be rather limited.[4,8,9] As our research so far seems to suggest to the contrary, we believe this employment of 2–2 connectivity configuration in pyroelectricity requires further exploration, which could potentially uncover PY coef. enhancements of even greater proportions.

At the outset in Sec. II, we first examine the theoretical and mathematical background behind this subject by applying thermodynamic and plate theory, results of which are presented in later section with the use of Mathematics package MAPLE 9.50.[16] In order to analyze the effects of increased thermal mass due to the introduction of NP elastic layer, we also define a quantity termed efficiency and utilize it to assess the trade-off between increased thermal mass and PY response by defining a figure of merit for efficiency.

Section III consists of a brief introduction to the materials considered for our simulation. This should clarify the

a)Electronic mail: h.chang@cranfield.ac.uk.

C.2 Article on Journal of Applied Physics - OC (2009)

JOURNAL OF APPLIED PHYSICS **106**, 014101 (2009)

Pyroelectric effect enhancement through product property under open circuit condition

H. H. S. Chang[a] and Z. Huang
Department of Materials, Cranfield University, Bedfordshire, MK43 0AL, United Kingdom

(Received 20 January 2009; accepted 30 May 2009; published online 6 July 2009)

An analytical model for the pyroelectric (PY) effect under open circuit condition and 2-2 connectivity laminates of various pairs of PY and nonpyroelectric (NP)/elastic materials has been developed. It is evident from our analysis that there indeed is a substantial dissimilarity between the PY coefficients and figure of merit for efficiency for various PY-NP pairs under short circuit and open circuit conditions. We believe this implies that there should be a greater distinction made between the PY coefficients under these two electrical conditions than previously thought. The indicators for various PY-NP material pairs that can be utilized to determine their PY coefficient enhancement potential under open circuit condition have been identified. The investigated PY materials are lead zirconate titanate (PZT-5H and PZT-5A), barium titanate, lithium tantalate, lithium niobate, and polyvinylidene fluoride (PVDF), while the NP materials are stainless steel, polytetrafluoroethylene (PTFE or Teflon), chlorinated polyvinyl chloride thermoplastic (CPVC), aluminum, zinc, and Invar 36. Extraordinarily large PY coefficient of 97×10^{-4} C m^{-2} K^{-1} at minimum thickness ratio R_{min} is expected for PZT-5H-CPVC pair while PVDF-CPVC could show increase in the secondary PY coefficient of up to 350%. In addition, where the figure of merit for efficiency is concerned, for the same volume of the composite PZT-5A-PTFE pair it reaches 24, a 24-fold increase in efficiency at R_{min}. Our analysis techniques should provide a methodological way for appraising the potentials of particular PY material and its 2-2 laminates for applications under open circuit condition such as PY X-ray generation, electron accelerator, and nuclear fusion.
 [DOI: 10.1063/1.3158472]

I. INTRODUCTION

It is well established that the pyroelectric coefficient (PY coef.), usually measured at constant stress $\mathbf{p}^{T,E}$, consists of the primary PY coef. at the constant strain $\mathbf{p}^{S,E}$ and the secondary PY coef. arising from strain,[1]

$$p_m^{T,E} = p_m^{S,E} + d_{mkl}^{E,\Theta} c_{ijkl}^{E,\Theta} \alpha_{ij}^{T,E}. \tag{1}$$

Here, T is the stress, E is the electric field, Θ is the temperature, $p_m^{T,E}$ is the PY coefficient at constant stress (free boundary condition) and electric field, $d_{mkl}^{E,\Theta}$ is the piezoelectric constant, $c_{ijkl}^{E,\Theta}$ is the elastic stiffness at constant temperature and electric field, and $\alpha_{ij}^{T,E}$ is the thermal expansion coefficient at constant stress and electric field. Notice the Einstein summation convention is used throughout this article along with the Voigt notation and the secondary PY effect can be regarded as a product property of piezoelectricity and thermal expansion.[2]

In our other communication,[3] with Eq. (1) in mind, the laws of thermodynamics dictated the PY coefficient for 2-2 laminates under short circuit (SC) condition to be

$$P_m = \frac{dD_m}{d\Theta} = p_m^{T,E} - (d_{mkl}^{E,\Theta})(c_{ijkl}^{E,\Theta})\left[\alpha_{ij}^{T,E} - \frac{dS_{ij}}{d\Theta}\right], \tag{2}$$

where p_m is the PY coefficient, D_m is the electric displacement, and dS_{ij} is the total strain experienced by the PY material.

This extended version of the PY coefficient expression, Eq. (2), describes the pyroelectricity of any PY material experiencing strain under SC condition. However, in practice, some applications such as PY X-ray generation,[4–6] electron accelerator,[7] and nuclear fusion[8] are conducted under conditions most closely approximated by open circuit (OC). We believe there is a difference between the PY coefficient under OC and SC conditions, and it is paramount that this disparity between the two be formulized to provide better insights into these applications of pyroelectricity. We also believe that this PY coefficient $p^{T,D}$ under OC condition is the one that should be utilized when evaluating the "voltage figure of merit" F_V and hence be distinguished from $p^{T,E}$ used in "current figure of merit" F_I.[9]

Under SC condition, the electric potential on the whole of the surface of the crystal is perceived as being the same, in other words $\mathbf{E}$ is assumed to be zero and constant, i.e., $\mathbf{E}=0=d\mathbf{E}$. Sometimes also termed as electrically free, this is the condition under which most measurements of PY coefficient are taken and therefore is the condition conventionally used for the derivation of PY coefficient, including Eq. (2). Under OC condition, however, $\mathbf{D}$ is assumed to be constant

[a]Electronic mail: h.chang@cranfield.ac.uk.

C.3 Article on Applied Physics Letters (2008)

APPLIED PHYSICS LETTERS **92**, 152903 (2008)

Substantial pyroelectric effect enhancement in laminated composites

H. H. S. Chang and Z. Huang[a)]
Department of Materials, School of Applied Sciences, Cranfield University, Bedfordshire MK43 0AL, United Kingdom

(Received 7 February 2008; accepted 19 March 2008; published online 16 April 2008)

A mathematical model has been developed to determine the pyroelectric coefficient (PY coef.) enhancement through secondary pyroelectric effect, utilizing a 2-2 connectivity of the pyroelectric lead zirconate titanate (PZT) and elastic laminate layers. Based on the prediction of this analysis, laminar stainless steel (St) PZT/St structures have been fabricated and more than 100% enhancement in PY coef. has been observed in these structures. Good agreement between the theoretical and experimental results was obtained by taking into account of the stain transfer loss at the St and PZT interface. © *2008 American Institute of Physics*. [DOI: 10.1063/1.2907701]

The pyroelectric (PY) effect concerns the release of the charge upon the change in temperature. It occurs in any material which possesses a polar point symmetry. This effect has been widely used for thermal radiation detection in applications such as fire alarms, intruder detection, and thermal imaging. All PY materials are also piezoelectric, so the pyroelectric coefficient (PY coef.), which is usually measured at constant stress $p^{T,E}$, consists of the primary PY coef. at the constant strain $p^{S,E}$ and the secondary PY coef. arising from strain,[1]

$$p_m^{T,E} = p_m^{S,E} + d_{mkl}^{E,\Theta} c_{ijkl}^{E,\Theta} \alpha_{ij}^{T,E}. \tag{1}$$

Here, $d_{mkl}^{E,\Theta}$ is the piezoelectric constant, $c_{ijkl}^{E,\Theta}$ is the elastic stiffness, $\alpha_{ij}^{T,E}$ is the thermal expansion coefficient, E is the electric field, and Θ is the temperature. Notice the use of Einstein summation convention.

There has been a number of research on the secondary PY coef. over the years.[2,3] Particularly, the effect of a substrate on PY thin films, arising from thermal expansion mismatch, has been extensively investigated by various researchers.[2,4–7] Generally speaking, for perovskite-based ferroelectric materials, the product term $d_{mkl}^{E,\Theta} c_{ijkl}^{E,\Theta} c_{ij}^{T,E}$ is much smaller than the primary term $p^{S,E}$, and hence the effect of this mismatch is limited.[4,5]

The possibility of utilizing secondary PY effect to enhance the total PY coef. was suggested by Newnham *et al.*[8] and Nan.[9] Their works led to the development of various composites with superior mechanical flexibility accompanied by good PY performances.[10–14] They concluded that in most cases due to the small hydrostatic piezoelectric effect, arising from cancellation between coefficients of opposite signs, the enhancement available through the secondary contribution is rather limited. We report in this communication more than 100% enhancement in PY coef., utilizing a 2-2 connectivity of PY lead zirconate titanate (PZT) and elastic laminate configuration.

A symmetrical configuration, where a PY PZT layer sandwiched between two elastic layers, or vice versa, was adopted to avoid bending (Fig. 1). From thermodynamics, as shown by Nye,[1] at constant external electric field, the total PY coef. of the system was obtained as (for $i,j,k,l,m=1.3$)

$$\frac{dD_m}{d\Theta} = p_m^{T,E} - (d_{mkl}^{E,\Theta})(c_{ijkl}^{E,\Theta})\left[\alpha_{ij}^{T,E} - \frac{dS_{ij}}{d\Theta}\right], \tag{2}$$

where $dD_m/d\Theta$ is the measured PY coef., dS_{ij} is the strain experienced by PY material, and $d\Theta$ is the temperature change.

It is evident from Eq. (2) that the larger the strain the nonpyroelectric (NP) component can exert on the PY component and the greater the piezoelectric coefficient of the PY material, the bigger the change in the secondary contribution. This leads to the conclusion that stiffer NP material with greater disparity in thermal expansion coefficient (α) with that of PY and more compliant PY material with high piezoelectric coefficients would be desirable. Hence, stainless steel (St) was chosen as the NP material and the PZT for the PY material.

Expression (2) is the general PY coef. for any PY material under strain. With the symmetry of PZT in mind, Eq. (2) can be simplified further to

$$p_3 = p_3^{T,E} - d_{31}^{E,\Theta} \sum_{j=1}^{3} \left[(c_{1j}^{E,\Theta} + c_{2j}^{E,\Theta}) \left(\alpha_j^{T,E} - \frac{dS_j}{d\Theta} \right) \right] - d_{33}^{E,\Theta} \sum_{j=1}^{3} \left[c_{3j}^{E,\Theta} \left(\alpha_j^{T,E} - \frac{dS_j}{d\Theta} \right) \right]. \tag{3}$$

When Eq. (3) is evaluated for a typical PZT, e.g., PZT-5*H*,[15,16] the sums of $d_{mkl}^{E,\Theta} c_{ijkl}^{E,\Theta}$ terms for each direction, i.e., corresponding to dS_1 or dS_2 and dS_3, termed as $dc1$ or $dc2$, and $dc3$, are $dc1=dc2=-15.9$ and $dc3=16.0$ C m^{-2}. This implies that positive strains in one and two directions,

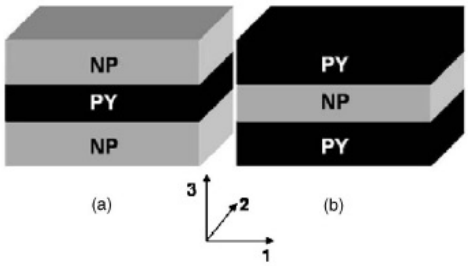

FIG. 1. 2-2 connectivity three layer laminate composite configurations.

a)Electronic mail: z.huang@cranfield.ac.uk.

C.4 Articles on Magnetoelectric composites

Journal of Electroceramics, Volume 20, Number 1, February 2008, pp53-58

Direct and converse magnetoelectric effect at resonant frequency in laminar piezoelectric-magnetostrictive composite

C. Popov[2], H. Chang[1], P.M. Record[2], E. Abraham[2], R.W. Whatmore[1,3] and Z. Huang[1,*]

[1]*Department of Materials, School of Applied Science, Cranfield University, Beds, MK43 0AL, UK*

[2]*School of Engineering and Physical Sciences, Heriot-Watt University, Edinburgh EH14 4AS, UK*

[3]*Current Address: Tyndall National Institute, Cork, Ireland.*

[*]*Corresponding author e-mail: Z.Huang@cranfield.ac.uk*

Abstract

Laminar piezoelectric-magnetostrictive composites using piezoelectric lead zirconate titanate ceramics and the giant magnetostrictive rare-earth-iron alloy Terfenol-D were prepared by epoxy bonding. The direct and converse magnetoelectric (ME) effects at and off the mechanical resonant frequency were characterized and compared to the theoretical modelling. The mechanical resonant frequency of the composites depended on the sample orientation and the magnetic DC bias field. In the longitudinal configuration, the resonant frequency shifted down monotonically with the increasing bias field. When the sample was in the transverse configuration, the resonant frequency decreased with the increasing field at first. However, at higher bias, it shifted up with the increasing bias. A phenomenological model based on the ΔE effect of magnetostrictive materials is proposed to explain the observed phenomena.

Keywords: magnetoelectric effect, piezoelectric, magnetostrictive, PZT, ΔE effect, orientation dependence.

ELSEVIER

Available online at www.sciencedirect.com
ScienceDirect

Sensors and Actuators B 126 (2007) 344–349

SENSORS AND ACTUATORS B CHEMICAL

www.elsevier.com/locate/snb

Direct and converse magnetoelectric effect in laminate bonded Terfenol-D–PZT composites

P. Record [a,*], C. Popov [a], J. Fletcher [a], E. Abraham [a], Z. Huang [b], H. Chang [b], R.W. Whatmore [c]

[a] *Electrical, Electronics and Computer Engineering, School of EPS, Herriot-Watt University, Riccarton, Edinburgh EH14 4AS, UK*
[b] *Department of Advanced Materials, SIMS, Cranfield University, Beds MK43 0AL, UK*
[c] *Tydnal National Institute, Lee Maltings, Prospect Row, Cork, Ireland*

Available online 12 June 2007

Abstract

Results from measurements of the direct and converse magnetoelectric (ME) effect on a three-layer, epoxy-bonded, laminate composite are presented. The laminae are a single transversely polarized piezoelectric elements (PZ29) sandwiched between two longitudinal-magnetically polarized magnetostrictive TD elements (Terfenol-D—TX GMM). The direct ME effect was determined by measuring laminate output with a Helmholtz-generated AC field (up to 7 Oe) in the range 50 Hz–100 kHz biased by a DC field (0–1000 Oe). Peak voltage output occurred at the sample's mechanical resonant frequency, its value depending on the strength and direction of the applied magnetic field. The peak output was 3061 mV at 3 Oe AC field and 1000 Oe bias, equivalent to 74.4 V cm^{-1} Oe^{-1}. The peak output coefficient, however, was 93.6 V cm^{-1} Oe^{-1} at 0.1 Oe AC field and 1000 Oe DC bias. The reduction at higher drive amplitudes was attributed to increased Young's modulus of the TD phase. Anomalous peaks in the low frequency spectrum of sample's output are explained. The converse magnetoelectric effect was measured by recording the voltage induced in a solenoid encompassing the ME while exposed to a DC bias field and the PZ phase driven by a 10 V_{AC} source. The peak output is shown to depend on the strength of the applied DC magnetic field and developed a maximum field of 15.4 Oe at the sample's mechanical resonant frequency. This equates to a converse magnetoelectric coefficient of 55 Oe cm kV^{-1}.

Keywords: Magnetoelectric effect; Magnetoelectric composites; Magnetostriction; Piezoelectricity; MEMS

1. Introduction

The magnetoelectric (ME) effect represents the coupling between an applied magnetic field and a change in electric polarization in a solid. While the effect can occur in single-phase materials, such as Cr_2O_3, it is usually small. Much larger effects can be obtained in composites consisting of two functional phases—a magnetostrictive material, in which a strain is produced by application of a magnetic field, coupled to a piezoelectric material, in which a change in electric polarization is produced by an applied stress. Reciprocally, an electric field applied to the piezoelectric phase of such a composite will cause a change in the magnetization of the magnetostrictive phase—described here as the converse magnetoelectric effect. The magnetoelectric effect is generally characterized by the magnetoelectric voltage coefficient:

$$\alpha_E = \frac{\partial E}{\partial H} \quad \mathrm{V\,Oe^{-1}\,m^{-1}}$$

Likewise, the converse magnetoelectric effect, being the exact reverse process, would be characterized by an converse coefficient:

$$\beta_M = \frac{\mathrm{d}H}{\mathrm{d}E} \quad \mathrm{Oe\,m\,V^{-1}}$$

A variety of materials have been used to produce magnetoelectric composites; comprehensively reviewed in the papers of Ryu et al. [1] and of Fiebig [2]. For the magnetostrictive phase, (MS) Terfenol-D, is the preferred material of choice [1–9] and lead magnesium niobate-lead titanate, PMN-PT, produced the highest ME coefficient. The most commonly used piezoelectric material in current research [1–9] was lead zirconium titanate, PZT, and this was the material used in this work. Other than Terfenol-D, a variety of ferrites have been

* Corresponding author. Tel.: +44 131 451 3341.
E-mail address: p.record@hw.ac.uk (P. Record).

0925-4005/$ – see front matter © 2007 Elsevier B.V. All rights reserved.
doi:10.1016/j.snb.2007.05.047

Appendix D

ANSYS and Maple codes

D.1 ANSYS code

```
!++++++++++++++++++++++++++++++++
!+++++++++++++++++++ Details ++++
!++++++++++++++++++++++++++++++++
!W=1e-2, L=2e-2 and appTemp=26 are set
!Bot electrode is grounded (Voltage set to zero)
!
!Epoxy layer introduced
!
!
/TITLE,PZT
/PMETH,OFF,1
KEYW,PR_SET,1
KEYW,PR_STRUC,1
KEYW,PR_THERM,1
KEYW,PR_FLUID,0
KEYW,PR_ELMAG,1
KEYW,MAGNOD,0
KEYW,MAGEDG,0
KEYW,MAGHFE,0
KEYW,MAGELC,1
KEYW,PR_MULTI,2
KEYW,PR_CFD,0
/GO
/COM,Preferences for GUI filtering have been set to display:
/COM, Structural
/COM, Thermal
/COM, Electric
!
!===============!===============!
!========== Pre-processing ======!
!===============!===============!
/PREP7
!+++++++++++++++!+++++++++++++++!
!+++ Define general parameters +++!
!+++++++++++++++!+++++++++++++++!
!!!!!!!!!!!!!!!!!!!!!!!!!!!!!!!! -latest edition
!+++ Define Epoxy thickness
tEpo = 40e-6
!+++
!++++++++++++=== Open or not ====+++!
!Set to see if open circuit or not
OpenC=0
!++++++++++++== Open or not ===+++++!
!+++++ Define condition parameters
epsilon0=8.8541878176e-12 ! C2N-1m-2
!+++ Testing Options (1 means yes, 0 means no.)
CTESame=0 ! Sets CTE of PZT and St the same for testing purposes
StPerm=0 ! Assigns permittivity (Stepsilon) to St
DsymApp=0 ! DSYM symmetric boundary conditions applied if=1
UseNdiv=1 ! NDIV used if=1, and SIZE used if=0
!+++
!+++ Finite element parameters (One of the two will be used)
SIZE=40e-6 ! Define the size of each element
NDIV=20 ! No. of element divisions along region boundaries in ESIZE
!+++
!+++ Which electrode to be used and coupled (1 means yes, 0 means no.) ← Only one value must be non-zero for smooth running
VeryThin=1 ! Very thin electrodes (TopElec1 & BotElec1 or TopElec2 & BotElec2) are used (1 means TopElec1 & BotElec1, 2 means TopElec2 & BotElec2 and 3 means both are used) and only TopElec1 & BotElec1 are coupled
    ! NB: TopElec1 (at HTop), BotElec1 (at HBot), TopElec2 (at HTop-HEl/NDIV) and BotElec2 (at HBot+HEl/NDIV)
ElUsed=0 ! This defines if electrodes (TpEl and BtEl) are used (and they are coupled)
    ! NB: TpEl (between HTop-HEl and HTop) and BtEl (between HBot and HBot+HEl)
ThinUsed=0 ! This defines if thin electrodes (ThinTpEl and ThinBtEl) are used (and they are coupled)
    ! NB: ThinTpEl (between HTop-HEl/NDIV and HTop) and ThinBtEl (between HBot and HBot+HEl/NDIV)
!Doesn't work (CpEl)
!CpEl=1 ! When TpEl and BtEl are used, this will couple all the electrodes nodes so that their displacement are identical (Hence removing any mechanical influence this layer will have, i.e. as if HEl is zero)
!+++
!+++ Boundary conditions (1 means yes, 0 means no.)
BotSurf=0 ! Define the strain (in z-direction) in the bottom surface to be zero
MidPlZ=1 ! Define the mid-plane (in Z-axis) and set the strain in z-direction of the mid-plane to zero
MidPlY=1 ! Define the mid-plane (in Y-axis) and set the strain in Y-direction of the mid-plane to zero
MidPlX=1 ! Define the mid-plane (in X-axis) and set the strain in X-direction of the mid-plane to zero
MidPt=1 ! Select the mid-point of all the mid-planes and fix it
ConvVt=0 ! Set convergence for voltage with convVolt1 and convVolt2
!+++
!+++++
!+++++ Define temperatures (Uniform/reference temperature and applied load temperature)
refTemp=25 ! Define Uniform/reference temperature
appTemp=26 ! Define Applied temperature
TREF,refTemp
!+++++
!+++++ Define convergence tolerance values for VOLT (Optional)
convVolt1=1.e-10
convVolt2=1e-6
!+++++
!+++++ Define element types
elePZT=1
ET,elePZT,SOLID5 !Define element type for PZT
eleSt=2
ET,eleSt,SOLID5 !Define element type for St
eleEpo=3
ET,eleEpo,SOLID5 !Define element type for Epoxy
!+++++
!+++++ Define model dimensions (to create physical and FE model)
!+++ Physical dimensions
*IF,DsymApp,EQ,1,THEN
    L=(2e-2)/2 !Set length (X-direction)
    W=(1e-2)/2 !Set Width (Y-direction)
    *ELSE
    L=2e-2 !Set length (X-direction)
    W=1e-2 !Set Width (Y-direction)
*ENDIF
H1=250e-6 !Set Height of St layer
H2=127e-6 !Set Height of PZT layer
HT=H1+tEpo+H2+tEpo+H1 !Total thickness
HBot=H1+tEpo ! Height of bottom electrode
HTop=H1+tEpo+H2 ! Height of top electrode
HEl=tEpo/2 ! To set tolerance range for NSEL
!+++
!+++++
!++++++++++++++++!++++++++++++++!
!
!++++++++++++++++!++++++++++++++!
!++++++ Specify material properties +++++++!
!++++++++++++++++!++++++++++++++!
!+++++ For PZT in Solid5 element type
!+++ Material constants for PZT-5H (Material no. elePZT)
!+ Thermal material properties
!— Assign reference temperature (refTemp)
```

```
UIMP,elePZT,REFT,,,refTemp,, ! This sets the reference temp to be refTemp (All thermal strains are set to zero at refTemp)
!—
!— Define coeff. of thermal expansion (instantaneous CTE, in K-1)
cte=3.00e-6
!-In each direction
CTE1=cte
CTE2=cte
CTE3=cte
!-
!—
!+
!+ Elastic material properties (Nm-2)
!— Stiffness (c) in Nm-2
mpC11=1.34e11
mpC12=8.97e10
mpC13=8.57e10
mpC33=1.09e11
mpC44=1.85e10
mpC66=2.20e10
c11=mpC11
c12=mpC12
c13=mpC13
c33=mpC33
c44=mpC44
c66=mpC66
!- From the symmetry of PZT-5H
c22=mpC11
c21=mpC12
c23=mpC13
c31=mpC13
c32=mpC13
c55=mpC44
c61=0
c41=0
c51=0
c62=0
c42=0
c52=0
c63=0
c43=0
c53=0
c46=0
c56=0
c54=0
!-
!—
!+
!+ Electric material properties
!— Relative dielectric constant (permittivity)
epsilon=3800
!—
!— Piezoelectric coefficients (d, in CN-1)
mpD31=-320e-12
mpD33=650e-12
mpD15=800e-12 ! Calculated from ferroperm, so d15 may be wrong
mpD24=mpD15
mpD32=mpD31
!- From the symmetry of PZT-5H
d11=0
d12=0
d13=mpD31
d21=0
d22=0
d23=mpD32
!d31=0
d31=mpD31
!d32=0
d32=mpD32
d33=mpD33
d61=0
d62=0
d63=0
d41=0
d42=mpD24
d43=0
d51=mpD15
d52=0
d53=0
!-
!—
!+
!+++
!+++ Input defined material properties
!+ Thermal material properties
!— Define CTE matrix (Reference temp=refTemp)
MPTEMP,,refTemp,,,,,
!UIMP,elePZT,REFT,,,refTemp,, ! This sets the reference temp to be refTemp (All thermal strains are set to zero at refTemp)
MPDE,CTEX,elePZT
MPDATA,CTEX,elePZT,,CTE1
MPDATA,CTEY,elePZT,,CTE2
MPDATA,CTEZ,elePZT,,CTE3
!—
!+
!+ Elastic material properties
!— Define stiffness matrix (Temperature for table=refTemp)
TB,ANEL,elePZT,1,21,0
TBTEMP,refTemp ! Defines temperature for data table (Originally was set to zero)
TBDATA,,c11,c21,c31,c61,c41,c51
TBDATA,,c22,c32,c62,c42,c52,c33
TBDATA,,c63,c43,c53,c66,c46,c56
TBDATA,,c44,c54,c55,,,
!—
!+
!+ Electric material properties
!— Assign permittivity
mpPer=epsilon
!- In each direction
mpPERX=mpPer
mpPERY=mpPer
mpPERZ=mpPer
!-
MPDATA,PERX,elePZT,,mpPERX ! Creates permittivity matrix
MPDATA,PERY,elePZT,,mpPERY
MPDATA,PERZ,elePZT,,mpPERZ
!—
!— Define Piezo coeff matrix (d)
TB,PIEZ,elePZT,,,1
TBMODIF,1,1,d11
! Modifies data for the data table (TBMODIF,ROw,COL,VALUE)
TBMODIF,1,2,d12
TBMODIF,1,3,d13
TBMODIF,2,1,d21
TBMODIF,2,2,d22
TBMODIF,2,3,d23
TBMODIF,3,1,d31
TBMODIF,3,2,d32
TBMODIF,3,3,d33
TBMODIF,4,1,d61
TBMODIF,4,2,d62
TBMODIF,4,3,d63
TBMODIF,5,1,d41
TBMODIF,5,2,d42
TBMODIF,5,3,d43
TBMODIF,6,1,d51
TBMODIF,6,2,d52
```

```
TBMODIF,6,3,d53
!—
!+
!+++
!+++++
!+++++ For NP in Solid5 element type
!+++ Material constants for St (Material no. eleSt)
!+ Thermal material properties
!— Assign reference temperature (refTemp)
UIMP,eleSt,REFT,,,refTemp,, ! UIMP for defining constant mat prop, this defines ref temp to refTemp
!—
!— Define thermal conductivity
TherCon=16.2 ! Thermal conductivity of St-304 used instead (Wm-1K-1)
!—
!— Define coeff. of thermal expansion (instantaneous CTE, in K-1)
*IF,CTESame,EQ,1,THEN
      cteSt=cte ! For checking, let CTE of NP be the same as PZT's
      *ELSE
      cteSt=1.44e-5 ! Coefficient of thermal expansion (intantaneous, K-1)
*ENDIF
!- In each direction
CTESt1=cteSt
CTESt2=cteSt
CTESt3=cteSt
!-
!—
!+
!+ Elastic material properties
StDen=7.81e3 ! Density (kgm-3)
StYoMod=1.93e11 ! Young's modulus (Nm-2) -> Shear modulus auto sets to EX/{2(1+NUXY)}
PoiRat=0.30 ! Poisson's ratio (NB:Ansys defaults this to 0.3 anyways)
!+
!+ Electric material properties
!— Relative dielectric constant (permittivity)
Stepsilon=1
!—
!+
!+++
!+++ Input defined material properties
!+ Thermal material properties
!— Assign thermal conductivity
MP,REFT,elePZT,refTemp
MP,REFT,eleSt,refTemp
MP,KXX,eleSt,TherCon ! Thermal conductivity of St-304 used instead (Wm-1K-1)
!—
!— Define CTE matrix (Reference temp=refTemp)
MPDE,CTEX,eleSt ! Delete CTE table of eleSt
MPDATA,CTEX,eleSt,,CTESt1
MPDATA,CTEY,eleSt,,CTESt2
MPDATA,CTEZ,eleSt,,CTESt3
!—
!+
!+ Elastic material properties
MP,DENS,eleSt,StDen ! Density (kgm-3)
MP,EX,eleSt,StYoMod ! Young's modulus (Nm-2) -> Shear modulus auto sets to EX/{2(1+NUXY)}
MP,NUXY,eleSt,PoiRat ! Poisson's ratio (NB:Ansys defaults this to 0.3 anyways)
!+
!+ Electric material properties (Optional)
!— Assign permittivity for St
*IF,StPerm,EQ,1,THEN
      StmpPer=Stepsilon
      !- In each direction
      StmpPERX=StmpPer
      StmpPERY=StmpPer
      StmpPERZ=StmpPer
      !-
      MPDATA,PERX,eleSt,,StmpPERX ! Create permittivity matrix
      MPDATA,PERY,eleSt,,StmpPERY
      MPDATA,PERZ,eleSt,,StmpPERZ
      *ELSE
*ENDIF
!—
!+
!+++
!+++++
!
!++++++++++++++++++++++++++++++
!+++++ For Epo in Solid5 element type
!+++ Material constants for Epoxy (Material no. eleEpo)
!+ Thermal material properties
!— Assign reference temperature (refTemp)
UIMP,eleEpo,REFT,,,refTemp,, ! UIMP for defining constant mat prop, this defines ref temp to refTemp
!—
!— Define thermal conductivity
EpoTherCon=6.92 ! Thermal conductivity (Wm-1K-1)
!—
!— Define coeff. of thermal expansion (instantaneous CTE, in K-1)
*IF,CTESame,EQ,1,THEN
      cteEpo=cte ! For checking, let CTE of NP be the same as PZT's
      *ELSE
      cteEpo=3.7e-5 ! Coefficient of thermal expansion (intantaneous, K-1)
*ENDIF
!- In each direction
CTEEpo1=cteEpo
CTEEpo2=cteEpo
CTEEpo3=cteEpo
!-
!—
!+
!+ Elastic material properties
EpoDen=1.15e3 ! Density (kgm-3)
EpoYoMod=3.65e9 ! Young's modulus (Nm-2) -> Shear modulus auto sets to EX/{2(1+NUXY)}
EpoPoiRat=0.358 ! Poisson's ratio (NB:Ansys defaults this to 0.3 anyways)
!+
!+ Electric material properties
!— Relative dielectric constant (permittivity)
Epoepsilon=3.80 ! from Epotek301_2_GoodInfo.doc
!—
!+
!+++
!+++ Input defined material properties
!+ Thermal material properties
!— Assign thermal conductivity
MP,REFT,eleEpo,refTemp
MP,KXX,eleEpo,EpoTherCon ! Thermal conductivity (Wm-1K-1)
!—
!— Define CTE matrix (Reference temp=refTemp)
MPDE,CTEX,eleEpo ! Delete CTE table of eleSt
MPDATA,CTEX,eleEpo,,CTEEpo1
MPDATA,CTEY,eleEpo,,CTEEpo2
MPDATA,CTEZ,eleEpo,,CTEEpo3
!—
!+
!+ Elastic material properties
MP,DENS,eleEpo,EpoDen ! Density (kgm-3)
```

```
MP,EX,eleEpo,EpoYoMod ! Young's modulus (Nm-2) -> Shear modulus auto sets to EX/{2(1+NUXY)}
MP,NUXY,eleEpo,EpoPoiRat !  Poisson's ratio (NB:Ansys defaults this to 0.3 anyways)
!+
!+ Electric material properties (Optional)
!— Assign permittivity for St
*IF,StPerm,EQ,1,THEN
      EpompPer=Epoepsilon
      !- In each direction
      EpompPERX=EpompPer
      EpompPERY=EpompPer
      EpompPERZ=EpompPer
      !-
      MPDATA,PERX,eleEpo,,EpompPERX ! Create permittivity matrix
      MPDATA,PERY,eleEpo,,EpompPERY
      MPDATA,PERZ,eleEpo,,EpompPERZ
      *ELSE
*ENDIF
!—
!+
!+++
!+++++
!++++++++++++++++++++
!
!
!+++++++++++++++!++++++!
!
!+++++++++++++++!+++++++++++++++!
!++++ Create physical and FE model ++++!
!+++++++++++++++!+++++++++++++++!
!+++++ Create physical model
!+++ Define keypoints
SELTOL,0.5*(HEl/NDIV) ! Define tolerance range for selection procedures below (NSEL)
K,1
K,2,L
K,3,L,W
K,4,,W
!+ Generate more keypoints (in other layers) based on existing ones
!++++++++++++++++++++
KGEN,2,1,4,1,,,H1 ! Second layer keypoints from KP1-4 (Bottom St layer)
KGEN,2,5,8,1,,,tEpo !  Third layer keypoints from KP5-8 (Bottom Epoxy layer)
KGEN,2,9,12,1,,,H2 ! Fourth layer keypoints from KP9-12 (PZT layer)
KGEN,2,13,16,1,,,tEpo !  Fifth layer keypoints from KP13-16 (Top Epoxy layer)
KGEN,2,17,20,1,,,H1 ! Second layer keypoints from KP17-20 (Top St layer)
!+
!+++
!+++ Create volumes using keypoints and assign material properties/element type
V,1,2,3,4,5,6,7,8 ! Creates volume from keypoints
VATT,eleSt ! Assign mat prop of St to vol 1
TYPE,eleSt ! Assign element type of St to vol 1
!VATT,elePZT ! To Test, Assign mat prop of PZT to vol 1
!TYPE,elePZT ! To Test, Assign element type of PZT to vol 1
V,5,6,7,8,9,10,11,12
VSEL,S,VOLU,,2 ! Select vol 2 (S indicates we are selecting a new set and VOLU indicates the data is a volume)
VATT,eleEpo ! Assign mat prop of Epoxy to vol 2
TYPE,eleEpo ! Assign element type of Epoxy to vol 2
!VATT,elePZT ! To test, Assign mat prop of PZT to vol 2
!TYPE,elePZT ! To test, Assign element type of PZT to vol 2
V,9,10,11,12,13,14,15,16
VSEL,S,VOLU,,3
VATT,elePZT ! Assign mat prop of PZT to vol 3
TYPE,elePZT ! Assign element type of PZT to vol 3
V,13,14,15,16,17,18,19,20
VSEL,S,VOLU,,4
VATT,eleEpo ! Assign mat prop of Epoxy to vol 4
TYPE,eleEpo ! Assign element type of Epoxy to vol 4
!VATT,elePZT ! To test, Assign mat prop of PZT to vol 4
!TYPE,elePZT ! To test, Assign element type of PZT to vol 4
V,17,18,19,20,21,22,23,24
VSEL,S,VOLU,,5
VATT,eleSt ! Assign mat prop of St to vol 5
TYPE,eleSt ! Assign element type of St to vol 5
!VATT,elePZT ! To test, Assign mat prop of PZT to vol 5
!TYPE,elePZT ! To test, Assign element type of PZT to vol 5
!+++
!++++++++++++++++++++++++++
!+++++
!+++++ Create FE model
VSEL,All ! Select all the volumes
!+++ Define the size of element for meshing (decides no. of elements)
*IF,UseNdiv,EQ,1,THEN
      ESIZE,,NDIV
      *ELSE
      ESIZE,SIZE
*ENDIF
VGLUE,ALL ! Glue all the volumes
MSHK,1 ! Mapped vol mesh
MSHA,0,3D ! Using Hex
VMESH,ALL ! Mesh the volume
/COM,NUMMRG,NODE ! Merge coincident and equivalently defined nodes
X=NODE(W/2,L/2,HT)
SELTOL ! Reset the tolerance range to 0.005*Value
!+++
!+++++
!+++++ Apply boundary conditions
SELTOL,0.5*(HEl/NDIV) ! Define tolerance range for selection procedures below (NSEL)
!+++ Define electrodes on PZT surface and apply equi-potential condition to their nodes
/COM, Define electrodes and couple their nodes
!++++++++++++++++++++++
HT=H1+tEpo+H2+tEpo+H1
HBot=H1+tEpo ! Height of bottom electrode
HTop=H1+tEpo+H2 ! Height of top electrode
NSEL,S,LOC,Z,0,H1 ! Define bottom St layer
*GET,node_BSt,NODE,,NUM,MIN ! Get node numbers of bottom St layer (node_BSt)
CM,BotStLay,NODE
NSEL,S,LOC,Z,HBot,HTop ! Define PZT layer
*GET,node_PZT,NODE,,NUM,MIN ! Get node numbers of PZT layer (node_PZT)
CM,PZTLay,NODE
NSEL,S,LOC,Z,HTop+tEpo,HT ! Define top St layer
*GET,node_TSt,NODE,,NUM,MIN ! Get node numbers of top St layer (node_TSt)
CM,TopStLay,NODE
NSEL,S,LOC,Z,HBot ! Define bottom electrode 1 (Right bottom)
*GET,node_BE1,NODE,,NUM,MIN ! Get node numbers of right bottom electrode (node_BE1)
CM,BotElec1,NODE ! Nodes forming bottom electrodes are named as 'BotElec1'
NSEL,S,LOC,Z,HTop ! Define Top electrode 1 (Right top)
*GET,node_TE1,NODE,,NUM,MIN ! Get node numbers of right top electrode (node_TE1)
CM,TopElec1,NODE ! Nodes forming top electrodes are named as 'TopElec1'
!++++==== Open or not ==++++++++++!
NSEL,S,LOC,Z,HBot
```

```
NSEL,A,LOC,Z,HTop
CM,AllElec,NODE ! Top and bottom electrode together
!+++ Select electrodes and fix potential in the electrode
*IF,OpenC,EQ,1,THEN
CP,1,VOLT,BotElec1 ! Couple bottom electrode
D,BotElec1,VOLT,0 ! Ground bottom electrode
!*GET,BotNod,NODE,0,NUM,MIN ! Get master node on bottom electrode
CP,2,VOLT,TopElec1 ! Couple Top electrode
!*GET,TopNod,NODE,0,NUM,MIN ! Get master node on top electrode
    *ELSE
    CP,3,VOLT,AllElec ! Couple top and bottom electrodes
    D,AllElec,Volt,0 ! Set voltage to zero
*ENDIF
!+++
!+++ Define nodes to display data after analysis
NSEL,S,LOC,Z,HBot,HTop ! Define PZT layer
CM,PZTLayer,NODE
NSEL,R,LOC,X,L
CM,EdgeX,NODE ! Define nodes on one shorter edge
CMSEL,S,PZTLayer
NSEL,R,LOC,Y,W
CM,EdgeY,NODE ! Define nodes on one longer edge
!+++
!++++++++++===Open or not ++++++!
!++++++++++++++++++++++++++++++++
!++++++++++++++++++++++++++++++++++
!++++ Define mid node of electrodes
CMSEL,S,BotElec1 ! Select BotElec1, bottom electrode's nodes
NSEL,R,LOC,X,L/2 ! Select the mid point
NSEL,R,LOC,Y,W/2
CM,midBot,NODE ! Name it midBot
CMSEL,S,TopElec1
NSEL,R,LOC,X,L/2
NSEL,R,LOC,Y,W/2
CM,midTop,NODE
!++++++++++++++++++
!+++ Define the strain (in z-direction) in the bottom surface to be zero
NSEL,S,LOC,Z,0
CM,BotSurf,NODE
*IF,BotSurf,EQ,1,THEN
    /COM, Set bottom surface Z-strain zero
    D,BotSurf,UZ,0,0
    *ELSE
*ENDIF
!+++
!+++ Define the mid-plane (in Z-axis) and set the strain in z-direction of the mid-plane to zero
NSEL,S,LOC,Z,HT/2
CM,MidPlane,NODE
*IF,MidPlZ,EQ,1,THEN
    /COM, Set mid-plane (Z-axis)'s Z-strain Zero
    D,MidPlane,UZ,0,0
    *ELSE
*ENDIF
!+++
!+++ Define the mid-plane (in Y-axis) and set the strain in Y-direction of the mid-plane to zero
NSEL,S,LOC,Y,W/2
CM,MidPlanY,NODE
*IF,MidPlY,EQ,1,THEN
    /COM, Set mid-plane (Y-axis)'s Y-strain Zero
    D,MidPlanY,UY,0,0
    *ELSE
*ENDIF
!+++
!+++ Define the mid-plane (in X-axis) and set the strain in X-direction of the mid-plane to zero
NSEL,S,LOC,X,L/2
CM,MidPlanX,NODE
*IF,MidPlX,EQ,1,THEN
    /COM, Set mid-plane (X-axis)'s X-strain Zero
    D,MidPlanX,UX,0,0
    *ELSE
*ENDIF
!+++
!+++ Select the mid-point of all the mid-planes and fix it
!NSEL,S,LOC,Z,HT/2
CMSEL,S,MidPlane
NSEL,R,LOC,X,L/2
NSEL,R,LOC,Y,W/2
CM,midPoint,NODE ! Define the mid-point
*IF,MidPt,EQ,1,THEN
    /COM, Fix the mid-point of the whole structure
    D,midPoint,UX,0,0 ! Fix the midPoint
    D,midPoint,UY,0,0
    D,midPoint,UZ,0,0
    *ELSE
*ENDIF
!+++
!+++ Apply symmetric boundary conditions with DSYM
*IF,DsymApp,EQ,1,THEN
    CSYS,0 ! Activates default Cartesian coordinate system
    NSEL,S,LOC,X,0 ! Select nodes in X=0
    DSYM,SYMM,X,0 !  Apply symmetric boundary condition to selected nodes about plane perpendicular to X-axis (coord sys 0)
    NSEL,S,LOC,Y,0
    DSYM,SYMM,Y,0
    !NSEL,S,LOC,Z,0
    !DSYM,SYMM,Z,0
    *ELSE
*ENDIF
!+++
!+++ Select the surface (area) of PZT's electrodes
ASEL,S,LOC,Z,HBot ! Select an area at Z=HBot
CM,ArBot,AREA ! Group this gemetry into a componet 'ArBot'
ASEL,S,LOC,Z,HTop ! Select an area at Z=HTop
CM,ArTop,AREA ! Group this gemetry into a componet 'ArTop'
!+++
!+++ Set convergence for voltage
*IF,ConvVt,EQ,1,THEN
    /COM, Set convergence tolerance
    CNVTOL,VOLT,convVolt1,convVolt2
    *ELSE
*ENDIF
!+++
!+++++
SELTOL ! Reset the tolerance range to 0.005*Value
NSEL,ALL ! Select all nodes
FINISH ! Exit Pre-processor
!++++++++++++++++!++++++++++++++++!
!
!================!================!
!========== Solve (Solution) ======!
!================!================!
!++++++++++++++++!++++++++++++++++!
!++++++ Apply appTemp to all nodes and solve +++!
!++++++++++++++++!++++++++++++++++!
!+++++ Change the view of the model
/VIEW,1,1,1,1
/ANG,1
/REP,FAST
/SOLU
ANTYPE,STATIC,NEW ! Define the type of analysis as static (Steady-state)
```

```
FLST,2,63,1,ORDE,2
FITEM,2,1
FITEM,2,-63
!+++++
!+++++ Apply appTemp to all nodes to model thermal expansion
/GO
/COM, Apply the thermal load to all the nodes
NSEL,ALL
TUNIF,refTemp ! Assign Uniform temp to all nodes
D,ALL,TEMP,appTemp ! Assign a fixed temperature to all nodes
!+++++
!+++++ Now, solve
/STATUS,SOLU
SOLVE
FINISH ! Exit Solution processor
!+++++
!+++++++++++++++!+++++++++++++++!
!
!===============!===============!
!========== Post-processing ========!
!===============!===============!
/POST1
!+++++++++++++++!+++++++++++++++!
!++++++ For results viewing +++++!
!+++++++++++++++!+++++++++++++++!
!+++++ Plot electric potential (Deformed and undeformed edge)
PLNSOL, VOLT,, 1,1.0
!+++++
!+++++ Print Electric flux density vector sum (Cm-2) of both elec-
trodes
NSEL,ALL
!!SAVE,Bimorph,txt
CMSEL,S,BotElec1 ! Select BotElec1 nodes (at HBot)
PRVECT,D
PRNSOL,VOLT ! Print DSUM
CMSEL,S,TopElec1 ! Select TopElec1 nodes (at HTop)
PRVECT,D
PRNSOL,VOLT ! Print DSUM
CMSEL,S,midBot
PRNSOL,VOLT
CMSEL,S,midTop
PRNSOL,VOLT
!++++++++++==== Open or not ==+++++!
!++ Print out strain results for PZT edges
CMSEL,S,EdgeX
PRVECT,U,,,EdgeLonger
CMSEL,S,EdgeY
PRVECT,U,,,EdgeShorter
!++++++++++== Open or not =====++++!
NSEL,ALL
```

D.2 Maple code

```
# PZT5H and St
# Define matrices and vectors
with(LinearAlgebra):
# Define colour, 'skyblue'
macro(skyblue = COLOR(RGB, 0.1960, 0.6000, 0.8000));
# Set basic parameters..
epsi0:=8.8541878176e-12; # Permittivity of free space
d_Theta:=90; # Temperature change we are interested in
SetL3:=127e-6; # Sets the thickness of PY layer
SetNPL3:=250e-6; # Sets the thickness of NP layer (One layer only, so in R, it is multiplied by two)
SetLength:=2e-2; # Sets the length of the sample
SetWidth:=2e-2; # Sets the width of the sample
# For pyroelectric coefficient enhancement
# - For PY
# Input data (Put in as sE, cE, alphaE and epsiT data, which can be used to calculate sD, cD, alphaD and epsiS values)
# Pyro coef at free body condition (pT,E)
Setpyro1:= 0:
Setpyro2:= 0:
Setpyro3:= -5E-4: # Sets pyro coef under SC free body condition (From Piezo.com)
# Piezo coefficients
Setd11:
Setd12: Setd13: Setd14:
Setd15:= 724E-12: # For testing purposes Piezo.com's data
Setd16:
Setd21: Setd22: Setd23: Setd24: Setd25: Setd26:
Setd31:= -320E-12: # From Piezo.com's data
Setd32:
Setd33:= 650E-12: # From Piezo.com's data
Setd34:
Setd35: Setd36:
# Elastic compliance (sE) # From Ferroperm
Sets11:= 17E-12:
Sets12:= -5.78E-12:
Sets13:= -8.79E-12:
Sets14:
Sets15: Sets16: Sets22: Sets23: Sets24: Sets25: Sets26:
Sets33:= 22.9E-12:
Sets34:
Sets35: Sets36:
Sets44:= 54.1E-12:
Sets45:
Sets46: Sets55: Sets56:
Sets66:= 45.6E-12:
# Elastic stiffness (cE) # From Ferroperm
Setc11:= 134E9:
Setc12:= 89.7E9:
Setc13:= 85.7E9:
Setc14:
Setc15: Setc16: Setc22: Setc23: Setc24: Setc25: Setc26:
Setc33:= 109E9:
Setc34:
Setc35: Setc36:
Setc44:= 18.5E9:
Setc45:
Setc46: Setc55: Setc56: Setc66:= 22E9:
# Thermal expansion coefficient (alphaE) # From Piezo.com
Setalpha1:= 3E-6:
Setalpha2:= 3E-6:
Setalpha3:= 3E-6:
Setalpha4:
Setalpha5: Setalpha6:
# Relative dielectric constant (epsiT) # From Ferroperm
Setepsi11:= 2438:
Setepsi22:= 2438:
Setepsi33:= 2874:
# ———————- For NP
SetE[np]:=193E9: # Young's modulus
Setnu[np]:=0.3: # Poisson's ratio
Setalpha[np]:=14.4E-6: # Linear thermal expansion coefficient
# ———————-
# For Efficiency calculations
# ———————- PY
SetEf_PYCvol:=3.15E6; # Sets Vol. heat capacity of PY
# ———————- NP
SetEf_NPCvol:=3.91E6; # Sets Vol. heat capacity of NP
# ———————-
PyroTE:=Vector(3):
PyroTD:=Vector(3):
SC_dS:=Vector(6):
SC_dS[1]:=SC_dS1:
SC_dS[2]:=SC_dS2:
SC_dS[3]:=SC_dS3:
OC_dS:=Vector(6):
OC_dS[1]:=OC_dS1:
OC_dS[2]:=OC_dS2:
OC_dS[3]:=OC_dS3:
d:=Matrix(3,6):
g:=Matrix(3,6):
sE:=Matrix(6,6):
cE:=Matrix(6,6):
sD:=Matrix(6,6):
cD:=Matrix(6,6):
alphaD:=Vector(6):
epsiT:=Matrix(3,3):
epsiS:=Matrix(3,3):
d_cE_alphaE_Strain:=Vector(3):
d_cD_alphaD_Strain:=Vector(3):
# For PZT5H
#———
# Define symmetry first...
PyroTE[1]:=pyro1:
PyroTE[2]:=pyro2:
PyroTE[3]:=pyro3:
PyroTE;
d[1,1]:=0;
d[1,2]:=0; d[1,3]:=0; d[1,4]:=0;
d[1,5]:=d15;
d[1,6]:=0;
d[2,1]:=0; d[2,2]:=0; d[2,3]:=0;
d[2,4]:=d15;
d[2,5]:=0;
d[2,6]:=0;
d[3,1]:=d31;
d[3,2]:=d31;
d[3,3]:=d33;
d[3,4]:=0;
d[3,5]:=0; d[3,6]:=0;
sE[1,1]:=s11;
sE[1,2]:=s12;
sE[1,3]:=s13;
sE[2,1]:=s12;
sE[2,2]:=s11;
sE[2,3]:=s13;
sE[3,1]:=s13;
sE[3,2]:=s13;
sE[3,3]:=s33;
sE[4,4]:=s44;
sE[5,5]:=s44;
sE[6,6]:=s66;
sE;
```

```
cE[1,1]:=c11:
cE[1,2]:=c12:
cE[1,3]:=c13:
cE[2,1]:=c12:
cE[2,2]:=c11:
cE[2,3]:=c13:
cE[3,1]:=c13:
cE[3,2]:=c13:
cE[3,3]:=c33:
cE[4,4]:=c44:
cE[5,5]:=c44:
cE[6,6]:=c66:
cE;
alphaE[1]:=alpha1:
alphaE[2]:=alpha2:
alphaE[3]:=alpha3:
alphaE[4]:
alphaE[5]:
alphaE[6]:
Transpose(alphaE);

epsiT[1,1]:=epsi0*epsi11:
epsiT[2,2]:=epsi0*epsi22:
epsiT[3,3]:=epsi0*epsi33:
epsiT;

# Relations between coefficients to be used later...
# sD and sE
Diff_sD_sE:=-Multiply(Multiply(Transpose(d),MatrixInverse(epsiT)),d):
sD:=sE+Diff_sD_sE:
# sE:=sD-Diff_sD_sE;
# g and d
# d:=Multiply(epsiT,g):
g:=Multiply(MatrixInverse(epsiT),d):
# epsiS and epsiT
epsiS:=(epsiT-Multiply(Multiply(d,cE),Transpose(d))):
# cD and cE
ePiezo:=Multiply(cE,Transpose(d)):
Diff_cD_cE:=Multiply(Multiply(ePiezo,MatrixInverse(epsiS)),Transpose(ePiezo)):
cD:=cE+Diff_cD_cE:
# cE:=cD-Diff_cD_cE;
# alphaD and alphaE
Diff_alphaD_alphaE:=-Multiply(Multiply(Transpose(d),MatrixInverse(epsiT)),PyroTE):
alphaD:=alphaE+Diff_alphaD_alphaE:
# alphaE:=alphaD-Diff_alphaD_alphaE;
# PyroTD and PyroTE
d_cE_alphaE:=Multiply(Multiply(d,cE),alphaE):
#PyroSecTE:=(1-epsi0/epsiT[3,3])*(d_cE_alphaE):
PyroSecTE:=d_cE_alphaE
#d_cD_alphaD:=Multiply(Multiply(d,cD),alphaD):
d_cD_alphaD:=-Multiply(Multiply(d,cD),alphaD):
#PyroSecTD:=(epsi0 * (epsiT[3, 3]/epsi0 - 1)(1/epsiT[3, 3]))(d_c D_a lphaD):
PyroSecTD:=d_cD_alphaD:
PyroTE:
PyroPrimE:=PyroTE-PyroSecTE:
PyroTD:=PyroTE-PyroSecTE+PyroSecTD:
PyroPrimD:=PyroTD-PyroSecTD:
# Input corresponding data (Put in as sE, cE, alphaE and epsiT data, which can be used to calculate sD, cD, alphaD and epsiS values)
# Pyro coef at free body condition (T,E)
pyro1:= Setpyro1: pyro2:= Setpyro2: pyro3:= Setpyro3:
# Piezo coefficients
d11:= Setd11: d12:= Setd12: d13:= Setd13: d14:= Setd14: d15:= Setd15: d16:= Setd16:
d21:= Setd21: d22:= Setd22: d23:= Setd23: d24:= Setd24: d25:= Setd25: d26:= Setd26:
d31:= Setd31: d32:= Setd32: d33:= Setd33: d34:= Setd34: d35:= Setd35: d36:= Setd36:
# Elastic compliance
s11:= Sets11: s12:= Sets12: s13:= Sets13: s14:= Sets14: s15:= Sets15: s16:= Sets16:
s22:= Sets22: s23:= Sets23: s24:= Sets24: s25:= Sets25: s26:= Sets26:
s33:= Sets33: s34:= Sets34: s35:= Sets35: s36:= Sets36:
s44:= Sets44: s45:= Sets45: s46:= Sets46:
```

```
s55:= Sets55: s56:= Sets56:
s66:= Sets66:
# Elastic stiffness
c11:= Setc11: c12:= Setc12: c13:= Setc13: c14:= Setc14: c15:= Setc15: c16:= Setc16:
c22:= Setc22: c23:= Setc23: c24:= Setc24: c25:= Setc25: c26:= Setc26:
c33:= Setc33: c34:= Setc34: c35:= Setc35: c36:= Setc36:
c44:= Setc44: c45:= Setc45: c46:= Setc46:
c55:= Setc55: c56:= Setc56:
c66:= Setc66:
# Thermal expansion coefficient
alpha1:= Setalpha1: alpha2:= Setalpha2: alpha3:= Setalpha3:
alpha4:= Setalpha4: alpha5:= Setalpha5: alpha6:= Setalpha6:
# Relative dielectric constant (permittivities)
epsi11:= Setepsi11:
epsi22:= Setepsi22:
epsi33:= Setepsi33:
# To evaluate pyroelectric coefficients..
d_cE_alphaE;
d_cE_alphaE_Strain:=Multiply(Multiply(d,cE),alphaE-(SC_dS/d_Theta));

#PyroSecEnTE:=(1-epsi0/epsiT[3,3])(d_cE_alphaE_Strain);
PyroSecEnTE:=d_cE_alphaE_Strain;
eval(PyroSecEnTE,[SC_dS1=alphaE[1]*d_Theta,SC_dS2=alphaE[2]*d_Theta,SC_dS3=alphaE[3]*d_Theta]);

d_cD_alphaD;
d_cD_alphaD_Strain:=-Multiply(Multiply(d,cD),(alphaD-(OC_dS/d_Theta)));
eval(d_cD_alphaD_Strain,[OC_dS1=alphaD[1]*d_Theta,OC_dS2=alphaD[2]*d_Theta,OC_dS3=alphaD[3]*d_Theta]);
PyroSecEnTD:=d_cD_alphaD_Strain;
eval(PyroSecEnTD,[OC_dS1=alphaD[1]*d_Theta,OC_dS2=alphaD[2]*d_Theta,OC_dS3=alphaD[3]*d_Theta]);

SCTotalPyro:=PyroTE-PyroSecEnTE;
OCTotalPyro:=PyroTD-PyroSecEnTD;
# To evaluate dc1, dc2 and dc3
# dc1=d_cE[1] or =d_cD[1], dc2=d_cE[2] or =d_cD[2] and so on...
d_cE:=Multiply(d,cE);
d_cE_:=Vector(6):
d_cE_[1]:=DotProduct(Multiply(d_cE,Vector([1,0,0,0,0,0])),Vector([1,1,1])):
d_cE_[2]:=DotProduct(Multiply(d_cE,Vector([0,1,0,0,0,0])),Vector([1,1,1])):
d_cE_[3]:=DotProduct(Multiply(d_cE,Vector([0,0,1,0,0,0])),Vector([1,1,1])):
d_cE_[4]:=DotProduct(Multiply(d_cE,Vector([0,0,0,1,0,0])),Vector([1,1,1])):
d_cE_[5]:=DotProduct(Multiply(d_cE,Vector([0,0,0,0,1,0])),Vector([1,1,1])):
d_cE_[6]:=DotProduct(Multiply(d_cE,Vector([0,0,0,0,0,1])),Vector([1,1,1])):
Transpose(d_cE_);

d_cD:=Multiply(d,cD);
d_cD_:=Vector(6):
d_cD_[1]:=DotProduct(Multiply(d_cD,Vector([1,0,0,0,0,0])),Vector([1,1,1])):
d_cD_[2]:=DotProduct(Multiply(d_cD,Vector([0,1,0,0,0,0])),Vector([1,1,1])):
d_cD_[3]:=DotProduct(Multiply(d_cD,Vector([0,0,1,0,0,0])),Vector([1,1,1])):
d_cD_[4]:=DotProduct(Multiply(d_cD,Vector([0,0,0,1,0,0])),Vector([1,1,1])):
d_cD_[5]:=DotProduct(Multiply(d_cD,Vector([0,0,0,0,1,0])),Vector([1,1,1])):
d_cD_[6]:=DotProduct(Multiply(d_cD,Vector([0,0,0,0,0,1])),Vector([1,1,1])):
Transpose(d_cD_);

# To check if cD/cE is inverse of sD/sE
Multiply(cE,sE):
Multiply(cD,sD):
# Force balance equation and theories...
# To carry out force balance equation solving process..
PYLength:=[L1,L2,L3]; NPLength:=[L1,L2,NPL3];
PYA:=[PYLength[2]*PYLength[3], PYLength[1]*PYLength[3]];
NPA:=[NPLength[2]*NPLength[3],NPLength[1]*NPLength[3]];
# For NP
npX[1]:=npE[1]/(1-npnu[2,1]*npnu[1,2]); npX[2]:=npE[1]*npnu[2,1]/(1-npnu[2,1]*npnu[1,2]);
npY[1]:=npE[2]*npnu[1,2]/(1-npnu[2,1]*npnu[1,2]);
npY[2]:=npE[2]/(1-npnu[2,1]*npnu[1,2]);
# For latter stage with calculation of S3 from S1 and S2 of PY
Lambda[1]:=(s[3,1]*c[1,1]+s[3,2]*c[2,1])/(1-(s[3,1]*c[1,3]+s[3,2]*c[2,3]));
Lambda[2]:=(s[3,1]*c[1,2]+s[3,2]*c[2,2])/(1-(s[3,1]*c[1,3]+s[3,2]*c[2,3]));
```

```
# For the force balance equation PYF[1]:=PYT[1]*PYA[1]; PYF[2]:=PYT[2]*PYA[2];
NPF[1]:=NPT[1]*NPA[1]; NPF[2]:=NPT[2]*NPA[2];
# The force balance equations are:
FEqu[1]:=PYF[1]+NPF[1]=0:
FEqu[2]:=PYF[2]+NPF[2]=0:
FEqu:=[FEqu[1],FEqu[2]];
# However, we know that..
# For PY
_PYS[3]:=simplify(Lambda[1]*PYS[1]+Lambda[2]*PYS[2]);
#_PYT[1]:=simplify(c[1,1]*PYS[1]+c[1,2]*PYS[2]+c[1,3]*PYS[3]);
jat:=c[1,1]*PYS[1]+c[1,2]*PYS[2]+c[1,3]*PYS[3]:
_PYT[1]:=eval(jat,PYS[3]=_PYS[3]);
#_PYT[2]:=simplify(c[2,1]*PYS[1]+c[2,2]*PYS[2]+c[2,3]*PYS[3]);
jat:=c[2,1]*PYS[1]+c[2,2]*PYS[2]+c[2,3]*PYS[3]:
_PYT[2]:=eval(jat,PYS[3]=_PYS[3]);
# For NP
_NPT[1]:=simplify(npX[1]*NPS[1]+npX[2]*NPS[2]);
_NPT[2]:=simplify(npY[1]*NPS[1]+npY[2]*NPS[2]);
_FEqu:=eval(FEqu,[PYS[3]=_PYS[3],PYT[1]=_PYT[1],PYT[2]=_PYT[2],NPT[1]=_NPT[1],NPT[2]=_NPT[2]]);
# However, we can also apply an interface factor...
# PYS_k1:=Multiply(PYS,k1); ← k1=k_2
# For NP into PY (To introduce k, we must set PYS to be 1/k times that of what it should have been since PYS=PYS_k1/k1)
_NPS[1]:=((1/k_2)*PYS[1]*(1+PY(alpha)[1]*d_(Theta))+(PY(alpha)[1]-NP(alpha)[1])*d_(Theta))/(1+NP(alpha)[1]*d_(Theta));
_NPS[2]:=((1/k_2)*PYS[2]*(1+PY(alpha)[2]*d_(Theta))+(PY(alpha)[2]-NP(alpha)[2])*d_(Theta))/(1+NP(alpha)[2]*d_(Theta));
# Therefore, the force balance equation to solve becomes..
__FEqu:=eval(_FEqu,[NPS[1]=_NPS[1],NPS[2]=_NPS[2]]);
eqns:=__FEqu[1],__FEqu[2]:
soln:=solve(eqns,PYS[1],PYS[2]):
pyS[1]:=simplify(subs(soln,PYS[1])):
pyS[2]:=simplify(subs(soln,PYS[2])):
pyS[3]:=simplify(Lambda[1]*pyS[1]+Lambda[2]*pyS[2]):
#dS[1]:=(pyS[1]+1)*(1+PY(alpha)[1]*d_(Theta))-1:
#dS[2]:=(pyS[2]+1)*(1+PY(alpha)[2]*d_(Theta))-1:
#dS[3]:=(pyS[3]+1)*(1+PY(alpha)[3]*d_(Theta))-1:

# The strain expressions in their most general form are... (Solutions to the force balance equation)
dS[1]:=simplify((pyS[1]+1)*(1+PY(alpha)[1]*d_(Theta))-1):
dS[2]:=simplify((pyS[2]+1)*(1+PY(alpha)[2]*d_(Theta))-1):
dS[3]:=simplify((pyS[3]+1)*(1+PY(alpha)[3]*d_(Theta))-1):

# General pyroelectric coefficient expressions...
SCTotalPyro_Gen:=eval(SCTotalPyro,[SC_dS1=dS[1],SC_dS2=dS[2],SC_dS3=dS[3]]):
OCTotalPyro_Gen:=eval(OCTotalPyro,[OC_dS1=dS[1],OC_dS2=dS[2],OC_dS3=dS[3]]):
# From above, define general pyroelectric coefficient...

# Define material properties according to general theory
# Common parameters
d_(Theta):=d_Theta;
L1:=SetLength; L2:=SetWidth; L3; NPL3;
# For NP
# Young's modulus
E[np]:=SetE[np]:
npE[1]:=E[np]; npE[2]:=E[np]; npE[3]:=E[np];
# Poisson's ratio
nu[np]:=Setnu[np]:
npnu[1,2]:=nu[np]; npnu[2,1]:=nu[np]; npnu[1,3]:=nu[np]; npnu[2,3]:=nu[np];
# Linear thermal expansion coefficient
alpha[np]:=Setalpha[np]:
NP(alpha)[1]:=alpha[np]; NP(alpha)[2]:=alpha[np];

# For PY
# As an example, in case of SC (s=sE, c=cE and PY(alpha)=alphaE)
# s[3,1]:=sE[3,1]; s[3,2]:=sE[3,2];
# c[1,1]:=cE[1,1]; c[1,2]:=cE[1,2]; c[1,3]:=cE[1,3];
# c[2,1]:=cE[2,1]; c[2,2]:=cE[2,2]; c[2,3]:=cE[2,3];
# PY(alpha)[1]:=alphaE[1]; PY(alpha)[2]:=alphaE[2]; PY(alpha)[3]:=alphaE[3];

# To be used for defining SC conditions on Force balance equation
# jat:=
```

```
# eval(jat,[s[3,1]=sE[3,1], s[3,2]=sE[3,2], c[1,1]=cE[1,1], c[1,2]=cE[1,2],
c[1,3]=cE[1,3], c[2,1]=cE[2,1], c[2,2]=cE[2,2], c[2,3]=cE[2,3], PY(alpha)[1]=alphaE[1], PY(alpha)[2]=alphaE[2], PY(alpha)[3]=alphaE[3]]);
# To be used for defining OC conditions on Force balance equation
# jat:= # eval(jat,[s[3,1]=sD[3,1], s[3,2]=sD[3,2], c[1,1]=cD[1,1], c[1,2]=cD[1,2], c[1,3]=cD[1,3],
c[2,1]=cD[2,1], c[2,2]=cD[2,2], c[2,3]=cD[2,3], PY(alpha)[1]=alphaD[1], PY(alpha)[2]=alphaD[2], PY(alpha)[3]=alphaD[3]]);

# To find the shorter form of the whole pyroelectric coefficient expression...
# For SC
#s[3,1]:=sE[3,1];
#s[3,2]:=sE[3,2];
#c[1,1]:=cE[1,1];
#c[1,2]:=cE[1,2];
#c[1,3]:=cE[1,3];
#c[2,1]:=cE[2,1];
#c[2,2]:=cE[2,2];
#c[2,3]:=cE[2,3];
#PY(alpha)[1]:=alphaE[1];
#PY(alpha)[2]:=alphaE[2];
#PY(alpha)[3]:=alphaE[3];
#SCFEqu:=FEqu;

jat:=FEqu;
SCFEqu:= eval(jat,[s[3,1]=sE[3,1], s[3,2]=sE[3,2], c[1,1]=cE[1,1], c[1,2]=cE[1,2], c[1,3]=cE[1,3], c[2,1]=cE[2,1], c[2,2]=cE[2,2], c[2,3]=cE[2,3],
PY(alpha)[1]=alphaE[1], PY(alpha)[2]=alphaE[2], PY(alpha)[3]=alphaE[3]]);
# However, we know that..
# For PY
#_SCPYS[3]:=Lambda[1]*PYS[1]+Lambda[2]*PYS[2];
jat:=Lambda[1]*PYS[1]+Lambda[2]*PYS[2];
_SCPYS[3]:=eval(jat,[s[3,1]=sE[3,1], s[3,2]=sE[3,2], c[1,1]=cE[1,1], c[1,2]=cE[1,2], c[1,3]=cE[1,3], c[2,1]=cE[2,1], c[2,2]=cE[2,2], c[2,3]=cE[2,3],
PY(alpha)[1]=alphaE[1], PY(alpha)[2]=alphaE[2], PY(alpha)[3]=alphaE[3]]);

#_SCPYT[1]:=c[1,1]*PYS[1]+c[1,2]*PYS[2]+c[1,3]*PYS[3];
jat:=c[1,1]*PYS[1]+c[1,2]*PYS[2]+c[1,3]*PYS[3];
#_SCPYT[1]:=eval(jat,PYS[3]=_SCPYS[3]);
jat2:=eval(jat,PYS[3]=_SCPYS[3]);
_SCPYT[1]:=eval(jat2,[s[3,1]=sE[3,1], s[3,2]=sE[3,2], c[1,1]=cE[1,1], c[1,2]=cE[1,2], c[1,3]=cE[1,3], c[2,1]=cE[2,1], c[2,2]=cE[2,2], c[2,3]=cE[2,3],
PY(alpha)[1]=alphaE[1], PY(alpha)[2]=alphaE[2], PY(alpha)[3]=alphaE[3]]);

#_SCPYT[2]:=c[2,1]*PYS[1]+c[2,2]*PYS[2]+c[2,3]*PYS[3];
jat:=c[2,1]*PYS[1]+c[2,2]*PYS[2]+c[2,3]*PYS[3];
#_SCPYT[2]:=eval(jat,PYS[3]=_SCPYS[3]);
jat2:=eval(jat,PYS[3]=_SCPYS[3]);
_SCPYT[2]:=eval(jat2,[s[3,1]=sE[3,1], s[3,2]=sE[3,2], c[1,1]=cE[1,1], c[1,2]=cE[1,2], c[1,3]=cE[1,3], c[2,1]=cE[2,1], c[2,2]=cE[2,2], c[2,3]=cE[2,3],
PY(alpha)[1]=alphaE[1], PY(alpha)[2]=alphaE[2], PY(alpha)[3]=alphaE[3]]);

# For NP
_SCNPT[1]:=npX[1]*NPS[1]+npX[2]*NPS[2];
_SCNPT[2]:=npY[1]*NPS[1]+npY[2]*NPS[2];
#_SCFEqu:=eval(SCFEqu,[PYS[3]=_SCPYS[3],PYT[1]=_SCPYT[1],PYT[2]=_SCPYT[2],NPT[1]=_SCNPT[1],NPT[2]=_SCNPT[2]]);
jat:=eval(SCFEqu,[PYS[3]=_SCPYS[3],PYT[1]=_SCPYT[1],PYT[2]=_SCPYT[2],NPT[1]=_SCNPT[1],NPT[2]=_SCNPT[2]]);
_SCFEqu:=eval(jat,[s[3,1]=sE[3,1], s[3,2]=sE[3,2], c[1,1]=cE[1,1], c[1,2]=cE[1,2], c[1,3]=cE[1,3], c[2,1]=cE[2,1], c[2,2]=cE[2,2], c[2,3]=cE[2,3],
¡PY(alpha)[1]=alphaE[1], PY(alpha)[2]=alphaE[2], PY(alpha)[3]=alphaE[3]]);
# However, we also know that...
# PYS_k1:=Multiply(PYS,k1);
# For NP into PY (To introduce k, we must set PYS to be 1/k times that of what it should have been since PYS=PYS_k1/k1)
#NPS[1]:=((1/k_2)*PYS[1]*(1+PY(alpha)[1]*d_(Theta))+(PY(alpha)[1]-NP(alpha)[1])*d_(Theta))/
(1+NP(alpha)[1]*d_(Theta)):
#_SCNPS[1]:=eval(((1/k_2)*PYS[1]*(1+PY(alpha)[1]*d_(Theta))+(PY(alpha)[1]-NP(alpha)[1])*d_(Theta))/
(1+NP(alpha)[1]*d_(Theta)),[s[3,1]=sE[3,1], s[3,2]=sE[3,2], c[1,1]=cE[1,1], c[1,2]=cE[1,2], c[1,3]=cE[1,3],
c[2,1]=cE[2,1], c[2,2]=cE[2,2], c[2,3]=cE[2,3], PY(alpha)[1]=alphaE[1], PY(alpha)[2]=alphaE[2], PY(alpha)[3]=alphaE[3]]);

jat:=((1/k_2)*PYS[1]*(1+PY(alpha)[1]*d_(Theta))+(PY(alpha)[1]-NP(alpha)[1])*d_(Theta))/(1+NP(alpha)[1]*d_(Theta)):
_SCNPS[1]:=eval(jat,[s[3,1]=sE[3,1], s[3,2]=sE[3,2], c[1,1]=cE[1,1], c[1,2]=cE[1,2], c[1,3]=cE[1,3], c[2,1]=cE[2,1], c[2,2]=cE[2,2], c[2,3]=cE[2,3],
PY(alpha)[1]=alphaE[1], PY(alpha)[2]=alphaE[2], PY(alpha)[3]=alphaE[3]]);

#NPS[2]:=((1/k_2)*PYS[2]*(1+PY(alpha)[2]*d_(Theta))+(PY(alpha)[2]-NP(alpha)[2])*d_(Theta))/
(1+NP(alpha)[2]*d_(Theta)):
#_SCNPS[2]:=eval(((1/k_2)*PYS[2]*(1+PY(alpha)[2]*d_(Theta))+(PY(alpha)[2]-NP(alpha)[2])*d_(Theta))/
(1+NP(alpha)[2]*d_(Theta)),[s[3,1]=sE[3,1], s[3,2]=sE[3,2], c[1,1]=cE[1,1], c[1,2]=cE[1,2], c[1,3]=cE[1,3],
```

```
c[2,1]=cE[2,1], c[2,2]=cE[2,2], c[2,3]=cE[2,3], PY(alpha)[1]=alphaE[1], PY(alpha)[2]=alphaE[2], PY(alpha)[3]=alphaE[3]]);

jat:=((1/k_2)*PYS[2]*(1+PY(alpha)[2]*d_(Theta))+(PY(alpha)[2]-NP(alpha)[2])*d_(Theta))/(1+NP(alpha)[2]*d_(Theta)):
_SCNPS[2]:=eval(jat,[s[3,1]=sE[3,1], s[3,2]=sE[3,2], c[1,1]=cE[1,1], c[1,2]=cE[1,2], c[1,3]=cE[1,3], c[2,1]=cE[2,1], c[2,2]=cE[2,2], c[2,3]=cE[2,3],
PY(alpha)[1]=alphaE[1], PY(alpha)[2]=alphaE[2], PY(alpha)[3]=alphaE[3]]);
# Therefore, the force balance equation to solve becomes..
__SCFEqu:=eval(_SCFEqu,[NPS[1]=_SCNPS[1],NPS[2]=_SCNPS[2]]);
SCeqns:=__SCFEqu[1],__SCFEqu[2];
SCsoln:=solve(SCeqns,PYS[1],PYS[2]);
#SCsoln[1];
#SCsoln[2];
SCpyS[1]:=simplify(subs(SCsoln,PYS[1])):
SCpyS[2]:=simplify(subs(SCsoln,PYS[2])):
#SCpyS[3]:=simplify(Lambda[1]*SCpyS[1]+Lambda[2]*SCpyS[2]);
jat:=simplify(Lambda[1]*SCpyS[1]+Lambda[2]*SCpyS[2]):
SCpyS[3]:=eval(jat,[s[3,1]=sE[3,1], s[3,2]=sE[3,2], c[1,1]=cE[1,1], c[1,2]=cE[1,2], c[1,3]=cE[1,3], c[2,1]=cE[2,1], c[2,2]=cE[2,2], c[2,3]=cE[2,3],
PY(alpha)[1]=alphaE[1], PY(alpha)[2]=alphaE[2], PY(alpha)[3]=alphaE[3]]);
#SCdS[1]:=(SCpyS[1]+1)*(1+PY(alpha)[1]*d_(Theta))-1;
#SCdS[2]:=(SCpyS[2]+1)*(1+PY(alpha)[2]*d_(Theta))-1;
#SCdS[3]:=(SCpyS[3]+1)*(1+PY(alpha)[3]*d_(Theta))-1;
##
# jat:=(SCpyS[1]+1)*(1+PY(alpha)[1]*d_(Theta))-1:
jat:=(k_1*SCpyS[1]+1)*(1+PY(alpha)[1]*d_(Theta))-1:
SCdS[1]:= eval(jat,[s[3,1]=sE[3,1], s[3,2]=sE[3,2], c[1,1]=cE[1,1], c[1,2]=cE[1,2], c[1,3]=cE[1,3], c[2,1]=cE[2,1], c[2,2]=cE[2,2], c[2,3]=cE[2,3],
PY(alpha)[1]=alphaE[1], PY(alpha)[2]=alphaE[2], PY(alpha)[3]=alphaE[3]]);
##
# jat:=(SCpyS[2]+1)*(1+PY(alpha)[2]*d_(Theta))-1:
jat:=(k_1*SCpyS[2]+1)*(1+PY(alpha)[2]*d_(Theta))-1:
SCdS[2]:= eval(jat,[s[3,1]=sE[3,1], s[3,2]=sE[3,2], c[1,1]=cE[1,1], c[1,2]=cE[1,2], c[1,3]=cE[1,3], c[2,1]=cE[2,1], c[2,2]=cE[2,2], c[2,3]=cE[2,3],
PY(alpha)[1]=alphaE[1], PY(alpha)[2]=alphaE[2], PY(alpha)[3]=alphaE[3]]);
##
# jat:=(SCpyS[3]+1)*(1+PY(alpha)[3]*d_(Theta))-1:
jat:=(k_1*SCpyS[3]+1)*(1+PY(alpha)[3]*d_(Theta))-1:
SCdS[3]:= eval(jat,[s[3,1]=sE[3,1], s[3,2]=sE[3,2], c[1,1]=cE[1,1], c[1,2]=cE[1,2], c[1,3]=cE[1,3], c[2,1]=cE[2,1], c[2,2]=cE[2,2], c[2,3]=cE[2,3],
PY(alpha)[1]=alphaE[1], PY(alpha)[2]=alphaE[2], PY(alpha)[3]=alphaE[3]]);

SCTotalPyro;
Gen_SCTotalPyro:=eval(SCTotalPyro,[SC_dS1=SCdS[1],SC_dS2=SCdS[2],SC_dS3=SCdS[3]]):
eval(SCTotalPyro[1],[SC_dS1=SCdS[1],SC_dS2=SCdS[2],SC_dS3=SCdS[3]]):
eval(SCTotalPyro[2],[SC_dS1=SCdS[1],SC_dS2=SCdS[2],SC_dS3=SCdS[3]]):
eval(SCTotalPyro[3],[SC_dS1=SCdS[1],SC_dS2=SCdS[2],SC_dS3=SCdS[3]]):
SCTotalPyro_Contri:=SCTotalPyro-PyroPrimE;
##
#- SC Pyroelectric coefficient with k=k_1 applied after force balance equation
##R_SCTotalPyro:=eval(eval(SCTotalPyro[3],[SC_dS[1]=SCdS[1],SC_dS[2]=SCdS[2],SC_dS[3]=SCdS[3]]),[NPL3=1,L3=R]);
#R_SCTotalPyro:=eval(eval(SCTotalPyro[3],[SC_dS1=SCdS[1],SC_dS2=SCdS[2],SC_dS3=SCdS[3]]),[NPL3=1,L3=R]);
k_1_R_SCTotalPyro:=eval(eval(SCTotalPyro[3],[SC_dS1=SCdS[1],SC_dS2=SCdS[2],SC_dS3=SCdS[3]]),[NPL3=1,L3=R,k_2=1]);
#R_SCTotalPyro_Contri:=eval(eval(SCTotalPyro_Contri[3],[SC_dS1=SCdS[1],SC_dS2=SCdS[2],SC_dS3=SCdS[3]]),[NPL3=1,L3=R]);
k_1_R_SCTotalPyro_Contri:=eval(eval(SCTotalPyro_Contri[3],[SC_dS1=SCdS[1],SC_dS2=SCdS[2],SC_dS3=SCdS[3]]),[NPL3=1,L3=R,k_2=1]);
SCPrimaryPyro:=PyroPrimE;
SCPyroTE:=PyroTE;
SCSecPyro:=PyroSecTE;
k_1_R_SCTotalPyro_k1:=eval(k_1_R_SCTotalPyro,[R=127/500,k_1=1]);
k_1_R_SCTotalPyro_k0:=eval(k_1_R_SCTotalPyro,[R=127/500,k_1=0]);
k_1_R_SCTotalPyro_Contri_k1:=eval(k_1_R_SCTotalPyro_Contri,[R=127/500,k_1=1]);
k_1_R_SCTotalPyro_Contri_k0:=eval(k_1_R_SCTotalPyro_Contri,[R=127/500,k_1=0]);
##
#- SC Pyroelectric coefficient with k=k_2 applied before force balance equation
##R_SCTotalPyro:=eval(eval(SCTotalPyro[3],[SC_dS[1]=SCdS[1],SC_dS[2]=SCdS[2],SC_dS[3]=SCdS[3]]),[NPL3=1,L3=R]);
#R_SCTotalPyro:=eval(eval(SCTotalPyro[3],[SC_dS1=SCdS[1],SC_dS2=SCdS[2],SC_dS3=SCdS[3]]),[NPL3=1,L3=R]);
R_SCTotalPyro:=eval(eval(SCTotalPyro[3],[SC_dS1=SCdS[1],SC_dS2=SCdS[2],SC_dS3=SCdS[3]]),[NPL3=1,L3=R,k_1=1]);
#R_SCTotalPyro_Contri:=eval(eval(SCTotalPyro_Contri[3],[SC_dS1=SCdS[1],SC_dS2=SCdS[2],SC_dS3=SCdS[3]]),[NPL3=1,L3=R]);
R_SCTotalPyro_Contri:=eval(eval(SCTotalPyro_Contri[3],[SC_dS1=SCdS[1],SC_dS2=SCdS[2],SC_dS3=SCdS[3]]),[NPL3=1,L3=R,k_1=1]);
SCPrimaryPyro:=PyroPrimE;
SCPyroTE:=PyroTE;
SCSecPyro:=PyroSecTE;
R_SCTotalPyro_k1:=eval(R_SCTotalPyro,[R=127/500,k_2=1]);
R_SCTotalPyro_k0:=eval(R_SCTotalPyro,[R=127/500,k_2=0]);
R_SCTotalPyro_Contri_k1:=eval(R_SCTotalPyro_Contri,[R=127/500,k_2=1]);
```

```
R_SCTotalPyro_Contri_k0:=eval(R_SCTotalPyro_Contri,[R=127/500,k_2=0]);

## For OC
#s[3,1]:=sD[3,1];
#s[3,2]:=sD[3,2];
#c[1,1]:=cD[1,1];
#c[1,2]:=cD[1,2];
#c[1,3]:=cD[1,3];
#c[2,1]:=cD[2,1];
#c[2,2]:=cD[2,2];
#c[2,3]:=cD[2,3];
#PY(alpha)[1]:=alphaD[1];
#PY(alpha)[2]:=alphaD[2];
#PY(alpha)[3]:=alphaD[3];

jat:=FEqu;
OCFEqu:= eval(jat,[s[3,1]=sD[3,1], s[3,2]=sD[3,2], c[1,1]=cD[1,1], c[1,2]=cD[1,2], c[1,3]=cD[1,3], c[2,1]=cD[2,1], c[2,2]=cD[2,2], c[2,3]=cD[2,3],
PY(alpha)[1]=alphaD[1], PY(alpha)[2]=alphaD[2], PY(alpha)[3]=alphaD[3]]);

# However, we know that..
# For PY
#_OCPYS[3]:=Lambda[1]*PYS[1]+Lambda[2]*PYS[2];
jat:=Lambda[1]*PYS[1]+Lambda[2]*PYS[2];
_OCPYS[3]:=eval(jat,[s[3,1]=sD[3,1], s[3,2]=sD[3,2], c[1,1]=cD[1,1], c[1,2]=cD[1,2], c[1,3]=cD[1,3], c[2,1]=cD[2,1], c[2,2]=cD[2,2], c[2,3]=cD[2,3],
PY(alpha)[1]=alphaD[1], PY(alpha)[2]=alphaD[2], PY(alpha)[3]=alphaD[3]]);

##_OCPYT[1]:=c[1,1]*PYS[1]+c[1,2]*PYS[2]+c[1,3]*PYS[3];
jat:=c[1,1]*PYS[1]+c[1,2]*PYS[2]+c[1,3]*PYS[3];
#_OCPYT[1]:=eval(jat,PYS[3]=_OCPYS[3]);
jat2:=eval(jat,PYS[3]=_OCPYS[3]);
_OCPYT[1]:=eval(jat2,[s[3,1]=sD[3,1], s[3,2]=sD[3,2], c[1,1]=cD[1,1], c[1,2]=cD[1,2], c[1,3]=cD[1,3], c[2,1]=cD[2,1], c[2,2]=cD[2,2], c[2,3]=cD[2,3],
PY(alpha)[1]=alphaD[1], PY(alpha)[2]=alphaD[2], PY(alpha)[3]=alphaD[3]]);

##_OCPYT[2]:=c[2,1]*PYS[1]+c[2,2]*PYS[2]+c[2,3]*PYS[3];
jat:=c[2,1]*PYS[1]+c[2,2]*PYS[2]+c[2,3]*PYS[3];
#_OCPYT[2]:=eval(jat,PYS[3]=_OCPYS[3]);
jat2:=eval(jat,PYS[3]=_OCPYS[3]);
_OCPYT[2]:=eval(jat2,[s[3,1]=sD[3,1], s[3,2]=sD[3,2], c[1,1]=cD[1,1], c[1,2]=cD[1,2], c[1,3]=cD[1,3], c[2,1]=cD[2,1], c[2,2]=cD[2,2], c[2,3]=cD[2,3],
PY(alpha)[1]=alphaD[1], PY(alpha)[2]=alphaD[2], PY(alpha)[3]=alphaD[3]]);

# For NP
_OCNPT[1]:=npX[1]*NPS[1]+npX[2]*NPS[2];
_OCNPT[2]:=npY[1]*NPS[1]+npY[2]*NPS[2];
#_OCFEqu:=eval(OCFEqu,[PYS[3]=_OCPYS[3],PYT[1]=_OCPYT[1],PYT[2]=_OCPYT[2],NPT[1]=_OCNPT[1],NPT[2]=_OCNPT[2]]);
jat:=eval(OCFEqu,[PYS[3]=_OCPYS[3],PYT[1]=_OCPYT[1],PYT[2]=_OCPYT[2],NPT[1]=_OCNPT[1],NPT[2]=_OCNPT[2]]);
_OCFEqu:=eval(jat,[s[3,1]=sD[3,1], s[3,2]=sD[3,2], c[1,1]=cD[1,1], c[1,2]=cD[1,2], c[1,3]=cD[1,3], c[2,1]=cD[2,1], c[2,2]=cD[2,2], c[2,3]=cD[2,3],
PY(alpha)[1]=alphaD[1], PY(alpha)[2]=alphaD[2], PY(alpha)[3]=alphaD[3]]);
# However, we also know that...
# PYS_k1:=Multiply(PYS,k1);
# For NP into PY (To introduce k, we must set PYS to be 1/k times that of what it should have been since PYS=PYS_k1/k1)
##NPS[1]:=((1/k_2)*PYS[1]*(1+PY(alpha)[1]*d_(Theta))+(PY(alpha)[1]-NP(alpha)[1])*d_(Theta))/
(1+NP(alpha)[1]*d_(Theta)):
#_OCNPS[1]:=eval(((1/k_2)*PYS[1]*(1+PY(alpha)[1]*d_(Theta))+(PY(alpha)[1]-NP(alpha)[1])*d_(Theta))/
(1+NP(alpha)[1]*d_(Theta)),[s[3,1]=sD[3,1], s[3,2]=sD[3,2], c[1,1]=cD[1,1], c[1,2]=cD[1,2], c[1,3]=cD[1,3],
c[2,1]=cD[2,1], c[2,2]=cD[2,2], c[2,3]=cD[2,3], PY(alpha)[1]=alphaD[1], PY(alpha)[2]=alphaD[2], PY(alpha)[3]=alphaD[3]]);

jat:=((1/k_2)*PYS[1]*(1+PY(alpha)[1]*d_(Theta))+(PY(alpha)[1]-NP(alpha)[1])*d_(Theta))/(1+NP(alpha)[1]*d_(Theta)):
_OCNPS[1]:=eval(jat,[s[3,1]=sD[3,1], s[3,2]=sD[3,2], c[1,1]=cD[1,1], c[1,2]=cD[1,2], c[1,3]=cD[1,3], c[2,1]=cD[2,1], c[2,2]=cD[2,2], c[2,3]=cD[2,3],
PY(alpha)[1]=alphaD[1], PY(alpha)[2]=alphaD[2], PY(alpha)[3]=alphaD[3]]);

##NPS[2]:=((1/k_2)*PYS[2]*(1+PY(alpha)[2]*d_(Theta))+(PY(alpha)[2]-NP(alpha)[2])*d_(Theta))/(1+NP(alpha)[2]*d_(Theta)):
#_OCNPS[2]:=eval(((1/k_2)*PYS[2]*(1+PY(alpha)[2]*d_(Theta))+(PY(alpha)[2]-NP(alpha)[2])*d_(Theta))/
(1+NP(alpha)[2]*d_(Theta)),[s[3,1]=sD[3,1], s[3,2]=sD[3,2], c[1,1]=cD[1,1], c[1,2]=cD[1,2], c[1,3]=cD[1,3],
c[2,1]=cD[2,1], c[2,2]=cD[2,2], c[2,3]=cD[2,3], PY(alpha)[1]=alphaD[1], PY(alpha)[2]=alphaD[2], PY(alpha)[3]=alphaD[3]]);

jat:=((1/k_2)*PYS[2]*(1+PY(alpha)[2]*d_(Theta))+(PY(alpha)[2]-NP(alpha)[2])*d_(Theta))/(1+NP(alpha)[2]*d_(Theta)):
_OCNPS[2]:=eval(jat,[s[3,1]=sD[3,1], s[3,2]=sD[3,2], c[1,1]=cD[1,1], c[1,2]=cD[1,2], c[1,3]=cD[1,3], c[2,1]=cD[2,1], c[2,2]=cD[2,2], c[2,3]=cD[2,3],
PY(alpha)[1]=alphaD[1], PY(alpha)[2]=alphaD[2], PY(alpha)[3]=alphaD[3]]);
```

```
# Therefore, the force balance equation to solve becomes..
__OCFEqu:=eval(_OCFEqu,[NPS[1]=_OCNPS[1],NPS[2]=_OCNPS[2]]);
OCeqns:=__OCFEqu[1],__OCFEqu[2];
OCsoln:=solve(OCeqns,PYS[1],PYS[2]);
#OCsoln[1];
#OCsoln[2];
OCpyS[1]:=simplify(subs(OCsoln,PYS[1])):
OCpyS[2]:=simplify(subs(OCsoln,PYS[2])):
#OCpyS[3]:=simplify(Lambda[1]*OCpyS[1]+Lambda[2]*OCpyS[2]);
jat:=simplify(Lambda[1]*OCpyS[1]+Lambda[2]*OCpyS[2]):
OCpyS[3]:=eval(jat,[s[3,1]=sD[3,1], s[3,2]=sD[3,2], c[1,1]=cD[1,1], c[1,2]=cD[1,2], c[1,3]=cD[1,3], c[2,1]=cD[2,1], c[2,2]=cD[2,2], c[2,3]=cD[2,3],
PY(alpha)[1]=alphaD[1], PY(alpha)[2]=alphaD[2], PY(alpha)[3]=alphaD[3]]);
#OCdS[1]:=(OCpyS[1]+1)*(1+PY(alpha)[1]*d_(Theta))-1;
#OCdS[2]:=(OCpyS[2]+1)*(1+PY(alpha)[2]*d_(Theta))-1;
#OCdS[3]:=(OCpyS[3]+1)*(1+PY(alpha)[3]*d_(Theta))-1;
# jat:=(OCpyS[1]+1)*(1+PY(alpha)[1]*d_(Theta))-1:
jat:=(k_1*OCpyS[1]+1)*(1+PY(alpha)[1]*d_(Theta))-1:
OCdS[1]:= eval(jat,[s[3,1]=sD[3,1], s[3,2]=sD[3,2], c[1,1]=cD[1,1], c[1,2]=cD[1,2], c[1,3]=cD[1,3], c[2,1]=cD[2,1], c[2,2]=cD[2,2], c[2,3]=cD[2,3],
PY(alpha)[1]=alphaD[1], PY(alpha)[2]=alphaD[2], PY(alpha)[3]=alphaD[3]]);
# jat:=(OCpyS[2]+1)*(1+PY(alpha)[2]*d_(Theta))-1:
jat:=(k_1*OCpyS[2]+1)*(1+PY(alpha)[2]*d_(Theta))-1:
OCdS[2]:= eval(jat,[s[3,1]=sD[3,1], s[3,2]=sD[3,2], c[1,1]=cD[1,1], c[1,2]=cD[1,2], c[1,3]=cD[1,3], c[2,1]=cD[2,1], c[2,2]=cD[2,2], c[2,3]=cD[2,3],
PY(alpha)[1]=alphaD[1], PY(alpha)[2]=alphaD[2], PY(alpha)[3]=alphaD[3]]);
# jat:=(OCpyS[3]+1)*(1+PY(alpha)[3]*d_(Theta))-1:
jat:=(k_1*OCpyS[3]+1)*(1+PY(alpha)[3]*d_(Theta))-1:
OCdS[3]:= eval(jat,[s[3,1]=sD[3,1], s[3,2]=sD[3,2], c[1,1]=cD[1,1], c[1,2]=cD[1,2], c[1,3]=cD[1,3], c[2,1]=cD[2,1], c[2,2]=cD[2,2], c[2,3]=cD[2,3],
PY(alpha)[1]=alphaD[1], PY(alpha)[2]=alphaD[2], PY(alpha)[3]=alphaD[3]]);
OCTotalPyro;
Gen_OCTotalPyro:=eval(OCTotalPyro,[OC_dS1=OCdS[1],OC_dS2=OCdS[2],OC_dS3=OCdS[3]]):
eval(OCTotalPyro[1],[OC_dS1=OCdS[1],OC_dS2=OCdS[2],OC_dS3=OCdS[3]]);
eval(OCTotalPyro[2],[OC_dS1=OCdS[1],OC_dS2=OCdS[2],OC_dS3=OCdS[3]]);
eval(OCTotalPyro[3],[OC_dS1=OCdS[1],OC_dS2=OCdS[2],OC_dS3=OCdS[3]]);
OCTotalPyro_Contri:=OCTotalPyro-PyroPrimD;
##
#- OC Pyroelectric coefficient with k=k_1 applied before force balance equation
#R_OCTotalPyro:=eval(eval(OCTotalPyro[3],[OC_dS1=OCdS[1],OC_dS2=OCdS[2],OC_dS3=OCdS[3]]),[NPL3=1,L3=R]);
k_1_R_OCTotalPyro:=eval(eval(OCTotalPyro[3],[OC_dS1=OCdS[1],OC_dS2=OCdS[2],OC_dS3=OCdS[3]]),[NPL3=1,L3=R,k_2=1]);
#R_OCTotalPyro_Contri:=eval(eval(OCTotalPyro_Contri[3],[OC_dS1=OCdS[1],OC_dS2=OCdS[2],OC_dS3=OCdS[3]]),[NPL3=1,L3=R]);
k_1_R_OCTotalPyro_Contri:=eval(eval(OCTotalPyro_Contri[3],[OC_dS1=OCdS[1],OC_dS2=OCdS[2],OC_dS3=OCdS[3]]),[NPL3=1,L3=R,k_2=1]);
OCPrimaryPyro:=PyroPrimD;
OCPyroTD:=PyroTD;
OCSecPyro:=PyroSecTD;
R_OCTotalPyro_k1:=eval(k_1_R_OCTotalPyro,[R=127/500,k_1=1]);
R_OCTotalPyro_k0:=eval(k_1_R_OCTotalPyro,[R=127/500,k_1=0]);
R_OCTotalPyro_Contri_k1:=eval(k_1_R_OCTotalPyro_Contri,[R=127/500,k_1=1]);
R_OCTotalPyro_Contri_k0:=eval(k_1_R_OCTotalPyro_Contri,[R=127/500,k_1=0]);

## #- OC Pyroelectric coefficient with k=k_2 applied before force balance equation
#R_OCTotalPyro:=eval(eval(OCTotalPyro[3],[OC_dS1=OCdS[1],OC_dS2=OCdS[2],OC_dS3=OCdS[3]]),[NPL3=1,L3=R]);
R_OCTotalPyro:=eval(eval(OCTotalPyro[3],[OC_dS1=OCdS[1],OC_dS2=OCdS[2],OC_dS3=OCdS[3]]),[NPL3=1,L3=R,k_1=1]);
#R_OCTotalPyro_Contri:=eval(eval(OCTotalPyro_Contri[3],[OC_dS1=OCdS[1],OC_dS2=OCdS[2],OC_dS3=OCdS[3]]),[NPL3=1,L3=R]);
R_OCTotalPyro_Contri:=eval(eval(OCTotalPyro_Contri[3],[OC_dS1=OCdS[1],OC_dS2=OCdS[2],OC_dS3=OCdS[3]]),[NPL3=1,L3=R,k_1=1]);
OCPrimaryPyro:=PyroPrimD;
OCPyroTD:=PyroTD;
OCSecPyro:=PyroSecTD;
R_OCTotalPyro_k1:=eval(R_OCTotalPyro,[R=127/500,k_2=1]);
R_OCTotalPyro_k0:=eval(R_OCTotalPyro,[R=127/500,k_2=0]);
R_OCTotalPyro_Contri_k1:=eval(R_OCTotalPyro_Contri,[R=127/500,k_2=1]);
R_OCTotalPyro_Contri_k0:=eval(R_OCTotalPyro_Contri,[R=127/500,k_2=0]);

#### For thermal mass calculations...
# Define parameters to be used for thermal mass (efficiency)...
Ef_Temp:=25; # Temperature in degC at which Ef_SCPYCv was measured
Ef_SCPYCv:=Ef_PYCvol;
Ef_SCNPCv:=Ef_NPCvol;
Ef_L:=Ef_Length;
Ef_W:=Ef_Width;
Ef_L3:=Ef_TotalThickness;
```

```
Ef_R;
Ef_PYt:=(Ef_L3*Ef_R)/(R+1);
Ef_NPt:=Ef_L3/(R+1);

# for SC
SCPyroTE[3];
#SCPY_Ef:=eval(SCPyroTE[3]/(Ef_L3*Ef_L*Ef_W*Ef_SCPYCv),R=Ef_R);
SCPY_Ef:=abs(eval(SCPyroTE[3]/(Ef_L3*Ef_L*Ef_W*Ef_SCPYCv),R=Ef_R)); # In case Pyro coef changes signs
#SCPY_Ef_PYt:=eval(SCPyroTE[3]/(Ef_PYt*Ef_L*Ef_W*Ef_SCPYCv),R=Ef_R);
SCPY_Ef_PYt:=abs(eval(SCPyroTE[3]/(Ef_PYt*Ef_L*Ef_W*Ef_SCPYCv),R=Ef_R)); # In case Pyro coef changes signs
#Ef_R_SCTotalPyro:=eval(R_SCTotalPyro,R=Ef_R);
Ef_R_SCTotalPyro:=abs(eval(R_SCTotalPyro,R=Ef_R)); # In case Pyro coef changes signs

#SCCom_Ef:=Ef_R_SCTotalPyro/(Ef_L3*Ef_L*Ef_W*(Ef_SCPYCv*Ef_R+Ef_SCNPCv)/(Ef_R+1));
SCCom_Ef:=abs(Ef_R_SCTotalPyro/(Ef_L3*Ef_L*Ef_W*(Ef_SCPYCv*Ef_R+Ef_SCNPCv)/(Ef_R+1))); # In case Pyro coef changes signs

#SC_R_Ef:=SCCom_Ef/SCPY_Ef;
SC_R_Ef:=abs(SCCom_Ef/SCPY_Ef); # In case Pyro coef changes signs
#SC_R_Ef_PYt:=SCCom_Ef/SCPY_Ef_PYt;
SC_R_Ef_PYt:=abs(SCCom_Ef/SCPY_Ef_PYt); # In case Pyro coef changes signs
#SC_R_Ef_Calc:=(Ef_R_SCTotalPyro*Ef_SCPYCv*(Ef_R+1))/(SCPyroTE[3]*(Ef_SCPYCv*Ef_R+Ef_SCNPCv));
SC_R_Ef_Calc:=abs((Ef_R_SCTotalPyro*Ef_SCPYCv*(Ef_R+1))/(SCPyroTE[3]*(Ef_SCPYCv*Ef_R+Ef_SCNPCv))); # In case Pyro coef changes
signs
eval(SC_R_Ef-SC_R_Ef_Calc);

# for OC
Ef_AbsTemp:=273.15+Ef_Temp;
Ef_OCPYCv:=Ef_SCPYCv-Ef_AbsTemp*Multiply(Transpose(PyroTE),Multiply(MatrixInverse(epsiT),PyroTE));
Ef_OCNPCv:=Ef_SCNPCv;

OCPyroTD[3];

#OCPY_Ef:=eval(OCPyroTD[3]/(Ef_L3*Ef_L*Ef_W*Ef_OCPYCv),R=Ef_R);
OCPY_Ef:=abs(eval(OCPyroTD[3]/(Ef_L3*Ef_L*Ef_W*Ef_OCPYCv),R=Ef_R)); # In case Pyro coef changes signs
#OCPY_Ef_PYt:=eval(OCPyroTD[3]/(Ef_PYt*Ef_L*Ef_W*Ef_OCPYCv),R=Ef_R);
OCPY_Ef_PYt:=abs(eval(OCPyroTD[3]/(Ef_PYt*Ef_L*Ef_W*Ef_OCPYCv),R=Ef_R)); # In case Pyro coef changes signs
#Ef_R_OCTotalPyro:=eval(R_OCTotalPyro,R=Ef_R);
Ef_R_OCTotalPyro:=abs(eval(R_OCTotalPyro,R=Ef_R)); # In case Pyro coef changes signs

#OSCom_Ef:=Ef_R_OCTotalPyro/(Ef_L3*Ef_L*Ef_W*(Ef_OCPYCv*Ef_R+Ef_OCNPCv)/(Ef_R+1));
OSCom_:=abs(Ef_R_OCTotalPyro/(Ef_L3*Ef_L*Ef_W*(Ef_OCPYCv*Ef_R+Ef_OCNPCv)/(Ef_R+1))); # In case Pyro coef changes signs

#OC_R_Ef:=OSCom_Ef/OCPY_Ef;
OC_R_Ef:=abs(OSCom_Ef/OCPY_Ef); # In case Pyro coef changes signs
#OC_R_Ef_PYt:=OSCom_Ef/OCPY_Ef_PYt;
OC_R_Ef_PYt:=abs(OSCom_Ef/OCPY_Ef_PYt); # In case Pyro coef changes signs
#OC_R_Ef_Calc:=(Ef_R_OCTotalPyro*Ef_OCPYCv*(Ef_R+1))/(OCPyroTD[3]*(Ef_OCPYCv*Ef_R+Ef_OCNPCv));
OC_R_Ef_Calc:=abs((Ef_R_OCTotalPyro*Ef_OCPYCv*(Ef_R+1))/(OCPyroTD[3]*(Ef_OCPYCv*Ef_R+Ef_OCNPCv))); # In case Pyro coef
changes signs
eval(OC_R_Ef-OC_R_Ef_Calc);

# Input material data...
Ef_PYCvol:=SetEf_PYCvol;
Ef_NPCvol:=SetEf_NPCvol;
Ef_Length:=SetLength;
Ef_Width:=SetWidth;
Ef_TotalThickness:=SetL3+2*SetNPL3;

Ef_OCPYCv;
# Evaluate the values to see....
Ef_SC_PYOnly:=SCPY_Ef;
Ef_OC_PYOnly:=OCPY_Ef;
Ef_SC_PYOnly_PYt:=eval(SCPY_Ef_PYt,[Ef_R=127/500,k_2=1]);
Ef_OC_PYOnly_PYt:=eval(OCPY_Ef_PYt,[Ef_R=127/500,k_2=1]);
Ef_SC_All:=eval(SCCom_Ef,[Ef_R=127/500,k_2=1]);
Ef_OC_All:=eval(OSCom_Ef,[Ef_R=127/500,k_2=1]);
R_Ef_SC:=eval(SC_R_Ef,[Ef_R=127/500,k_2=1]);
R_Ef_OC:=eval(OC_R_Ef,[Ef_R=127/500,k_2=1]);
R_Ef_SC_PYt:=eval(SC_R_Ef_PYt,[Ef_R=127/500,k_2=1]);
```

```
R_Ef_OC_PYt:=eval(OC_R_Ef_PYt,[Ef_R=127/500,k_2=1]);
eval(SC_R_Ef_Calc,[Ef_R=127/500,k_2=1]);
eval(OC_R_Ef_Calc,[Ef_R=127/500,k_2=1]);

# Plot the efficiencies of PY material (PYt is used) with varying R and perfect bonding under SC and OC
# This is meaningless as this expression is only derived for the use with the efficiency ratios
# by itself, this has no meaning
plot([eval(SCPY_Ef_PYt,k_2=1),eval(OCPY_Ef_PYt,k_2=1)],Ef_R=0..10):
plot([eval(SCPY_Ef_PYt,k_2=1),eval(OCPY_Ef_PYt,k_2=1)],Ef_R=0..1/2):
# Plot the efficiencies of the composite with varying R and perfect bonding under SC and OC
# Ef_L3 is the total thickness
# As R reaches infinity, this should settle to the efficiency value of just PZT5H of Ef_L3 thickness..
Ef_SC_PYOnly:=SCPY_Ef;
Ef_OC_PYOnly:=OCPY_Ef;
Efficiency_R0_10000000000;
plot([eval(SCCom_Ef,k_2=1),eval(OSCom_Ef,k_2=1)],Ef_R=0..1e10,
color=[red,skyblue],labels=["R",""],legend=["Short circuit","Open
circuit"],thickness=2,axesfont=[HELVETICA,bold,12],labelfont=[HELVETICA,BOLD,12],labeldirections=[horizontal,vertical] );
Efficiency_R0_100000;
plot([eval(SCCom_Ef,k_2=1),eval(OSCom_Ef,k_2=1)],Ef_R=0..1e5,
color=[red,skyblue],labels=["R",""],legend=["Short circuit","Open
circuit"],thickness=2,axesfont=[HELVETICA,bold,12],labelfont=[HELVETICA,BOLD,12],labeldirections=[horizontal,vertical] );
Efficiency_R0_100;
plot([eval(SCCom_Ef,k_2=1),eval(OSCom_Ef,k_2=1)],Ef_R=0..1e2,
color=[red,skyblue],labels=["R",""],legend=["Short circuit","Open
circuit"],thickness=2,axesfont=[HELVETICA,bold,12],labelfont=[HELVETICA,BOLD,12],labeldirections=[horizontal,vertical] );
Efficiency_R0_10;
plot([eval(SCCom_Ef,k_2=1),eval(OSCom_Ef,k_2=1)],Ef_R=0..1e1,
color=[red,skyblue],labels=["R",""],legend=["Short circuit","Open
circuit"],thickness=2,axesfont=[HELVETICA,bold,12],labelfont=[HELVETICA,BOLD,12],labeldirections=[horizontal,vertical] );
Efficiency_R0_3;
plot([eval(SCCom_Ef,k_2=1),eval(OSCom_Ef,k_2=1)],Ef_R=0..3e0,
color=[red,skyblue],labels=["R",""],legend=["Short circuit","Open
circuit"],thickness=2,axesfont=[HELVETICA,bold,12],labelfont=[HELVETICA,BOLD,12],labeldirections=[horizontal,vertical] );
Efficiency_R0_05;
plot([eval(SCCom_Ef,k_2=1),eval(OSCom_Ef,k_2=1)],Ef_R=0..5e-1,
color=[red,skyblue],labels=["R",""],legend=["Short circuit","Open
circuit"],thickness=2,axesfont=[HELVETICA,bold,12],labelfont=[HELVETICA,BOLD,12],labeldirections=[horizontal,vertical] );
# Plot the efficiency ratios of the composite with varying R and perfect bonding under SC and OC
# With total thickness being the same (L3 used for both PY and composite)
# As R reaches infinity, this should approach 1 as the whole composite starts to become dominantly
# PY material only...
Ratio_Efficiency_R0_100000;
plot([eval(SC_R_Ef,k_2=1),eval(OC_R_Ef,k_2=1)],Ef_R=0..1e5,
color=[red,skyblue],labels=["R",""],legend=["Short circuit","Open
circuit"],thickness=2,axesfont=[HELVETICA,bold,12],labelfont=[HELVETICA,BOLD,12],labeldirections=[horizontal,vertical] );
Ratio_Efficiency_R0_100;
plot([eval(SC_R_Ef,k_2=1),eval(OC_R_Ef,k_2=1)],Ef_R=0..1e2,
color=[red,skyblue],labels=["R",""],legend=["Short circuit","Open
circuit"],thickness=2,axesfont=[HELVETICA,bold,12],labelfont=[HELVETICA,BOLD,12],labeldirections=[horizontal,vertical] );
# Plot the efficiency ratios of the composite with varying R and perfect bonding under SC and OC
# With the same PY material thickness (PYt is the thickness of PY material and L3 is the total thickness of the composite)
# As R reaches infinity, this should approach 1 as the whole composite starts to become dominantly
# PY material only...
Ratio_Efficiency_R0_100000;
plot([eval(SC_R_Ef_PYt,k_2=1),eval(OC_R_Ef_PYt,k_2=1)],Ef_R=0..1e5,
color=[red,skyblue],labels=["R",""],legend=["Short circuit","Open
circuit"],thickness=2,axesfont=[HELVETICA,bold,12],labelfont=[HELVETICA,BOLD,12],labeldirections=[horizontal,vertical] );
Ratio_Efficiency_R0_100;
plot([eval(SC_R_Ef_PYt,k_2=1),eval(OC_R_Ef_PYt,k_2=1)],Ef_R=0..1e1,
color=[red,skyblue],labels=["R",""],legend=["Short circuit","Open
circuit"],thickness=2,axesfont=[HELVETICA,bold,12],labelfont=[HELVETICA,BOLD,12],labeldirections=[horizontal,vertical] );

# For stresses under SC with 127 micron PZT-5H and 2x250 micron St
MatrixInverse(sE);
cE;
d_Theta;
Multiply(cE,d_Theta);
SCdS[1];
```

```
SCdS[2];
SCdS[3];
_SCdS:=Vector(6):
_SCdS[1]:=eval(SCdS[1],[NPL3=2*SetNPL3,L3=SetL3,k_1=1,k_2=1]):
_SCdS[2]:=eval(SCdS[2],[NPL3=2*SetNPL3,L3=SetL3,k_1=1,k_2=1]):
_SCdS[3]:=eval(SCdS[3],[NPL3=2*SetNPL3,L3=SetL3,k_1=1,k_2=1]):
_SCdS;
alphaE;
_SCdS-Multiply(alphaE,d_Theta);
SCdT:=Multiply(cE,_SCdS-Multiply(alphaE,d_Theta));
ToCheckSimplifedExpression;
CheckSCdT1:=(E[np]*(cE[1,1]+cE[1,2])*(1+alphaE[1]*d_Theta)*(alpha[np]-alphaE[1])*d_Theta)/
((1-nu[np])*(cE[1,1]+cE[1,2])*(1+alpha[np]*d_Theta)*R+E[np]*(1-2*sE[1,3]*cE[1,3])*(1+alphaE[1]*d_Theta));
RtoEval:=SetL3/(2*SetNPL3);
EvaluatedValueIs;
eval(CheckSCdT1,[R=RtoEval]);
CheckSCdT3:=CheckSCdT1*(2*(cE[1,3]-sE[1,3]*(2*(cE[1,3])^2-cE[3,3]*(cE[1,1]+cE[1,2]))))/(cE[1,1]+cE[1,2]);
EvaluatedValueIs;
eval(CheckSCdT3,[R=RtoEval]);
# For stress expression under SC
ks_SCdS:=Vector(6):
ks_SCdS[1]:=eval(SCdS[1],[NPL3=1,L3=R]):
ks_SCdS[2]:=eval(SCdS[2],[NPL3=1,L3=R]):
ks_SCdS[3]:=eval(SCdS[3],[NPL3=1,L3=R]):
ks_SCdS;
ks_SCdT:=Multiply(cE,ks_SCdS-Multiply(alphaE,d_Theta));
k1_SCdT:=eval(ks_SCdT,[k_2=1]);
k2_SCdT:=eval(ks_SCdT,[k_1=1]);
ToCompareWithStressFromAbove;
RtoEval:=SetL3/(2*SetNPL3);
SCdT;
SCdT-eval(k1_SCdT,[R=RtoEval,k_1=1]);
SCdT-eval(k2_SCdT,[R=RtoEval,k_2=1]);
# For stresses under OC with 127 micron PZT-5H and 2x250 micron St
_OCdS:=Vector(6):
_OCdS[1]:=eval(OCdS[1],[NPL3=2*SetNPL3,L3=SetL3,k_1=1,k_2=1]):
_OCdS[2]:=eval(OCdS[2],[NPL3=2*SetNPL3,L3=SetL3,k_1=1,k_2=1]):
_OCdS[3]:=eval(OCdS[3],[NPL3=2*SetNPL3,L3=SetL3,k_1=1,k_2=1]):
_OCdS-Multiply(alphaD,d_Theta);
OCdT:=Multiply(cD,_OCdS-Multiply(alphaD,d_Theta));
ToCheckSimplifiedExpression;
CheckOCdT1:=(E[np]*(cD[1,1]+cD[1,2])*(1+alphaD[1]*d_Theta)*(alpha[np]-alphaD[1])*d_Theta)/
((1-nu[np])*(cD[1,1]+cD[1,2])*(1+alpha[np]*d_Theta)*R+E[np]*(1-2*sD[1,3]*cD[1,3])*(1+alphaD[1]*d_Theta));
RtoEval:=SetL3/(2*SetNPL3);
EvaluatedValueIs;
eval(CheckOCdT1,[R=RtoEval]);
CheckOCdT3:=CheckOCdT1*(2*(cD[1,3]-sD[1,3]*(2*(cD[1,3])^2-cD[3,3]*(cD[1,1]+cD[1,2]))))/(cD[1,1]+cD[1,2]);
EvaluatedValueIs;
eval(CheckOCdT3,[R=RtoEval]);
The_evaluated_values_are_different_from_our_model_under_OC_since_alphaD3_is_not_equal_to_alphaD1_or_alphaD2_under_OC;
# For stress expression under OC
ks_OCdS:=Vector(6):
ks_OCdS[1]:=eval(OCdS[1],[NPL3=1,L3=R]):
ks_OCdS[2]:=eval(OCdS[2],[NPL3=1,L3=R]):
ks_OCdS[3]:=eval(OCdS[3],[NPL3=1,L3=R]):
ks_OCdS;
ks_OCdT:=Multiply(cD,ks_OCdS-Multiply(alphaD,d_Theta));
k1_OCdT:=eval(ks_OCdT,[k_2=1]);
k2_OCdT:=eval(ks_OCdT,[k_1=1]);
ToCompareWithStressFromAbove;
RtoEval:=SetL3/(2*SetNPL3);
OCdT;
OCdT-eval(k1_OCdT,[R=RtoEval,k_1=1]);
OCdT-eval(k2_OCdT,[R=RtoEval,k_2=1]);
```

References

[1] For the thermal properties of BTO, values provided by Surfacenet GmbH were used, 2003.

[2] For the material properties Al, data from Ing. Buro R. Tschaggelar were used, 2005.

[3] For the detailed mechanical properties of both PZTs, data from Ferroperm piezoceramics for the corresponding Ferroperm PZTs, namely Pz27 for PZT-5A and Pz29 for PZT-5H, were used, 2006.

[4] For the thermal and piezoelectric properties of PZT-5H (PSI-5H4E) and PZT-5A (PSI-5A4E), values provided by Piezo systems Inc. were used, 2006.

[5] Amptek Inc. Miniature X-ray generator with pyroelectric crystal, 2007.

[6] For the material properties of 3M-TC2810 epoxy, data provided by 3M were used, 2007.

[7] For the material properties of EPOTEK epoxies, data provided by Epotek technology, Inc. were used, 2007.

[8] For the material properties of ERA-182 epoxy, data provided by Eastern resins corp. were used, 2007.

[9] For the material properties of stainless steel (Stainless steel-15-7PH) and Zn, data from Goodfellow were used, 2007.

[10] For the material properties of TIM- epoxies, data provided by Timtronics (Thermal Interface Material) were used, 2007.

[11] For the material properties of WLK30 epoxy, data provided by Fischer Elektronik GmbH were used, 2007.

[12] For the thermal and pyroelectric properties of LTO and LNO, values provided by Crystal Technology Inc. were used, 2007.

[13] Data from eFunda, Engineering fundamentals were used, 2008.

[14] For the material properties of CPVC, Al, and Zn, data from Wikipedia Foundation Inc. were used, 2008.

[15] For the material properties of PTFE, values provided by Gentech Engineering Plastics were used, 2008.

[16] M. Achenback and I. A. Mueller. A model for shape memory. *J. Phys.*, **12**(43):163–167, 1982.

[17] A. Amin. The role of connectivity in thermal imaging. *J. Electroceram.*, **61**:73–80, 1980.

[18] J. Asano, S. Iwasaki, M. Okuyama, and Y. Hamakawa. Electron emission from PZT ceramic by external pulsed electric fields - Pulse voltage dependence of emitted charge. *Jpn. J. Appl. Phys.*, **32**(Part 1, 9B):4284–4287, 1993.

[19] ASME. *Energy harvesting by pyroelectric effect using PZT*, volume Proceedings of SMASIS08, Ellicott city, Maryland, USA, October 2008. ASME.

[20] A. Badel, D. Guyomar, E. Lefeuvre, and C. Richard. Efficiency enhancement of a piezoelectric energy harvesting device in pulsed operation by synchronous charge inversion. *J. Intell. Mater. Syst. Struct.*, **16**:889–901, 2005.

[21] A. Barzegar, D. Damjanovic, N. Ledermann, and P. Muralt. Piezoelectric response of thin films determined by charge integration technique: Substrate bending effects. *Journal of Applied Physics*, **93**(8):4756–4760, 2003.

[22] B. Baumslag and B. Chandler. *Schaum's outline of Group Theory*. McGraw-Hill, 1968.

[23] S. P. Beeby, M. J. Tudor, and N. M. White. Energy harvesting vibration sources for microsystems applications. *Meas. Sci. Technol.*, **17**:R175–R195, 2006.

[24] A. J. Bell. On the origin of the large piezoelectric effect in morphotropic phase boundary perovskite single crystals. *Appl. Phys. Lett.*, **76**(1):109–111, 2000.

[25] A. J. Bell and E. Furman. A two order parameter thermodynamic model for $Pb(Zr_{1-x}Ti_x)O_3$. *Jpn. J. Appl. Phys.*, **42**:7418–7423, 2003.

[26] D. Berlincourt, H. H. A. Krueger, and C. Near. Properties of piezoelectricity ceramics. Technical Report Technical Publication Report No. TP-226, Morgan Electro Ceramics, 2003.

[27] A. S. Bhalla and R. E. Newnham. Primary and secondary pyroelectricity. *Phys. Status solidi(a)*, **58**(1):K19–K24, 1980.

[28] A. S. Bhalla, R. E. Newnham, L. E. Cross, and W. A. Schulze. Pyroelectric PZT-Polymer composites. *Ferroelectrics*, 33:139–146, 1981.

[29] M. I. Bichurin, V. M. Petrov, and G. Srinivasan. Theory of low-frequency magnetoelectric effects in ferromagnetic-ferroelectric layered composites. *Journal of Applied Physics*, **92**(12):7681–7683, 2002.

[30] K. Biedrzycki. Polarization reversal-induced electron emission from triglycine sulphate crystals. *Ferroelectrics*, **119**:33–39, 1991.

[31] S. V. Bogdanov. The origin of the piezoelectric effect in pyroelectric crystals. *IEEE T Ultrason Ferr*, **49**(11):1469–1473, 2002.

[32] E. M. Bourim, C.-W. Moon, S.-W. Lee, and I. K. Yoo. Investigation of pyroelectric electron emission from monodomain lithium niobate single crystals. *Physica B*, **383**:171–182, 2006.

[33] J. G. Boyd and D. C. Lagoudas. A thermodynamic constitutive model for the shape memory materials. Part I: the monolithic shape memory alloys. *Int. J. Plas.*, **12**(6):805–842, 1996.

[34] L. C. Brinson. One dimensional constitutive behavior of shape memory alloys: thermomechanical derivation with non-constant material functions and redefined martensite internal variable. *J. Int. Mat. Sys. and Str.*, **4**:229–242, 1993.

[35] J. D. Brownridge. Pyroelectric X-ray generator. *Nature*, **358**:287–288, 1992.

[36] J. D. Brownridge and S. Raboy. Investigation of pyroelectric generation of X rays. *J. Appl. Phys.*, **86**(1):640–647, 1999.

[37] J. D. Brownridge and S. M. Shafroth. The effect of vacuum chamber size on maximum electron energy for pyroelectric crystal electron accelerators. In *CAARI 2004: 18th International conference on the applications of accelerators in research and industry*, 2004.

[38] J. D. Brownridge and S. M. Shafroth. *Trends in Lasers and Electro-Optics Research*, chapter Electron and Positive Ion Beams and X-rays Produced by Heated and Cooled Pyroelectric Crystals such as $LiNbO_3$ and $LiTaO_3$ in Dilute Gases: Phenomenology and Applications, pages 59–95. Nova Science Publishers, 2006.

[39] J. D. Brownridge, S. M. Shafroth, D. W. Trott, B. R. Stoner, and W. M. Hooke. Observation of multiple nearly monoenergetic electron production by heated pyroelectric crystals in ambient gas. *Appl. Phys. Lett.*, **78**(8):1158, 2001.

[40] W. G. Cady. *Piezoelectricity.* New York: McGraw-Hill Book Company, Inc., 1946.

[41] H. H. S. Chang. *First year review report: Enhanced pyroelectric effect through product property & its applications. Unpublished report (PhD)*, (2007).

[42] H. H. S. Chang. *Second year review report: Enhanced pyroelectric effect through product property & its applications. Unpublished report (PhD)*, (2008).

[43] H. H. S. Chang and Z. Huang. Substantial pyroelectric effect enhancement in laminated composites. *Applied Physics Letters*, **92**(15):152903, 2008.

[44] H. H. S. Chang and Z. Huang. Pyroelectric effect enhancement through product property under open circuit condition. *Journal of Applied Physics*, **106**(1):014101, 2009.

[45] H. H. S. Chang, R. W. Whatmore, and Z. Huang. Pyroelectric effect enhancement in laminate composites under short circuit condition. *Journal of Applied Physics*, **106**(11):114110, 2009.

[46] S. Chen, S. Zheng, Z. Zhu, X. Dong, and C. Tang. Electron emission and plasma generation in a modulator electron gun using ferroelectric cathode. *Nucl. Instrum. Meth. A*, **566**:662–667, 2006.

[47] K. H. Chew, F. G. Shin, B. Ploss, H. L. W. Chan, and C. L. Choy. Primary and secondary pyroelectric effects of ferroelectric 0-3 composites. *Journal of Applied Physics*, **94**(2):1134–

1145, 2003.

[48] H. C. Chung. *The development of a piezoelectric fan system for the flapping wing micro-air-vehicle application*. Phd thesis, Cranfield University, 2008.

[49] A. G. Chynoweth. Dynamic method for measuring the pyroelectric effect with special reference to barium titanate. *Journal of Applied Physics*, **27**:78, 1956.

[50] D. K. Das-Gupta. On the nature of pyroelectricity in polyvinylidene fluoride. *Ferroelectrics*, **33**:75–89, 1981.

[51] A. V. Dixit, N. R. Rajopadhye, and S. V. Bhoraskar. Secondary electron emission of doped PZT ceramics. *J. Mat. Sci.*, **21**:2798–2802, 1986.

[52] J. Drescher, H. Balke, H. A. Bahr, G. Milde, and G. Gerlach. Finite element modeling of the thermo-electro-mechanical coupling in pyroelectric infrared sensor arrays. In *MOEMS and Miniaturized Systems II*, volume 4561, pages 333–338. SPIE, 2nd Oct. 2001.

[53] H. Dvey-Aharon and P. L. Taylor. Thermodynamics of pyroelectricity and piezoelectricity in polymers. *Ferroelectrics*, **33**:103–110, 1981.

[54] T. G. Engel, C. Keawboonchuay, and W. C. Nunnally. Energy conversion and high power pulse production using miniature piezoelectric compressors. *IEEE T Plasma Sci*, **28**(5):1338–1341, 2000.

[55] F. Falk and P. Konopka. Three-dimensional Landau theory describing the martensitic transformation of shape memory alloys. *J. Phys.*, **2**:61–77, 1990.

[56] F. D. Fischer and K. Tanaka. A micromechanical model for the kinetics of martensitic transformation. *Int. J. Sol. and Str.*, **29**(14-15):1723–1728, 1992.

[57] M. Fukuhara and A. Sampei. Stress-induced pyroelectric properties of devitrified fused quartz in elevated temperature. *J. Mat. Sci.*, **12**:131–135, 2001.

[58] K. Gall, H. Sehitoglu, R. Anderson, I. Karaman, Y. I. Chumlyakov, and I. V. Kireeva. On the mechanical behavior of single crystal Ni-Ti shape memory alloys and related polycrystalline phenomenon. *Mat. Sci. and Eng.*, **A317**:85–92, 2001.

[59] F. G. Gaudette, A. E. Giannakopoulos, and S. Suresh. Interface cracks in layered materials subjected to a uniform temperature change. *Int. J. Fracture*, **110**:325–349, 2001.

[60] J. M. Gere and S. P. Timoshenko. *Mechanics of materials*. Wadsworth International, 1985.

[61] J. A. Geuther and Y. Danon. Development of a pyroelectric neutron source. Technical report, DOE NEER: Highlights-III, 2005.

[62] J. A. Geuther and Y. Danon. Electron and positive ion acceleration with pyroelectric crystals. *J. Appl. Phys.*, **97**:074109, 2005.

[63] J. A. Geuther and Y. Danon. High-energy x-ray production with pyroelectric crystals. *J. Appl. Phys.*, **97**:104916, 2005.

[64] J. A. Geuther and Y. Danon. Pyroelectric electron acceleration: Improvements and future applications. Technical report, DOE NEER: Highlights of recent and current research-I, 2005.

[65] J. A. Geuther and Y. Danon. Radiation generation using pyroelectric crystals. Poster for Nuclear engineering education research, 2007.

[66] J. A. Geuther, Y. Danon, and F. Saglime. Nuclear reactions induced by a pyroelectric accelerator. *Phys. Rev. Lett.*, **96**(5):054803, 2006.

[67] J. N. Grima, P. S. Farrugia, R. Gatt, and V. Zammit. Connected triangles exhibiting negative Poisson's ratios and negative thermal expansion. *J. Phys. Soc. Jap.*, **76**(2):025001, 2007.

[68] P. J. Grout, N. H. March, and T. L. Thorp. Pyroelectricity: microscopic estimates and upper bounds. *J. Phys. C: Solid State Phys.*, **8**:2167–2182, 1975.

[69] D. Guyomar, A. Badel, E. Lefeuvre, and C. Richard. Towards energy harvesting using active materials and conversion improvement by nonlinear processing. *IEEE T Ultrason Ferr*, **52**(4):584–595, 2005.

[70] D. Guyomar, S. Pruvost, and G. Sebald. Energy harvesting based on FE-FE transition in ferroelectric single crystals. *IEEE T Ultrason Ferr*, **55**(2):279–285, 2008.

[71] D. Guyomar, G. Sebald, E. Lefeuvre, and A. Khodayari. Toward heat energy harvesting using pyroelectric material. *J. Intell. Mater. Syst. Struct.*, **20**(3):265–271, 2009.

[72] A. Haris, N. S. Goo, H. C. Park, and K. J. Yoon. Modeling and analysis for the development of Lightweight Piezoceramic Composite Actuators (LIPCA). *Com. Mat. Sci.*, **30**:474–481, 2004.

[73] N. P. Hartley, P. T. Squire, and E. H. Putley. A new method of measuring pyroelectric coefficients. *J. Phys. E: Scientific Instruments*, **5**:787–789, 1972.

[74] E. Hausler and L. Stein. Implantable physiological power supply wiht PVDF film. *Ferroelectrics*, **60**:277–282, 1984.

[75] Y. Hayashi, D. Flechtner, and E. Hotta. Characteristics of electron emission from PZT ferroelectric cathode under strong accelerating field. *J. Phys. D: Appl. Phys.*, **35**:281–286, 2002.

[76] K. H. Hellwege, editor. *Landolt-Bornstein: Numerical data and functional relationships in science and technology: Group III: Crystal and Solid State Physics.* Springer-Verlag Berlin-Heidelberg, 1981.

[77] K. H. Hellwege, editor. *Landolt-Bornstein: Numerical data and functional relationships in science and technology: Group III: Crystal and Solid State Physics.* Springer-Verlag Berlin-Heidelberg, 1982.

[78] H. Hilton. *Mathematical crystallography.* Oxford: Clarendon Press, 1903.

[79] D. Hodgson. *Using Shape Memory Alloys*. Sunnyvale, CA: Shape Memory Applications, Inc., 1988.

[80] J. M. Horton and G. E. Tupholme. Axial loading of elliptical-section bonded rubber blocks. *Int. J. Solids and Struc.*, **44**:5101–5110, 2007.

[81] IEEE. *Design and comparison of high strain shape memory alloy actuators*, ROBOT, Albuquerque, New Mexico, April 1997. IEEE.

[82] T. Ikeda. *Fundamentals of Piezoelectricity*. New York: Oxford University Press, 1990.

[83] Y. Ivshin and T. J. Pence. A constitutive model for hysteretic phase transition behavior. *Int. J. Eng. Sci.*, **32**(4):681–704, 1994.

[84] R. W. Newsome Jr. and E. Y. Andrei. Measurement of the pyroelectric coefficient of poly(vinylidene fluoride) down to 3K. *Phys. Rev. B*, **55**(11):7264–7271, 1997.

[85] I. Kanno, Y. Yokoyama, H. Kotera, and K. Wasa. Thermodynamic study of c-axis-oriented epitaxial $Pb(Zr,Ti)O_3$ thin films. *Phys. Rev. B*, **69**:064103, 2004.

[86] S. Kapuria, P. C. Dumir, and A. Ahmed. An efficient coupled layerwise theory for static analysis of piezoelectric sandwich beams. *Arc. Appl. Mech.*, **73**:147–159, 2003.

[87] C. Keawboonchuay and T. G. Engel. Design, modeling and implementation of a 30-kW piezoelectric pulse generator. *IEEE T Plasma Sci*, **30**(2):679–686, 2002.

[88] C. Keawboonchuay and T. G. Engel. Maximum power generation in a piezoelectric pulse generator. *IEEE T Plasma Sci*, **31**(1):123–128, 2003.

[89] C. Keawboonchuay and T. G. Engel. Scaling relationships and maximum peak power generation in a piezoelectric pulse generator. *IEEE T Plasma Sci*, **32**(5):1879–1885, 2004.

[90] R. G. Kepler and R. A. Anderson. Piezoelectricity and pyroelectricity in polyvinylidene fluoride. *Journal of Applied Physics*, **49**(8):4490, 1978.

[91] A. Khodayari, S. Pruvost, G. Sebald, D. Guyomar, and S. Mohammadi. Nonlinear pyroelectric energy harvesting from relaxor single crystals. *IEEE T Ultrason Ferr*, **56**(4):693–699, 2009.

[92] H. W. Kim, A. Batra, S. Priya, K. Uchino, D. Markley, R. E. Newnham, and H. F. Hofmann. Energy harvesting using a piezoelectric "Cymbal" transducer in dynamic environment. *Jpn J. Appl. Phys.*, **43**(9A):6178–6183, 2004.

[93] P. Kloucek, D. R. Reynolds, and T. I. Seidman. Computational modeling of vibration damping in SMA wires. *Cont. Mech. and Therm.*, **16**(5):495–514, 2004.

[94] L. S. Kokhanchik and E. B. Yakimov. The pulse electron emission and local changes of pyroelectric potential in lithium niobate crystals. *Ferroelectrics*, **225**:41–48, 1999.

[95] P. W. Kruse. *Uncooled thermal imaging: Arrays, systems and applications*. SPIE Press, 2002.

[96] V. D. Kugel, G. Rosenman, and D. Shur. Electron emission from $LiNbO_3$ crystals with

domains of inverted polarization. *J. Phys. D: Appl. Phys.*, **28**:2360–2364, 1995.

[97] J. Kymissis, C. Kendall, J. A. Paradiso, and N. Gershenfeld. Parasitic power harvesting in shoes. *Proc. 2nd IEEE Int. Conf. Wearable Computing (California)*, pages 132–139, 1998.

[98] K. S. Lam, Y. W. Wong, L. S. Tai, Y. M. Poon, and F. G. Shin. Dielectric and pyroelectric properties of lead zirconate titanate/polyurethane composites. *Journal of Applied Physics*, **96**(7):3896–3899, 2004.

[99] S. B. Lang. *Pyroelectricity*: From ancient curiosity to modern imaging tool. *Phys. Today*, **58**:31, 2005.

[100] S. B. Lang and S. Muensit. Lesser-known piezoelectric and pyroelectric applications of electroactive polymers. *Mat. Res. Soc. Symp. Proc.*, **889**:3–14, 2006.

[101] T. Lauwagie, H. Sol, G. Roebben, W. Heylen, Y. Shi, and O. Van der Biest. Mixed numerical-experimental identification of elastic properties of orthogropic metal plates. *NDT & E Int.*, **36**:487–495, 2003.

[102] H. J. Lee and D. A. Saravanos. The effect of temperature dependent material properties on the response of piezoelectric composite materials. *J. Int. Mat. Sys. and Str.*, **9**:503–508, 1998.

[103] M. H. Lee, R. Guo, and A. S. Bhalla. Pyroelectric sensors. *J. Electroceramics*, **2**(4):229–242, 1998.

[104] E. Lefeuvre, A. Badel, C. Richard, and D. Guyomar. Piezoelectric energy harvesting device optimization by synchronous electric charge extraction. *J. Intell. Mater. Syst. Struct.*, **16**(10):865–876, 2005.

[105] E. Lefeuvre, A. Badel, C. Richard, L. Petit, and D. Guyomar. A comparison between several vibration-powered piezoelectric generators for standalone systems. *SENSOR ACTUAT A-PHYS*, **126**:405–416, 2006.

[106] Y. L. Li, S. Y. Hu, Z. K. Liu, and L. Q. Chen. Effect of electrical boundary conditions on ferroelectric domain structures in thin films. *Appl. Phys. Lett.*, **81**(3):427–429, 2002.

[107] C. Liang and C. A. Rogers. One-dimensional thermomechanical constitutive relations for shape memory materials. *J. Int. Mat. Sys. and Str.*, **1**:207–234, 1990.

[108] W. M. Lin, R. Koehler, G. Suchaneck, and G. Gerlach. Thermal analysis of pyroelectric sensors in scanning thermal microscopy. *Jpn. J. Appl. Phys. Part 1*, **41**(11B):7239–7241, 2002.

[109] M. E. Lines and A. M. Glass. *Applications of ferroelectrics and related materials.* Oxford: Oxford University Press, 1977.

[110] S. T. Liu and D. Long. Pyroelectric detectors and materials. In *Proceedings of the IEEE*, volume **14-26**, pages 310–321. IEEE, 1978.

[111] A. E. H. Love. *Mathematical theory of elasticity*. Cambridge: Cambridge University Press, 4th edition, 1927.

[112] Z. K. Lu and G. J. Weng. A self-consistent model for the stress-strain behavior of shape memory alloy polycrystals. *ACTA Materialia*, **46**(15):5423–5433, 1998.

[113] K. Makihara, J. Onoda, and T. Miyakawa. Low energy dissipation electric circuit for energy harvesting. *Smart Mater. Struct.*, **15**:1493–1498, 2006.

[114] L. F. Malmonge, J. A. Malmonge, and W. K. Sakamoto. Study of pyroelectric activity of PZT/PVDF-HFP composite. *Materials research*, **6**(4):469–473, 2003.

[115] N. Merah, M. Irfan-Ul-Haq, and Z. Khan. Temperature and weld-line effects on mechanical properties of CPVC. *J. Mat. Proc. Tech.*, **142**:247, 2003.

[116] V. Michaud. Can shape memory alloy composites be smart. *Scripta Materialia*, **50**:249–253, 2004.

[117] G. Min, D. M. Rowe, and K. Kontostavlakis. Thermoelectric figure-of-merit under large temperature differences. *J. Phys. D: Appl. Phys.*, 37(8):1301–1304, 2004.

[118] C.-W. Moon, D.-W. Kim, G. Rosenman, T. K. Ko, and I. K. Yoo. Patterned pyroelectric electron emitters and their feasibility study for lithography applications. *Jpn. J. Appl. Phys.*, 42:3523–3525, 2003.

[119] K. M. Mossi and R. P. Bishop. Characterization of different types of high performance Thunder^{TM} actuators. In *Smart structures and materials*, volume 3675, pages 43–52. SPIE, 1999.

[120] K. M. Mossi, Z. Ounaies, R. C. Smith, and B. L. Ball. Prestressed curved actuators: characterization and modeling of thei piezoelectric behavior. In *Smart structures and materials*, volume 5053, pages 423–435. SPIE, 2003.

[121] I. Muller and S. Seelecke. Thermodynamic aspects of shape memory alloys. *Mat. and Com. Mod.*, **34**(12-13):1307–1355, 2001.

[122] R. W. Munn and R. J. Newham. Thermodynamics of internal strain in perfect crystals. III. Piezoelectric and related properties. *J. Phys. C: Solid State Phys.*, **7**(5):848–863, 1974.

[123] P. Muralt. Micromachined infrared detectors based on pyroelectric thin films. *Rep. Prog. Phys.*, **64**:1339–1388, 2001.

[124] H. S. Nalwa, editor. *Ferroelectric polymers: chemistry, physics, and applications*. New York: Marcel Dekker, Inc., 1995.

[125] C. W. Nan. Product property between thermal expansion and piezoelectricity in piezoelectric composites: pyroelectricity. *J. Mat. Sci. Lett.*, **13**:1392–1394, 1994.

[126] C. W. Nan. Theoretical approach to the coupled thermal-electrical-mechanical properties of inhomogeneous media. *Physical Review B*, **49**(18):12619–12624, 1994.

[127] B. Naranjo, J. K. Gimzewski, and S. Putterman. Observation of nuclear fusion driven by a pyroelectric crystal. *Nature*, **434**:1115–1117, 2005.

[128] B. Naranjo and S. Putterman. Search for fusion from energy focusing phenomena in ferroelectric crystals, 2002.

[129] R. E. Newnham, D. P. Skinner, and E. Cross. Connectivity and piezoelectric-pyroelectric composites. *Mat. Res. Bull.*, **13**:525–536, 1978.

[130] R. E. Newnham, D. P. Skinner, K. A. Klicker, A. S. Bhalla, B. Hardiman, and T. R. Gururaja. Ferroelectric ceramic-plastic composites for piezoelectric and pyroelectric applications. *Ferroelectrics*, **27**(1):49–55, 1980.

[131] Z. Nishiyama. *Martensitic transformation*. New York: Academic Press, 1978.

[132] E. L. Nix, J. Nanayakkara, G. R. Davies, and I. M. Ward. Primary and secondary pyroelectricity in highly oriented polyvinylidene fluoride. *J. Poly. Sci. Part B: Poly. Phys.*, **26**(1):127–140, 1988.

[133] J. F. Nye. *Physical properties of crystals*. Oxford: Oxford University Press, 1979.

[134] K. S. Olofsson. Temperature predictions in thick composite laminates at low cure temperatures. *Appl. Comp. Mat.*, **4**:1–11, 1997.

[135] R. B. Olsen, D. Bruno, and J. Briscoe. Cascaded pyroelectric energy converter. *Ferroelectrics*, **59**:205–219, 1984.

[136] R. B. Olsen, D. Bruno, and J. Briscoe. Pyroelectric conversion cycle of vinylidene fluoride-trifluoroethylene copolymer. *J. Appl. Phys.*, **57**:5036–5042, 1985.

[137] R. B. Olsen, D. Bruno, and J. Briscoe. Pyroelectric conversion cycles. *J. Appl. Phys.*, **58**:4709–4716, 1985.

[138] R. B. Olsen and D. Evans. Pyroelectric energy conversion: Hysteresis loss and temperature sensitivity of a ferroelectric material. *J. Appl. Phys.*, **57**:5941–5944, 1983.

[139] G. K. Ottman, H. F. Hofmann, and G. A. Lesieutre. Optimized piezoelectric energy harvesting circuit using step-down converter in discontinuous conduction mode. *IEEE T Power Electr.*, **18**(2):696–703, 2003.

[140] Z. Ounaies, K. M. Mossi, R. C. Smith, and J. Bernd. Low-field and high-field characterization of THUNDER actuators. In *Smart structures and materials*, volume 4333, pages 399–407. SPIE, 2001.

[141] R. A. Paquin. *Handbook of Optics*. McGraw-Hill, 2nd edition, 1995.

[142] R. A. Paquin. *Handbook of optomechanical engineering*. CRC Press, 1997.

[143] J. Perkins. *Shape memory effects in alloys*. New York: Plenum Press, 1975.

[144] S. Pinarbasi, U. Akyuz, and Y. Mengi. A new formulation for the analysis of elastic layers bonded to rigid surfaces. *Int. J. Solids and Struc.*, **43**:4271–4296, 2006.

[145] B. Ploss, B. Ploss, S. Kopf, and F. G. Shin. The pyroelectric coefficient of composites.

ISE-12 Int. Symp. Electrets, pages 487–490, 2005.

[146] C. Popov, H. Chang, P. M. Record, E. Abraham, R. W. Whatmore, and Z. Huang. Direct and converse magnetoelectric effect at resonant frequency in laminated piezoelectric-magnetostrictive composite. *J. Electroceramics*, **20**(1):53–58, 2008.

[147] P. M. Record, C. Popov, J. Fletcher, E. Abraham, Z. Huang, H. Chang, and R. W. Whatmore. Direct and converse magnetoelectric effect in laminate bonded Terfenol-D-PZT composites. *Sen. and Act. B: Chemical*, **126**(1):344–349, 2007.

[148] K. Ren, Y. Liu, X. Geng, H. F. Hofmann, and Q. M. Zhang. Single crystal PMN-PT/Epoxy 1-3 composite for energy-harvesting application. *IEEE T Ultrason Ferr*, **53**(3):631–638, 2006.

[149] M. Renaud, T. Sterken, P. Fiorini, R. Puers, K. Baert, and C. van Hoof. Scavenging energy from human body: design of a piezoelectric transducer. *Tech. Digest 13th Int. Conf. on Solid-state sensors and actuators transducers '05 (Seoul, South Korea)*, **1**:784–787, 2005.

[150] S. Riffat and X. Ma. Thermoelectrics: a review of present and potential applications. *Apl. Therm. Eng.*, 23:913–935, 2003.

[151] W. F. Riley and L. W. Zachary. *Introduction to mechanics of materials*. John Wiley & Sons, Inc., 1989.

[152] Y. Roh, V. V. Varadan, and V. K. Varadan. Characterization of all the elastic, dielectric, and piezoelectric constants of uniaxially oriented poled PVDF films. *IEEE trans. on ultrason., ferro., and freq. contr.*, **49**(6):836, 2002.

[153] G. Rosenman, D. Shur, Ya. E. Krasik, and A. Dunaevsky. Electron emission from ferroelectrics. *J. Appl. Phys.*, **88**(11):6109–6161, 2000.

[154] S. Roundy, P. K. Wright, and J. Rabaye. A study of low level vibrations as a power source for wireless sensor nodes. *Comput. Commun.*, **26**:1131–1144, 2003.

[155] V. Sandomirsky, A. V. Butenko, Y. Schlesinger, and R. Levin. Enhancement of voltage, ion current and neutron yield in pyroelectric accelerators. *arXiv:0904.0329v1*, 2009.

[156] V. Sandomirsky, Y. Schlesinger, and R. Levin. The edge electric field of a pyroelectric and its applications. *J. Appl. Phys.*, **100**(11):113722, 2006.

[157] G. D. Sao and H. V. Tiwary. Thermal expansion of poly(vinylidene fluoride) films. *Journal of Applied Physics*, **53**(4):3040, 1981.

[158] L. B. Schein, P. J. Cressman, and L. E. Cross. Electrostatic measurements of tertiary pyroelectricity in partially clamped $LiNbO_3$. *Ferroelectrics*, **22**(1):945–948, 1979.

[159] B. Scott and K. Michelle. Consider CPVC for process applicaitons. *Chem. Eng. Prog.*, **90**:36, 1994.

[160] G. Sebald, E. Lefeuvre, and D. Guyomar. Pyroelectric energy conversion: Optimization principles. *IEEE T Ultrason Ferr*, **55**(3):538–551, 2008.

[161] G. Sebald, S. Pruvost, and D. Guyomar. Energy harvesting based on Ericsson pyroelectric cycles in a relaxor ferroelectric ceramic. *Smart Mater. Struct.*, **17**:015012, 2008.

[162] A. Sharma, Z. G. Ban, S. P. Alpay, and J. V. Mantese. Effect of operating temperature and film thickness on the pyroelectric response of ferroelectric materials. *Applied Physics Letters*, **84**(24):4959–4961, 2004.

[163] A. Sharma, Z. G. Ban, S. P. Alpay, and J. V. Mantese. Pyroelectric response of ferroelectric thin films. *Journal of Applied Physics*, **95**(7):3618–3625, 2004.

[164] N. S. Shenck and J. A. Paradiso. Energy scavenging with shoe-mounted piezoelectrics. *IEEE Micro.*, **21**:30–42, 2001.

[165] Y. C. Shu and I. C. Lien. Efficiency of energy conversion for a piezoelectric power harvesting system. *J. Micromech. Microeng.*, **16**:2429–2438, 2006.

[166] D. Shur and G. Rosenman. Figures of merit for ferroelectric electron emission cathodes. *J. Appl. Phys.*, **80**(6):3445–3450, 1996.

[167] P. Sittner and V. Novˊk. Anisotropy of martensitic transformations in modeling of shape memory alloy polycrystals. *Int. J. Plas.*, **16**(10-11):1243–1268, 2000.

[168] H. A. Sodano, D. J. Inman, and G. Park. A review of power harvesting from vibration using piezoelectric materials. *The Shock Vib. Digest*, **36**(3):197–205, 2004.

[169] H. A. Sodano, D. J. Inman, and G. Park. Comparison of piezoelectric energy harvesting devices for recharging batteries. *J. Intell. Mater. Syst. Struct.*, **16**(10):799–807, 2005.

[170] H. A. Sodano, D. J. Inman, and G. Park. Generation and storage of electricity from power harvesting devices. *J. Intell. Mater. Syst. Struct.*, **16**(1):67–75, 2005.

[171] A. V. Srinivasan and D. M. McFarland. *Smart structures: Analysis and design*. Cambridge University Press, 2001.

[172] N. G. Stephen. On energy harvesting from ambient vibration. *J. Sound Vib.*, **293**:409–425, 2006.

[173] E. Suhir. Calculated thermally induced stresses in adhesively bonded and soldered assemblies. In *Proc. ISHM Int. Symp. Microelectron*, pages 383–392, Atlanta, Georgia, 6th Oct. 1986.

[174] E. Suhir. Modeling of Thermal Stress in Microelectronic and Photonic Structures: Roles, Attributes, Challenges, and Brief Review. *J. Electronic Packaging*, **125**(2):261–267, 2003.

[175] Q. P. Sun and K. C. Hwang. Micromechanics modeling for the constitutive behavior of polycrystalline shape memory alloys - part I. Derivation of general relations. *J. Mech. and Phys. Sol.*, **41**(1):1–17, 1993.

[176] K. Tanaka and S. Nagaki. Thermomechanical description of materials with internal variables in the process of phase transitions. *Ing.-Arc.*, **51**:287–299, 1982.

[177] H. Taunaumang, I. L. Guy, and H. L. Chan. Electromechanical properties of 1-3 piezoelec-

tric ceramic/piezoelectric polymer composites. *Journal of Applied Physics*, **76**(1):484–489, 1994.

[178] H.-C. Tsai. Compression analysis of rectangular elastic layers bonded between rigid plates. *Int. J. Solids and Struc.*, **42**:3395–3410, 2005.

[179] H.-C. Tsai. Tilting analysis of rectangular elastic layers bonded between rigid plates. *J. Eng. Mech.*, **133**(9):1030–1036, 2007.

[180] M. Umeda, K. Nakamura, and S. Ueha. Energy storage characteristics of a piezo-generator using impact induced vibrations. *Jpn J. Appl. Phys.*, **36**:3146–3151, 1997.

[181] J. van Suchtelen. Product properties: A new application of composite materials. *Philips Res. Rep.*, 27:28–37, 1972.

[182] D. Vanderpool, J. H. Yoon, and L. Pilon. Simulations of a prototypical device using pyroelectric materials for hearvesting waste heat. *Int. J. Heat and Mass Trans.*, **51**:5052–5062, 2008.

[183] B. Wang and C. H. Woo. Curie-Weiss law in thin-film ferroelectrics. *Journal of Applied Physics*, **100**:044114, 2006.

[184] H. Warlimont, L. Delaey, R. V. Krishnan, and H. Tas. Thermoelasticity, pseudoelasticity and the memory effects associated with martensitic transformations - Part 3: Thermodynamics and kinetics. *J. Mat. Sci.*, **9**(9):1545–1555, 1974.

[185] A. W. Warner, M. Onoe, and G. A. Coquin. Determination of elastic and piezoelectric constants for crystal in class (3m). *J. Acoustical Soc. of America*, **42**(6):1223, 1967.

[186] R. W. Whatmore. Pyroelectric devices and materials. *Rep. Prog. Phys.*, **49**:1335–1386, 1986.

[187] R. W. Whatmore and A. J. Bell. Pyroelectric ceramics in the Lead zirconate-Lead titanate-Lead iron niobate system. *Ferroelectrics*, **35**:155–160, 1981.

[188] R. W. Whatmore, J. M. Herbert, and F. W. Ainger. Recent developments in ferroelectrics for Infrared detectors. *Phys. Stat. Sol. A*, **61**:73–80, 1980.

[189] R. W. Whatmore, P. C. Osbond, and N. M. Shorrocks. Ferroelectric materials for thermal IR detectors. *Ferroelectrics*, **76**:351–367, 1987.

[190] R. W. Whatmore and R. Watton. *Infrared Detectors and Emitters: Materials and Devices*, chapter 5. Pyroelectric materials and devices, pages 99–148. Kluwer academic publishers, 2001.

[191] J. Wood. Pyroelectric crystal used to drive neutron source: Electronic materials. *Materials today*, **8**(6):9, 2005.

[192] W. A. Wooster. *Tensors and group theory for the physical properties of crystals.* Oxford: Clarendon Press, 1973.

[193] S. Xing. Preparation and structure of RAINBOW piezoelectric ceramics. *J. Wuhan Uni.*

Tech., **18**(4), 2003.

[194] Y. Xu. *Ferroelectric materials and their applications*. Amsterdam: North-Holland, 1991.

[195] H. Yamazaki and T. Kitayama. Pyroelectric properties of polymer-ferroelectric composites. *Ferroelectrics*, 33:147–153, 1981.

[196] F. Yang, D. Zhang, B. Yu, K. Zheng, and Z. Li. Pyroelectric properties of ferroelectric ceramic/ferroelectric polymer 0-3 composites. *Journal of Applied Physics*, **94**(4):2553–2558, 2003.

[197] R. Yimnirun, Y. Laosiritaworn, and S. Wongsaenmai. Effect of uniaxial compressive pre-stress on ferroelectric properties of soft PZT ceramics. *J. Phys. D: Appl. Phys.*, **39**:759–764, 2006.

[198] I. K. Yoo, C. Moon, W. Choi, S. Kim, E. Bae, and S. Chung. Feasibility studies on pyroelectric emission for lithography application. *Integrated Ferroelectrics*, **41**:17–24, 2001.

[199] J. Zhao and Q. M. Zhang. Effect of mechanical stress on the electromechanical performance of PZT and PMN-PT ceramics. In *ISAF '96 Proceedings of the Tenth IEEE Int. Symp. on App. Fer.*, volume **2**, pages 971–974. IEEE, 1996.

[200] D. Zhou and M. Kamlah. High-field dielectric and piezoelectric performance of soft lead zirconate titanate piezoceramics under combined electromechanical loading. *Journal of Applied Physics*, **96**(11):6634–6641, 2004.

[201] D. Zhou, M. Kamlah, and D. Munz. Effects of unizxial prestress on the ferroelectric hysteretic response of soft PZT. *J. Eur. Cer. Soc.*, **25**:425–432, 2005.

[202] J. D. Zook and S. T. Liu. Pyroelectric effects in thin film. *Journal of Applied Physics*, **49**(8):4604–4606, 1978.